THE UNIVERSITY
of EDINBURGH

Learning in Adaptive Networks: Analytical and Computational Approaches

Guoli Yang

Doctor of Philosophy
Laboratory for Foundations of Computer Science
School of Informatics
University of Edinburgh
2016

Abstract

The dynamics *on* networks and the dynamics *of* networks are usually entangled with each other in many highly connected systems, where the former means the evolution of state and the latter means the adaptation of structure. In this thesis, we will study the coupled dynamics through analytical and computational approaches, where the adaptive networks are driven by learning of various complexities.

Firstly, we investigate information diffusion on networks through an adaptive voter model, where two opinions are competing for the dominance. Two types of dynamics facilitate the agreement between neighbours: one is pairwise imitation and the other is link rewiring. As the rewiring strength increases, the network of voters will transform from consensus to fragmentation. By exploring various strategies for structure adaptation and state evolution, our results suggest that network configuration is highly influenced by range-based rewiring and biased imitation. In particular, some approximation techniques are proposed to capture the dynamics analytically through moment-closure differential equations.

Secondly, we study an evolutionary model under the framework of natural selection. In a structured community made up of cooperators and cheaters (or defectors), a new-born player will adopt a strategy and reorganise its neighbourhood based on social inheritance. Starting from a cooperative population, an invading cheater may spread in the population occasionally leading to the collapse of cooperation. Such a collapse unfolds rapidly with the change of external conditions, bearing the traits of a critical transition. In order to detect the risk of invasions, some indicators based on population composition and network structure are proposed to signal the fragility of communities. Through the analyses of consistency and accuracy, our results suggest possible avenues for detecting the loss of cooperation in evolving networks.

Lastly, we incorporate distributed learning into adaptive agents coordination, which emerges as a consequence of rational individual behaviours. A generic framework of work-learn-adapt (WLA) is proposed to foster the success of agents organisation. To gain higher organisation performance, the division of labour is achieved by a series of events of state evolution and structure adaptation. Importantly, agents are able to adjust their states and structures through quantitative information obtained from distributed learning. The adaptive networks driven by explicit learning pave the way for a better understanding of intelligent organisations in real world.

Lay Summary

This thesis focuses on the interplay between state evolution and structure adaptation in adaptive networks. In real world, the adaptive dynamics drives the formation of complex topologies in social, biological, and technical systems. Generally speaking, the nodes connected with each other by various edges can change their states and structures locally in a distributed manner. With different levels of learning, individual behaviours give rise to a rich landscape in adaptive networks. The aim of this study is to explore various macroscopic emergence out of microscopic behaviours, where three types of learning methods are adopted to drive the adaptive dynamics.

To investigate the diffusion of information over networks, an adaptive voter model is proposed by means of some basic social learning strategies. For example, individuals holding different opinions may imitate or repel each other. This model can be used to reveal the transition from network consensus to fragmentation by varying some external parameters. Both numerical simulations and analytical calculations are developed in our study to analyse the system-level phenomena. We also try to adapt natural selection into adaptive networks, where the individual holding higher fitness would be more likely to reproduce. This family of models usually encompass a variety of games in networks, which are used to characterize the fitness of an individual. In particular, the collapse of cooperation attracts more and more attention in the fields of ecology, biology and even sociology, where some early-warning indicators are required to detect the coming risks. Furthermore, when the individuals are capable of learning, their behaviours of state evolution and structure adaptation should facilitate higher organisation performance. As no one is in global control, each individual aggregates local and historical information in the process of learning. A self-organising framework is proposed in our study to incorporate distributed learning into adaptive networks.

To conclude, we illustrate adaptive networks in information network, biological population, and technical system. By exploring various levels of learning, we gain deeper insights into the emergence, fragmentation, self-organisation, etc. More importantly, our research is helpful to (1) analyse the diffusion of information over networks; (2) detect the collapse of cooperation in an evolutionary population; (3) develop a system with autonomy, robustness and adaptability.

Acknowledgements

First, I would like to thank my supervisor, Vincent Danos, for his guidance and support throughout these years. I am very grateful to him for all the encouragement, inspiration and help. Many thanks to my second supervisor, Michael Herrmann, for his advice and suggestions. I would especially thank Matteo Cavaliere for his guidance in a core part of this thesis, which helps me gain a deep understanding in this research field.

Thanks to the people in Rule-Based Modelling group for their help along the way. Thanks to all my colleagues and friends in the school of Informatics, I have a very happy time in Edinburgh together with them.

Last but not least, I want to thank all my family members for their love.

Declaration

I declare that this thesis was composed by myself, that the work contained herein is my own except where explicitly stated otherwise in the text, and that this work has not been submitted for any other degree or professional qualification except as specified.

(*Guoli Yang*)

Table of Contents

Chapter 1

Introduction

In the past decades, a large variety of networks are illustrated in abstract or concrete ways (Strogatz, 2001; Albert and Barabási, 2002) to model complex systems in the highly connected world. Since the end of last century, complex networks have been widely noted by Refs. (Dorogovtsev and Mendes, 2002; Newman, 2003; Boccaletti et al., 2006; Jackson et al., 2008; Barrat et al., 2008) from the perspectives of topological structures, statistical properties, dynamical evolution, etc. As is known, a large number of realistic systems are present in the form of information networks (Albert et al., 1999), social networks (Redner, 1998; Newman, 2001), economic networks (Easley and Kleinberg, 2010), biological networks (Jeong et al., 2000) and ecological networks (Dunne et al., 2002).

Complex networks in real world have very different origins, while all of them can be demonstrated in the form of nodes connected by edges. To gain a deep insight into the interplay between structure and function, Newman *et al.* (Newman, 2003) have studied a variety of complex networks from both microscopic perspective and macroscopic perspective, where the former relates to local actions and the latter to global patterns. It is clear that, the interacting individuals change their behaviours locally, which will foster the emergence of some global phenomena. To understand the dynamical processes on complex networks, Barrat *et al.* (Barrat et al., 2008) have illustrated a large number of collective properties (synchronization, criticality, emergence, self-organisation, etc.) led by individual behaviours.

Complex adaptive theory (Holland, 1992; Miller and Page, 2009) has been proven to be a generic and fundamental framework for studying complex dynamical systems, where network theory, statistics, and self-organisation are involved. In general, complex adaptive systems can be characterized by three properties: individual components,

localised interactions and autonomous reactions (Levin, 2003). Well-known examples of adaptive systems have been observed from tissues to species and societies, which are "*systems that have a large numbers of components, often called agents, that interact and adapt or learn*"(Holland, 2006).

The main purpose of our study is to shed light upon the interrelationships between local behaviours and collective patterns in adaptive networks (Gross and Blasius, 2008), which are entangled by state evolution (i.e. changes of nodes' states) and structure adaptation (i.e. changes of network topology). In particular, we will explore different dynamics in adaptive networks driven by learning of various complexities, and then provide effective methods in inference and prediction.

1.1 Adaptive Networks

Recently, numerous studies have characterized the dynamical structures of complex systems by means of node (or link) creation, node (or link) deletion, link rewiring, etc. These dynamical structures are widely observed in the generation of various complex networks, for example the formation of scale-free networks based on preferential attachment (Barabási and Albert, 1999). More interestingly, for a network with a given structure, some dynamical processes may occur on top of it. In this case, the state of a node, which may be a discrete or continuous variable, is not static, but will change over time. In general, the changes of nodes' states are dependent on the underlying topology and neighbourhood configuration. We can easily find this kind of dynamical process from information cascade to opinion formation and epidemic spreading. However, the above two types of dynamics (dynamical structure and dynamical process) are addressed almost separately in many researches, ignoring the intrinsic interplay between each other.

From complex networks to adaptive networks (Gross and Blasius, 2008; Blasius and Gross, 2009; Zschaler, 2012), people will gain a deeper insight into the complexity in biological, social or technical systems, where both the states of nodes and the structure of network are dynamical. As illustrated in Ref. (Sayama et al., 2013), many real-world complex systems are entangled by the "dynamics *on* networks" and the "dynamics *of* networks" as shown in Figure 1.1. In the former, we focus on the evolution of nodes' states in a network with a given structure; while in the latter, we are more interested in the adaptation of network structure.

It is natural to couple the two types of dynamics, especially when we need to op-

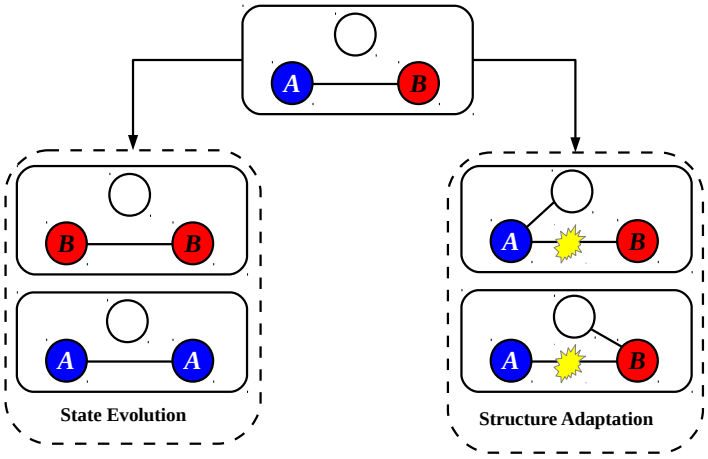

Figure 1.1: Adaptive mechanism in an example of voter model (Durrett et al., 2012), where the dynamics is driven by a bunch of specific rules of state evolution (i.e. imitation) and structure adaptation (i.e. repelling).

timize or build some networks with changing states and structures. In many realistic cases (Myers and Leskovec, 2014; Weng et al., 2013), the two types of dynamics are interdependent on each other. As shown in Figure 1.1, the structure of network usually influences the evolution of node's state, which in turn will affect the adaptation of neighbourhood. The formed feedback loop between state evolution and structure adaptation would drive the system from chaos to order or the other way around. For example, in Twitter networks, the process of tweets posting and sharing will let some users far away be visible and followed, so that the network structure is changed. On the other hand, the evolving structure will influence the propagation of information in the network.

Adopting some local actions and reactions, the adaptive dynamics can draw a spectacular picture to reveal various system-level phenomena, such as complex topology formation, critical phase transition, and robust self-organisation. As reviewed in Refs. (Gross and Blasius, 2008; Sayama et al., 2013), many researches have started exploring adaptive networks from different directions, ranging from information to biology, chemistry, sociology, ecology, etc. In particular, understanding the dynamics in adaptive networks mainly involves two aspects: (1) what individual behaviours are effective to direct the system towards desired outcomes; (2) how do the collective properties emerge out of individual behaviours. In this thesis, we will shed light upon the above issues through analytical and computational approaches, where the dynamics originates from learning of various complexities.

1.2 Learning in Adaptive Networks

In many real-world adaptive networks, individual behaviours have a great influence on global properties, which relate to collective benefit or organisation performance. Therefore, how to foster effective individual behaviours is key to the evolution of state and the adaptation of structure. As individuals in complex networks usually just possess local and historical information (of external environment, neighbourhood configuration, past experience etc.), some learning techniques implemented in a distributed manner are required for themselves to behave rationally.

As is known, learning is the ability to acquire, aggregate and analyse information (such as training data, past experience, interactions) used to guide future actions (Conte and Paolucci, 2001; Sen and Weiss, 1999). Some well-known learning methods are observation, imitation, advice-taking, reinforcement learning, etc. In a structured community, each individual can play as a learner, and its behaviour is a consequence of learning. Based on the complexities in the process of learning, we will focus on the following three types:

- **pairwise imitation** (Miller and Dollard, 1941; Sen and Weiss, 1999) is a typical form of social learning, where an individual would like to imitate the strategy of her/his neighbours. In this case, state evolution and structure adaptation would be implemented instantaneously without considering the historical interactions.

- **natural selection** (Darwin and Bynum, 2009; Hinton and Nowlan, 1987) is implemented based on the principles of Darwinian mechanism to shape the configuration of a community, where individuals with higher fitness are more likely to be promoted. In essential, natural selection is a kind of global imitation based on fitness.

- **distributed learning** (Sayed, 2014; Abdallah and Lesser, 2007; Gaston, 2005) allows each individual to make use of local and historical information in the process of decision-making, as a consequence the system can be reconfigured through a series of local actions. In a dynamical environment caused by changing tasks and neighbours, reinforcement learning (Barto, 1998) is widely adopted to make decisions.

In most of the existing researches (Zschaler, 2012), the coupled dynamics is usually driven by imitation. Here, we will integrate the above learning methods into three adaptive network models respectively, so that a more broad view can be obtained.

1.3 Primary Contributions

The main purpose of our work is to develop analytical and computational approaches for a better understanding of the dynamics in adaptive networks. The common framework is based on various social and physical dynamical processes on top of dynamical networks, which are driven by different forms of learning. The primary contributions are some adaptive network models and generalised methods.

1.3.1 Models

On the basis of existing researches, three typical complex adaptive systems are studied in this thesis. At first, an **adaptive voter model** (Chapter 3) focuses on the diffusion of information on networks, which are driven by a series of pairwise imitation and link rewiring. Secondly, an **evolutionary population model** (Chapter 4) is investigated based on the Darwinian mechanisms, where the dynamics of population is dependent on natural selection. Finally, **adaptive agents coordination** (Chapter 5) incorporates distributed learning into adaptive networks, so that state evolution and structure adaptation can be implemented under quantitative guidance to achieve higher performance. Essentially, these adaptive network models are just particular cases of graph transformation system (GTS) with colours for nodes (Danos et al., 2014).

1.3.1.1 Adaptive Voter Model

Information diffusion or spreading on networks is a fundamental topic in network science. In particular, the voter model (Holley and Liggett, 1975; Sznajd-Weron and Sznajd, 2000) describes a stochastic process for two or more competing opinions, which are held by the interacting voters and can be transmitted through the network. When the network structure is changing at the same time, an adaptive voter model (Holme and Newman, 2006) is present to highlight the coupled dynamics. In detail, state evolution indicates the process that the opinion of a voter is imitated by one of her/his neighbours, and structure adaptation results from the disconnection of those discordant edges (connecting two voters with different opinions).

Adaptive voter models are usually driven by two simple rules in social learning: pairwise imitation and link rewiring. In general, this family of models can exemplify well the adaptive nature through a rich landscape of behaviours from opinion consensus to network fragmentation. Based on the work (Durrett et al., 2012), some extensions

are developed in our study (Chapter 3). First, we discuss the influence of various adaptation strategies on the system-level behaviours, where an early fragmentation is obtained through rewire-to-foaf (here foaf is short for *friend of a friend*). Afterwards, we explore a more natural strategy for state evolution through approximate majority approach, where a neutral state will be created when two discordant voters meet. When taking neighbourhood information into consideration, a weight is assigned to the node as a measure for biased imitation. All these extensions foster a variety of collective dynamics, contributing to a better understanding of adaptive networks.

1.3.1.2 Evolutionary Population Model

The dynamics of evolutionary population focuses on the changing frequencies of individuals holding a certain state in an evolving community. In most cases, the state of an individual acts as a strategy, which is adopted by that individual to interact with all the neighbours. Evolutionary game theory (EGT) (Smith and Price, 1973) incorporates game theory into the evolving populations, where each individual holds a strategy of either cooperation or defection. The population usually evolves following the principles of natural selection, which is dependent on the fitness of individuals. An individual with higher fitness is more likely to be selected to reproduce offsprings, who would inherit the strategy from the parent unless mutation arises.

Based on the model discussed in Ref. (Cavaliere et al., 2012), we study the evolution of cooperation in dynamical networks (Chapter 4). Under the framework of evolutionary game theory, a birth-death update rule (Jiang et al., 2013) based on the Moran process (Moran, 1958) is adopted to depict the dynamics on networks, where the frequencies of cooperators and defectors (or cheaters) are varying as time goes by. Considering the dynamics of networks, we let the new-born individual to reconstruct its local neighbourhood by connecting to its parent and the friends of parent. This idea is rooted in social science, where the fresh person would like to form links with the friends of a friend. This model reveals the coupled dynamics through state-structure inheritance, which can be significantly helpful for the researches in ecology, biology and even sociology.

1.3.1.3 Adaptive Agents Coordination

Complex adaptive networks may arise in multi-agent systems (MAS), where agents interact with each other to solve some complicated tasks. As far as we are concerned,

global organisation performance is highly dependent on the functionality of agents and the interactions between each other. Combining self-organisation (Kohonen, 1988) with adaptive networks, some multi-agent systems (MAS) are able to achieve better performance in a distributed and adaptive manner (Gaston and desJardins, 2005; Kota et al., 2012). Recent researches have witnessed the success of adaptive multi-agent systems in the fields of robotic group (Gaston and desJardins, 2005; Abdallah and Lesser, 2007), traffic systems (Guimerà et al., 2002; Guimera et al., 2005), gene networks (Bornholdt and Rohlf, 2000; Bornholdt and Schuster, 2006), etc. In these applications, a successful organisation is usually fostered by a series of effective evolution and adaptation strategies. But how to evolve the states and adjust the structure in a distributed manner is not trivial.

In our study (Chapter 5), we investigate the adaptive dynamics in the field of agents coordination, where agents work and interact locally to achieve some global targets. As before, the adaptation of structure indicates the change of network topology and the evolution of state means the change of agent's functionality. In this family of models, both the dynamics of structure and the dynamics of state can influence the organisation performance and be influenced by it. Interestingly, the adaptive dynamics and agents coordination are entangled through a work-learn-adapt (WLA) framework. This framework extends the traditional adaptive network model by allowing distributed learning, through which both state evolution and structure adaptation can be performed quantitatively to gain better organisation performance.

1.3.2 Methods

In practice, it is not easy to capture the adaptive dynamics accurately, especially when the system size is large and the strategies for evolution and adaptation are complicated. To the best of our knowledge, differential equations and agent-based numerical simulations (Barrat et al., 2008) are two main methods used for analysing the transient processes and steady states in complex adaptive systems.

- Analytical Approach

Differential equations can characterize the dynamics by providing a cruder picture in a more efficient and simpler way, but more work is required to derive them. Through this analytical approach, some quantitative estimations are obtained to capture the equilibrium of some interesting observables. Let's define $p(G_i)(t)$ as the probability that

the network state (including the states of nodes and the interactions between them) is $G_i \in \Omega_G$ at time t, and we have $\sum_{G_i} p(G_i)(t) = 1$. Based on the general theory of Markov chains (Norris, 1998), we can write the forward equation for the vector p, which indicates the probability distribution of network states:

$$\frac{\mathrm{d}}{\mathrm{dt}} p^T = p^T Q \tag{1.1}$$

where p^T is the transpose of p and Q is the rate matrix whose element $q(G_i, G_j)$ represents the jump rate from network G_i to G_j. This function can be derived further to calculate some quantities of interest. Let's define an observable f, which is a function of $\mathbb{R}^{\Omega_G}$, and then the differential equation for $E_p(f)$ can be written as:

$$\frac{\mathrm{d}}{\mathrm{dt}} E_p(f) = p^T Q(f) \tag{1.2}$$

where $Q(f)$ is a vector with $Q(f)(G_i)$ as the mean rate of change of f at G_i, and

$$Q(f)(G_i) = \sum_{G_j} q(G_i, G_j)[f(G_j) - f(G_i)] \tag{1.3}$$

where $f(G_i)$ means the observable f at G_i.

- Computational Approach

Considering the difficulty in building and solving the fine-grained differential equations, some studies turn to the computational approach. Agent-based numerical simulations are usually adopted to verify the accuracy of analytical approach, where all detailed information can be obtained. By observing the state of any node at any time, we can capture the transient process precisely but costly. In addition, this method has been proven to be a powerful tool in dealing with some complicated adaptive processes, when it is hard to derive the coupled dynamics through differential equations. Notably, a single agent-based simulation may lead to inevitable noises or stochastic fluctuations, thus a large number of identical and independent trials are required to obtain the average observables and statistical distributions. Of course, the computation cost for agent-based simulations is usually expensive, especially for large-scale adaptive systems.

With a unified framework entangled by state evolution and structure adaptation, we adopt both analytical and computational methods to study these adaptive network models. In particular, three main points are focused respectively in the following Chapter 3, 4 and 5.

1.3.2.1 Approximation Techniques

When we are writing the differential equations for adaptive systems, some approximation techniques are required to make the equations solvable. In order to capture the dynamics of a certain observable under a series of rules $\gamma \in \mathcal{R}$, for example the average number of a motif $[g]$, we can obtain the differential equation as:

$$\begin{aligned} \frac{\mathrm{d}}{\mathrm{d}t}[g] &= p^T Q(g) \\ &= \sum_{\gamma \in \mathcal{R}} k_\gamma ([g]_\gamma^+ - [g]_\gamma^-) \end{aligned} \tag{1.4}$$

where k_γ is the rate of the rule γ, $[g]_\gamma^+$ means the average number of gain contributions under the rule γ and $[g]_\gamma^-$ means the average number of loss contributions. Notably, the calculations for $[g]_\gamma^+$ and $[g]_\gamma^-$ usually involve some bigger motifs. As a result, we need to write more differential equations for those bigger motifs so as to keep the system of equations closed (Danos et al., 2014).

As far as we are concerned, moments expansion will lead to a large number of differential equations, which are usually costly to establish. For this reason, some approximation techniques should be adopted to make the system of differential equations smaller and closed. In our study (Chapter 3), two approximation methods are developed to truncate bigger motifs through smaller ones. One approximation is improved from pair approximation (Ellner, 2001), where we take the relevant correlations of the observables into consideration. As the rules usually occur in the interface, we re-calculate the number of nodes located in the interface to avoid the overestimation. This interface approximation is as cheap as pair approximation in cost but will bring a higher accuracy. Another improvement is based on approximate master equation (Gleeson, 2011; Durrett et al., 2012), where neighbourhood configuration of a node is represented by a star-structure observable, and neighbourhood configuration of the neighbours is estimated through double stars approximation. This approximation makes the performance better but at the expense of higher computation cost, which is mainly caused by big variance in degree distribution. Nonetheless, through the study for approximations, we can grasp the technology to estimate the equilibrium of dynamical systems in a very efficient way relative to the agent-based simulations.

1.3.2.2 Critical Transitions

The adaptive dynamics sometimes demonstrates many very interesting phase transitions by varying a certain parameter gradually. This kind of phenomenon is extensively observed in structured biological, social, economic and ecological communities, whose

success is determined by the presence of evolutionary competition. Combining evolutionary games with adaptive networks, we intend to reveal the influence of network adaptation on the level of cooperation (Chapter 4). It is noted that a critical phase transition from the regime of cooperation to that of defection is obtained with the change of an adaptation parameter.

Such a collapse of cooperation usually unfolds rapidly and unexpectedly, which is crucial for the stability and sustainability of many evolutionary systems in real world. In the co-evolution of population composition and network structure, we associate the loss of cooperation with a number of generic indicators. Interestingly, some proposed indicators reflecting the dynamical structural information can perform very well in the tests of consistency and accuracy. Specifically, we adopt Kendall's τ correlation (Abdi, 2007) and receiver operating characteristic (ROC) (Boettiger and Hastings, 2012) to verify the performance of indicators in early-warnings. Both models and methods discussed in this study provide a deeper insight into the critical transition in evolving communities, which are widely observed in ecology, biology and even sociology. Some potential applications can be found in financial market prediction, ecological system detection and cultural diversity protection, where the early-warning signals are key to future catastrophes.

1.3.2.3 Distributed Learning

When it comes to the optimization problems on top of adaptive networks, the organisation performance is highly dependent on the states of nodes and the structure how they are organised. Considering the difficulty in communication, management and synchronization, it is impractical to adopt centralised methods with global information. In order to achieve a favourable organisation, the interacting agents should be endowed with some learning abilities, based on which they can self-organise the state and structure in a distributed manner (Chapter 5).

We study the adaptive dynamics in agents coordination, where the agents need to complete the tasks cooperatively. In particular, a module of distributed learning is performed by each agent in real time to acquire and aggregate feedbacks from external environment. After a long time of continuous agent learning, useful information or knowledge is obtained for quantitative state evolution and structure adaptation (Figure 1.2). Notably, the learning method in our study is adapted from reinforcement learning (Barto, 1998), where the dynamics is controlled by the difference between desired target and current case. In this way, we don't need to consider a huge state-action

space to make decisions.

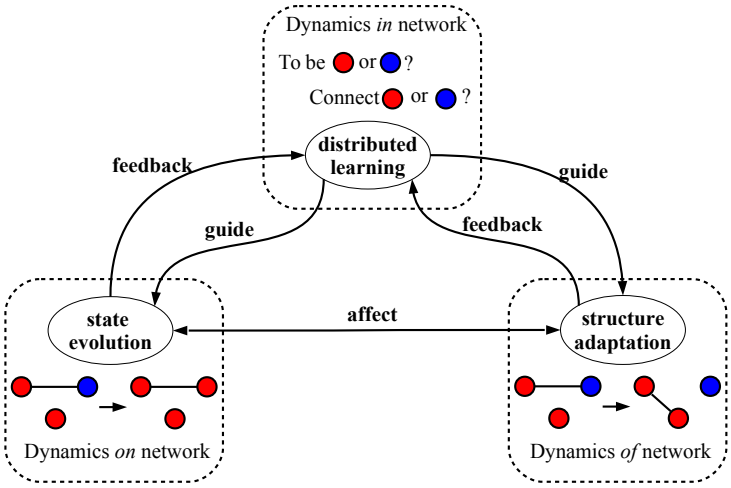

Figure 1.2: A schematic framework to show the adaptive networks incorporated by state evolution, structure adaptation and distributed learning.

As we can see, the adaptive network models are able to work in a more natural way by considering the dynamics *in* networks as well as the dynamics *on* and *of* networks (Figure 1.2). All types of dynamics are highly related to the organisation performance, where the details for state evolution and structure adaptation are quantified by continuous learning. In real world, this framework has a huge potential in the fields of robotic groups, sensor networks, resource allocation, etc.

1.4 Thesis Structure

In this thesis, we focus on the coupled dynamics between state and structure on top of complex adaptive networks, where the macroscopic phenomena emerge out of a series of microscopic interactions. Three adaptive network models are discussed in different research fields, namely adaptive voter model, evolutionary population model and adaptive agents coordination. All these models are characterized by state evolution and structure adaptation, but they are driven by different levels of learning as shown in Figure 1.3.

In chapter 2, we introduce the background and related work for complex adaptive networks. Some classic models and methods are reviewed for dynamical networks, dynamical processes and coupled dynamics.

In chapter 3, we focus on an adaptive voter model, whose dynamics is triggered by a series of pairwise imitation and link rewiring. In this chapter, we are going to

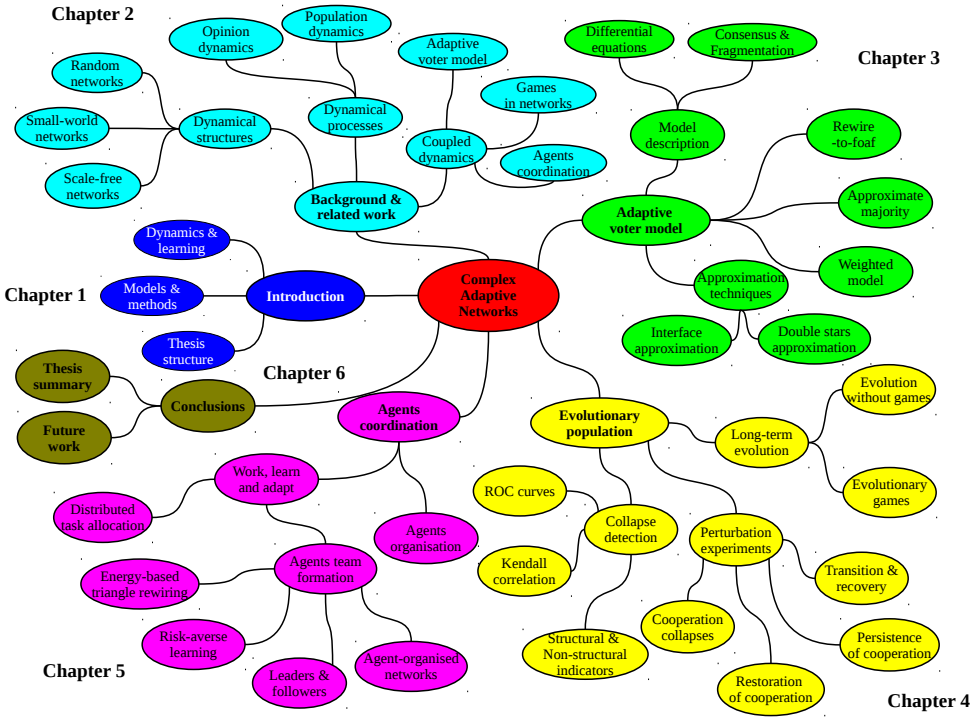

Figure 1.3: The structure of thesis.

make some extensions to understand the influences of various evolution and adaptation strategies on global patterns. Furthermore, the coupled dynamics is captured by some approximate differential equations.

In chapter 4[1], we study the evolution of cooperation in a group of structured population, where the dynamics originates from natural selection. A critical phase transition from the regime of cooperation to that of defection is obtained with the change of a certain structure adaptation parameter. To detect the loss of cooperation, some indicators are proposed to signal the resilience of communities.

In chapter 5[2], the adaptive networks are incorporated by state evolution, structure adaptation and distributed learning. We explore adaptive agents coordination through a work-learn-adapt (WLA) framework. Driven by organisation performance, the agents are able to adapt their states and structures through some quantitative information obtained from distributed learning.

Finally, we conclude our work in chapter 6, and discuss some possible directions for future work.

[1]Some of the contents are from our paper *Learning in Open Adaptive Networks*, Scientific Reports, 2016.

[2]It is exteneded from our paper *Detecting the Collapse of Cooperation in Evolving Networks*, SASO, 2016.

Chapter 2

Background

Complex networks have been widely studied since the end of last century to reason about the highly connected world, where a variety of natural and artificial systems offer fascinating properties. As present in Ref. (Zschaler, 2012), this chapter will give an overview of complex adaptive networks by providing a large number of models and methods as the state of the art. In the beginning, we will introduce several well-known network models as the first step towards complex adaptive systems, where the network structures are dynamically formed. Statistical analysis acts as a useful mathematical tool to understand the structure and function of these complex networks. We then explore some dynamical processes on static networks, where the states of nodes will change because of endogenous or exogenous factors. Interestingly, many global properties arise as a consequence of local behaviours (imitation, contagion, competition, etc.). When both structure and state are allowed to change, adaptive networks are built to shed light upon the coupled dynamics. We study the adaptive networks by considering three typical applications: adaptive voter model, games in adaptive networks and adaptive agents coordination, through which we can have a better understanding of modern complex systems from different perspectives.

2.1 Dynamical Networks

The formation of complex networks usually comes along with the dynamics of structures. In this section, we introduce some dynamical networks on the basis of graph theory and statistics, where different network models bring the differences in statistical properties. In particular, three classic network models are reviewed in the following, which are random networks, small-world networks and scale-free networks

respectively.

2.1.1 Random Networks

The random network model was studied originally by Erdős and Rényi in 1960s (Erdős and Rényi, 1959, 1960), which is usually referred as ER or Poisson random graph. In addition, we can find a variety of similar models in Refs. (Van Der Hofstad, 2009; Bollobás et al., 2010).

In the ER model, there are N isolated nodes in the beginning, and then each pair will be connected by an edge with probability p ($0 \leq p \leq 1$). Given an ER network denoted as $G_{N,p}$, when $p = 0$, the number of edges in the network is $E = 0$, namely a totally isolated network; while $p = 1$, the number of edges is $E = N(N-1)/2$, namely a complete network. Let's set $M = N(N-1)/2$, at a given p the expected number of edges is $\langle E \rangle = Mp$, and the average degree is $\langle k \rangle = (N-1)p \approx Np$.

As for the degree distribution in an ER random network, we can compute the probability a node with degree k as $p(k)$:

$$p(k) = \binom{N-1}{k} p^k (1-p)^{N-1-k} \approx \frac{\langle k \rangle^k e^{-\langle k \rangle}}{k!} \tag{2.1}$$

which is a Poisson distribution for the scaling $N \to \infty$ with a constant average degree.

In an ER random network, the clustering coefficient C is highly dependent on the linking probability p. For any connected triplet, the probability that the two ends are connected by an edge is p, so the network clustering coefficient is:

$$C = p \tag{2.2}$$

Ignoring the loops, the number of nodes within a distance l can be estimated as $\langle k \rangle^l$. When we have $\langle k \rangle^{\langle l \rangle} \approx N$, the average shortest path length can be obtained as (Bollobás, 1981):

$$\langle l \rangle \approx \log_{\langle k \rangle} N = \frac{\log N}{\log \langle k \rangle} \tag{2.3}$$

Network structures and statistical characteristics in ER random networks vary a lot when changing p. There is a critical value $p_c = 1/N$, which indicates the average degree is $\langle k \rangle_c = 1$. As discussed in Ref. (West et al., 2001), if $p < p_c$ then there are many small isolated sub-graphs; otherwise if $p > p_c$, then with a high probability there is a single giant component in the network. In Ref. (Erdős and Rényi, 1961), it is shown that if the linking probability is bigger than $\log(N)/N$, then the ER network will be connected with a probability approaching 1.

Given a linking probability p, the probability of an event I_u that a node u is isolated can be computed as:

$$p(I_u) = (1-p)^{N-1} \leq e^{-p(N-1)} \tag{2.4}$$

In this way, the probability that a network contains at least one isolated node is upper bounded as:

$$p(\cup I_u) \leq \sum_u p(I_u) \leq Ne^{-p(N-1)} \tag{2.5}$$

The ER random model can be extended to various generalised forms (Bollobás, 2001; Molloy and Reed, 1995; Newman et al., 2001), where the configuration model (Bender and Canfield, 1978) is a famous one. In the configuration model, a sequence of degree $[k_1, k_2, \cdots k_N]$ is assigned to nodes in the network, and then edges are assigned uniformly at random to match the given degree distribution.

Let's define k_u as the degree of a node u and k_v as that of a node v, the probability of an edge between u and v can be computed as:

$$p_{uv} = k_u k_v / 2E = k_u k_v / \sum_w k_w$$

Furthermore, let's define n_{uv} as the number of common neighbours of u and v, and then we can expect that:

$$\langle n_{uv} \rangle = \sum_w \frac{k_u k_w}{2E} \times \frac{k_v(k_w-1)}{2E} = p_{uv} \frac{\langle k^2 \rangle - \langle k \rangle}{\langle k \rangle}$$

As for the clustering coefficient, it can be calculated by (Newman, 2003):

$$\begin{aligned} C &= \frac{1}{N} \sum_u \sum_v \frac{k_u k_v}{2E} \frac{\sum_w [(k_u-1)k_w/2E] \times [(k_v-1)(k_w-1)/2E]}{(k_u-1)k_u} \\ &= \frac{1}{N} \sum_u \sum_v \frac{k_v(k_v-1)}{(2E)^2} \frac{\langle k^2 \rangle - \langle k \rangle}{\langle k \rangle} \\ &= \frac{1}{N} \sum_u \frac{1}{2E} \left(\frac{\langle k^2 \rangle - \langle k \rangle}{\langle k \rangle} \right)^2 = \frac{1}{N} \frac{(\langle k^2 \rangle - \langle k \rangle)^2}{\langle k \rangle^3} \end{aligned} \tag{2.6}$$

where we can find a strong relationship between the average degree $\langle k \rangle$ and the higher moment $\langle k^2 \rangle$. When $\langle k^2 \rangle$ is much larger, the clustering coefficient in the configuration model is bigger than that in an ER random model.

2.1.2 Small-world Networks

"Six degrees of separation" is a well-known story in social networks, as explained in (Karinthy, 1929) "*nobody from the group needed more than five links in the chain to reach, just by using the method of acquaintance, any inhabitant of our Planet.*"

A notion of random network with a higher clustering coefficient and smaller average shortest path length than the ER model can be constructed as a "small-world" network. These examples in real world have been observed in navigation networks (Kleinberg, 2000), protein networks (Bork et al., 2004) and transcriptional networks (Van Noort et al., 2004).

In 1998, Watts and Strogatz (Watts and Strogatz, 1998) proposed a WS model to describe the collective dynamics in small-world networks. As shown in Figure 2.1, we can obtain a series of small-world networks originated from a regular graph by increasing the randomness parameter q (rewiring probability), which is the probability that each edge connected to a right-hand side neighbour is rewired randomly.

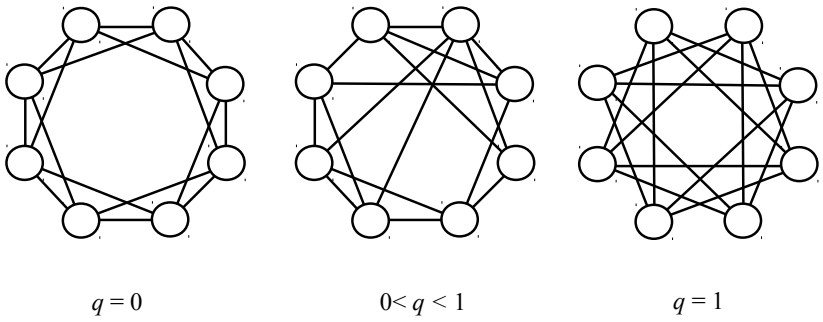

Figure 2.1: Increasing randomness will give rise to to some small-world networks at $0 < q < 1$, and then a random network at $q = 1$. Starting from a regular ring lattice, each edge on right-hand side is randomly rewired with probability q. The distant pairs may be connected by some short-cuts in the generated small-world networks. Figure is adapted from Ref. (Watts and Strogatz, 1998).

As we can see, at $q = 0$ the network is regular with a quite large clustering coefficient and a big average path length. After random rewirings in the range $0 < q < 1$, some distant pairs may be connected by short-cuts, which reduces the average path length meanwhile keeps the clustering coefficient high. If all edges are rewired, a random network with a smaller clustering coefficient and a quite shorter average path length is obtained at $q = 1$. Notably, the number of edges is constant. More statistical characteristics about the small-world networks can be found in Refs. (Barthélémy and Amaral, 1999; Barrat and Weigt, 2000).

Specifically, the degree distribution of a WS small-world model can be computed

as (Barrat and Weigt, 2000):

$$p(k) = \sum_{n=0}^{\min(k-\langle k\rangle/2,\langle k\rangle/2)} \binom{\langle k\rangle/2}{n} (1-q)^n q^{\langle k\rangle/2-n} \frac{(q\langle k\rangle/2)^{k-n-\langle k\rangle/2}}{(k-n-\langle k\rangle/2)!} e^{-q\langle k\rangle/2} \quad (2.7)$$

where $\langle k\rangle$ is the average degree of the network and q is the rewiring probability. The degree of a node contains three aspects: (I) the $\langle k\rangle/2$ rewired connections by itself; (II) the $\binom{\langle k\rangle/2}{n}(1-q)^n q^{\langle k\rangle/2-n}$ untouched edges from the left-hand side neighbours; (III) $\frac{(q\langle k\rangle/2)^{k-n-\langle k\rangle/2}}{(k-n-\langle k\rangle/2)!} e^{-q\langle k\rangle/2}$ rewired links towards the node itself. In addition, the minimum degree in a WS network is $\langle k\rangle/2$, and the degree distribution has a smaller variance in this case.

When $q \to 1$, the degree distribution follows a Poisson distribution:

$$p(k) = \frac{(\langle k\rangle/2)^{k-\langle k\rangle/2}}{(k-\langle k\rangle/2)!} e^{-\langle k\rangle/2} \quad (2.8)$$

Barrat and Weight (Barrat and Weigt, 2000) measured the clustering coefficient through some analytical calculations as follows. When $q = 0$, the network is a regular graph, and we can have the clustering coefficient $C = \frac{3(\langle k\rangle-2)}{4(\langle k\rangle-1)}$, which tends to $3/4$ as the network average degree is quite large. When $0 < q < 1$, the triangle remains connected with probability $(1-q)^3$, thus the clustering coefficient can be approximated as:

$$C \approx \frac{3(\langle k\rangle-2)}{4(\langle k\rangle-1)}(1-q)^3 \quad (2.9)$$

As the rewiring probability increases to $q = 1$, all edges are rewired and the network turns into a random graph, so the clustering coefficient is $C = \langle k\rangle/N$.

When it comes to the average shortest path length, we can obtain $\langle l\rangle = N/(2\langle k\rangle)$ at $q = 0$, and $\langle l\rangle = \frac{\ln N}{\ln\langle k\rangle}$ at $q = 1$. Interestingly, when $1/N < q \ll 1$, Refs. (Barthélémy and Amaral, 1999; Barrat and Weigt, 2000) pointed out that the average shortest path length decreases rapidly to a quite small value close to the one at $q = 1$, meanwhile the clustering coefficient remains high. In this way, an evident small-world phenomenon is obtained in the range of $1/N < q \ll 1$.

2.1.3 Scale-free Networks

Recently, more and more researches have illustrated that many realistic networks such as Internet, biological networks and social networks demonstrate power-law degree distributions. These networks are usually known as scale-free networks, whose degree distribution follows a form like $p(k) \sim k^{-\gamma}$, where γ usually ranges from 2 to 3. The

scale-free networks mainly focus on the dynamical growth process and the emergence of non-trivial configurations, which present an obvious "heavy tail" in degree distribution. There have been a large number of generation models explored in this field since the late 1990s, and the mechanism proposed by Barabási and Albert (Barabási and Albert, 1999) (known as the BA model) has attracted the most attention.

In the BA model (Barabási and Albert, 1999), two ingredients are required to construct the scale-free network:

- **Network growth**: the size of network is not constant, and it will increase continuously by adding a certain number of new nodes and edges at each step. In the beginning, we have a small connected component. Afterwards, one node and m edges are added into the network at each step.

- **Preferential attachment**: the new edges are not assigned to the nodes at random but prefer to connect to those nodes with higher degree. This principle is also known as the phenomenon of "rich get richer" or Matthew effect (Merton, 1968), which indicates the accumulated advantage (Perc, 2014).

As shown in Figure 2.2, we provide a schematic diagram to show the evolving network from step t to $t+1$, where a new node and two new edges are added into the graph.

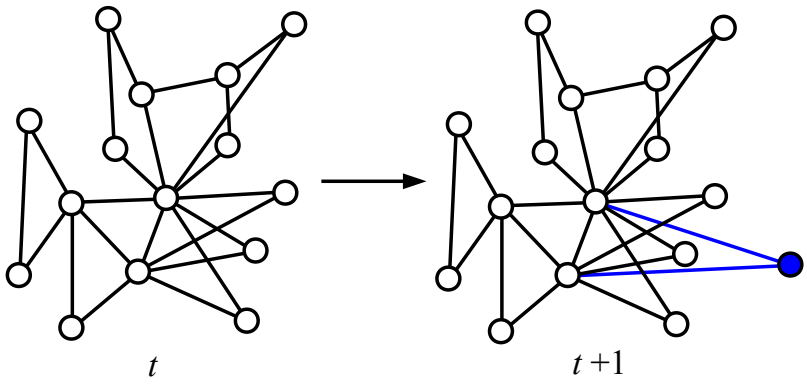

Figure 2.2: Network growth and preferential attachment in a scale-free network. The new edge (blue one in the graph) is connected to an existing node with probability proportional to its degree.

Now, let's come to some analytical investigations for the dynamical process of the BA model. The new node u connects to an old node v with probability p_{uv} at step t,

which is proportional to the corresponding degree of v.

$$p_{uv} = \frac{k_v(t)}{\sum_w k_w(t)} \tag{2.10}$$

Suppose we have m_0 edges in the initial component, as m edges are added at each step, there are $mt + m_0$ edges in the network at step t. The evolution equation for the degree of u can be approximated as:

$$\frac{\mathrm{d}k_u(t)}{\mathrm{dt}} = m\frac{k_u(t)}{2(mt+m_0)} \tag{2.11}$$

Furthermore, we can obtain the solution for $k_u(t)$ as:

$$k_u(t) = m\sqrt{t/t_u} \tag{2.12}$$

where t_u is the step at which u is added into the network, and the boundary condition is $k_u(t_u) = m$.

Now, let's see some statistical properties of the scale-free networks. The degree distribution at time $t \to +\infty$ can be calculated as follows to obtain a power law form (Barrat et al., 2008):

$$\begin{aligned} p(k,t) &\approx \frac{1}{t}\int_0^t \delta(k-k_u(t))\mathrm{d}u \\ &\approx 2m^2k^{-3} \end{aligned} \tag{2.13}$$

where $\delta(k-k_u(t))$ is the Dirac delta function. Similar results can be obtained through master equations (Dorogovtsev et al., 2000) and rate equations (Krapivsky et al., 2000).

The clustering coefficient in the BA model has been calculated analytically in Refs. (Klemm and Eguiluz, 2002b,a; Szabó et al., 2003), where a relatively higher clustering coefficient can be obtained for those scale-free networks. In addition, the average shortest path length in a BA network is smaller than that in an ER random network, when both have same size (Albert and Barabási, 2002; Bollobás and Riordan, 2003).

2.2 Dynamical Processes

It is known that, some simple local strategies, for example neighbourhood imitations, can affect individual state and then global properties. In order to analyse the dynamical process in a mathematical way, approximate differential equations are usually adopted to capture the microscopic processes and then the macroscopic phenomena. In addition, agent-based numerical simulations also play an important role in understanding

the collective dynamics and statistical properties. Ref. (Porter and Gleeson, 2014) gives several fascinating examples and generalised calculations for the study of dynamical systems on networks, and it is a great start point for those who are interested in this topic. In this section, we will introduce two typical dynamical processes taking place on static networks: one is opinion dynamics and the other is population dynamics.

2.2.1 Opinion Dynamics

The family of voter models is widely used to characterize opinion dynamics or information diffusion on networks. In general, they can be described by a stochastic process for two or more competing opinions. In voter models, the voters are represented by nodes, and the edges mean the interactions between each other. The state of a node is the corresponding opinion held by itself, which may change due to the influence from neighbourhood. The first voter model was introduced in Ref. (Clifford and Sudbury, 1973), where two species competed for territory within a spatial structure. Afterwards, a wide variety of researches (Holley and Liggett, 1975; Sznajd-Weron and Sznajd, 2000; Galam, 2002; Sood and Redner, 2005) have been launched to explore the dynamics of opinions.

As we all know, the collective patterns, such as emergence, synchronization, bifurcation, are usually fostered by a series of local behaviours. We can find numerous relevant examples in real world, like innovation cascade, rumour spreading and alliance formation. Recently, a variety of voter models (including link (or node)-centric voter model (San Miguel et al., 2005), majority voter model (Galam, 2002; Krapivsky and Redner, 2003), Sznajd model (Sznajd-Weron and Sznajd, 2000), threshold voter model (Durrett et al., 1993), continuous voter model (Deffuant et al., 2000), etc.) have arisen to throw light upon the propagation of opinions. In addition, a large number of variants (Colaiori and Castellano, 2015; Varghese and Durrett, 2013; Mellor et al., 2015) are explored from different perspectives (public media, a third state, long-range evolution, etc.) to illustrate information diffusion on complex networks. For more details on statistical physics of social dynamics, we can find a comprehensive review in Ref. (Castellano et al., 2009).

Generally speaking, there are N voters in the system, and each of them has a state $s_i \in \{A, B\}$, which indicates two different political choices or opinions. After that, the state of a voter will change along with the interactions. Some rules are introduced to

drive the evolution of state, which will converge to a frozen configuration when none of the rules can be applied to the agents. In the following, we will give a brief overview of some classic voter models mentioned above.

2.2.1.1 Node-centric Voter Model

In general, it is assumed that individuals are not self-confident and they may adopt the states of their neighbours. The dynamical process in a node-centric voter model can be shown as below:

(1) A voter i is selected at random.

(2) An arbitrary neighbour $j \in NB(i)$ is selected as the imitation target.

(3) The voter i updates her/his state as: $s_i = s_j$.

(4) Repeat step $(1) - (3)$ until the opinion consensus is reached in the finite system.

This process follows a proportional rule as shown in Figure 2.3(a), where the focal agent is more likely to imitate the state of the majority. In a finite connected system, we have two absorbing states: all As and all Bs. This voter model is similar to the Ising model when the temperature is decreased to a low level, and the system will evolve from a chaotic one to an ordered one. As illustrated in the coarsening process (Scheucher and Spohn, 1988) shown in Figure 2.3(b), some larger homogeneous regions with voters sharing same state are obtained with time going by.

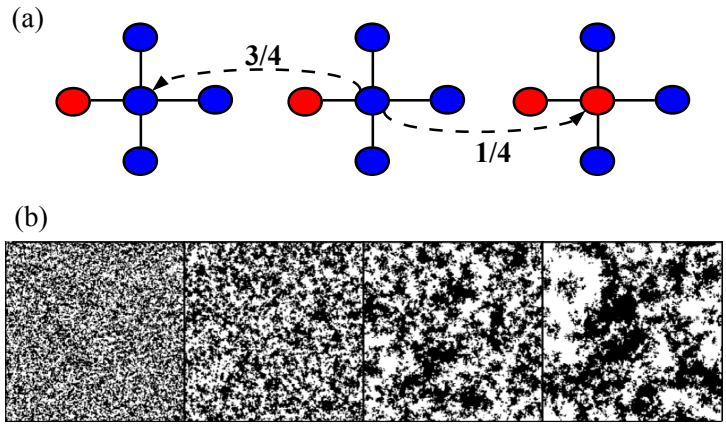

Figure 2.3: The evolution of voter model. (a) The flipping of state follows a proportional rule. (b) The evolution of 2-dimensional voter model from a fully disordered lattice to a coarsening structure. Figures are from Ref. (Dornic et al., 2001).

When the voter model is embedded into various complex networks, we can acquire a more interesting landscape. In detail, some statistical properties will be concerned in the evolution of opinions, such as the number of a certain type of opinion holders ($[A]$ or $[B]$), the number of active links (connecting opposite opinions, i.e. $[AB]$), and the expected consensus time.

Specifically, let's consider a network with a degree distribution $p(k)$, and then the probability that a given neighbour has degree k can be approximated by $kp(k)/\langle k\rangle$. Let ρ_k be the density of voters holding A in the group constituted by nodes of degree k, and then the probability that a voter A with degree k changes her/his state to B is:

$$p_k(A \to B) = p(k)\rho_k \sum_{k'} \frac{k'p(k')}{\langle k\rangle}(1-\rho_{k'}) \tag{2.14}$$

Similarly, we can have $p_k(B \to A)$ as the probability that a voter B with degree k changes to A:

$$p_k(B \to A) = p(k)(1-\rho_k) \sum_{k'} \frac{k'p(k')}{\langle k\rangle}\rho_{k'} \tag{2.15}$$

In this way, the density of As with degree k evolves as (Barrat et al., 2008):

$$\frac{\mathrm{d}}{\mathrm{d}t}\rho_k = \frac{p_k(B \to A) - p_k(A \to B)}{p(k)} = \sum_{k'} \frac{k'p(k')}{\langle k\rangle}(\rho_{k'} - \rho_k) \tag{2.16}$$

which leads to $\rho_k = \sum_{k'} \frac{k'p(k')}{\langle k\rangle}\rho_{k'}$ at stationary state (Sood and Redner, 2005).

In addition, we can approximate the expected consensus time through a recursion equation (Barrat et al., 2008; Sood et al., 2008), where a network with a heterogeneous structure (high variance in degree distribution) is more likely to reach consensus (Castellano et al., 2003).

2.2.1.2 Link-centric Voter Model

The link-centric voter model (Suchecki et al., 2005) focuses on the changes of edges in networks. The dynamical process is considered as follows: a random edge is selected at each step, and then one node at a randomly chosen end imitates the state of the node at the other end. In the node-centric model, the probability to pick an edge uv is $1/N(1/k_u + 1/k_v)$, but here the probability to pick uv is $1/E$. The differential equations can be obtained as (see more details in Chapter 3):

$$\begin{aligned} \tfrac{\mathrm{d}}{\mathrm{d}t}[A] &= [AB] - [BA] \\ \tfrac{\mathrm{d}}{\mathrm{d}t}[AB] &= -[AB] + [ABB] - [ABA] - [BA] + [BAA] - [BAB] \end{aligned} \tag{2.17}$$

where $[AB] = [BA]$ and $[AA]$ is not discounted for symmetries. A schematic diagram is presented in Figure 2.4.

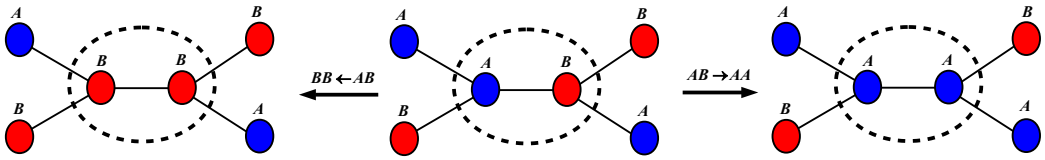

Figure 2.4: An example to show the link-centric voter model. (a) In the case of $AB \rightarrow AA$, the voter B changes her/his state to A and those edges connecting that original "B" are affected as well. (b) Similarly, in the case of $BA \rightarrow BB$, the voter A changes her/his state to B and the corresponding edges are changed as well.

As we can see, the differential equation for the average number of $[A]$ or $[B]$ equals 0, which means that the expected size of As or Bs is invariant. However, the differential equations for edges contain some triple motifs (ABA, ABB, BAB, etc.), resulting in an unclosed system. To address this problem, some moment-closure approximations are required as reviewed in Ref. (Demirel et al., 2014).

2.2.1.3 Majority Voter Model

Another interesting evolution mechanism for the voter model is based on the majority rule (Galam, 2002; Chen and Redner, 2005), where a group of connected voters (chains, cliques, circles, etc.) are selected at each step, and then all of them adopt the state of the majority in that group. This majority voter model is inspired by the social influence as illustrated in the following example (Figure 2.5).

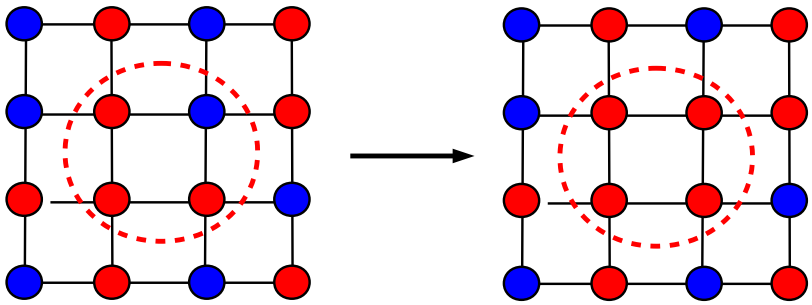

Figure 2.5: A schematic diagram to show the majority voter model. A group of selected nodes in the red circle are updated by adopting the majority state.

In particular, let's consider a well-mixed network with N voters, where the initial fraction of voters holding A is denoted by ϕ_0. At each step, for example, 3 voters are picked to update their states. The flipping to AAA occurs as: $AAB \to AAA$, $ABA \to AAA$, and $BAA \to AAA$. The flipping to BBB occurs as: $ABB \to BBB$, $BAB \to BBB$, and $BBA \to BBB$. We can obtain the evolution equation for the average number of voters holding A:

$$\begin{aligned} \frac{\mathrm{d}}{\mathrm{dt}}[A] &= p(AAB) + p(ABA) + p(BAA) \\ &\quad - p(ABB) - p(BAB) - p(BBA) \end{aligned} \tag{2.18}$$

where the probability to pick two As and one B is $p(AAB) = p(ABA) = p(BAA) = [A]^2[B]/N^3$, and the probability to pick one A and two Bs is $p(ABB) = p(BAB) = p(BBA) = [A][B]^2/N^3$. When $\mathrm{d}[\mathrm{A}]/\mathrm{dt} = 0$, we have $[A] = 0, N/2, N$ at stationary state. The consensus time is scaled as $\log N$ (Galam, 2002), which can be obtained through a recursion equation:

$$T_n = \frac{[A]^2[B]}{N^3}(T_{n+1} + \delta t) + \frac{[A][B]^2}{N^3}(T_{n-1} + \delta t) + (1 - \frac{[A]^2[B] + [A][B]^2}{N^3})(T_n + \delta t) \tag{2.19}$$

where T_n is the expected consensus time in the case of n voters holding A.

When it comes to a variety of realistic networks, the topology plays an important role, where the mean field theory can't work very well due to the heterogeneous neighbourhood configurations and big variance in degree distribution. For this reason, we need to consider various bigger motifs in the network, leading to a very complicated problem. Nonetheless, some studies (Liggett, 2013) modified the above model like that: a randomly selected voter would update its state by adopting the majority state in the neighbourhood, which can be seen as a combination of node-centric rule and majority rule.

2.2.1.4 Sznajd Model

In the Sznajd model (Sznajd-Weron and Sznajd, 2000; Sznajd-Weron, 2005), the dynamics follows " *United we Stand, Divided we Fall* ", where a voter will be convinced by more than one neighbours. Two rules are introduced for a given chain of four nodes.

- **Social validation**: two neighbouring voters sharing same state will convince the nearest neighbours to imitate their opinion: $XAAY \to AAAA$ or $XBBY \to BBBB$, where $X, Y \in \{A, B\}$.

- **Discord destruction**: two voters holding different opinions will cause the disagreement from other neighbours: $XABY \rightarrow BABA$ or $XBAY \rightarrow ABAB$, where $X, Y \in \{A, B\}$.

As shown in Figure 2.6, the evolution of voters' states follows the above rules, where a quadruplet chain is picked randomly to evolve at each step. Eventually, we have absorbing states of: (1) all As; (2) all Bs; (3) alternating As and Bs.

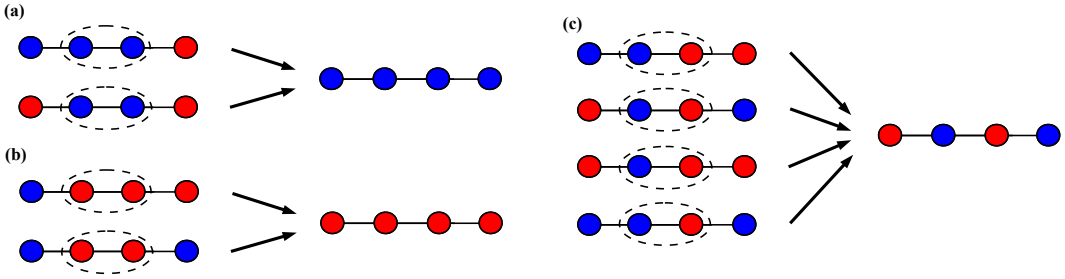

Figure 2.6: The Sznajd voter model. (a,b) Social validation occurs in the situation where the neighbours imitate the connected pair sharing same state. (c) Discord destruction arises when the selected nodes are holding different states, and then their neighbours will argue with them by adopting an opposite state.

Moreover, some alternative recipes have been explored through different update rules. For example, the alternating opinions led by discord destruction may change to a partially ordered form by a rule in Ref. (Sánchez, 2004). In this model, if two conflict nodes are connected by an edge, then they would turn to the other direction, and imitate the states of those neighbours. This model enables the voters to stand together with at least one neighbour. As a result, we can have the evolution of state as $XABY \rightarrow XXYY$ or $XBAY \rightarrow XXYY$, where $X, Y \in \{A, B\}$. At stationary state, the "ferromagnetic" configurations with all As or all Bs will be obtained.

2.2.1.5 Deffuant model

The family of bounded confidence models (Castellano et al., 2009) is usually adopted to characterize continuous states in opinion dynamics. Initially, the state of a voter is presented by a real number randomly picked from a certain range. After that, two neighbouring voters are selected to update their states through some compromise strategies if and only if the difference between their states is smaller than a tolerance ε. Finally, several clusters are formed, each of which contains the voters sharing same or

similar state. Here, we will focus on a typical bounded confidence model: the Deffuant model (Deffuant et al., 2000).

The Deffuant model defines $s_i(t)$ as the state of voter i at step t. At each step, a pair of voters i and j are selected to update their states. If $|s_i(t) - s_j(t)| \geq \varepsilon$, then nothing happens. Otherwise, if $|s_i(t) - s_j(t)| < \varepsilon$, the states are updated as:

$$\begin{aligned} s_i(t+1) &= s_i(t) + \mu[s_j(t) - s_i(t)] \\ s_j(t+1) &= s_j(t) + \mu[s_i(t) - s_j(t)] \end{aligned} \tag{2.20}$$

where $\mu \in [0, 0.5]$ is the compromise rate. And we have $s_i(t+1) + s_j(t+1) = s_i(t) + s_j(t)$, but the difference is shrinking $|s_i(t+1) - s_j(t+1)| \leq |s_i(t) - s_j(t)|$, which indicates the compromise after a debate.

The tolerance threshold ε affects the number of clusters at stationary state. Given a uniform initial distribution where the state values are ranging from 0 to 1, there will be more clusters formed at a smaller ε (Figure 2.7).

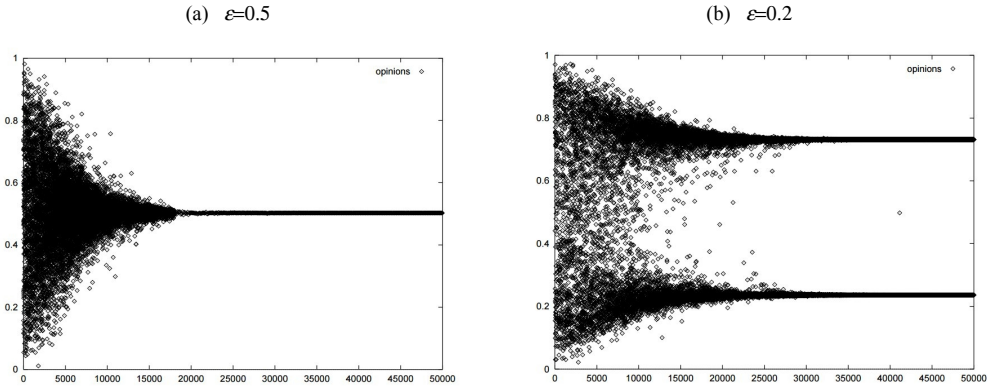

Figure 2.7: The evolution of Deffuant mode at $\varepsilon = 0.5$ and $\varepsilon = 0.2$. Figures are from Ref. (Deffuant et al., 2000).

For a given tolerance threshold ε, more clusters will be formed in a structured community than in a well-mixed case (Castellano et al., 2009).This phenomenon is caused by the structure restriction in space, where it is impossible for the distant voters to make a compromise. As a result, many clusters are formed, each of which contains the voters sharing similar states and are close in space.

2.2.1.6 Axelrod Model

As we can see, the above opinion dynamics considers a single variable as the state to evolve on a static network. When the state of a node is defined as a vector of variables,

the dynamics would be much more complicated. The Axelrod model (Axelrod, 1997) was proposed to study the dissemination of culture represented by a vector, where both assimilation and diversity are possible at stationary state. Cultural assimilation indicates the case where various culture traits converge to a single one; while cultural diversity means the co-existence of different types of culture. The vectorial state of culture in reality may involve language, art, science, etc.

In detail, we can describe the state of a node through a set of discrete values. For example, let's define the state by a set of features $\sigma = \{\sigma_1, \sigma_2, \cdots, \sigma_F\}$, each of which has q traits to choose, namely $\sigma_f \in \{t_1^f, t_2^f, \cdots t_q^f\}$. For any two connected nodes, let's say i and j, we have $\sigma(i)$ as the culture features for i and $\sigma(j)$ for j. The similarity between i and j can be computed by:

$$s_{ij} = \frac{1}{F} \sum_{f=1}^{F} \delta_{\sigma_f(i),\sigma_f(j)} \tag{2.21}$$

where δ indicates the Kronecker's delta function and $\delta_{x,y} = 1$ if $x = y$, otherwise $\delta_{x,y} = 0$. On the contrary, the difference between i and j can be obtained as $d_{ij} = 1 - s_{ij}$.

A large number of studies (Axelrod, 1997; Castellano et al., 2009) for the Axelrod model follows two principles (Castellano et al., 2000):

- similar agents are more likely to interact with each other;
- more interactions increase the similarity between the agents.

At each step, a pair of neighbouring agents i and j are selected uniformly at random. With probability s_{ij}, an interaction happens between them, and an inconsistent feature $\sigma_f(i) \neq \sigma_f(j)$ is set to be consistent $\sigma_f(i) = \sigma_f(j)$. The dynamics between two neighbours stops at one of the steady states: all features are same ($s_{ij} = 1$) or none of the feature is same ($s_{ij} = 0$). A network at steady state may contain one or several frozen regions, each of which consists of nodes holding completely same state, but any two adjacent regions don't share any same feature.

Figure 2.8 describes a 3×3 lattice, where the state of a node contains two features (namely $F = 2$) and each feature has two $q = 2$ traits to choose: (a) shows a frozen situation where all nodes have same state $(0,1)$ and (c) shows a frozen situation where all nodes have same state $(1,0)$. However, there are two frozen regions in (b): one is all $(0,1)$ and the other is all $(1,0)$, the edges between the two regions are connecting nodes without sharing any same feature.

Starting from a random distribution for the states in a finite size lattice with a size L^2, the above dynamical evolution will run until a frozen network is reached. Ref.

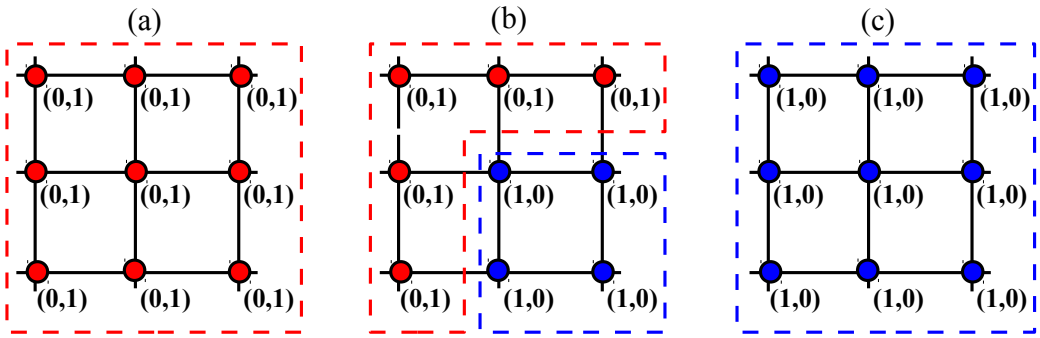

Figure 2.8: The frozen states in the Axelrod model. (a) All nodes are sharing same state $(0,1)$. (b) Two regions are separated by discordant edges . (c) All nodes are sharing same state $(1,0)$.

(Castellano et al., 2000) varied the parameters L, F and q to explore their influences on steady states, where it is found that a smaller q and F would be more likely to bring about large-size frozen regions and even global consensus.

2.2.2 Population Dynamics

In recent years, the evolutionary population (Hofbauer and Sigmund, 1998) is attracting more and more attention in the fields of biology, statistical physics and computer science, where population composition changes in a dynamical community. Specifically, the dynamics in an evolutionary population focuses on the changing frequencies of a certain type of individuals in a finite population. We can find this kind of dynamics through natural selection, mutation and genetic drift (Masel, 2011). In the following, some related models are introduced step by step to shed light upon the evolutionary population.

2.2.2.1 Wright-Fisher Model

The Wright-Fisher model (Fisher, 1930; Wright, 1931) describes a typical stochastic evolution in a group of individuals. In this model, the size of population is finite and constant as N, and each individual is considered as a diploid with two alleles selected from A and B. Therefore, any individual holds a state in a set $\{AA, AB, BA, BB\}$. In this model, there are not overlapping agents between the previous generation and the following generation, which means that all individuals have same and fixed lifespan. Each allele in a new-born individual inherits the genetic information from the previous generation uniformly and independently.

Let's define $[A]_t$ as the number of alleles of A at step t and $[B]_t$ as the number of alleles of B, and then we have $[A]_t + [B]_t = 2N$. The evolution of $[A]_t$ or $[B]_t$ in the Wright-Fisher model will converge to two absorbing states: $[A]_t = 0$ or $[A]_t = 2N$. Starting from an initial configuration with $[A]_0$ and $[B]_0$, the fixation probability for $[A]_t = 2N$ is $[A]_0/2N$. Specifically, given a previous state $[A]_t$, the following state $[A]_{t+1}$ follows a binomial distribution, where any allele in the next generation has a probability $[A]_t/2N$ to select A and a probability $[B]_t/2N$ to select B. In this way, the expected size $\mathbb{E}([A]_{t+1})$ at $t+1$ is equal to $[A]_t$.

Under this framework, some more complicated situations are explored further, such as varying population size, dynamical interacting structures, and biased selection. More details can be found in Refs. (Hudson, 2002; Charlesworth, 2009).

2.2.2.2 Moran Process

The Moran process (Moran, 1958; Moran et al., 1962) can be seen as a slower Wright-Fisher model, where overlapping generations are allowed. Instead of replacing all individuals in the previous generation, the Moran process adopts a single birth-death mechanism to update the composition of population, namely one new-born individual and one old-removal at each step. In this way, the number of certain type of individuals changes by $-1, 0, 1$ per step, which gives an easier mathematical calculation. But it requires more rounds to update the states of all individuals.

Let's consider a population of N individuals, and each individual has a state of either A or B. Under neutral drift, a random individual is selected to reproduce and then a random one is chosen to be removed at each step (see Figure 2.9), consequently the size of the population is constant. The new-born individual adopts the parent's state in the case when no mutation arises, but adopts the opposite state in the case when mutation arises. This model provides a generic framework for the evolutionary population by means of reproduction, selection and mutation (Nowak, 2006a).

In a well-mixed population, let $[A]_t$ and $[B]_t$ be the number of individuals of A and of B at step t. Here, we will discuss two typical cases, one is the mutation and the other is selection.

- Mutation case

  When the population is influenced by mutation, a parameter μ is defined as the probability that a new-born individual adopts the state different from that of her/his parent. Mutation is an effective route to promote the diversity of the

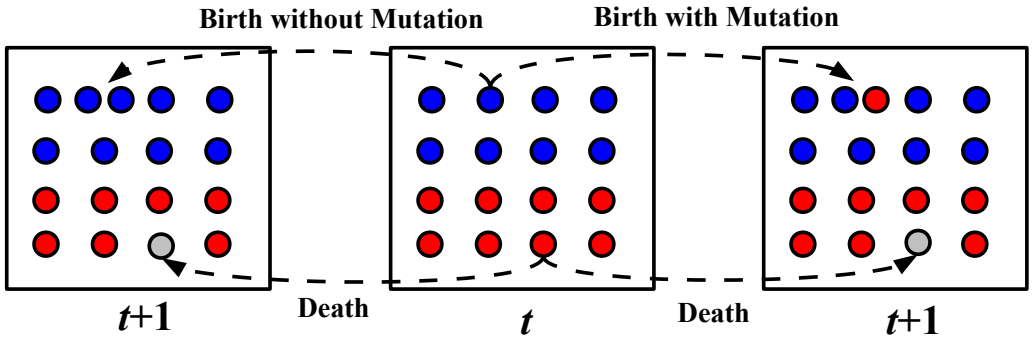

Figure 2.9: A schematic diagram is provided to show the evolution of Moran process in a well-mixed population. The middle box indicates the previous population at t, and one *blue* individual is chosen to reproduce and one *red* individual is chosen to be removed. In the case when no mutation arises (left box), the new-born individual adopts a state of *blue*, but in the case when mutation occurs (right box), a state of *red* is taken by the new-born individual.

population, but there are not frozen states in this case. In a well-mixed population, the transition probability $p_{i,j}$ from the case $[A]_t = i$ to $[A]_{t+1} = j$ can be written as:

$$\begin{aligned} p_{i,j} &= (1-\mu)(N-i)i/N^2 + \mu i^2/N^2 && \text{if} \quad 0 < i \leq N, j = i-1 \\ p_{i,j} &= 1 - 2(N-i)i/N^2 - \mu(N-2i)^2/N^2 && \text{if} \quad 0 \leq i \leq N, j = i \\ p_{i,j} &= (1-\mu)(N-i)i/N^2 + \mu(N-i)^2/N^2 && \text{if} \quad 0 \leq i < N, j = i+1 \end{aligned} \tag{2.22}$$

- Selection case

  When it comes to the situation of selection, we need to consider the fitness of individuals. As is known, an individual with higher fitness is more likely to be chosen to reproduce, but the death process is usually random. Let's suppose that the individuals holding A have same fitness f_A and then the total fitness of them is $F_t(A) = [A]_t f_A$; similarly for the individuals holding B, the total fitness is $F_t(B) = [B]_t f_B$. In a well-mixed population under the circumstance where no mutation arises, the probability that an individual of A is chosen to reproduce and an individual B is chosen to be removed at t is:

$$p_{[A]_t,[A]_t+1} = \frac{F_t(A)}{F_t(A)+F_t(B)} \frac{[B]_t}{N} = \frac{[A]_t f_A}{[A]_t f_A + [B]_t f_B} \frac{[B]_t}{N} \tag{2.23}$$

  On the contrary, the probability that the number of individuals of A decreases

can be computed by:

$$p_{[A]_t,[A]_t-1} = \frac{F_t(B)}{F_t(A)+F_t(B)}\frac{[A]_t}{N} = \frac{[B]_t f_B}{[A]_t f_A + [B]_t f_B}\frac{[A]_t}{N} \tag{2.24}$$

2.2.2.3 Evolutionary Game Theory

Evolutionary game theory (EGT) (Smith and Price, 1973; Weibull, 1997; Hofbauer and Sigmund, 1998) studies a mathematical framework combining game theory with evolutionary population characterized by the Darwinian process. The strategies of the previous generation can be inherited by their successors based on natural selection. The competing strategies are formulated by the principles of game theory, where the fitness of an individual is dependent on the interacting neighbours as well as the game settings. For example, A and B are the two strategies in the population, and then a payoff matrix is provided to determine the corresponding payoffs in the interactions.

$$\Pi = \begin{array}{c} \\ A \\ B \end{array} \begin{array}{c} \begin{array}{cc} A & B \end{array} \\ \begin{pmatrix} R & S \\ T & P \end{pmatrix} \end{array} \tag{2.25}$$

where the payoff obtained by a player can be calculated by $\pi_i = \sum_{j \in NB(i)} \Pi(s_i, s_j)$. In a well-mixed population, the players holding same strategy have same payoffs.

Depending on the relative order of the four coefficients in the payoff matrix, four main dilemmas (Macy and Flache, 2002) are widely investigated: Prisoner's Dilemma (PD) $T > R > P > S$, Stag-Hunt game (SH) $R > T > P > S$, Snowdrift Game (SG) $T > R > S > P$, and Coordinate Game (CG) $R \simeq P > S \simeq T$. In particular, the Prisoner's Dilemma (PD) illustrates that the optimal individual decision should be defection but the collective benefit reaches maximum in the regime of cooperation (Hofbauer and Sigmund, 1998). In most cases, it is hard for cooperators to survive due to the disadvantageous fitness under natural selection. However, Nowak *et al.* (Nowak, 2006b) pointed out that some specific mechanisms (such as indirect reciprocity, network adaptation, and group selection) can promote the cooperation effectively in an evolutionary population.

When adapting game theory into evolutionary populations, the dynamics focuses on the ability to survive among competing individuals. A successful strategy should be the one dominating the population (Vincent and Brown, 2005). In general, population dynamics can be described in a discrete way or a continuous way, where the fitter individuals are more likely to be selected to reproduce offsprings. Specifically, the

Moran process introduced above is a typical discrete form for evolutionary games. As for the continuous update mechanism, replicator equations (Schuster and Sigmund, 1983) are often adopted by people, where the evolution of individuals can be written as a differential equation:

$$\dot{\rho}_A = \rho_A[f_A - (\rho_A f_A + \rho_B f_B)] \tag{2.26}$$

where $\rho_A = [A]/N$ is the density of As and f_A is the corresponding fitness of A. The evolutionary stable state (ESS) is reached when the strategies in the population are maintained around some stationary values.

A generic framework for the evolutionary game model can be shown as Figure 2.10, where the fitness is characterized by a series of game rules and the population is updated through the replicator dynamics.

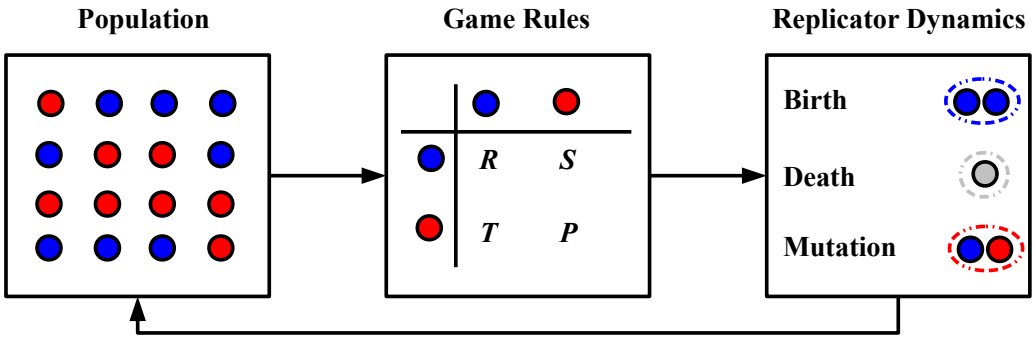

Figure 2.10: We have a schematic diagram for the evolutionary game model. The population works under the rules of game, and different payoffs are obtained by these individuals through payoff matrix. Based on the resulting fitness, the population will be updated following the replicator dynamics. After a series of birth, death and mutation, we obtain a new generation of population, who will continue the above process until a stationary state is reached.

2.2.2.4 Evolutionary Population on Networks

When the population is located on a network, where the individuals only meet and interact with their neighbours, we should take the underlying network structure into consideration. In 1992, Nowak *et al.* (Nowak and May, 1992) demonstrated some evolutionary games in a grid, where a co-existence of cooperators and defectors can be obtained at stationary state. From then on, a large number of investigations have been

launched to reveal the evolutionary dynamics on networks (see more details in Refs. (Nowak, 2012; Allen et al., 2013; Shakarian et al., 2012)).

For the evolutionary population on a static network, the payoff π_i of an individual i is dependent on the neighbourhood configuration and interaction matrix Π. Usually, the fitness of an individual is a function of her/his payoff, for example $f_i = (1+\delta)^{\pi_i}$, where δ means the strength of selection. When $\delta \to 0$, it is under weak selection and all individuals are selected uniformly to reproduce; when δ goes to a big value, an individual with a higher payoff is more likely to be selected to reproduce.

The evolutionary population on static networks can be characterized by three types of update rules (Jiang et al., 2013; Ohtsuki et al., 2006; Nowak et al., 2010), which are death-birth rule, birth-death rule and imitation rule. In the case of death-birth, a random individual is removed from the graph with an empty site left, subsequently the neighbours compete for that empty site with probability proportional to the fitness. The birth-death rule is implemented as follows: an individual is chosen for reproduction with probability proportional to her/his fitness, and the state of a random neighbour will be replaced by the strategy of the chosen player. Under the rule based on imitation, a pair of adjacent individuals will compete with each other. One can either remain the current strategy with probability proportional to her/his fitness or adopt the strategy of the neighbour with the complementary probability.

Specifically, we provide some examples on top of a static network to show the evolution of population according to the above three rules respectively (Figure 2.11).

For a simplifier case of PD, we can have the interaction payoff matrix as:

$$\Pi = \begin{array}{c} \\ C \\ D \end{array} \begin{array}{c} \begin{array}{cc} C & D \end{array} \\ \begin{pmatrix} R & S \\ T & P \end{pmatrix} \end{array} = \begin{array}{c} \\ C \\ D \end{array} \begin{array}{c} \begin{array}{cc} C & D \end{array} \\ \begin{pmatrix} b-c & -c \\ b & 0 \end{pmatrix} \end{array} \tag{2.27}$$

where C means the strategy of cooperation and D means the strategy of defection. In addition, b is the benefit obtained from the altruistic behaviour with a cost of c. A defector pays no cost for a complete benefit. Interestingly, Ohtsuki *et al.* (Ohtsuki et al., 2006) proposed a simple rule for the evolution of cooperation. Through numerical simulations in a variety of static structures (including rings, lattices, random graphs, and scale-free networks), they found that the fixation probability of cooperation will be higher when $b/c > \langle k \rangle$, where $\langle k \rangle$ is the average degree. This rule indicates the influence of some underlying network properties on the evolution of cooperation.

Using the form of interaction matrix 2.27, Tarnita *et al.* (Tarnita et al., 2009) proposed a generic structural coefficient σ to show the strategy of C would be dominant

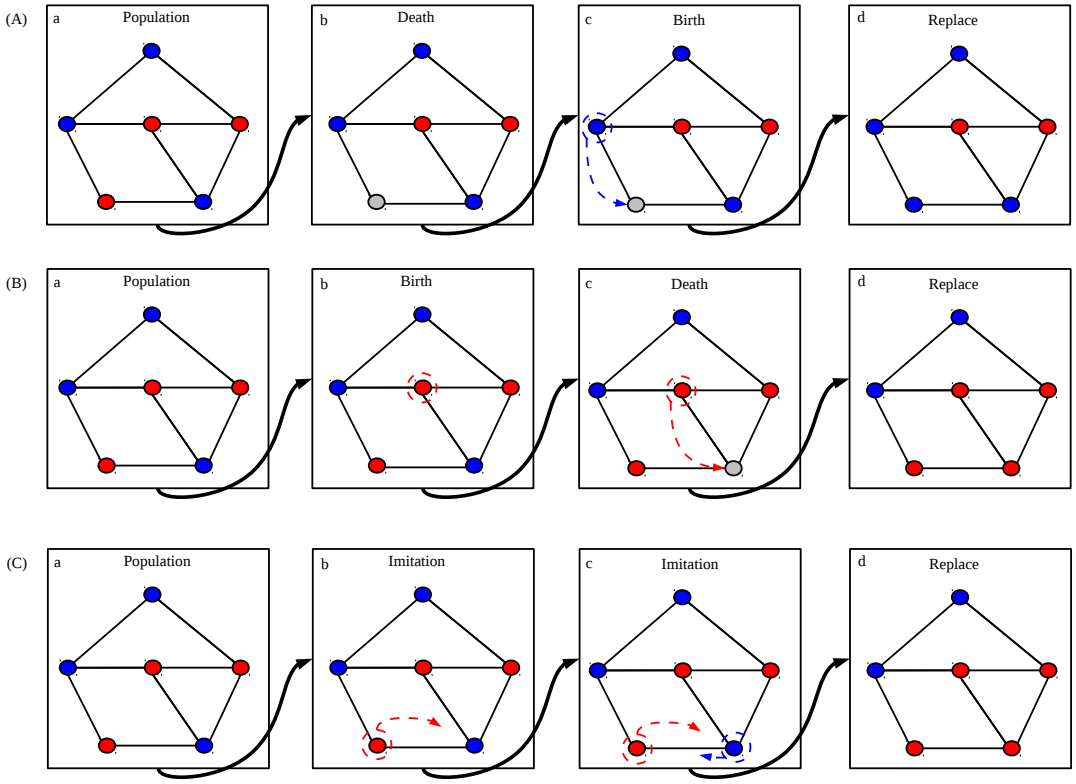

Figure 2.11: A schematic diagram is presented to illustrate the evolutionary dynamics. We have 6 nodes in the population, interacting on a static graph. The individual has a chance to reproduce proportional to the corresponding fitness, which is computed through the payoff matrix and neighbourhood configuration. Figure (A) illustrates the rule of death-birth, (B) explains the rule of birth-death and (C) shows the rule of pairwise imitation.

under weak selection when:

$$\sigma R + S > T + \sigma P \tag{2.28}$$

Furthermore, they also pointed out that $\sigma = \langle [D][CC] \rangle / \langle [D][CD] \rangle$ can be computed through a long-term numerical simulation, where that structural coefficient is highly dependent on the structure of population. In Chapter 4, we will explore the indicator based on σ in the detection of cooperation collapse.

2.3 Coupled dynamics

The above two sections illustrate the dynamical processes running much slower and much faster than the dynamical structures respectively. Recently, more and more peo-

ple pay attention to the coupled dynamics in adaptive networks (Gross and Sayama, 2009; Holme and Newman, 2006; Sayed, 2014; Kozma and Barrat, 2008), where both the structure of network and the states of agents can change at comparable time scales. As is known, the dynamics on networks focuses on the changes of individuals' states; however, the dynamics of networks relates to the topological changes through some hard actions, such as rewiring, deleting, and adding. In real world, the coupled dynamics are usually interdependent on each other, displaying a plethora of amazing phenomena (Holme and Newman, 2006; Zimmermann et al., 2004; Durrett et al., 2012). In this section, we will give a brief overview of the coupled dynamics in the fields of adaptive voter model, games in adaptive networks and adaptive agents coordination.

2.3.1 Adaptive Voter Model

Let's first start from a brief introduction for the opinion dynamics in adaptive networks. The voter models reviewed before mainly consider the situation that the underlying network is static and only the states of nodes change over time. However, in the adaptive voter model (Holme and Newman, 2006), both the states of individuals and the structure of network are allowed to change, in which case the opinion dynamics is ranging from consensus to diversity. This family of models couples the dynamics on networks with the dynamics of networks tightly in a very natural manner. On the one hand, an agent would like to imitate the states of neighbours or be influenced by social pressure, where network topology affects the evolution of state profoundly. On the other hand, the agent may get away from discordant neighbours and form new connections with some others, where the states of agents have a big influence on the adaptation of structure. Driven by the adaptive dynamics, some mathematical and numerical approaches have been applied into this field to reveal the critical transitions, stationary states and some other statistical properties.

In the following, we will review some classic adaptive voter models from the perspectives of node-centric rules and link-centric rules, to understand the entangled relationship between state evolution and structure adaptation. In particular, rewire-to-random and rewire-to-same are two major adaptation approaches for active links. Furthermore, some approximation techniques are provided for analytical calculations based on differential equations.

2.3.1.1 Node-centric Models

The adaptive voter models based on node-centric rules are usually implemented by picking a node at each step to change its state or adjust the neighbourhood. Originally, this family of models originates from Ref. (Holme and Newman, 2006), where Holme and Newman studied the phase transition from consensus to pluralism controlled by a single rewiring parameter, let's say α.

In general, the model runs on a network with fixed number of nodes (N) and edges (E). There are m possible opinions with a uniform distribution over the network in the beginning. Let's denote the state of an individual i by s_i, which is one of the m possible opinions. The adaptive voter model will be implemented as follows (Figure 2.12) at each step until a frozen network is reached.

(1) a random voter i is selected.

(2) with probability α, i disconnects from a random neighbour j and connects to a random node k who holds same opinion with i.

(3) with probability $1-\alpha$, i sets its state equal to the state of a random neighbour j, namely $s_i = s_j$.

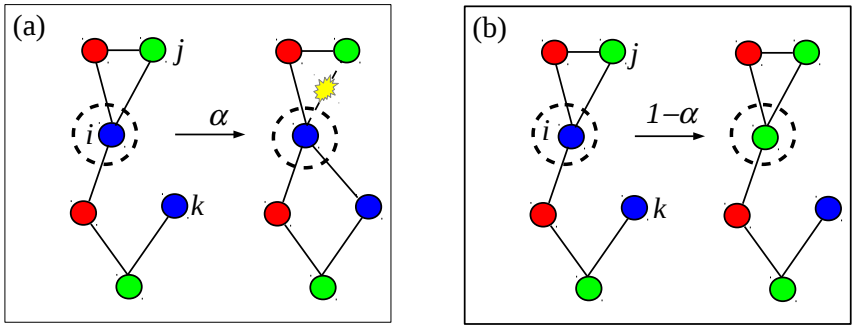

Figure 2.12: An illustration of the adaptive voter model of (Holme and Newman, 2006), where different colors mean different opinions. Figure (a) shows the adaptation of structure with probability α and (b) illustrates the evolution of state with $1-\alpha$.

It is the rewiring strength α that controls the competition between network consensus and opinion diversity at stationary state. When α is bigger, the rewiring event occurs frequently, and most of the opinions are conserved. However, when α is smaller, the size of monochrome component sharing same state is bigger, but the number of conserved opinions is smaller. When $\alpha \to 0$ the size of monochrome component is

close to N. More interestingly, a rich landscape is obtained by varying α. Let's use $P(s)$ to describe the fraction of monochrome components with a size s at stationary state, and we have the following numerical results at $\alpha = 0.04$, $\alpha = 0.458$ and $\alpha = 0.96$ in Figure 2.13 (Holme and Newman, 2006).

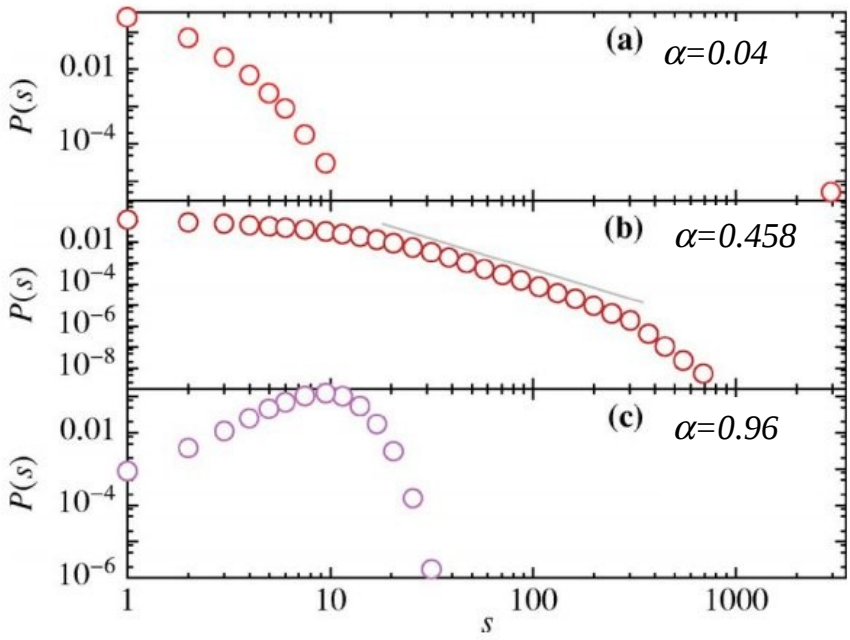

Figure 2.13: The distribution of the sizes of monochrome components at stationary state. The number of nodes is $N = 3200$, and the number of edges is $E = 6400$. In the beginning, $m = 320$ opinions are assigned to the network uniformly at random. A qualitative transition from a giant component to numerous fragmented components is observed with the increase of α. Figure is adapted from Ref. (Holme and Newman, 2006) and the values are binned logarithmic.

As we can see, the adaptive dynamics induced by a single parameter can lead to a transition from a giant monochrome component to a broad view of opinions. This phenomenon has attracted more and more attention in the fields of statistical physics, computer science and social networks. In order to gain a deeper insight into the transition from consensus to fragmentation, Vazquez *et al.* (Vazquez et al., 2008; Vazquez, 2013) studied a binary voter model, where two opinions are in the adaptive network. In their model, a node i is selected arbitrarily at each step and then a random neighbour j: (1) if $s_i = s_j$, then nothing happens; (2) if $s_i \neq s_j$, then i redirects the link from j to k such that $s_k = s_i$ with probability α, or i adopts j's state with probability $1 - \alpha$. Vazquez *et al.* (Vazquez et al., 2008) focused on the density of the active links

(connecting two nodes with different states) through a differential equation:

$$\begin{aligned}\frac{d\rho}{dt} &= \sum_k \frac{p(k)}{1/N} \sum_{n=0}^{k} B_{n,k} \frac{n}{k} \left[(1-\alpha)\frac{2(k-2n)}{\langle k\rangle N} - \frac{2\alpha}{\langle k\rangle N}\right] \\ &= \sum_k \frac{2p(k)}{\langle k\rangle k} \left[(1-\alpha)(k\langle n\rangle_k - 2\langle n^2\rangle_k) - \alpha\langle n\rangle_k\right] \end{aligned} \tag{2.29}$$

where $p(k)$ is the probability that a node has degree k, $\langle k\rangle$ means the average degree, and $B_{n,k}$ is the probability that a node with degree k has n active links, which is assumed to be a binomial distribution. In particular, a critical α_c can be obtained to predict the critical transition from an active phase (corresponding to a connected network) to a frozen phase (corresponding to a fragmented network) (Vazquez et al., 2008). Some numerical results are obtained in Ref. (Vazquez et al., 2008), where the average size of largest component dropped sharply around the critical point. Notably, this numerical value is far from the analytical one obtained through the approximate differential equation, which is due to the correlations among the links.

2.3.1.2 Link-centric Models

This part will review another common situation, where an edge instead of a node is selected at each step to do state evolution and structure adaptation.

Durrett *et al.* (Durrett et al., 2012) explored the graph fission in an adaptive voter model by dealing with the discordant links. As before, each agent holds one of the two opinions A and B, and the initial fraction of As is ϕ_0. Two rewiring strategies are studied: rewire-to-same and rewire-to-random, where rewire-to-same means to make a connection with an agent holding same opinion and rewire-to-random means to connect a random agent in the network. The adaptive process at each step is implemented as follows.

(1) a random active edge connecting i and j is selected, where $s_i \neq s_j$;

(2) a node randomly selected from i and j adopts the state of the other with probability $1-\alpha$;

(3) otherwise with probability α, that selected node rewires to a new neighbour based on rewire-to-same or rewire-to-random.

where α is the rewiring strength. With the increase of α, the system transforms from network consensus (most of the nodes are sharing same state) to network fragmentation

(disconnected monochrome communities are formed). Especially, when $\alpha = 0$, the system only does the flipping, and global consensus is obtained in the end. When $\alpha = 1$, the system only does the rewiring, and both opinions remain same as their initial fractions but the network is fragmented. The average fraction of the final minority (namely $\min\{[A],[B]\}/N$ at frozen state) is presented in Figure 2.14.

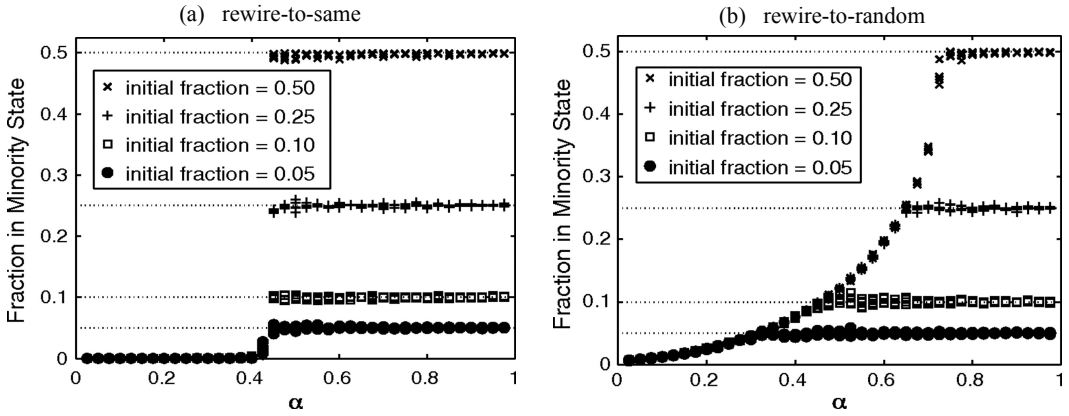

Figure 2.14: The fraction of the minority opinion at stationary state. Figure (a) illustrates the situation based on rewire-to-same, where a critical transition from consensus to fragmentation occurs at $\alpha_c \approx 0.43$ for varying ϕ_0s. When $\alpha \leq \alpha_c$, the final fraction of the minority is close to 0. When $\alpha > \alpha_c$, the final fraction of the minority is same as the initial fraction of the minority. Figure (b), however, presents a quite different result based on rewire-to-random, where the critical rewiring value is dependent on the initial fraction of the minority. Figures are from Ref. (Durrett et al., 2012).

In addition, Ref. (Durrett et al., 2012) also developed some approximation calculations (pair approximation and approximate master equations) to capture the adaptive dynamics, which will be introduced in detail in Chapter 3.

Another interesting work is the adaptive voter model on directed networks (Zschaler et al., 2012), where the agents have a fixed out-degree distribution, and the rewiring would change the in-degree distribution. The adaptive voter model on directed networks is implemented as follows at each step:

(1) a random edge $i \to j$ is selected;

(2) if $s_i = s_j$, then nothing happens;

(3) if $s_i \neq s_j$, with probability α, i rewires the edge $i \to j$ to a random agent k sharing the same state with i;

(4) otherwise with probability $1-\alpha$, i adopts the state of the j, so that $s_i = s_j$.

To shed light upon the influence of directed networks on the adaptive dynamics, Zschaler *et al.* compared the results from numerical simulations with the analytical approximations (see details in Ref. (Zschaler et al., 2012)). Interestingly, if the network presents a scale-free out-degree distribution, then the numerical critical point is far below the estimated one. In addition, they also focused on the formation of self-stabilizing network structure, which contains numerous smaller absorbing clusters with few out-going edges.

2.3.1.3 Other Variants

As we can see, network consensus comes from the basic fact that the edges connecting nodes with same state keep unchanged. We can find many situations by *homophily* attachment, namely the agents are more likely to redirect links to those holding same state. In reality, *heterophily* attachment is also important in many situations, for example the establishment of weak ties used for the communication between distinct communities. To understand the adaptive dynamics driven by different rewiring strategies, Kimura (Kimura and Hayakawa, 2008) proposed an adaptive voter model allowing the rewiring to different-opinion agents as well as same-opinion ones. This model in an adaptive network is implemented as follows:

(1) a random voter i is selected and then a random neighbour j.

(2) with probability ϕ, i disconnects from j and rewires to k who holds the same opinion as i.

(3) with probability ψ, i disconnects from j and rewires to l who holds a different opinion from i.

(4) with probability $1-\phi-\psi$, i adopts the state of j, namely $s_i = s_j$.

When $\psi = 0$, the above dynamical process is equivalent to the model in Ref. (Holme and Newman, 2006), where the communities reach consensus at stationary state. To investigate the case when $\psi > 0$, Ref.(Kimura and Hayakawa, 2008) carried out the dynamical process interplayed by homophily attachment and heterophily attachment. What should be noted is that even with a very small ψ, the heterophily rewiring can bring a quite different result from the discovery in Ref. (Holme and Newman, 2006). A small-world property (namely a bigger average clustering coefficient

and a smaller average path length) can be obtained for a certain range of ϕ and ψ, where the connected communities results from homophily attachment and the bridges among communities are created by heterophily attachment.

In most cases, the dynamics of state is influenced by the configuration of neighbourhood. For this reason, some researches (Benczik et al., 2008, 2009; Fu and Wang, 2008) allow the agent to adopt the majority state in its neighbourhood. Besides the network consensus, a mixture configuration is also possible at steady state, where the active links connecting different states may be conserved. In particular, Feng *et al.* (Fu and Wang, 2008) studied the adaptive dynamics through a majority-preference and minority-avoidance approach. This model presents a rich landscape from opinions diversity to global consensus by varying the rewiring parameters (more details in Ref. (Fu and Wang, 2008)). Interestingly, a critical transition from a broad variety of opinions coexistence to single opinion dominance arises around a critical value, which is quite similar to the results obtained in Refs. (Holme and Newman, 2006; Vazquez et al., 2008).

Recently, a large variety of models (Sood et al., 2008; Rogers and Gross, 2013; Xie et al., 2011) have been highlighted to reveal the entangled dynamics in adaptive voter models. Generally speaking, the main point lies in the following two aspects: (1) the influence of local behaviours on global properties; (2) how to build approximate calculations to estimate the equilibrium.

2.3.1.4 Approximation Techniques

In order to characterize the dynamical system analytically, a large number of moment-closure approximations are applied into the differential equations (Demirel et al., 2014). Here we will introduce three of the most popular methods.

- Mean field approximation (MFA) (Gleeson et al., 2012; Gleeson, 2011, 2013) is usually derived under the following assumptions: absence of local clustering, absence of modularity and absence of dynamical correlations (Gleeson et al., 2012). The main idea of this approximation is to let the nodes with same state to be equivalent, which are grouped into the same observational variable. This approximation can match the simulation results very well if the system is well-mixed and the correlations among the neighbourhood are negligible. However, the above assumptions clearly violate the characteristics of many real-world networks. As shown in Ref. (Gleeson et al., 2012), the performance of mean field

approximation is highly dependent on the degree distribution as well as the link correlation in the network.

- Pair approximation (PA) (Durrett et al., 2012; Gleeson, 2011, 2013) focuses on some more complicated motifs including various edges, triplets and chains. This analytical method deals with the bigger observables based on smaller ones. In order to make the differential system closed, pair approximation adapts the Bayes' theorem into graphs by estimating the bigger motifs through some existing smaller ones. For example, the number of triplet ABA can be calculated by: $[ABA] = [AB] \times [AB]/[B]$. However, this method ignores the distribution of some certain motifs, which may be only located in specific regions. In particular, the motifs in the intersection part may be easily overestimated.

- Approximate master equation (AME) (Durrett et al., 2012; Gleeson, 2011, 2013) considers the states of nodes and their neighbours by building a large number of master equations for the star-like motifs. This method puts the nodes with same state as well as same neighbourhood configuration into the same group, where the information regarding local structure can be captured correctly by the observational variables. For example, $[A_{m,n}]$ means the number of agents holding A with m neighbours of A and n neighbours of B. The system of AMEs can capture the dynamics better by considering a large number of "stars", but it is at the expense of higher computation cost. Fortunately, the maximal degree of a node $k_{\max}$ is a relatively small number compared with the size of network N, thus the number of equations is not that large.

To conclude, the above approximation techniques can do analytical calculations for adaptive networks in some simple cases, but it may fail to capture the dynamical process on many complex realistic networks (Gleeson et al., 2012), which are large-scale and highly correlated. Therefore, more work needs to be done for the development of effective and accurate approximation techniques (see more details in Chapter 3).

2.3.2 Games in Adaptive Networks

When individuals are interacting in a structured community, each of them may have a specific property (such as weight, payoff, fitness) to show its influence on others. In this section, we intend to explore the coupled dynamics of individuals, who play games with each other in adaptive networks.

In particular, when the individuals are playing the game of Prisoner's Dilemma (PD), cooperation (C) and defection (D) are two strategies held by them. The payoff matrix Π 2.27 in the PD has a sequential relation $T > R > P > S$, which leads the players to opt for defection as $T > R$ and $P > S$. Consequently, the dominance of defection is present as the Nash equilibrium at stationary state. However, it is the dominance of cooperation that gives the optimal collective outcome (Figure 2.15). Therefore, how to promote the cooperation in a population of self-interested individuals is a very interesting topic.

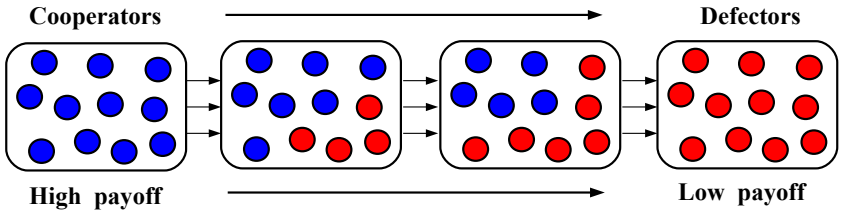

Figure 2.15: The trade-off between optimal individual choice and optimal group choice in the PD. Starting from a well-mixed community, the population will evolve from all cooperators to all defectors under natural selection.

Recently, many researches have been launched to explore the evolution of cooperation in dynamical communities (Pacheco et al., 2006b). Combining state evolution with structure adaptation, a large number of efforts have been made to promote the cooperation by changing network structures. With adjustable topologies, the adaptation based on preference enables the individuals to break up those "bad" links (connecting to defectors) and redirect to some "good" ones (namely cooperators) (Zimmermann and Eguíluz, 2005), leading to the formation of cooperative components. Wu *et al.* (Wu et al., 2010) modelled the evolution of cooperation in adaptive networks using differential equations, and they pointed out that the fragile *CD* links and robust *CC* links would increase the chances of cooperation. Santos *et al.* (Santos et al., 2012) investigated numerous factors (such as rewiring strength (Santos et al., 2006), pre-play signals (Santos et al., 2011) and selection pressure (Van Segbroeck et al., 2011)) that could promote the cooperation by increasing the diversity of population. Fu *et al.* (Fu et al., 2008) proposed a reputation-based adaptation strategy to enhance the cooperation, where agents will reorganise the local structure by disconnecting lower-reputation neighbours and connecting to higher-reputation ones. In addition, Poncela *et al.* (Poncela et al., 2009) conducted a model of evolutionary games in a growing structured

population, where they obtained a higher level of cooperation when increasing the size of network. Szolnoki *et al.* (Szolnoki and Perc, 2008; Szolnoki et al., 2008) proposed a teaching mechanism that allows the successful agents (whose states are imitated by others) to make new connections, which is effective in promoting the cooperative behaviour.

In the following, we will review some game models in adaptive networks from the perspectives of pairwise imitation and natural selection. In the case of pairwise imitation, the states and structures are updated locally through direct neighbourhood interactions, which is extended from the voter model with biased imitation and rewiring. However, the case of natural selection is implemented under the Darwinian mechanism (for example the Moran process), where the reproduction of an individual occurs with probability proportional to the corresponding fitness.

2.3.2.1 Pairwise Imitation

Given an interacting population under the PD, it is assumed that the players are designated as either C or D with equal probability in the beginning. The tendency to imitate a state is quantified by the payoffs π_i and π_j of two adjacent nodes i and j. As before, the payoff of a player i is calculated as $\pi_i = \sum_{j \in NB(i)} \Pi(s_i, s_j)$, where Π is the payoff matrix and $s_i \in \{C, D\}$ is the state of i. Some deterministic and stochastic approaches to implement state evolution have been explored in Ref. (Hofmann et al., 2011), such as imitate-best-neighbour, imitate-best-strategy, win-stay-lose-shift and imitate-random-neighbour.

Here, we focus on pairwise imitation by computing the imitation probability through the corresponding payoffs. Let $p(s_i \to s_j)$ be the probability that a player i imitates the strategy of j, and then we can compute this imitation probability based on the Fermi function (Traulsen et al., 2006):

$$p(s_i \to s_j) = \frac{1}{1 + e^{-\beta(\pi_j - \pi_i)}} \tag{2.30}$$

where $\beta > 0$ represents the selection strength. A smaller β means weaker selection, indicating a stochastic imitation; while a larger β enforces the agent to select the strategy with a higher payoff.

As for the adaptation of structure, a large number of papers have been reviewed in Ref. (Perc and Szolnoki, 2010), where the spatial interactions, population growth, teaching activity, mobility and ageing agents are the main factors affecting the evolution of cooperation. In general, structure adaptation mainly focuses on how to deal

with those links between the players. As we all know, the links of *DD* are usually unstable, because defectors intend to rewire from other defectors to some cooperators. The links of *CD* are more likely to be broken by cooperators while they will be preserved by defectors, thus they are unstable as well. However, the cooperative links of *CC* yield mutual benefit to each other, which are quite stable between cooperators.

This family of models is similar to the adaptive voter model in mathematics and simulations, and we can approximate them in same way. Notably, both the flipping and flapping are biased by payoffs in the situation of games, which involves many interesting stories in real life. For example, an individual with a higher payoff may convince other people to follow her/his state easily, though the flipping of state may be detrimental to herself/himself. In the following, we will present some relevant models based on pairwise imitation to illustrate the influences of various structure adaptation strategies on the level of cooperation.

Neighbourhood reorganisation to get away from the defective neighbours (Zimmermann et al., 2004; Zimmermann and Eguíluz, 2005) has been proven to be an effective way to promote the cooperation in a structured population. One of the generic models was investigated in Refs. (Santos et al., 2006; Pacheco et al., 2007), which combines pairwise imitation with neighbourhood reorganisation naturally. In that model, the sizes of nodes and edges are constant, and initially a player is assigned to be a cooperator or a defector with equal probability. The dynamics of state evolution is implemented by pairwise imitation based on the Fermi function, while a link will be rewired if at least one player is dissatisfied with that connection.

In detail, the event of state evolution occurs at each τ_e, when a random pair of connecting nodes i and j are selected. According to Eq. 2.30, the node i imitates the state of j with probability $p(s_i \to s_j)$, otherwise the node j imitates the state of i with probability $p(s_j \to s_i)$.

The event of structure adaptation occurs at each τ_a, when a random edge connecting i and j is selected to do neighbourhood reorganisation as follows:

- if $s_i = C$ and $s_j = C$, then nothing happens.
- if $s_i = C$ and $s_j = D$, then i rewires from j to a random node with probability $p_i = 1/(1+e^{-\beta(\pi_i-\pi_j)})$, otherwise with probability $p_j = 1-p_i$, i keeps the connection with j.
- if $s_i = D$ and $s_j = C$, then i stays together with j with probability $p_i = 1/(1+e^{-\beta(\pi_i-\pi_j)})$, otherwise with probability $p_j = 1-p_i$, j rewires from i to a random

node.

- if $s_i = D$ and $s_j = D$, then i rewires from j to a random node with probability $p_i = 1/(1+e^{-\beta(\pi_i-\pi_j)})$, otherwise with probability $p_j = 1-p_i$, j rewires from i to a random node.

As we can see, the time scale ratio $W = \tau_e/\tau_a$ measures the relative speed between state evolution and structure adaptation, where a larger W means a prompt reaction to adverse ties and a smaller W indicates a slowly changing network. Interestingly, with the increase of W, the cooperation is enhanced due to the formation of cooperative clusters (Figure 2.16).

Another important contribution is the active linking model (Pacheco et al., 2006a,b; Van Segbroeck et al., 2009), which assigns different rates for the formation or disconnection of different links. The dynamics of state evolution is implemented as before, which adopts pairwise imitation (based on Fermi function, see Eq. 2.30) to quantify the imitation probability. However, the links are formed and disconnected continuously according to the corresponding rates. The propensity to form a link for the player C is defined as α_C, similarly for the player D we have α_D. A new edge is formed between two unconnected players at a rate of $\alpha_X\alpha_Y$, and a connected link XY is removed at a rate of γ_{XY}, where $X,Y \in \{C,D\}$. The links evolve based on an ordinary differential equation as follows (Pacheco et al., 2006b):

$$\frac{\mathrm{d}}{\mathrm{dt}}[XY] = \alpha_X\alpha_Y(M_{XY} - [XY]) - \gamma_{XY}[XY] \tag{2.31}$$

where M_{XY} is the maximum possible number of XY links. This differential equation has an equilibrium solution for the links as $[XY]^\star = M_{XY}\alpha_X\alpha_Y/(\alpha_X\alpha_Y+\gamma_{XY}) = M_{XY}\phi_{XY}$, where we define $\phi_{XY} = \alpha_X\alpha_Y/(\alpha_X\alpha_Y+\gamma_{XY})$.

Of course, state evolution and structure adaptation are also coupled by the time scale ratio $W = \tau_e/\tau_a$. When $W \to +\infty$, the adaptation of structure runs much faster than the evolution of state, and the average payoff of a certain type of player at stationary state can be calculated as (Pacheco et al., 2006b):

$$\begin{aligned}
\pi_C &= \frac{\Pi(C,C)[CC]^\star}{[C]} + \frac{\Pi(C,D)[CD]^\star}{[C]} \\
&= R\phi_{CC}([C]-1) + S\phi_{CD}[D] \\
\pi_D &= \frac{\Pi(D,D)[DD]^\star}{[D]} + \frac{\Pi(D,C)[DC]^\star}{[D]} \\
&= T\phi_{DC}[C] + P\phi_{DD}([D]-1)
\end{aligned} \tag{2.32}$$

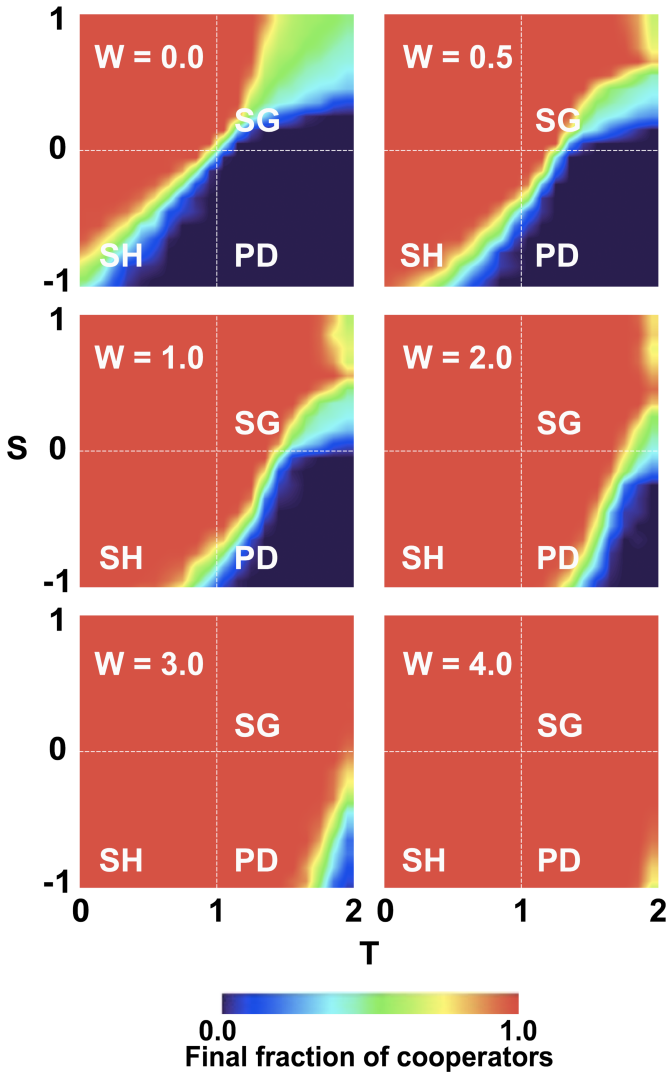

Figure 2.16: For a given payoff matrix Π, we have $R = 1$ and $P = 0$, but vary $S \in [-1, 1]$ and $T \in [0, 2]$. The average fraction of cooperators at stationary state is obtained at different Ws . For a lower value of W, the neighbourhood structure is modified slowly and the defectors prevail because of the higher temptation to defect. When the value of W is bigger, the adverse ties are removed promptly, and a heterogeneous structure is formed to promote the cooperation. Figures are from Ref. (Santos et al., 2006).

Besides the above work, a large number of researches (Wu et al., 2010; Santos et al., 2012; Van Segbroeck et al., 2008) have been launched to explore the success of cooperators in adaptive networks, where the cooperation is enhanced by rewiring from adverse ties and forging cooperative clusters. In particular, some heuristic strategies, such as tit-for tat behaviour (Szolnoki et al., 2014), state-changing penalty (Jin et al., 2012), reputation-based parter choice (Fu et al., 2008), imitating older friends (Yang et al., 2014) and prompt neighbourhood reaction (Yang et al., 2015), have been

proposed from different perspectives to enhance the cooperation.

2.3.2.2 Natural Selection

This part will introduce evolutionary models on networks derived from the basic Moran process, where natural selection determines the composition of population and fitter individuals are more likely to reproduce. We provide two typical models as below to illustrate the dynamics of an evolutionary population in evolving networks, one is multilevel selection model (Traulsen and Nowak, 2006) and the other is social inheritance model (Cavaliere et al., 2012).

Multilevel selection (also known as group selection) divides the population into several groups, each of which consists of well-mixed players. As before, the individuals play the Prisoner's Dilemma (PD) in the group, and gain the payoff according to the payoff matrix Π and population composition in the corresponding group. Notably, each individual interacts with all other members in the same group, but is separated from other groups. The individuals may reproduce and spread, where the new-born players will be added to the same group together with their parents.

Traulsen *et al.* (Traulsen and Nowak, 2006; Traulsen et al., 2008) considered an evolutionary population based on multilevel selection as follows. At each step,

(1) an individual i is selected to reproduce with probability proportional to her/his fitness f_i, which is a function of the corresponding payoff and selection strength;

(2) a new-born offspring is added to the same group as i;

(3) if the group size is bigger than n, then

  (3-1) with probability q, that group is divided into two daughter groups uniformly, and then a group randomly picked from the population will be removed;

  (3-2) otherwise with probability $1-q$, the group doesn't divide but one random member in that group is removed.

As we can see, the total number of groups is fixed as m, and each group has a maximal size n. Therefore, the size of population is $m \leq N \leq mn$. The coupled dynamics can be demonstrated as Figure 2.17. It is clear that the defectors (red nodes) are favoured in the well-mixed group under lower-level selection, but the defective groups

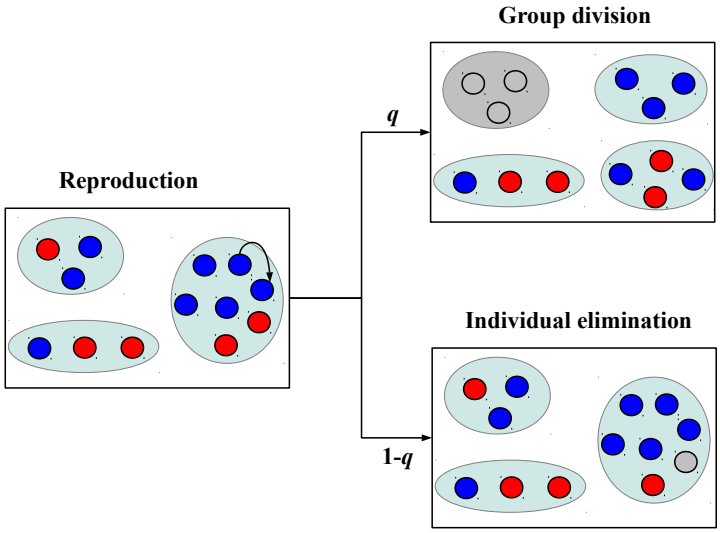

Figure 2.17: The evolution of population based on group selection is demonstrated by a schematic diagram. There are two levels of selection: one is the lower-level competition among the individuals, where a defective individual with higher fitness is more likely to reproduce; the other is the higher-level competition among the groups, where a group full of cooperative individuals splits more frequently.

are opposed by higher-level selection, where the groups full of cooperators are more competitive (Traulsen and Nowak, 2006; Traulsen et al., 2008).

Let the payoff matrix be: $R = b - c$, $S = -c$, $T = b$ and $P = 0$. When $q = 0$, this model is a disjoint sum of Moran processes. When $q \to 0$, we have a hierarchy of Moran processes. For the lower-level selection, the fixation probability of one cooperator prevails in a group of defectors is approximated as p_c. For the higher-level selection, the fixation probability that a group of cooperators takes over the whole population is approximated as P_C. Therefore, the fixation probability of a single cooperator in the population of defectors is computed as $\phi_c = p_c P_C$. The cooperation is favoured if $\phi_C > 1/mn$, which can be derived further as $b/c > 1 + n/(m-2)$ (see Refs. (Traulsen and Nowak, 2006; Traulsen et al., 2008) for more details). In addition, some people (Vural et al., 2015) also study the formation of bunches in an evolving interdependent population, which can be seen as hierarchical competitions as well.

Under natural selection, the reproduction or removal in a structured population is associated with network reorganisation. Cavaliere *et al.* (Cavaliere et al., 2012) proposed a simple reproduction-mutation-reorganisation model to demonstrate the fragmentation and reformation of an evolutionary community. In the reproduction, not only the state of the parent is inherited, but also the neighbourhood may be copied

by the new-born player. This phenomenon of social inheritance is widely observed in social networks, financial organisations and bacterial communities.

In the model of evolutionary population discussed in Ref. (Cavaliere et al., 2012), each agent holds a state of either cooperation (C) or defection (D), and the payoff obtained by a player is the accumulated payoff by interacting with all neighbours. The fitness of an agent is computed as $f_i = (1+\delta)^{\pi_i}$, where δ is a tunable intensity of selection. At each step,

(1) a role-model is selected to reproduce with probability proportional to the fitness, namely $f_i / \sum_j f_j$;

(2) the new-born agent adopts the state of her/his parent with probability $1-\mu$ and mutates to an alternative state with probability μ;

(3) the new-born agent connects to her/his parent with probability p and connects to each of her/his parent's neighbours with probability q;

(4) a randomly selected agent is removed form the network.

This model follows the Moran process, but the network structure is dynamically changed. When the mutation rate is $\mu \to 0$, the evolution of cooperation performs a series of transitions from all cooperators to all defectors. Interestingly, a highly connected network is obtained in the case of all cooperators and a sparsely fragmented network is observed in the case of all defectors.

Some very interesting results have been illustrated in Ref. (Cavaliere et al., 2012), where they found a correlation between network stability and prosperity. In addition, the embedding parameters p and q affect the persistence of cooperation as well as the prosperity of population. The collapse of cooperation occurs when q reaches a high value, which resembles a critical transition. This model combines evolutionary games with adaptive networks in a quite natural manner, based on which we will investigate more ingredients in the following Chapter 4.

2.3.3 Adaptive Agents Coordination

Multi-agent system (MAS) (Ferber, 1999) is composed of interacting agents, who work in an organised manner to solve some complicated problems. Those agents can work through methodic approach to achieve collective goals (Olfati-Saber et al., 2007),

where network topology is crucial to the organisation performance. Networks organised by agents in real world can be used to model the dynamics in robotic group (Gaston and desJardins, 2005; Abdallah and Lesser, 2007), traffic systems (Guimerà et al., 2002; Guimera et al., 2005), gene networks (Bornholdt and Rohlf, 2000; Bornholdt and Schuster, 2006), etc. where a core problem is agent coordination in solving tasks.

2.3.3.1 Organisation of Agents

In many real-world applications, individuals should be able to interact with each other locally and implement tasks cooperatively. Here, we will give a brief overview of the task model, the organisation model, the implementation method, and the adaptive dynamics.

- **Task model**

The overall performance of a system of agents is measured by how successful the agents are at solving tasks they pick up and at what rate they can pick these tasks from the task-flow. The structure of the task-flow depends on various choices which we detail below. These are the task composition or structure, the task advertisement mechanism and the task allocation mechanism.

Task composition indicates how many subtasks are in the task and how those subtasks are interdependent on each other. A subtask is atomic and requires a certain skill. In addition, the subtasks can be implemented in parallel or in a sequential order (Kota et al., 2012).

Task advertisement shows how a task is known to the agents (Glinton et al., 2008b). Usually, tasks can be globally advertised or locally advertised to the agents. Sometimes, the task known by an agent may be advertised to the neighbours in a P2P way.

Task allocation tells us how tasks are allocated to one or more agents. When a task arrives at an agent, it can be allocated to its neighbours randomly or with a preference. Once the tasks are pushed into an agent, they will be served in an order of first in first out (FIFO) or some other ways (Kota et al., 2012), depending on the structure of local task queue.

- **Organisation model**

An organisation is usually made up of interacting agents, which are used to implement the tasks.

Agents are represented by nodes in the network and are connected with each other through various links. The agents can be homogeneous or heterogeneous in implementing tasks, where the functionality of agents may differ from each other. For instance, the agents may be equipped with different skills and agents with the same skill may work at different service rates.

Interactions illustrate how the agents are connected in an organisation. The links can be undirected or directed, indicating the information or task flow on them. In addition, the links can be homogeneous or heterogeneous, where a weight is used to show the affinity between adjacent agents.

Organisation performance is the benefit obtained by completing the tasks, which can be measured by utilization rate, completion time, success rate, etc.

- **Implementation method**

When the models of task and organisation are provided, we can implement the tasks within an organisation using the following two methods.

Centralised method needs a central control to guide the task implementation within the whole organisation. This method can reach optimal solution at the expense of high cost and low robustness. Many centralised algorithms in the field of operational research exist to solve the tasks-agents assignment with polynomial complexity.

Recently, more and more studies consider to solve MAS optimization problems (Gaston and desJardins, 2005; Kota et al., 2012) through some local interactions without a central control. In general, a decentralised method enables the agents to implement tasks locally, and rational individual behaviours can foster high collective benefit. Notably, the communication cost in this case is much lower than that in a centralised way, meanwhile the system is more robust to random failures or attacks, thus enhancing the resilience of the organisation.

- **Adaptive dynamics**

Organisation performance in a decentralised system can be improved through adaptive dynamics, namely a series of effective state evolution and structure adaptation.

Learning is a kind of cognition capability used to transfer local and historical information into a form of knowledge. Generally speaking, learning is a decision-making process conducted by the agents in order to obtain an optimal policy for individual behaviours in the future. As no one is in global control, agent learning in a distributed

manner can only capture local information (task flow, information flow, policy, advertisement, etc.). Some common learning methods are observation-imitation, advice-taking, reinforcement learning, etc. Interestingly, there have been some concrete learning approaches (Sen and Weiss, 1999) applied in agents coordination.

Adaptation is the individual behaviours used to modify the organisation of agents based on the feedbacks (policy, guidance, reports, etc.) obtained from learning. The agents in an organisation may be self-interested or cooperative, which determines whether the changes of state and structure will fulfil the individual interest or collective benefit. In this thesis, we will only consider the simpler case where all agents are cooperating. In general, task implementing and agent learning run faster than individual behaviours for adaptation, as it usually takes a long time to form an effective and stable adaptation policy. But it is not always good to follow the data too closely, which may cause overfitting. In addition, cost will arise along with the adjustments of states and structures.

2.3.3.2 Network Adaptation in Organisations

Considering the uncertainty in realistic situations, multi-agent systems (MAS) should be flexible enough to modify their underlying structures, which are supposed to be robust to accidental faults. As far as we are concerned, the emergence of collective coordination in real world is usually achieved by a series of individual behaviours of evolution and adaptation.

Aiming at reaching higher organisation performance, many self-organisation approaches (Kohonen, 1988) have been adopted to solve agents coordination problems. Unfortunately, there is still no unified theory to incorporate self-organisation into adaptive networks. In the following, we will review some examples in the realms of agents team formation (Gaston and desJardins, 2005) and distributed task allocation (Abdallah and Lesser, 2007). As will be shown, designing an effective adaptation strategy is not trivial, and a key problem is how to foster favourable individual behaviours. What should be noted is that the dynamics discussed in the existing references mainly lies in the adaptation of structure by connecting, disconnecting, rewiring links, etc. However, in many situations, the evolution of state (the changes of agents' roles or functions) is important as well and should be considered in the research for adaptive networks.

We consider the adaptation of network for agents team formation (Gaston, 2005), where the tasks need to be implemented by teams of cooperative and connected agents. In this family of models for team formation, the requirement of a task is a set of skills,

and the agents with different skills are embedded in a network randomly in the beginning. The agents should form teams in a distributed manner to implement those tasks (Figure 2.18). In detail, each agent will do either of the following events at each step to be involved in a team:

- Initialize a team with a probability (which is the ratio between the number of uncommitted neighbours and that of total neighbours), if the team corresponding to a task is empty and that agent holds a required skill;
- Join an existing team with a probability (which is the ratio of current team size and actual task size), if a neighbour has been in the team and that agent holds a required skill for the corresponding task;

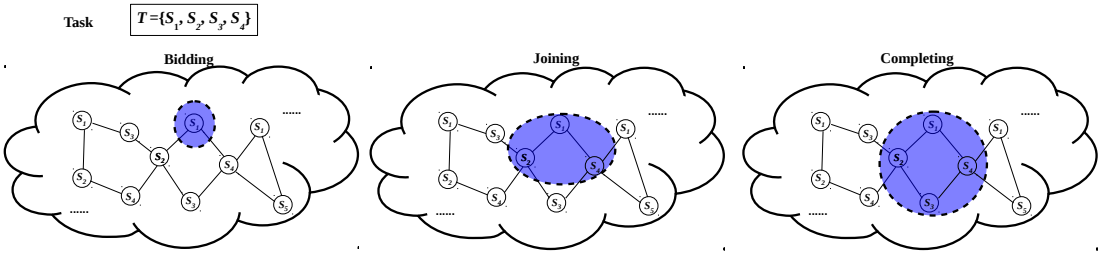

Figure 2.18: The process of team formation. When an agent bids for a task, some adjacent and uncommitted agents will join the team until all required skills are in the team. Once an agent is committed to a team, it will stay there until the task is completed or expired.

In general, the organisation performance (namely task success rate, defined by the ratio between the number of successful teams and that of imported tasks) is highly dependent on the underlying structure, which should be changed in real time. Here, we will focus on the action of *rewiring*, which disconnects one neighbour and connects to another one. The purpose of this research is to facilitate the formation of effective teams through network adaptation, which can work well as environment changes. In particular, a learning-based framework for network adaptation is proposed to address the team formation problem (Gaston, 2005). This framework is performed in an agent-organised network (AON), which is defined as "*an organizational network structure, or agent-to-agent interaction topology, that changes as a result of local network adaptation decisions made by the individual agents in a networked multi-agent system*" (Gaston, 2005). A major consideration for AON in agents team formation is when and how the agents adapt their local structure. In detail, we need to answer:

- *when* to adapt;

In Ref.(Gaston, 2005), a stateless Q-learning is adopted to decide whether it is necessary for an agent to do rewiring. For an agent, its Q value is updated as:

$$Q(a) \leftarrow Q(a) + \alpha[R_t - Q(a)] \tag{2.33}$$

where R_t is the change in local performance after taking a certain action a. Here, the local performance of an agent is the ratio between the number of successful teams joined and that of teams joined totally. In this way, an agent decides to adapt its structure if $Q(rewiring) > Q(nothing)$. In their study, two αs are used to discriminate the case where performance is increasing and the case where performance is decreasing.

- *which* connections to remove;

For each connection, a value is maintained to measure the benefit of that connection. At each step, the value of a connection is updated as:

$$V_{ij} \leftarrow V_{ij} + \beta[W_{ij} - V_{ij}] \tag{2.34}$$

where $W_{ij} = 1$ if the connection is in a successful team; otherwise $W_{ij} = 0$. When an agent decides to do rewiring, then it will remove the minimum-valued connection.

- *where* to make new connections.

In general, a push referral method is used to determine with whom to establish a new connection, which can guarantee the connectivity of the organisation. Specifically, if an agent i decides to rewire from a neighbour j, then j will refer its neighbour with maximum performance to i.

The above AON strategy is *Q/minNeighbor/pushMax*, which can foster a huge success in agents team formation and other similar applications. In addition, Gaston *et al.* (Gaston and desJardins, 2005) also developed two rule-based network adaptation strategies for dynamic multi-agent team formation. In the structure-based strategy, the adaptation of network follows the principle of preferential attachment, where the edges are rewired from lower-degree nodes to higher-degree ones. In the performance-based strategy, agents are enabled to remove the connections from the neighbours with lower performance and to establish new connections to the neighbour's neighbours with higher performance. Through their work, some interesting conclusions are obtained: (1) the network topology plays an important role in the performance of team

formation; (2) task success rate can be improved to a higher value using some adaptation strategies.

In addition, Glinton *et al.* (Glinton et al., 2008b,a) empirically analysed the characteristics of the above mentioned structure-based strategy, and proposed a token-based adaptation method to rewire to some distant agents. Barton *et al.* (Barton and Allan, 2007a,b, 2008) explored some strategic methods for team formation, where an interesting one is the strategy of diversity-based adaptation. In that model, an agent would like to connect to someone who holds a quite different skill from those nearby. In this way, a more robust team can be formed with diverse skills in the neighbourhood.

When it comes to the field of distributed task allocation, we focus on assigning tasks to suitable agents. Refs.(Kota et al., 2012, 2009; Ye et al., 2012) explored a decentralised approach in the organisation of agents, which comprises a set of structured and cooperative individuals. Interestingly, the cost for task completion (including load, communication, reorganisation) can be reduced by allowing the adjustments of network structure. In order to learn past experiences effectively, some researches (Abdallah and Lesser, 2006, 2007) studied the interplay between task allocation and self-organisation through multi-agent reinforcement learning (MARL). In that model, $p_i(s,a)$ is defined as the probability that action a is taken by agent i at state s, and is updated by reinforcement learning:

$$p_i(s,a) \leftarrow p_i(s,a) + \eta\left(Q_i(s,a) - \hat{Q}_i(s)\right) \tag{2.35}$$

where $Q_i(s,a)$ indicates the reward value by implementing a at s and the average reward at s is calculated by $\hat{Q}_i(s) = \sum_a p_i(s,a)Q_i(s,a)$. Notably, they also applied the Win or Lose Fast (WoLF) heuristic to recalculate the learning rate, which varies as $\Delta(a) = Q_i(s,a) - \hat{Q}_i(s)$ changes. In this way, the agent associated with a bigger $p_i(s,a)$ will be more likely to be connected; on the contrary the one associated with a smaller $p_i(s,a)$ will be more likely to be disconnected. Notably, this learning method needs to consider all the interacting information at each step, which leads to a quite large state-action space and then high computation cost.

In many realistic situations, the operation of agents organisation is dependent on the interacting functional agents, whose performance is recorded in the process of distributed learning, which in turn determines the adjustments of states and structures. Considering the trade-off between effectiveness and efficiency, a more explicit and simpler mechanism incorporating state, structure and learning should be studied, and we are going to explore that in Chapter 5.

Chapter 3

Network Consensus and Fragmentation in Information Diffusion

Ref. (Durrett et al., 2012) studies an adaptive voter model on a complex network whose nodes have one opinion from two options (A or B). Two types of dynamics facilitate the agreement between neighbours: one is pairwise imitation with a tendency $(1-\alpha)$ and the other is link rewiring with a tendency α. The adaptive dynamics stops at a frozen state when there is no active link AB left in the network. For a null rewiring force, $\alpha = 0$, the agent graph is static and the opinions converge to a consensus (per connected component). For null imitation, $\alpha = 1$, opinions never change, and eventually, the graph converges to a fragmented form where the two opinions are disconnected. For values between 0 and 1, both dynamics coexist. As α increases, the system will change from consensus to fragmentation.

The adaptive voter model studied above is driven by the dynamics of imitate-or-repel, which is a kind of simple social learning. In this chapter, a rich landscape will be revealed by varying the rewiring force α in the cases of various structure adaptation strategies and state evolution mechanisms. In detail, we try to explore the adaptive networks by rewire-to-foaf (friend of a friend), approximate majority and weighted model. Furthermore, moment-closure differential equations based on interface approximation (IA) and double stars approximation (DSA) are derived to capture the adaptive dynamics analytically. The adaptive voter model can be used to shed light on real world competitive phenomenologies among different groups (e.g. species, languages, cultures and opinions), where the coupled dynamics has a significant impact on the group fate.

3.1 Introduction

Network consensus and fragmentation are two important trends for information diffusion in adaptive networks. As reviewed before, the adaptive dynamics has been explored extensively to reveal neural systems (Bornholdt and Rohlf, 2000), epidemics spreading (Pastor-Satorras and Vespignani, 2001; Gross et al., 2006; Guerra and Gómez-Gardeñes, 2010), opinion formation (Holme and Newman, 2006; Zanette and Gil, 2006; Kozma and Barrat, 2008), etc. Typically, one may ask whether global transitions can be triggered by small changes in the parameters of rules, and how these transitions reflect on the underpinning graph structure. In this chapter, we will study the adaptive voter model by exploring the entangled dynamics between pairwise imitation and link rewiring.

The adaptive dynamics led by opinion spreading and social contacts was originally investigated by Holme *et al.* (Holme and Newman, 2006) in 2006, where the discordant edges (i.e. active links connecting two nodes holding different states) are eliminated by opinion imitation and link rewiring. Interestingly, they found a critical phase transition from opinion uniformity to opinion diversity with the increase of the rewiring strength. Afterwards, Fu *et al.* (Fu and Wang, 2008) studied the strategy of majority-preference (MP, the agent imitates the majority opinion in the neighbourhood) and minority-avoidance (MA, the agent rewires the link from a neighbour in the minority) to resolve the discord, where a variety of opinions are conserved when the strength of rewiring is stronger. Durrett *et al.* (Durrett et al., 2012) discovered that the fraction of nodes in minority state is highly dependent on the rewiring strength and initial fraction. Under two different rewiring strategies: rewire-to-same and rewire-to-random, the transitions from consensus to fragmentation are different dramatically. In order to gain a deeper insight into the phase transition, Vazquez *et al.* (Vazquez et al., 2008; Demirel et al., 2014) adopted some approximate differential equations to obtain the statistical properties analytically, but the results are not accurate enough, which is due to the correlations among links in the dynamical process.

Adaptive voter models entangle state evolution and structure adaptation naturally in order to deal with the conflict (or discord) caused by discordant edges. As shown in Figure 3.1, link rewiring and state imitation are two major ways to improve the agreement between neighbours, where the **rewiring force** α ($0 \leq \alpha \leq 1$) indicates the tendency to rewire from the current neighbour.

In this chapter, we base our work on an example in Ref.(Durrett et al., 2012) to

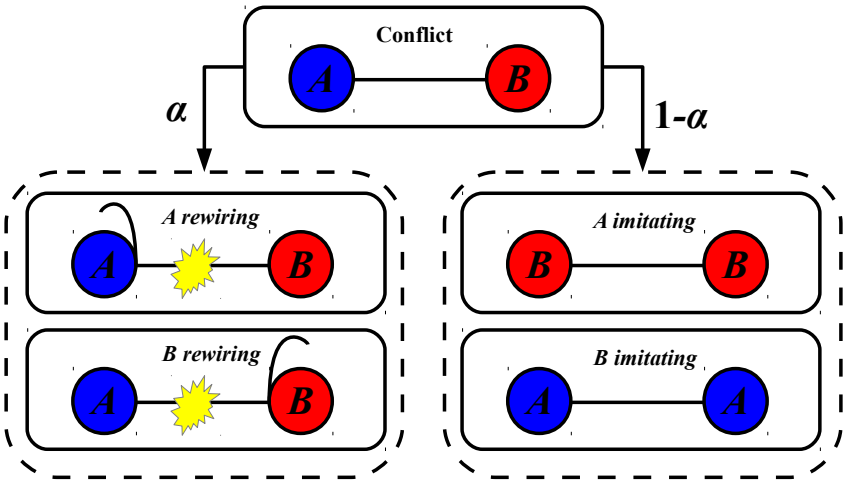

Figure 3.1: The discordant edges can be resolved by either rewiring an adjacent AB edge (with probability α) or imitating the neighbour (with probability $1-\alpha$).

explore the adaptive voter model from the following perspectives:

- different rewiring strategies are used to uncover the influence of adaptation on network fragmentation;
- an approximate majority method is adopted in state evolution to promote the consensus of network;
- the voters are assigned with weights, and the model is extended to weighted voter model;
- some approximation techniques are proposed to capture the adaptive dynamics more accurately.

3.2 Adaptive Voter Model

A variety of adaptive voter models have been reviewed in Chapter 2. In this study, the model discussed in Ref. (Durrett et al., 2012) is adopted in the following analytical calculations and numerical simulations. This section is a re-exposition of the paper (Durrett et al., 2012) with some simulations and remarks.

The adaptive voter model reflects the competition between two opinions: A and B, and each voter holds a single opinion as its state $s_i \in \{A, B\}$. In the beginning, all the voters are distributed uniformly in a random network with N nodes and E edges. We

assume that the voters holding A has a fraction of ϕ_0 initially, and $\phi_0 \leq 0.5$ unless noted otherwise. The adaptive dynamics between state and structure runs as follows. At each step, an active link AB is picked at random for pairwise imitation or link rewiring. With probability $1-\alpha$, a random voter from that selected AB adopts the opinion of the other. Otherwise, with probability α that voter redirects the active link to other target (depending on the rewiring strategy) in the network. The adaptive dynamics continues until there is no active link left in the network.

This adaptive voter model is parametrized by the rewiring force α: when $\alpha = 0$ the model always flips in a static graph, and when $\alpha = 1$ the model always rewires to form a few fragmented communities, otherwise the model is a mixture with a rate α to rewire and $1-\alpha$ to imitate. As the rewiring force α increases, network fragmentation becomes more likely (Figure 3.2).

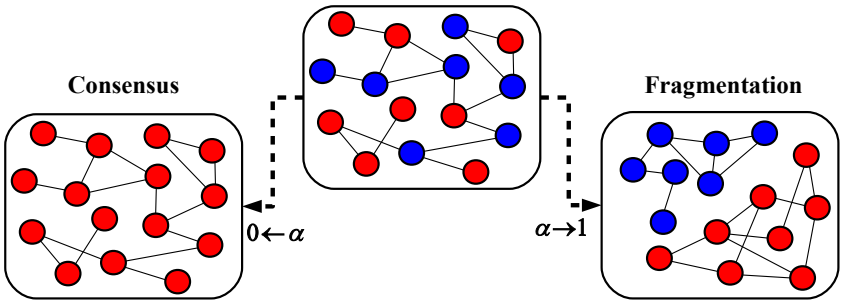

Figure 3.2: A schematic diagram illustrates the transition from consensus to fragmentation as α increases.

The macroscopic emergence is caused by various microscopic behaviours, such as varying rewiring forces, state evolution rules and structure adaptation rules. In all cases, the number of nodes N and the number of edges E are invariant.

3.2.1 Analytical Description

Clearly, the family of adaptive voter models can be represented as Markov chains (Gilks, 2005), where the states are node-coloured graphs. The node set is invariant (as said earlier) and so is the number of edges. We write Ω_G for the finite set of graphs with N nodes and E edges, which are reachable from a given initial node-coloured graph G_0 (with same set of nodes and edges). For convenience, we will set the dynamics as a continuous-time Markov chain (CTMC) (Norris, 1998). This means that the rewiring force α is construed as a rate rather than a probability. We will write $p(t)(G_i)$

for the probability to be at G_i in Ω_G at time t. Thus, $p(t)$ can be seen as a vector (or finite function) in the finite-dimensional real vector space $\mathbb{R}^{\Omega_G}$.

From the general theory of finite Markov chains we have the so-called forward equation:

$$\frac{\mathrm{d}}{\mathrm{d}t}p^T = p^T Q \tag{3.1}$$

where p^T is the transpose of p, and Q is the generator, or rate matrix, of our continuous-time Markov chain (CTMC). This linear ordinary differential equation (ODE) system defines the dynamics of p for a given initial condition. Whenever the state space is finite (namely finite number of reachable networks), then there exists a unique solution to the forward equation.

Consider an observable f, that is to say a function in $\mathbb{R}^{\Omega_G}$. We define $E_p(f) := p^T f$ as the (time-dependent) value of f averaged over p, and sometimes we also write it as $\mathbb{E}(f)$. From the forward equation we can derive a rate equation for $E_p(f)$:

$$\frac{\mathrm{d}}{\mathrm{d}t}E_p(f) = \frac{\mathrm{d}}{\mathrm{d}t}p^T f = p^T Q(f) = E_p(Q(f)) \tag{3.2}$$

This differential equation specifies the evolution of the average of f. Concretely, $Q(f)$ is a vector contains the following observables:

$$Q(f)(G_i) = \sum_{G_j} q(G_i, G_j)[f(G_j) - f(G_i)] \tag{3.3}$$

where $q(G_i, G_j)$ is the rate at which the system jumps from G_i to G_j. That is to say, $Q(f)$ is the mean rate of change of f under Q.

In the realm of graph transformation (Danos et al., 2015a), the rules and pattern matching are essential to understand the CTMC. In general, a rule is defined as:

$$\gamma := (L \to R, k_\gamma) \tag{3.4}$$

which runs on a left-hand side L to obtain a right-hand side R with a certain rate k_γ. A match $m : X \to Y$ is a graph morphism from X to Y, which "*preserves the graph structure and is injective on nodes*"(Danos et al., 2014). We say $m(X)$ the image of m in its codomain Y. For more details about graph transformation, we can find a good review in Ref. (Heindel, 2010).

Before establishing the ODEs based on a series of rules, we need to introduce an important ingredient, which is **minimal glueings** (Danos et al., 2014). A glueing μ of two motifs g_1 and g_2 is pair of matches: $\mu_1 : g_1 \to C$ and $\mu_2 : g_2 \to C$, to a common codomain C. The glueing μ is minimal if the codomain of μ is same as $\mu_1(g_1) \cup \mu_2(g_2)$.

Furthermore, we can write $mg(g_1, g_2)$ as the set of minimal glueing motifs for g_1 and g_2.

Given a motif g, we write $[g]$ as the number of that motif, and the ODE for average $[g]$ can be generated based on the rules. For a rule $\gamma \in \mathcal{R}$ with left-hand side L and right-hand side R, let $mg(g,L)$ be the set of motifs corresponding to the minimal glueings of g and L, which indicates the case of observable destructions. Similarly, $mg(g,R)$ be the set of motifs corresponding to the minimal glueings of g and R, which indicates the case of observable constructions. Be careful, the counting for $mg(g,R)$ should be done in the generated graph instead of the current graph. In order to obtain the number of generated motif g, we define $mg^{\neg}(g,R)$ as the reverse set of $mg(g,R)$, where each element is obtained by applying the reverse rule to the corresponding element in $mg(g,R)$. Therefore, we can calculate the constructions of g by counting the number of motifs in $mg^{\neg}(g,R)$ at current state.

For example, suppose we have a rule $AB \to AA$ and the observable is $[g] = [AB]$, the minimal glueings can be shown in Figure 3.3.

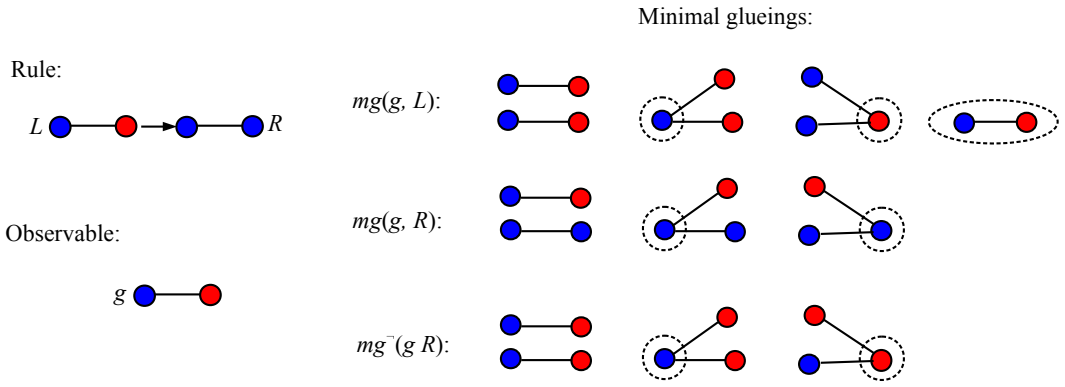

Figure 3.3: An example shows the transition triggered by a rule $AB \to AA$, where $mg(g,L)$ indicates the all possible destructions of g and $mg^{\neg}(g,R)$ indicates all possible constructions of g. The dashed circle indicates the overlapping part.

Using the ordinary differential equations (ODEs) generation method proposed in Ref. (Danos et al., 2015a,b), the ODE obtained to describe the dynamics of the average number of a certain motif can be shown in a general form as below.

$$\frac{\mathrm{d}}{\mathrm{dt}}[g] = \sum_{\gamma \in \mathcal{R}} k_\gamma \Big(\sum_{r \in mg^{\neg}(g,R)} [r] - \sum_{l \in mg(g,L)} [l] \Big) \tag{3.5}$$

where $[g]$ indicates the observable, and k_γ is the rate of rule γ. In fact, we write $\frac{\mathrm{d}}{\mathrm{dt}}[g]$

short for $\frac{\mathrm{d}}{\mathrm{dt}}\mathbb{E}([g])$ and all the observables in the ODEs are the average case, namely $[g] = \mathbb{E}([g])$.

Importantly, our convention is that motif counts are not discounted for symmetries. In technical terms, we are counting the number of coloured graph morphisms that are injective on nodes. For example, we have $[AA] = 2N$ for a graph consisting of a ring of N nodes of type A; whereas in a ring of N nodes where type alternates, we have $[AB] = [BA] = N$.

As all these monomials themselves are motif observables, the linear subspace generated by motif observables is closed under rate matrices led by local graph rewriting rules (see proof in Ref.(Danos et al., 2014)).

3.2.2 Pair Approximation

In adaptive voter models, we are interested in exploiting the differential equations to study observables corresponding to small graph motifs such as the number of nodes of type A, B, and the number of edges of type AB, AA and BB. In order to distinguish between motifs and their observables, we will write respectively $[A]$, $[B]$, $[AB] = [BA]$, $[AA]$ and $[BB]$ for the motif observables above (and use similar notations for larger motifs).

In terms of the simplest observable $[A]$, we will construct its differential equation. Here, we need only to consider imitation steps as $[A]$ is invariant under rewiring. Among imitation steps, we can distinguish ones where A gets imitated, and hence $[A]$ gets incremented, and dual steps where B gets imitated, and $[A]$ gets decremented. We then get:

$$\begin{aligned} \frac{\mathrm{d}}{\mathrm{dt}}[A] &= (1-\alpha)\textstyle\sum_{AB\in G}(k_{B\to A} - k_{A\to B}) \\ &= (1-\alpha)(k_{B\to A} - k_{A\to B})[AB] \end{aligned} \tag{3.6}$$

with $k_{A\to B}$ means the rate a voter of A imitates the neighbouring state of B.

Let's consider the strategy of rewire-to-random (Durrett et al., 2012), where the opinions are equally persuasive and the discordant node redirects the active link to a random one. The ordinary differential equations (ODEs) based on the above described method in Eq. 3.5 are provided as follows to capture the dynamics of small-motif observables.

$$\begin{aligned}
&\tfrac{\mathrm{d}}{\mathrm{dt}}[A] = (1-\alpha)\times 0\times [AB] \\
&\tfrac{\mathrm{d}}{\mathrm{dt}}[B] = (1-\alpha)\times 0\times [AB] \\
&\tfrac{\mathrm{d}}{\mathrm{dt}}[AB] = (1-\alpha)(-[AB]+[ABB]-[ABA]-[BA]+[BAA]-[BAB]) \\
&+\alpha[AB](-1+\tfrac{[B]}{N})+\alpha[BA](-1+\tfrac{[A]}{N}) \\
&\tfrac{1}{2}\tfrac{\mathrm{d}}{\mathrm{dt}}[AA] = (1-\alpha)([AB]+[ABA]-[BAA])+\alpha[AB]\tfrac{[A]}{N} \\
&\tfrac{1}{2}\tfrac{\mathrm{d}}{\mathrm{dt}}[BB] = (1-\alpha)([BA]+[BAB]-[ABB])+\alpha[BA]\tfrac{[B]}{N}
\end{aligned} \tag{3.7}$$

What should be noted is that the right-hand sides of the equations involve some triplet motifs (such as ABA, BAB, ABB, BAA). In order to make the set of equations closed, the following two options are available: (1) write more equations for those bigger motifs, which may be infinite for large-scale complex networks; (2) truncate those bigger motifs based on some approximation approaches. Many researches reviewed in Ref. (Demirel et al., 2014) have focused on moment-closure approximate differential equations, and the most widely-used one is pair approximation (PA) (Ellner, 2001). Pair approximation adapts the Bayes' theorem into the graphs by estimating the bigger motifs through some smaller ones. In detail, we can write following approximate equation to decompose the triplet:

$$[XYZ] \simeq \frac{[XY][YZ]}{[Y]} \tag{3.8}$$

where $X,Y,Z \in \{A,B\}$. In this way, we can have following approximations for the involved triplets. Notably, this approximation works under an assumption of conditional independence.

$$\begin{aligned}
&[BAB] \simeq \tfrac{[AB][AB]}{[A]} \qquad [ABA] \simeq \tfrac{[AB][AB]}{[B]} \\
&[BAA] \simeq \tfrac{[AA][AB]}{[A]} \qquad [ABB] \simeq \tfrac{[BB][AB]}{[B]}
\end{aligned} \tag{3.9}$$

3.2.3 Higher Order Moments

Besides the first order moment, it is also very interesting to explore the expressions and differential equations for some higher order ones. Before doing that, let's recall

the minimal glueings explained earlier, based on which we will study the minimal glueings of more than two motifs. For a higher order moment $[X]^n$, we can write it as:

$$[X]^n = \sum_{\mu \in mg(X,X,\cdots,X)} [\mu] \tag{3.10}$$

where $mg(X,X,\cdots,X)$ indicates the set of minimal glueing motifs for n Xs.

In particular, the second order items are widely used, which can be used to estimate the variance. For the second order observable $[X]^2$, we can express it using the disjoint parts and joint parts. For two motifs of X, the case without any intersection can be written in the way $X+X$. The number of this kind of disjoint pairs can be calculated as:

$$[X+X] = [X][X] - \sum_{\mu \in mg(X,X)\setminus\{X+X\}} [\mu] \tag{3.11}$$

where $mg(X,X)$ is the set of minimal glueing motifs for the two Xs.

If the motif X means a certain kind of node, then we can have:

$$\begin{aligned}
[X]^n &= \underbrace{[X][X]\cdots[X]}_{\text{n}} \\
&= ([X]+[X+X])\underbrace{[X][X]\cdots[X]}_{\text{n-2}} \\
&= ([X]+(2+1)[X+X]+[X+X+X])\underbrace{[X][X]\cdots[X]}_{\text{n-3}} \\
&\cdots \\
&= a_{n,1}[X]+a_{n,2}[X+X]+\cdots+a_{n,n-1}\underbrace{[X+\cdots+X]}_{\text{n-1}}+a_{n,n}\underbrace{[X+\cdots+X]}_{\text{n}}
\end{aligned} \tag{3.12}$$

Given a n^{th}-order $[X]^n$ as above, we can write the $(n+1)^{th}$-order $[X]^{n+1}$ by using a recurrence relation:

$$\begin{aligned}
[X]^{n+1} &= a_{n+1,1}[X]+a_{n+1,2}[X+X]+\cdots \\
&\quad +a_{n+1,i}\underbrace{[X+\cdots+X]}_{\text{i}}+\cdots \\
&\quad +a_{n+1,n}\underbrace{[X+\cdots+X]}_{\text{n}}+a_{n+1,n+1}\underbrace{[X+\cdots+X]}_{\text{n+1}} \\
&= a_{n,1}[X]+(a_{n,1}+2a_{n,2})[X+X]+\cdots \\
&\quad +(a_{n,i-1}+ia_{n,i})\underbrace{[X+\cdots+X]}_{\text{i}}+\cdots \\
&\quad +(a_{n,n-1}+na_{n,n})\underbrace{[X+\cdots+X]}_{\text{n}}+a_{n,n}\underbrace{[X+\cdots+X]}_{\text{n+1}}
\end{aligned} \tag{3.13}$$

where $a_{n,i}$ is the Stirling number (Sharp, 1968). We have the recurrence relation as $a_{n+1,i} = ia_{n,i} + a_{n,i-1}$ and $a_{n,i} = \frac{1}{i!}\sum_{j=1}^{i}(-1)^{i-j}\binom{i}{j}j^n$.

Return to the above described adaptive voter model, the average number of a certain type of nodes (e.g. A) is imitation relevant and rewiring free, and we can have that $\frac{d}{dt}[A] = 0$. Thus, the average number of As at stationary state should be fixed as $[A] = \phi_0 N$. However, the distribution of the final fraction of As is non-trivial with the change of rewiring force α (see more details in following section). Therefore, we can estimate the distribution of final As through its variance: $\mathbb{V}([A]) = \mathbb{E}([A]^2) - \mathbb{E}([A])^2$. The ODE for the second order of motif A (namely $[A]^2 = [A+A] + [A]$) can be written as:

$$\begin{aligned} \frac{\mathrm{d}}{\mathrm{dt}}[A]^2 &= \frac{\mathrm{d}}{\mathrm{dt}}[A+A] + \frac{\mathrm{d}}{\mathrm{dt}}[A] = \frac{\mathrm{d}}{\mathrm{dt}}[A+A] \\ &= 2 \times \big((1-\alpha)[A+AB] + (1-\alpha)[AB] - (1-\alpha)[A+BA]\big) \\ &= 2(1-\alpha)[AB] \end{aligned} \tag{3.14}$$

Furthermore, let's see the second order of the average number of active links AB, which can be written as: $[AB]^2 = [AB+AB] + [ABA] + [BAB] + [AB]$. Here $[AB+AB]$ means the totally disjoint items, $[ABA]$ means the two motifs with a common B, $[BAB]$ means the two motifs with a common A, and $[AB]$ means the completely overlapping case. As a result, the ODE for the second order of $[AB]$ can be written as:

$$\frac{\mathrm{d}}{\mathrm{dt}}[AB]^2 = \frac{\mathrm{d}}{\mathrm{dt}}[AB+AB] + \frac{\mathrm{d}}{\mathrm{dt}}[ABA] + \frac{\mathrm{d}}{\mathrm{dt}}[BAB] + \frac{\mathrm{d}}{\mathrm{dt}}[AB] \tag{3.15}$$

3.2.4 From Consensus to Fragmentation

Driven by the coupled dynamics, the system will eventually reaches one or more monochrome components due to the finite network size. The paper (Durrett et al., 2012) discussed the graph fission in the adaptive voter model, where they pointed out that the active links AB would converge to a quasi-stationary distribution (Collet et al., 2012) quickly, and stay there for a long time until a frozen network is reached. That is to say the edges and nodes have stationary distributions conditional on $[AB] > 0$. Starting from a random network with $\phi_0 = 0.4$ as the initial fraction of As, the quasi-stationary distributions for the edges and nodes are illustrated in Figure 3.4.

More interestingly, the evolving system will approaches a parabola of meta-stable state for a long time and drifts along the curve until the frozen state is reached. Given a certain $\alpha = 0.5$, Figure 3.5 illustrates the evolutionary trajectories for the fraction of As and that of ABs under different ϕ_0s, where an evident quadratic curve is obtained.

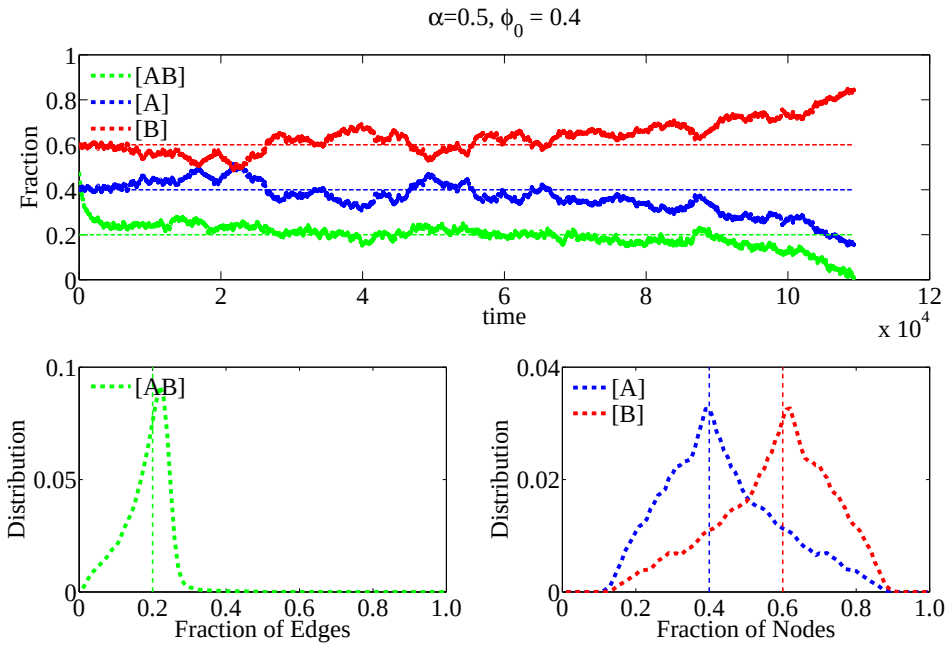

Figure 3.4: Quasi-stationary distributions for the edges and nodes at $\alpha = 0.5$. Starting from $\phi_0 = 0.4$, we plot the distributions for the fraction of ABs, As and Bs in the evolving process before $[AB] = 0$. It is clear that the fraction of As and Bs have a mean of ϕ_0 and $1 - \phi_0$ respectively, while the fraction of ABs moves around 0.2.

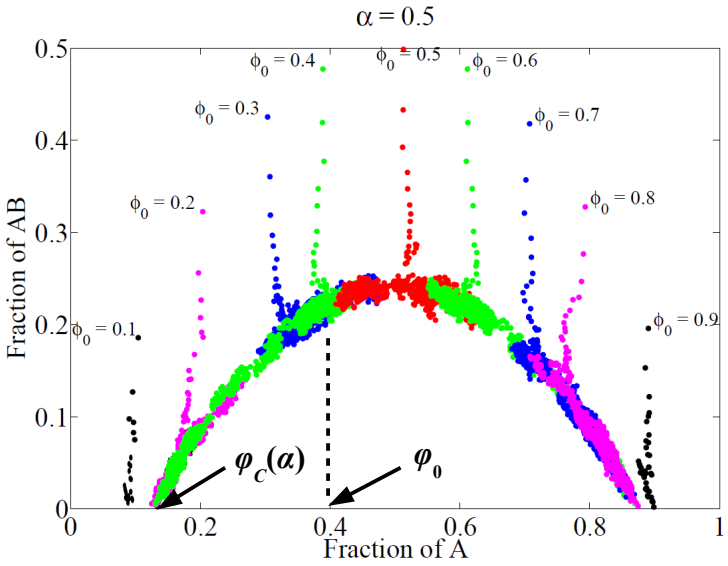

Figure 3.5: The evolutionary trajectories of the pairs: the fraction of ABs versus the fraction of As by rewire-to-random at $\alpha = 0.5$. Starting from $\phi_0 = 0.1, 0.2, \cdots 0.9$, we plot the pairs every 1000 time steps, finally a symmetric "arch" is presented. A critical fraction ϕ_C indicates the final minority. Figure is adapted from Ref. Durrett et al. (2012).

A critical fraction of As corresponding to the point where the fraction of ABs drops to 0 exactly along the quadratic curve. In above example, the critical fraction is around 0.125 and 0.875, which means the average final minority and majority. Let's define $\phi_C(\alpha)$ as the smaller **critical fraction** (namely the minority), and if $\phi_0 < \phi_C(\alpha)$, then the fraction of ABs goes straight down to 0 rapidly and the average fraction of final minority is ϕ_0. Otherwise, if $\phi_0 \geq \phi_C(\alpha)$, the average fraction of final minority is $\phi_C(\alpha)$. Therefore, the estimation for the final minority relies on the quasi-stationary distributions of ABs and As.

Besides the initial fraction ϕ_0, the rewiring force α is another important factor for the network configurations at stationary state. As we can see in Ref. (Vazquez et al., 2008; Durrett et al., 2012), the network will transform from consensus to fragmentation when the rewiring force α gets stronger. A simulation is conducted as a verification shown in Figure 3.6, where voters of A are the initial minority with a fraction of ϕ_0. We can find that voters holding A may become the majority when α is smaller, but remain as the minority when α is bigger.

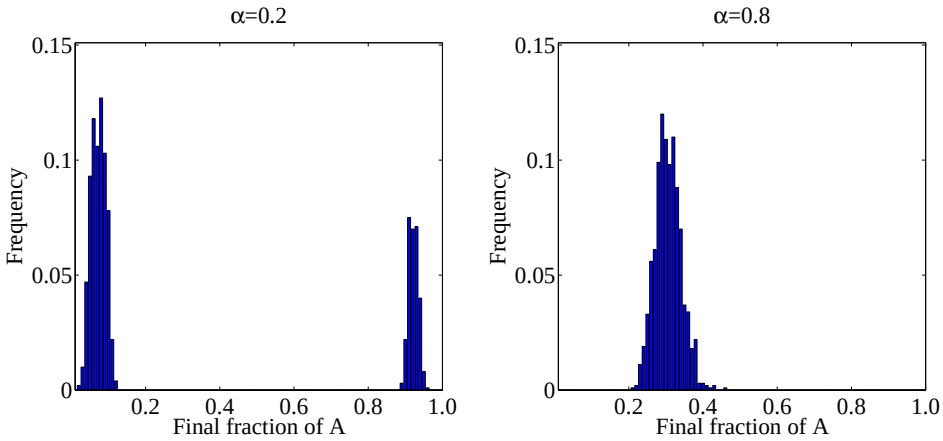

Figure 3.6: Simulation results display the distributions for the final fraction of As based on rewire-to-random strategy. Opinions are uniformly assigned into a random network with $N = 1000$, $E = 2000$, and 1000 independent simulations are conducted to get the distribution. The initial fraction of As is $\phi_0 = 0.3$. Two different rewiring forces $\alpha = 0.2$ and $\alpha = 0.8$ are adopted, where we can find an obvious shift from bimodal distribution at a smaller α to a unimodal distribution at a bigger α.

When we solve the above ODEs (Eq. 3.7) based on pair approximation (PA), the average number of various types of nodes and edges can be obtained. There are two situations for the quasi-stationary number of active links: one is $[AB] > 0$, where the initial minority has chance to be the final majority; the other one is $[AB] = 0$, where

the initial minority is always the final minority. Therefore, for a given ϕ_0, when the rewiring force α is increased from 0 to 1, we have a critical rewiring force α_C to distinguish the two situations:

- if $\alpha < \alpha_C$, then $[AB] > 0$ at quasi-stationary state and the distribution for the final fraction of As is bimodal.
- if $\alpha \geq \alpha_C$, then $[AB] = 0$ at quasi-stationary state and the distribution for the final fraction of As is unimodal.

As explained in Ref. (Durrett et al., 2012), the ODEs 3.7 at stationary state have $\frac{\mathrm{d}}{\mathrm{dt}}[AA] = 0$ and $\frac{\mathrm{d}}{\mathrm{dt}}[BB] = 0$, which can be rewritten as:

$$[AA] + [BB] - (\frac{\phi_0}{1-\phi_0} + \frac{1-\phi_0}{\phi_0})[AB] = [\frac{2(\phi_0^2 - \phi_0)\alpha + 1}{1-\alpha}]N$$

In this way, the critical rewiring force α_C can be calculated by:

$$\alpha_C = \frac{2E/N - 1}{2(\phi_0^2 - \phi_0) + 2E/N} \tag{3.16}$$

where the transition point from consensus to fragmentation is dependent on both the initial fraction ϕ_0 and the network connectivity (aka average degree) $2E/N$.

With the change the rewiring force α as well as the initial fraction ϕ_0, we can obtain the "arch" ($[AB]$ versus $[A]$) and the "heat-map" in Figure 3.7, by solving Eq. 3.7.

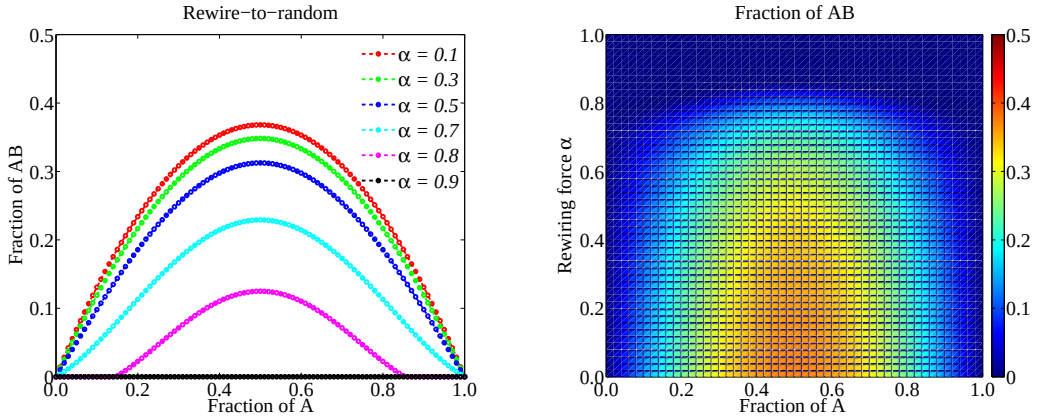

Figure 3.7: The quasi-stationary fraction of ABs obtained from the solutions of PA-based ODEs under rewire-to-random. When the initial fraction ϕ_0 and rewiring force α are varying from 0 to 1, a quite amazing landscape for the fraction of AB links at stationary state is illustrated. For a given ϕ_0, the critical rewiring force α_C is the point at which the stationary $[AB]$ just reaches 0.

3.3 Range-based Rewiring

In this section, we will explore a very interesting rewiring strategy: rewire-to-foaf (foaf is short for friend of a friend), based on which an early fragmentation will be obtained. In addition, we also try to understand the trade-off between minority survival and winning under various rewiring strategies. Both numerical simulations and approximate analyses are provided to illustrate the transitions from consensus to fragmentation.

3.3.1 Rewire-to-foaf

The rewiring strategy determines how to change the structure of network, and rewire-to-random and rewire-to-same are two popular methods which have been discussed in Ref. (Durrett et al., 2012). In detail, rewire-to-random means one of the voters connected by AB will redirect the active link AB to a random node in the network, whereas rewire-to-same means that one will disconnect from the neighbour he disagrees and make a new connection to someone holding the same opinion.

In this section, we are going to propose a new strategy: rewire-to-foaf (shown in Figure 3.8), where the voter breaks AB and rewires to his friend of a friend (foaf). A quite different point for the rewire-to-foaf is that it can reorganise the structure according to local spatial information, which is more feasible in real-world applications.

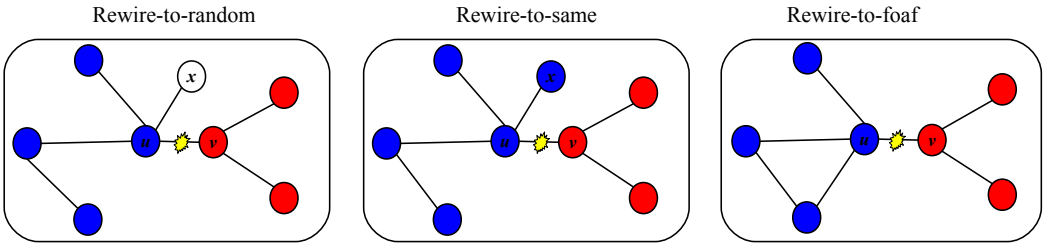

Figure 3.8: The schematic processes for (a) rewire-to-random, (b) rewire-to-same and (c) rewire-to-foaf, which reveal various social phenomena regarding how to reconstruct the local neighbourhood in real life.

The strategy of rewire-to-foaf originates from social science, where the friend of a friend is more likely to become a friend (Wasserman, 1994). As is known, the clustering coefficient is a measure to show the transitivity of a network, which is computed by the number of closed triplets ("$\triangle$") and the number of connected triplets ("$\vee$"). In social networks, we can interpret this transitivity by the probability that two individuals with a common friend also are friends.

From a global perspective, the clustering coefficient measures the density of closed triplets in a network, which can be computed by:

$$C = \frac{\#of\ closed\ triplets}{\#of\ connected\ triplets} \tag{3.17}$$

From a local perspective, we need to measure the clustering coefficient for a single node u according to Ref. Watts and Strogatz (1998):

$$C_u = |\{(v,w) : v,w \in NB(u) \wedge e_{vw} = 1\}|/k_u(k_u - 1) \tag{3.18}$$

which means the local density of the triangles connecting node u.

In this way, the average clustering coefficient in the network can be computed through $C = \sum_u C_u/N$. It is clear that a short-range rewiring can help the formation of small communities as well as big clustering coefficients as shown in Figure 3.9.

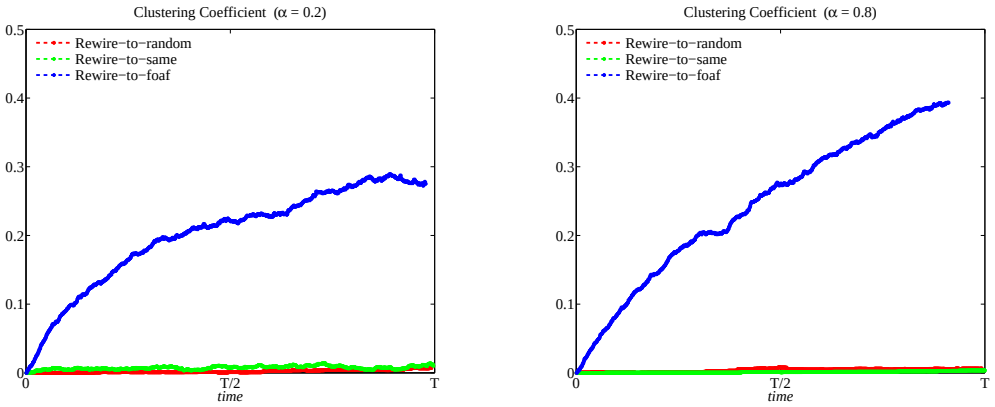

Figure 3.9: The clustering coefficient evolves with the change of time at $\alpha = 0.2$ and 0.8. The strategy of rewire-to-foaf brings a bigger clustering coefficient than the other two. We run the simulation in a random network with $N = 1000$ and $E = 2000$. The initial fraction of As is $\phi_0 = 0.4$, which are distributed within the network uniformly in the beginning.

3.3.2 Approximate Differential Equations

According to the descriptions presented above, we intend to explore some analytical calculations for this short-range rewiring, namely rewire-to-foaf. As before, we define $[A]$, $[B]$, $[AB]$, $[AA]$ and $[BB]$ as the average number of various types of nodes and edges. It is known that $[A] + [B] = N$ and $[AA] + 2[AB] + [BB] = 2E$.

As the number of nodes is rewiring free, we can have same ODEs as Eq. 3.7 for $[A]$ and $[B]$. In the process of rewire-to-foaf, the voter A from an active link AB will rewire

to another voter A with probability $\frac{[A?A]}{[A??]}$ approximately, where $[A?A] = [AAA] + [ABA]$ and $[A??] = [AAA] + [AAB] + [ABA] + [ABB]$. Similarly, the voter B from an active link AB will rewire to another voter B with probability $\frac{[B?B]}{[B??]}$, where $[B?B] = [BBB] + [BAB]$ and $[B??] = [BAA] + [BAB] + [BBA] + [BBB]$. In this situation, a node with a bigger degree will more likely to be redirected. We then arrive at the following differential equations under the strategy of rewire-to-foaf.

$$\begin{aligned}
&\tfrac{\mathrm{d}}{\mathrm{dt}}[AB] = (1-\alpha)(-[AB] + [ABB] - [ABA] - [BA] + [BAA] - [BAB]) \\
&+\alpha[AB](-1 + \tfrac{[A?B]}{[A??]}) + \alpha[BA](-1 + \tfrac{[B?A]}{[B??]}) \\
&\tfrac{1}{2}\tfrac{\mathrm{d}}{\mathrm{dt}}[AA] = (1-\alpha)([AB] + [ABA] - [BAA]) + \alpha[AB]\tfrac{[A?A]}{[A??]} \\
&\tfrac{1}{2}\tfrac{\mathrm{d}}{\mathrm{dt}}[BB] = (1-\alpha)([BA] + [BAB] - [ABB]) + \alpha[BA]\tfrac{[B?B]}{[B??]}
\end{aligned} \tag{3.19}$$

To handle the bigger motifs on the right-hand side, we adopt pair approximation (PA) to truncate the triplets into pairs. And this kind of moment-closure approximation is confluent and obtains a unique normal form.

3.3.3 Examples

Starting from an Erdös-Rényi (ER) random network, we have $N = 1000$ nodes and $E = 2000$ edges. In the beginning, the initial fraction of voters holding A is ϕ_0, which are distributed within the network uniformly.

3.3.3.1 The Fraction of the Final Minority

An early fragmentation means that the network can be fragmented even at a smaller rewiring force α. In general, the fragmentation of network can be illustrated by the final fraction of nodes in minority state. Figure 3.10 presents the average fraction of the final minority for varying rewiring force αs under different strategies.

As mentioned before, at a bigger rewiring force α, the network is fragmented; while at a smaller rewiring force most of the agents would reach consensus. The fraction of final minority increases from 0 to ϕ_0 with the increase of α, and the minority is better conserved under rewire-to-foaf. In addition, the strategy of rewire-to-same brings a sharp transition at a fixed α_C, which is independent of its initial fraction (see more details in Ref. (Durrett et al., 2012)).

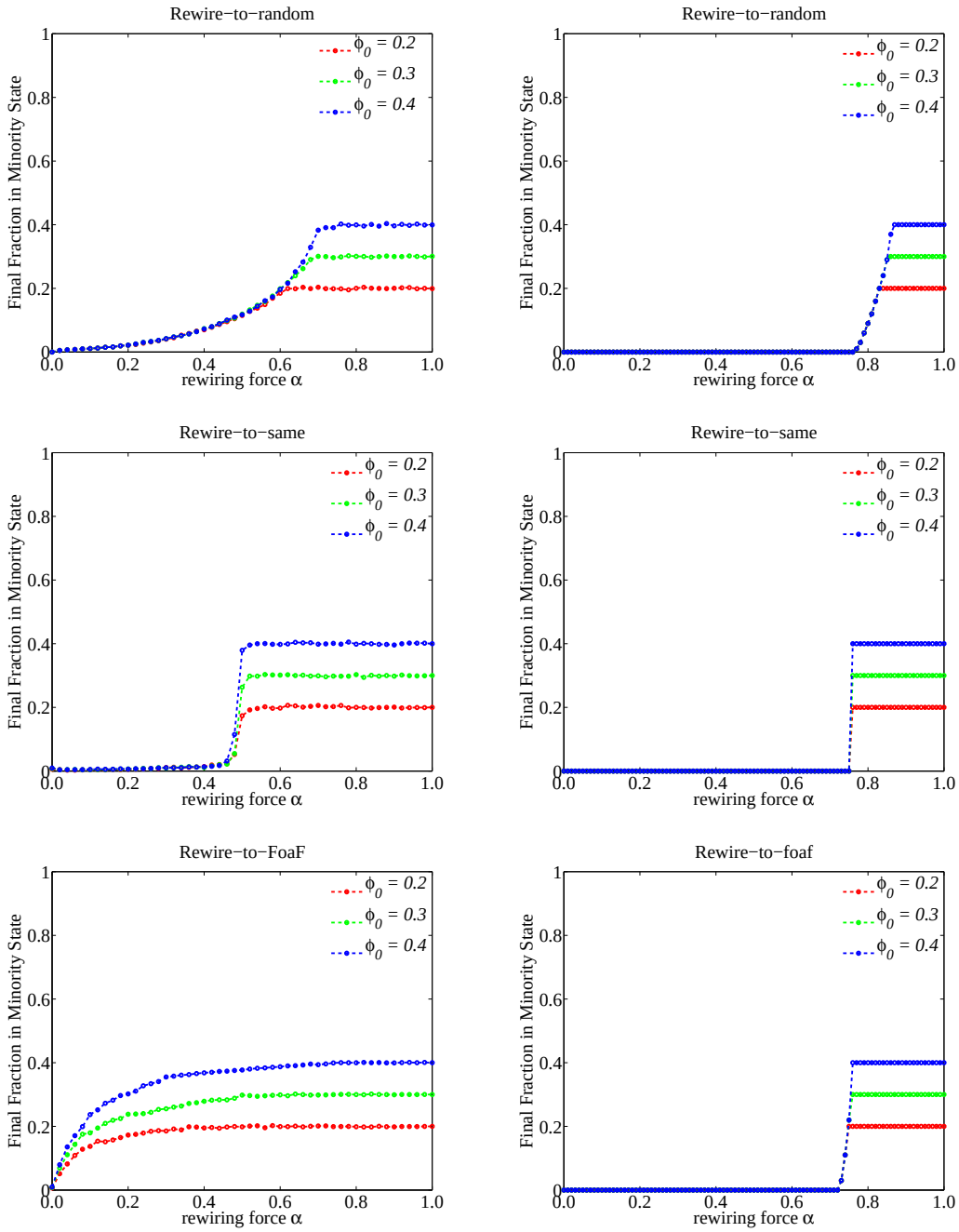

Figure 3.10: Simulation results (left column) and ODEs solutions (right column) for the average fraction of the final minority under rewire-to-random, rewire-to-same and rewire-to-foaf. Opinions are randomly assigned within the network and the initial fraction of As is $\phi_0 = 0.2, 0.3$ and 0.4 respectively. We run 1000 independent simulations to get the average. With the increase of α, the final fraction in minority state reaches ϕ_0. Notably, an early fragmentation is obtained under the strategy of rewire-to-foaf.

Furthermore, we also explore the analytical results obtained through PA-based ODEs, which are a little bit far from the numerical simulation results (see Figure 3.10

). The inaccuracy may be caused by following two aspects: (1) the number of ODEs is too small and more moment-closure ODEs should be created to capture the dynamics of bigger motifs; (2) pair approximation (PA) used to decompose the triplet $[XYZ]$ is not appropriate.

3.3.3.2 Survival and Winning

Voters holding opinion A are the minority in the beginning, but it is possible that they become the majority in the end. Here, we define two situations:

- **survival** means the case that the final fraction of As is not smaller than a certain proportion of its initial level $\rho\phi_0$, where $0 < \rho \leq 1$ is a tolerance coefficient.
- **winning** means the case that the final fraction of As is bigger than 0.5, namely the minority becomes the majority in the end.

In Figure 3.11, we can clearly see that higher survivability is available when the rewiring force α is bigger. Interestingly, during a range of $\alpha \in [0.4, 0.6]$, the strategy of rewire-to-random enables the voters holding A to survive better if they have a smaller ϕ_0. This phenomenon can be explained by the fact that network fragmentation is earlier for a smaller ϕ_0 (Figure 3.10), which leads to relatively higher survivability during that range of αs. A sharp transition at the critical point α_C is obtained under rewire-to-same. Notably, the strategy of rewire-to-foaf brings higher survivability even when α is smaller, which is associated with the early fragmentation shown before. In addition, Figure 3.11 also illustrates that a higher winning chance is obtained at a smaller rewiring force, and when α is 0, the chance to win is around ϕ_0. When the rewiring force is stronger, it is less likely for the minority to win. In detail, the strategy of rewire-to-foaf has a smaller winning chance than the strategy of rewire-to-random, and a sharp transition is obtained under rewire-to-same.

As we can see, a rich landscape is led by varying the rewiring force α. In this section, the adaptive voter model could reach an early fragmentation under rewire-to-foaf, which gives rise to many smaller monochrome communities. In addition, it is a trade-off between the survival and winning: a smaller α promotes the winning for the minority but hinders the survivability; vice versa for a higher α, the survivability of the minority is better but they will never win. It is inevitable to observe a transition from consensus to fragmentation when α changes from 0 to 1, but different rewiring strategies really can lead to different patterns of transition.

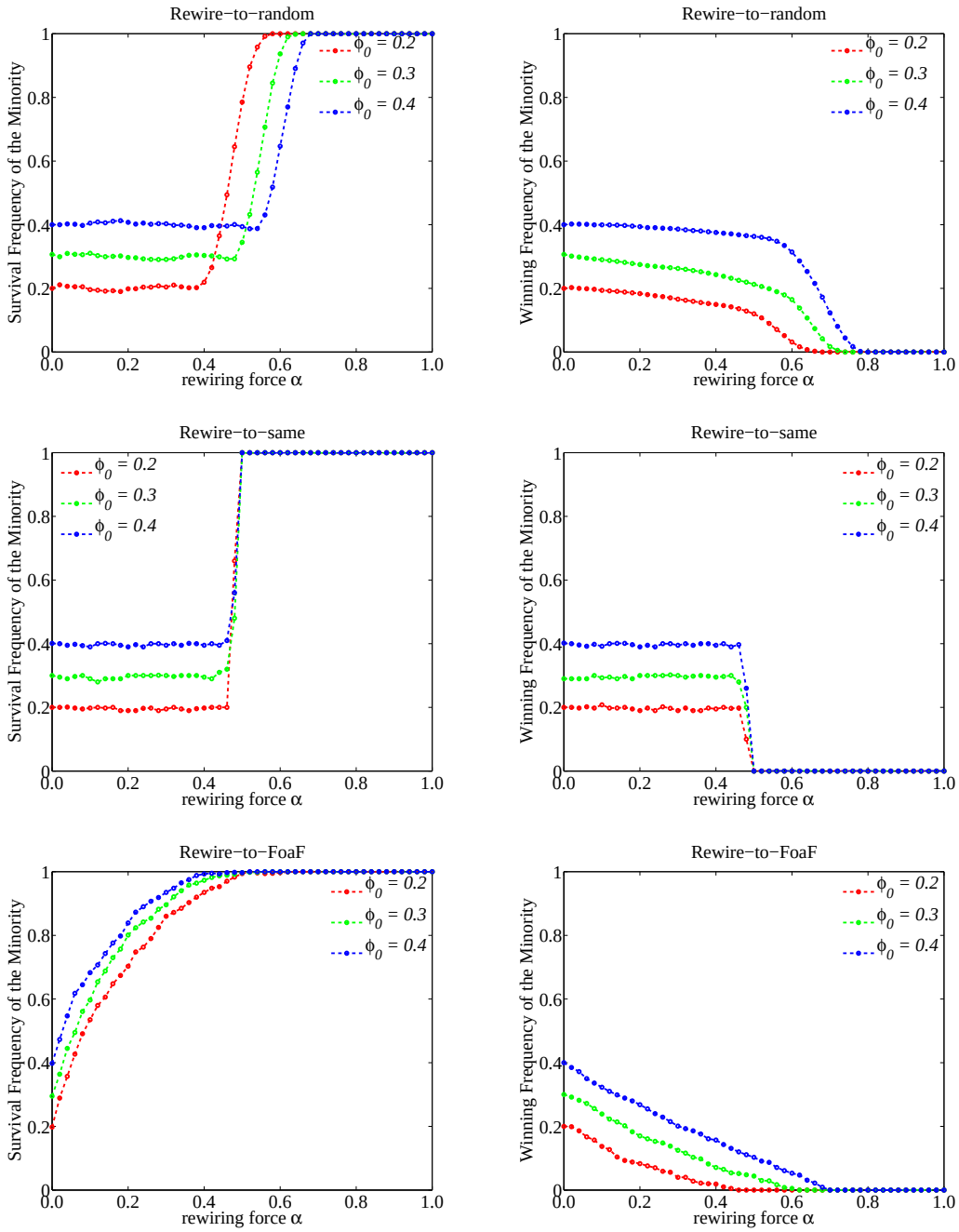

Figure 3.11: Simulation results of the survival (left column) and winning chances (right column) for the initial minority As under different rewiring strategies. Starting from a random network, 1000 independent simulations are run to get the average. The initial fraction of As is $\phi_0 = 0.2, 0.3$ and 0.4 respectively.

3.4 Approximate Majority Model

In most of adaptive voter models, the strategy of direct competition is used for state evolution. Under this strategy, two decided voters (A and B) meet each other and

deal with the discordant edge quickly by imitating the state of the other, for example $AB \rightarrow AA$ and $BA \rightarrow BB$, which are implemented at the same rate.

In many real-world situations, however, the discordant agents are more likely to adopt a neutral (or undecided) state to make a compromise (Vazquez et al., 2003; Castelló et al., 2006; Colaiori et al., 2015; Colaiori and Castellano, 2015). In particular, approximate majority model has been explored from evolving cell cycles (Cardelli and Csikász-Nagy, 2012) to population dynamics (Angluin et al., 2008; Aspnes and Ruppert, 2009), where a neutral state is used as an interim agreement between two discordant states.

3.4.1 A Neutral State

In this study, we will adopt approximate majority approach in the process of state evolution, where a neutral node with a type of C arises when a pair of connected nodes A and B interact. Based on the properties of approximate majority, one node at the end of AB will turn to be undecided, namely: $AB \rightarrow AC$ or $BA \rightarrow BC$. Moreover, the undecided voters will be convinced by any decided voter they meet, which can be shown as: $AC \rightarrow AA$ or $BC \rightarrow BB$. Notably, some flipping actions like $CA \rightarrow CC$ or $CB \rightarrow CC$ are not allowed in the evolution of state, because these actions will form a two-way communication which may lead to the loss of last decided voters (i.e. $[C] = N$). The state transition graph based on approximate majority can be illustrated as Figure 3.12.

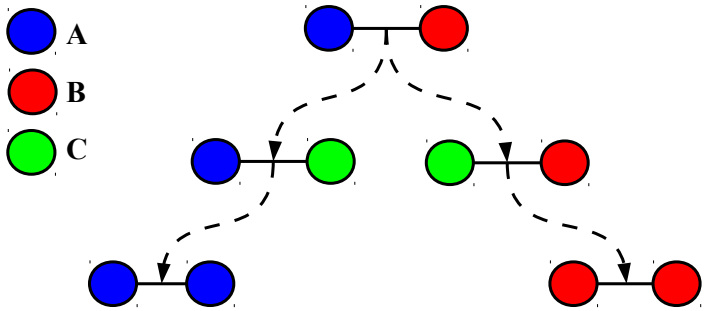

Figure 3.12: State transition graph based on approximate majority model. For any active link AB, a neutral state C is obtained when the two decided nodes A and B interact with each other. And the nodes holding the state of C will be assimilated when the links of AC or BC are in the network.

Many studies (Cardelli and Csikász-Nagy, 2012) have revealed that, under the strat-

egy of direct competition, the convergence is very slow as a random walk and the system is also fragile under a slight perturbation. However, under the strategy of approximate majority, the system will converge to a stationary state quickly, at which the majority turns into the totality. In the following, we will explore the influences of the two state evolution strategies (direct competition and approximate majority) on the adaptive dynamics.

3.4.2 Approximate Differential Equations

Here, we consider an adaptive voter model based on approximate majority like what follows. At each step, a random edge connecting X and Y is picked from the network, and the event of state evolution is implemented with probability $1-\alpha$:

- if $X = Y$, then nothing happens;
- if $X \neq Y \wedge X \neq C \wedge Y \neq C$, then $XY \to XC$ or $YX \to YC$;
- if $X \neq Y \wedge Y = C$, then $XY \to XX$.

Otherwise with probability α, the strategy of rewire-to-random is adopted to do the structure adaptation:

- if $X = Y$, then nothing happens;
- if $X \neq Y \wedge X \neq C \wedge Y \neq C$, then $(XY,Z) \to (XZ,Y)$ or $(YX,Z) \to (YZ,X)$;
- if $X \neq Y \wedge Y = C$, then nothing happens.

where Z is a random node in the network. The above dynamical process continues until all the connecting voters have same state.

In the following, let's derive the ordinary differential equations (ODEs) for the adaptive voter model based on approximate majority. Define $[A],[B],[C]$ as the average numbers of different voters, and $[AA],[AB],[AC],[BA],[BB],[BC],[CC]$ are the average numbers of various edges. The differential equations for voters of A, B and C can be written as Eq. 3.20.

$$\begin{aligned}
\tfrac{\mathrm{d}}{\mathrm{d}t}[A] &= (1-\alpha)([AC]-[BA]) \\
\tfrac{\mathrm{d}}{\mathrm{d}t}[B] &= (1-\alpha)([BC]-[AB]) \\
\tfrac{\mathrm{d}}{\mathrm{d}t}[C] &= (1-\alpha)([AB]+[BA]-[AC]-[BC])
\end{aligned} \tag{3.20}$$

In particular, when $\alpha = 0$ and the voters are interacting in a well-mixed structure, we can obtain following equations:

$$\begin{aligned} \frac{\mathrm{d}}{\mathrm{d}t}[A] &= [A][C] - [B][A] \\ \frac{\mathrm{d}}{\mathrm{d}t}[B] &= [B][C] - [A][B] \\ \frac{\mathrm{d}}{\mathrm{d}t}[C] &= 2[A][B] - [A][C] - [B][C] \end{aligned} \tag{3.21}$$

Let's define a 3-tuple $([A],[B],[C])$ to describe the state of this particular dynamical system, and clearly $[A]+[B]+[C] = N$. When the rewiring force is $\alpha = 0$ and the initial state is $(\phi_0 N, (1-\phi_0)N, 0)$, the system converges to $(0, N, 0)$ when $\phi_0 < 0.5$; while it converges to $(N/3, N/3, N/3)$ when $\phi_0 = 0.5$ (Figure 3.13).

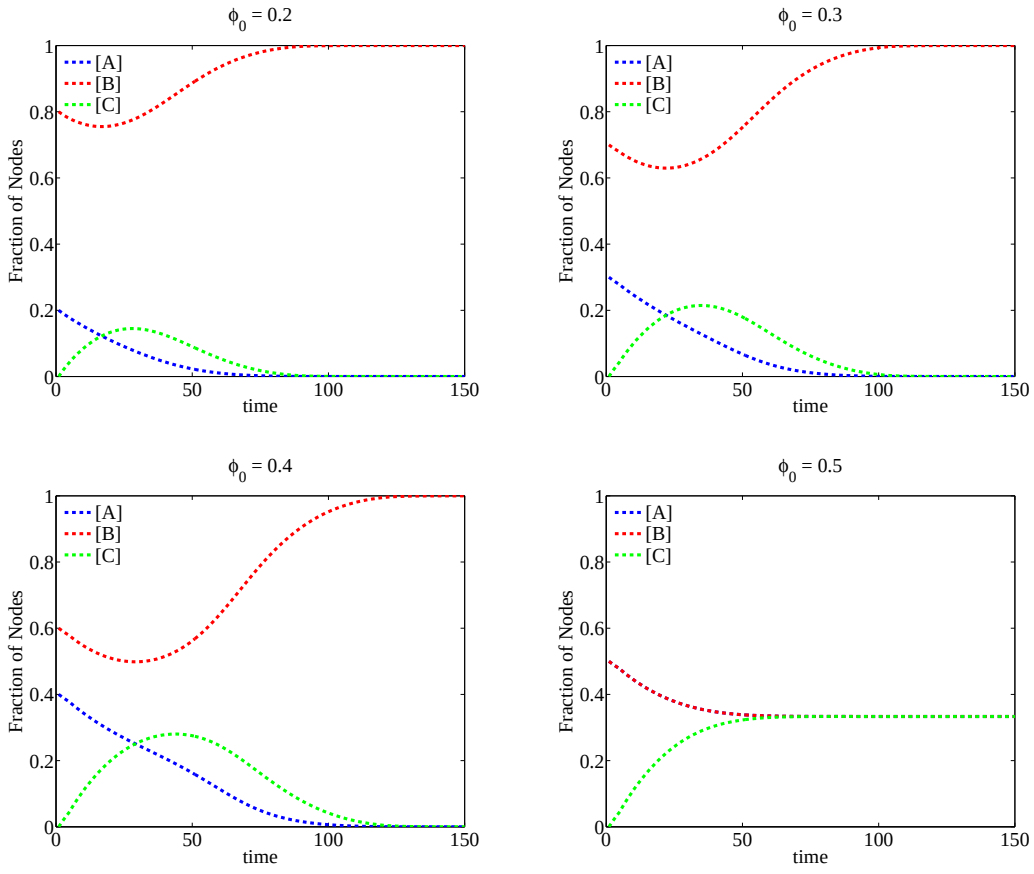

Figure 3.13: Starting from a state with $[C] = 0$, the initial minority with a fraction ϕ_0 will disappear and the majority will turn into the totality. If the two opinions are equal in the beginning, namely $\phi_0 = 0.5$, then we will come to a steady state with $[A] = [B] = [C] = N/3$.

Clearly, four steady states are available for this specified situation: $(N,0,0)$, $(0,N,0)$, $(0,0,N)$, and $(N/3,N/3,N/3)$. However, these steady states (or fixed points) have different stabilities. That is to say if we start from a value close to a certain steady state, then it may drive the development away from that state. For instance $(0,0,N)$, it is an unstable steady state. In addition, the state of $(N/3,N/3,N/3)$ is not stable either, unless we start from an initial state with $[A]_0 = [B]_0 = N/2$. In detail, a stream plot (Figure 3.14) is provided to illustrate the directions of the velocity vectors at different points, which can be used to demonstrate the overall dynamics of the system. It is clear that the majority will turn into the totality in the case of null link-rewiring ($\alpha = 0$) and asymmetric initial fractions ($\phi_0 \neq 0.5$).

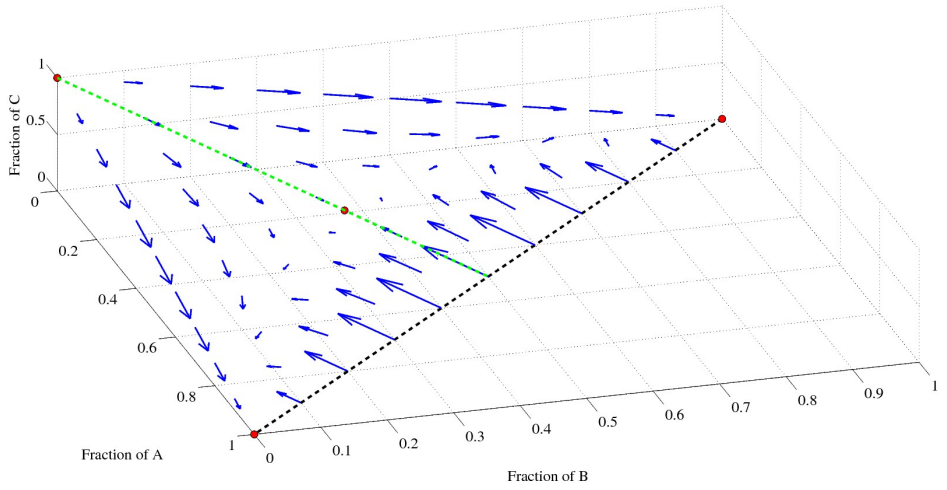

Figure 3.14: We have the directions of evolution presented to show the dynamical process at different points. The red points are the four steady states and the green dashed line indicates the boundary between the basin of all As and that of all Bs.

When the network structure is taken into consideration, we need to write more differential equations to describe the evolution of more detailed motifs. Eq. 3.22 is provided to illustrate the dynamics of various edges in the adaptive voter model based on approximate majority. As we can see, the constructions (or destructions) of a certain type of edges are consequences of local behaviours (namely state evolution and structure adaptation). Notably, some bigger motifs may arise due to the glueings discussed before. In order to make the equations closed, pair approximation (PA) will be adopted to decompose those larger motifs into smaller ones as Eq. 3.9. Implementing the moment-closure ODEs, we can easily obtain the stationary network configurations for varying αs and ϕ_0s.

$$
\begin{aligned}
\tfrac{1}{2}\tfrac{\mathrm{d}}{\mathrm{d}t}[AA] &= (1-\alpha)([AC]+[ACA]-[BAA])+\alpha[AB]\tfrac{[A]}{N} \\
\tfrac{\mathrm{d}}{\mathrm{d}t}[AB] &= (1-\alpha)(-[AB]-[ABA]+[ACB]-[BA]-[BAB]+[BCA]) \\
&\quad -\alpha([AB](1-\tfrac{[B]}{N})+[BA](1-\tfrac{[A]}{N})) \\
\tfrac{\mathrm{d}}{\mathrm{d}t}[AC] &= (1-\alpha)([AB]+[ABA]-[AC]-[ACA]+[ACC]-[BAC]+[BAA]-[BCA]) \\
&\quad +\alpha[AB]\tfrac{[C]}{N} \\
\tfrac{1}{2}\tfrac{\mathrm{d}}{\mathrm{d}t}[BB] &= (1-\alpha)([BC]+[BCB]-[ABB])+\alpha[BA]\tfrac{[B]}{N} \\
\tfrac{\mathrm{d}}{\mathrm{d}t}[BC] &= (1-\alpha)([BA]+[BAB]-[BC]-[BCB]+[BCC]-[ABC]+[ABB]-[ACB]) \\
&\quad +\alpha[BA]\tfrac{[C]}{N} \\
\tfrac{1}{2}\tfrac{\mathrm{d}}{\mathrm{d}t}[CC] &= (1-\alpha)(-[CCA]+[CBA]-[CCB]+[CAB])
\end{aligned}
\tag{3.22}
$$

3.4.3 Examples

We start from a random graph with the number of nodes N and the number of edges E to implement a series of simulations. There is not any neutral voter C in the beginning, and the voters holding A are the initial minority with a fraction of ϕ_0. All the nodes are uniformly distributed within the network. Under the strategy of approximate majority, the voters holding C will come into the system due to the disagreement between A and B, but they will be eliminated eventually according to the rules described before (namely $AC \to AA$ and $BC \to BB$). Meanwhile, the C-relevant links are rewiring free, which leads to $[C] = 0$ at frozen state. In the following, different initial fraction ϕ_0s and rewiring force αs are explored to illustrate some global properties.

3.4.3.1 The Dominance of Majority

First, let's see the final fraction of voters holding A based on direct competition and approximate majority in Figure 3.15, where the initial fraction of As is $\phi_0 = 0.2, 0.3$ and 0.4 respectively. When the rewiring force α is close to 1, the two strategies have similar results with the final fraction of As around the initial fraction ϕ_0. However, when α is smaller, the voters holding A under approximate majority drop to a much

lower level. While the average fraction of As under direct competition is still around its initial fraction ϕ_0.

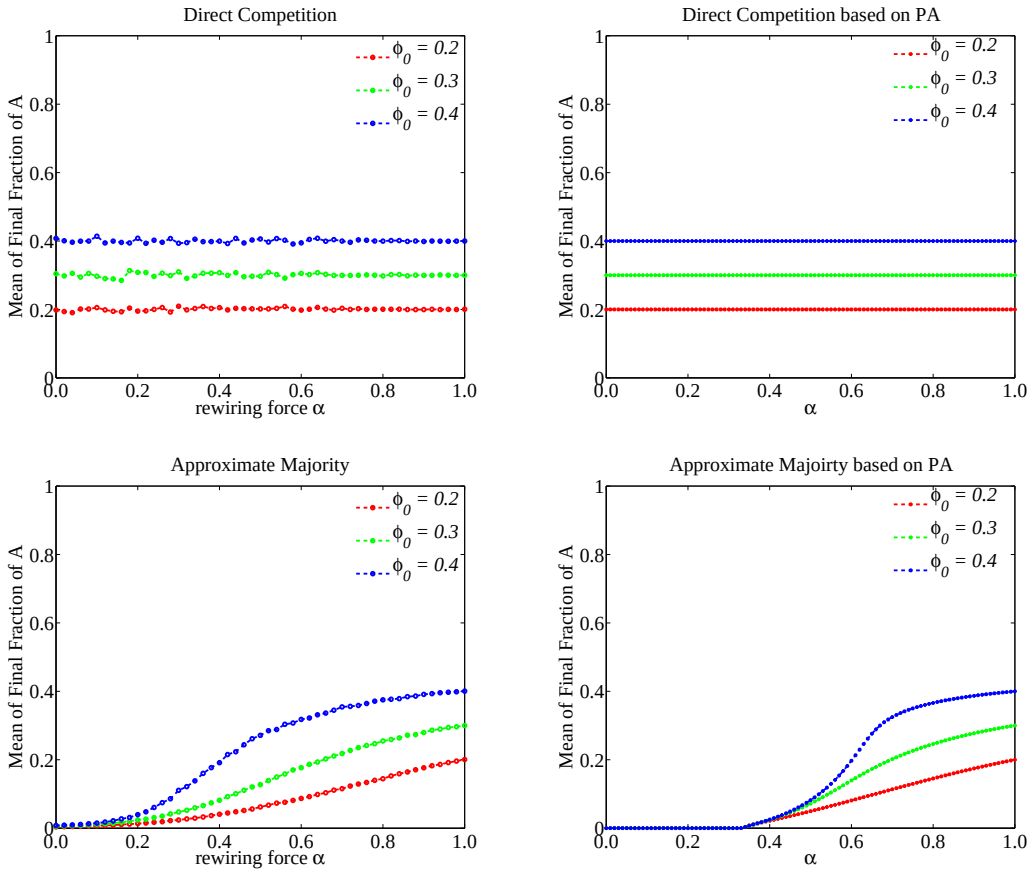

Figure 3.15: The final fraction of As is obtained from the numerical simulations (left column) and ODEs (right column). Given a random network with $N = 1000$ and $E = 2000$, 1000 identical and independent simulations are run to get the average. The stationary fraction of As is presented based on direct competition (upper row) and approximate majority (lower row). Interestingly, when the rewiring force is weaker, the minority becomes extinct under the strategy of approximate majority and the majority turns into the totality at $\alpha = 0$.

Intuitively, for an active link AB, both A and B may turn to C, but the number of generated BC is bigger that of AC due to the bigger fraction of Bs in the beginning. In this way, more nodes will be assimilated by Bs. When α gets smaller, the evolution of state runs quickly, and it is easier for the majority to convince most of the voters, leading to the dominance of majority.

3.4.3.2 Survival and Winning

Let's use the definitions for winning and survival described before, and a group of voters holding A are the minority in the beginning with an initial fraction of ϕ_0. As shown in Figure 3.16, under the strategy of approximate majority (lower row), the initial minority has no chance to win and the chance to survive drops to 0 at smaller αs. The undecided voter C is more likely to meet a voter with majority preference, which leads to a bigger pressure moving towards the majority state. Therefore, the introduction of a neutral state C in a binary network facilitates the dominance of the majority; on the other hand, it brings about the difficulty for the minority to win and even survive.

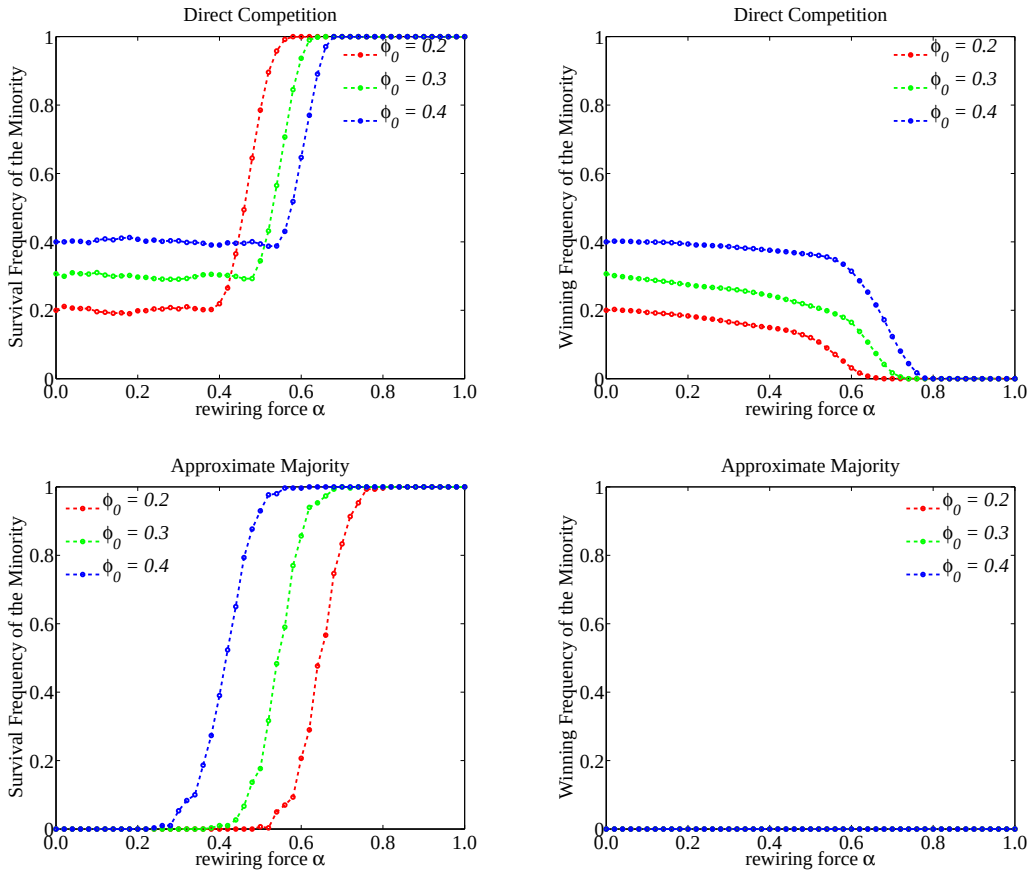

Figure 3.16: The chances of survival (left column) and winning (right column) are presented for the minority (namely As), whose initial fraction is $\phi_0 = 0.2, 0.3$ and 0.4 respectively. The strategy of direct competition (upper row) and approximate majority (lower row) give rise to quite different results for the fate of the minority.

3.5 Weighted Voter Model

The evolution of state discussed before (Durrett et al., 2012; Holme and Newman, 2006) lets all agents have equal weights, which are independent of their neighbourhood configurations. In this section, the original model in Ref. (Durrett et al., 2012) is generalized so that the imitation step is modulated by a local linear signal sent by each agent and which summarises their neighbourhoods.

3.5.1 Weighted Nodes and Biased Imitation

As before, each agent can be of one of two states (or colors, types): A or B. We write s_i for the state of agent i, and $NB(i)$ for the set of neighbours of i, who are the agents i can directly interact with. Here, we introduce the notion of weight of a node to indicate the fitness of the voter in the system, just like the games in adaptive networks (see more details (Zimmermann et al., 2004; Santos et al., 2006; Zschaler, 2012) in Chapter 2). Suppose given a 2×2 matrix Π with real coefficients, the weight of a node, in a given state of the system, is defined by:

$$\pi_i = \sum_{j \in NB(i)} \Pi(s_i, s_j) \tag{3.23}$$

In general, we will write:

$$\Pi = \begin{array}{c} \\ A \\ B \end{array} \begin{array}{c} \begin{array}{cc} A & B \end{array} \\ \begin{pmatrix} R & S \\ T & P \end{pmatrix} \end{array} \tag{3.24}$$

The relative weights of neighbours (of different states) are used to determine which is more likely to imitate which. The higher the weight ratio between i and j is, the likelier is j to imitate i.

Depending on how one sets up the interaction matrix Π, different types of propagation can be obtained. If $\Pi = I$, then the weight π_i measures the number of "same" in i's neighbourhood. Of two opposing neighbours, the one with most neighbours of the same type will dominate the imitation game. This effect is self-reinforcing, where imitation will tend to increase the dominant node's weight. On the contrary, one can set Π so that weights measure the number of "different" and obtain a negative feedback leading to homeostatic behaviours.

Given an interaction matrix Π, we can obtain the weights of two neighbouring agents: π_i and π_j, and then the probability that i adopts the state of j is defined as

$p(s_i \to s_j)$, which can be calculated based on the Fermi distribution (Traulsen et al., 2006):

$$p(s_i \to s_j) = \frac{1}{1+e^{-\beta(\pi_j - \pi_i)}} \tag{3.25}$$

where $\beta \geq 0$ is a parameter indicating the selection strength. If we think of π_i as (minus) the energy of a node, then β can be seen as the inverse of a temperature. The smaller β, the weaker the bias towards higher weights. For $\beta = 0$, we find again the original voter model from Ref.(Durrett et al., 2012). On the other hand, if $\beta \to +\infty$, the agent with a higher weight always wins and the imitation mechanism becomes directed (unless both nodes have the same weight).

In contrast to state evolution, the structure rewiring is unbiased in that when an active link is set to rewire with probability α, a random node is redirected by that link. The structure adaptation is a kind of dynamical spatial selection, where the weight of an agent will change with the adjustment of its local neighbourhood. While imitation promotes consensus, the rewiring facilitates the assortment of same-color nodes which leads to network fragmentation.

As we can see, the main difference in the weighted voter model is the biased state evolution, which will bring about a quite different result from that in Ref. (Durrett et al., 2012).

3.5.2 Approximate Differential Equations

There are correlations between *AB*, *AA* and *BB* motifs which one might need to take into account. To do this, we use triplet motifs, such as *AAA*, *AAB*, *ABA*, *BBA*, *BAB*, and *BBB*, to estimate local statistics on agents' neighbourhoods as in Figure 3.17.

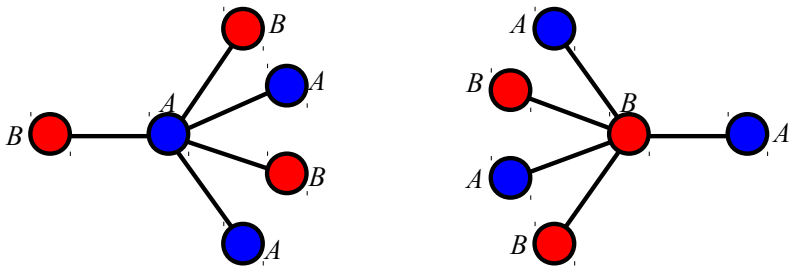

Figure 3.17: The approximate neighbourhood configurations: we assume agents of A with an active link AB have $[BAA]/[AB]$ neighbours of type A and $1+[BAB]/[AB]$ neighbours of type B; similarly for B agents.

Thus, we get refined approximations for the mean weights and imitation probabilities of agents connected by an edge of AB as follows.

$$\begin{aligned} \pi_A &= R[BAA]/[AB] + S(1+[BAB]/[AB]) \qquad p(A\to B) = \tfrac{1}{1+e^{-\beta(\pi_B-\pi_A)}} \\ \pi_B &= T(1+[ABA]/[AB]) + P[ABB]/[AB] \qquad p(B\to A) = \tfrac{1}{1+e^{-\beta(\pi_A-\pi_B)}} \end{aligned} \tag{3.26}$$

Putting things together, we get the ODEs for the weighted voter model as follows.

$$\begin{aligned} \tfrac{\mathrm{d}}{\mathrm{dt}}[A] &= (1-\alpha)[AB]\big(p(B\to A)-p(A\to B)\big) \\ \tfrac{\mathrm{d}}{\mathrm{dt}}[B] &= (1-\alpha)[AB]\big(p(A\to B)-p(B\to A)\big) \\ \tfrac{\mathrm{d}}{\mathrm{dt}}[AB] &= (1-\alpha)\big(p(A\to B)([BAA]-[BAB]) \\ &\quad + p(B\to A)([ABB]-[ABA])\big) + (\tfrac{\alpha}{2}-1)[AB] \\ \tfrac{1}{2}\tfrac{\mathrm{d}}{\mathrm{dt}}[AA] &= (1-\alpha)\big(p(B\to A)[ABA]-p(A\to B)[BAA]\big) \\ &\quad + [AB]\big((1-\alpha)p(B\to A)+\tfrac{\alpha[A]}{2N}\big) \\ \tfrac{1}{2}\tfrac{\mathrm{d}}{\mathrm{dt}}[BB] &= (1-\alpha)\big(p(A\to B)[BAB]-p(B\to A)[ABB]\big) \\ &\quad + [AB]\big((1-\alpha)p(A\to B)+\tfrac{\alpha[B]}{2N}\big) \end{aligned} \tag{3.27}$$

As we can see, it remains to close the above equations, and break our triplet observables into smaller ones. Here we adopt pair approximation (PA) to do that as discussed before.

3.5.3 Examples

We build an ER random network with N nodes and E edges to investigate our weighted voter model numerically and compare the approximations with simulations. The initial fraction of As is written by ϕ_0, and opinions are assigned uniformly at random once ϕ_0 is given. In particular, we will explore the dynamics by varying rewiring force α, network connectivity (namely average degree) $\langle k\rangle = 2E/N$ and selection strength β. The evolution stops when the simulation converges to a frozen state $[AB]=0$, and 30 independent simulations are run to compute an empirical average.

3.5.3.1 Simulations and Approximations

Now, let's come to the asymmetric imitation where the selection strength is set as $\beta = 10$, and the weight parameters are: $R = 1.0$, $S = -1.0$, $T = 2.0$ and $P = 0.0$. This choice implies that flipping from A to B always results in an increase of one's rate while, paradoxically, the aggregate weight decreases. We focus again on the long-term behaviour, especially the average fraction of As, for different αs. The simulation is led in a random network with $N = 1000$ and $E = 2000$. The initial fraction of As ranges in $\{0.1, 0.3, 0.5, 0.7, 0.9\}$. Figure 3.18 displays the results of average fraction of As at stationary state.

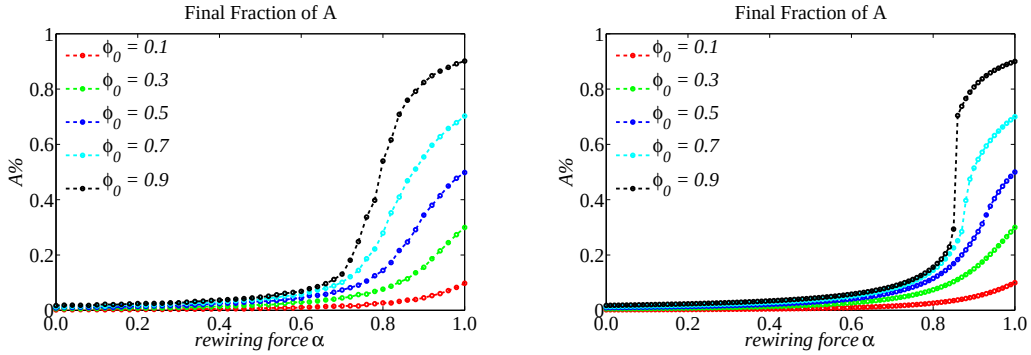

(a) Simulation results

(b) Approximation results

Figure 3.18: The final fraction of As under different rewiring force αs and initial fraction ϕ_0s. The numerical simulations (left panel) and PA-based ODEs (right panel) are carried out in a random network.

Under asymmetric imitation one can see that it is impossible for As to win over a consensus state. However, As are better conserved with higher αs where the network is more likely to be fragmented into several monochrome communities. At any rate, the final fraction of As is always less than its initial one ϕ_0. When $\alpha > 0$ the final fraction of As increases with α to reach the initial value ϕ_0 only when $\alpha = 1.0$. This phenomenon is quite different from symmetric imitation, where the average fraction of As is constant with the increase of α (see Figure 3.15). In the case of $\phi_0 > 0.5$, the initial majority will become extinct at a smaller α, which is due to the weighted agents and biased imitation. On the contrary, the initial minority with quite high weights will take over the population. This weighted voter model reflects rich behaviours in social networks, where a small fraction of "powerful" people are able to convince the majority to follow their opinions.

3.5.3.2 Network Connectivity

Ref. (Ranjbar-Sahraei et al., 2014) studies the influence of network connectivity on the consensus formation in static networks. We see similarities in the adaptive case. We take a set of weight parameters: $R = 1.0$, $S = -1.0$, $T = 2.0$ and $P = 0.0$, and the selection strength is $\beta = 10$. Figure 3.19 shows the final fraction of As using a sparser random network with $\langle k \rangle = 2E/N = 4$ and a denser random network with $\langle k \rangle = 2E/N = 10$. Of course, the two networks have same size $N = 1000$.

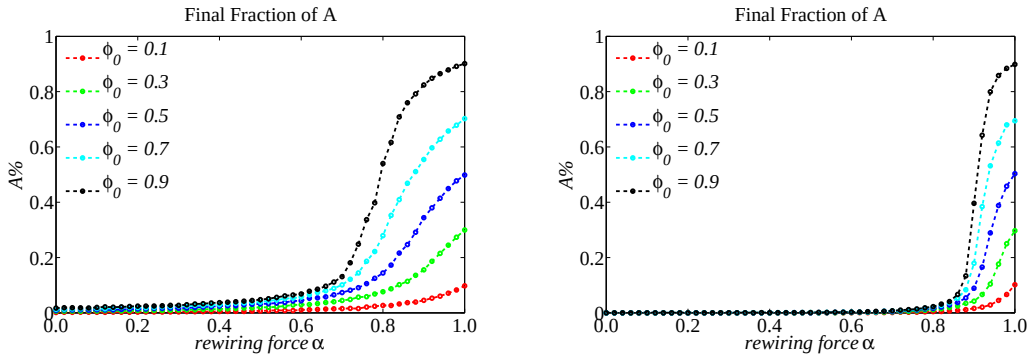

(a) $\langle k \rangle = 4$ (b) $\langle k \rangle = 10$

Figure 3.19: The final fraction of As under different rewiring force αs and initial fraction ϕ_0s. Figure (a) shows the results in a sparser network with $\langle k \rangle = 4$, and figure (b) shows the results in a denser network with $\langle k \rangle = 10$. Both networks have a size of $N = 1000$.

For this specific setting, we find that the higher network connectivity decreases the chance of fragmentation when $\alpha < 1$, meanwhile the final fraction of As decreases. The intuitive reason why a higher average degree inhibits the propagation of As (for our specific choices of Π parameters), is that Bs will get higher weights ($T\langle k \rangle/2 + P\langle k \rangle/2$), but As cannot increase theirs ($R\langle k \rangle/2 + S\langle k \rangle/2$). Essentially, network consensus is promoted due to Bs becoming stronger. When $\alpha = 1$, unsurprisingly, both A and B remain.

3.5.3.3 Selection Strength

Besides the rewiring force and network connectivity, another important factor is the selection strength β, which determines the imitation bias. As discussed earlier, the selection strength can be seen as the inverse of a temperature, where a high β brings deterministic imitation (namely a voter with a higher payoff will always win). Let's start from a random network with $N = 1000$, $E = 2000$ and $\langle k \rangle = 4$, and we have a

certain rewiring force $\alpha = 0.5$. A set of weight parameters are: $R = 1.0$, $S = -1.0$, $T = 2.0$ and $P = 0.0$. With the initial fraction of As in $\{0.1, 0.3, 0.5, 0.7, 0.9\}$, we provide their final fraction in Figure 3.20 with the selection strength varying from 0 to 10.

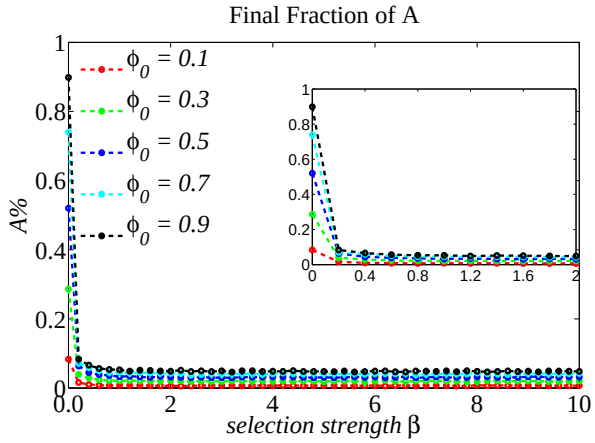

Figure 3.20: The final fraction of As under different selection strength βs ranging in $[0, 10]$ for various initial fraction ϕ_0s. The simulation is carried out in a network with $N = 1000$, $E = 2000$ and $\langle k \rangle = 4$, and the rewiring force is $\alpha = 0.5$.

Given a fixed α, the final fraction of As changes from ϕ_0 to a quite lower fraction with the increase of selection strength β. When β is smaller, the nodes of A fare better thanks to the randomness in imitation. This is especially true when $\beta = 0$, where the average final fraction of As is equal to its initial fraction ϕ_0. When β is just a little bit bigger, the selection gets stronger and the imitation becomes asymmetric, leading to the progressive demise of As.

3.6 Approximation Techniques

As mentioned before, the differential equation associated with a motif g generally involves bigger motifs led by overlapping g and the left-hand sides of various rules. For example, in Figure 3.21, a transition $AB \to AA$ leads to the changes of $ABA \to AAA$ and $ABB \to AAB$, which will influence the number of AB links. Specifically, besides the decrease of the focal AB, $ABA \to AAA$ will cause an additional decrease of AB, while $ABB \to AAB$ will bring an additional increase of AB.

In principle, one could iterate Eq. 3.5 to obtain a system of ODEs for the evolution of the observables of interest. But in general such a development will be infinite, especially when the size of network is quite large and network patterns are diverse.

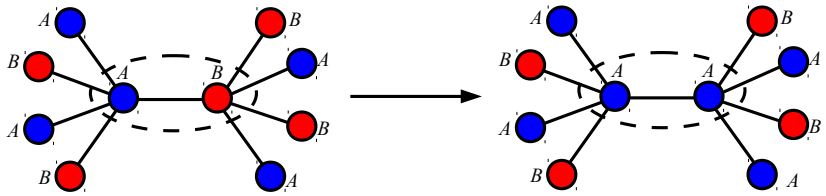

Figure 3.21: An example shows the coupled motifs under the rule $AB \to AA$, where the dynamics of motif observable $[AB]$ involves bigger motifs ABA and ABB.

Therefore, some methods to truncate the expansions and obtain a manageable finite approximate differential equations should be studied.

3.6.1 From Pair Approximation to Interface Approximation

Pair approximation (PA) (Ellner, 2001) is widely used to truncate and express the bigger motif as a function of smaller ones. Let $g = g_1 \cup g_2$ and $h = g_1 \cap g_2$, and then we can express the bigger motif through its subgraphs,

$$[g] \simeq \frac{[g_1][g_2]}{[h]} \tag{3.28}$$

which is based on an assumption of conditional independence. In pair approximation, it is assumed that the edges are uniformly distributed within the network, where each smaller motif g_1 is associated with $[g_2]/[h]$ bigger motif g. However, this approximation usually underestimates the observable $[g]$ by adopting an inaccurate denominator $[h]$, which contains some negative applicable cases. Therefore, some approaches are required to exclude those "special" hs.

In the voter model, the ODEs presented before involve many triplet observables $[AAB]$, $[ABA]$, $[BAB]$, etc. which are decomposed by pairs $[AA]$, $[AB]$, $[BB]$ and single nodes $[A]$ and $[B]$. Nevertheless, this approximation ignores correlations among edges of type AB, AA and BB. This is particularly consequential for fragmentable systems, as the distribution of AB links is (very) far from uniform. Specifically, the long-ranged motifs involving the active links, such as ABA and BAB, show a strong correlation close to the fragmentation.

To handle this problem, we distinguish agents of A which see no Bs and those who do (Figure 3.22). We write $[A_I]$ for the observable counting those interfacial agents.

The idea is that only agents in the interface should be used to approximate active triplet motifs. In PA, we suppose that AA and AB links are uniformly distributed among

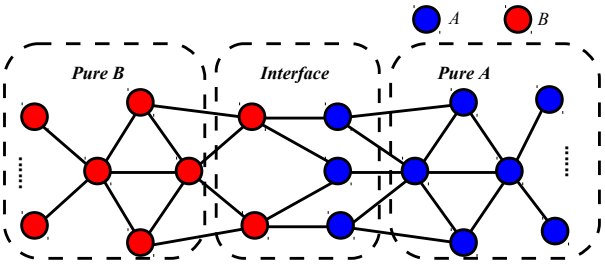

Figure 3.22: Decomposition of the network structure: agents of type A are either connected by active links in which case they belong to the interface, or all of their neighbours are of the same type, and they are in the *pure A* subset. Similarly for B agents.

all As, and each of them has $[AA]/[A]$ neighbours of type A and $[AB]/[A]$ neighbours of type B. But it is inaccurate to take some "special" As (connected only by the neighbours holding A) into the interface, where the voter A should have $[AB]/[A_I]$ neighbours of type B in average. Therefore, to obtain a better approximation, we need to estimate $[A_I]$, the number of As in the interface.

Starting from a random network, the random rewiring strategy doesn't affect the degree distribution of the network. Therefore, we make two assumptions as follows to illustrate the distribution of the degree as well as the configurations of the neighbourhood. For the nodes holding a state A, we have:

- the degree of node A follows a Poisson distribution with average degree $k_A = ([AA]+[AB])/[A]$;
- the neighbourhood configuration of an A follows a binomial distribution, namely any one of its neighbours will be the state of A with probability $p_{AA} = [AA]/([AA]+[AB])$ and be the state of B with probability $p_{AB} = [AB]/([AA]+[AB])$.

Similar method can be used for B, and we have $k_B = ([AB]+[BB])/[B]$, $p_{BB} = [BB]/([BB]+[AB])$, and $p_{BA} = [AB]/([BB]+[AB])$.

As a result, the interfacial agents can be approximated as:

$$\begin{aligned} [A_I] &= [A]\sum_{k=1}^{N-1} f(k,k_A)\left(\sum_{i=1}^{k}\binom{k}{i}p_{AB}^{i}p_{AA}^{k-i}\right) < [A] \\ [B_I] &= [B]\sum_{k=1}^{N-1} f(k,k_B)\left(\sum_{i=1}^{k}\binom{k}{i}p_{BA}^{i}p_{BB}^{k-i}\right) < [B] \end{aligned} \tag{3.29}$$

where $f(k,k_A) = \frac{k_A^k e^{k_A}}{k!}$ indicates the probability an agent of A has a degree k under the Poisson distribution.

This approximation computes the number of triplets associated with active links as:

$$[BAB] \simeq \frac{[AB][AB]}{[A_I]} > \frac{[AB][AB]}{[A]}$$
$$[ABA] \simeq \frac{[AB][AB]}{[B_I]} > \frac{[AB][AB]}{[B]} \tag{3.30}$$

The above approximation is called interface approximation (IA), which distinguishes the agents in the interface from the whole population. The differential equations are same as the case based on pair approximation, which means IA is equally cheap as PA in terms of computation cost.

3.6.1.1 Examples

Now, let's come to an example of adaptive voter model under rewire-to-random, where a random active link AB is selected at each step to do the evolution of state with probability $1-\alpha$ and to do the adaptation of structure with probability α. We capture the final fraction of the minority for different αs. As before, the simulation is led in a random network with $N = 1000$, $E = 2000$. The initial fraction of As is $\phi_0 = 0.2, 0.3$ and 0.4 respectively. Figure 3.23 displays the simulation results as well as the approximations (Eq. 3.7) based on PA and IA. Notably, the triplets truncations are different, where PA is implemented as Eq. 3.9 and IA is implemented as Eq. 3.30.

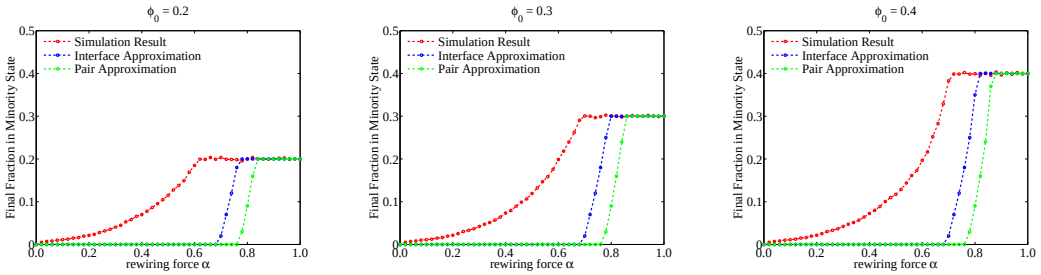

Figure 3.23: The final fraction of the minority under rewire-to-random with the increase of rewiring force α. The initial fraction of As is $\phi_0 = 0.2$ (left), 0.3 (middle) and 0.4 (right) respectively. We present the results from numerical simulation, PA-based ODEs and IA-based ODEs in different colors.

We also implement the weighted voter model to observe the performance of these approximation methods. In detail, we take a set of weight parameters $T > R > P > S$ to build a prisoner's dilemma (PD) interaction payoff matrix. As for the coupled dynamics, the evolution of state occurs with probability $1-\alpha$, where a biased imitation

based on Fermi distribution (see Eq. 3.25) is introduced to enhance the success of an agent with a higher weight. The structure rewiring is implemented by adopting the strategy of rewire-to-random. Figure 3.24 presents the results of numerical simulations and analytical calculations based on PA and IA .

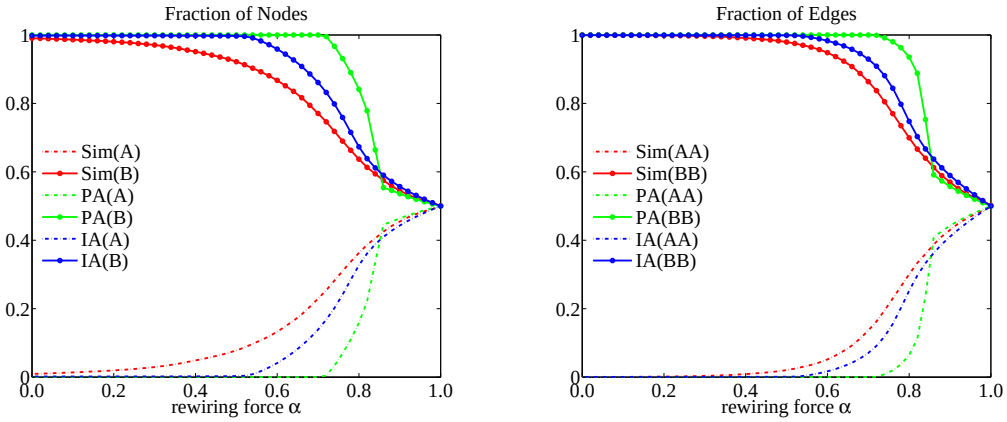

Figure 3.24: The final fraction of different types of nodes and edges under different rewiring force αs in the weighted voter model. With an initial fraction $\phi_0 = 0.5$, the numerical simulation, PA-based ODEs and IA-based ODEs are undertaken in a random network with $N = 1000$, $E = 2000$ and $\langle k \rangle = 4$, and the selection strength is $\beta = 0.1$. The weight parameters are $R = 1.0$, $S = -1.0$, $T = 2.0$ and $P = 0.0$.

When we change the weight parameters to the case of coordination game with $R \simeq P > S \simeq T$, we come to another example of weighted voter model. In this situation, two adjacent nodes sharing same state benefit mutually. Figure 3.25 demonstrates the results of numerical simulations and analytical calculations based on PA and IA.

As we can see in Figure 3.23, 3.24 and 3.25, the interface approximation (IA) method has promoted the accuracy to a relatively higher level than pair approximation (PA), but is same in computation cost.

3.6.2 From Approximate Master Equations to Double Stars Approximation

In this section, we intend to capture the adaptive dynamics through a series of master equations of more detailed motifs (Gleeson, 2011, 2013; Durrett et al., 2012). The motif observables are various star-like structures as shown in Figure 3.26.

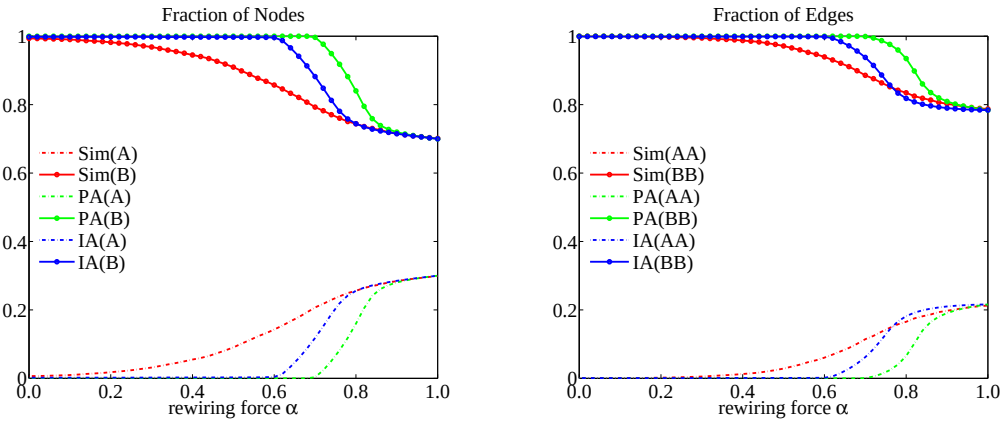

Figure 3.25: The final fraction of different types of nodes and edges under different rewiring force αs in the weighted voter model. With an initial fraction $\phi_0 = 0.3$, the numerical simulation, PA-based ODEs and IA-based ODEs are undertaken in a random network with $N = 1000$, $E = 2000$ and $\langle k \rangle = 4$, and the selection strength is $\beta = 0.1$. The weight parameters are $R = 1.0$, $S = 0.0$, $T = 0.0$ and $P = 1.0$.

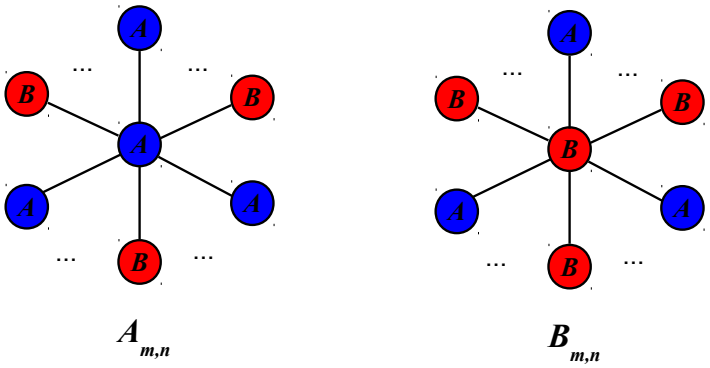

Figure 3.26: The star structure $A_{m,n}$ means a focal agent holding a state A has m neighbours of A and n neighbours of B. Similarly, for $B_{m,n}$, it means a focal agent holding a state of B has m neighbours of A and n neighbours of B.

3.6.2.1 Approximate Master Equations

Approximate master equations (AME) for adaptive voter models were studied in Ref. (Durrett et al., 2012), where people investigated to construct a system of closed star-like motifs. To capture the dynamics of the stars, we need to consider the following 5 types of dynamics, which are demonstrated through an motif $A_{m,n}$.

- the state flipping of the focal agent, where $A_{m,n} \to B_{m,n}$ leads to the decrease of $A_{m,n}$, but the reverse action $B_{m,n} \to A_{m,n}$ leads to the increase of $A_{m,n}$.

- the state flipping of the neighbours, where $A_{m,n} \to A_{m-1,n+1}$ (a neighbour holding A changes to B) and $A_{m,n} \to A_{m+1,n-1}$ (a neighbour holding B changes to A) will lead to the decrease of $A_{m,n}$, but the reverse actions will lead to the increase of $A_{m,n}$.

- the addition of edges, where $A_{m,n} \to A_{m+1,n}$ (adding a new neighbour holding A) and $A_{m,n} \to A_{m,n+1}$ (adding a new neighbour holding B) will lead to the decrease of $A_{m,n}$, but $A_{m-1,n} \to A_{m,n}$ and $A_{m,n-1} \to A_{m,n}$ will lead to the increase of $A_{m,n}$.

- the removal of edges, where $A_{m,n} \to A_{m-1,n}$ (removing a neighbour holding A) and $A_{m,n} \to A_{m,n-1}$ (removing a neighbour holding B) will lead to the decrease of $A_{m,n}$, but $A_{m+1,n} \to A_{m,n}$ and $A_{m,n+1} \to A_{m,n}$ will lead to the increase of $A_{m,n}$.

- the swapping of edges, where $A_{m,n} \to A_{m-1,n+1}$ (swapping a neighbour holding A to other one holding B) and $A_{m,n} \to A_{m+1,n-1}$ (swapping a neighbour holding B to other one holding A) will lead to the decrease of $A_{m,n}$, but the reverse actions $A_{m-1,n+1} \to A_{m,n}$ and $A_{m+1,n-1} \to A_{m,n}$ will lead to the increase of $A_{m,n}$.

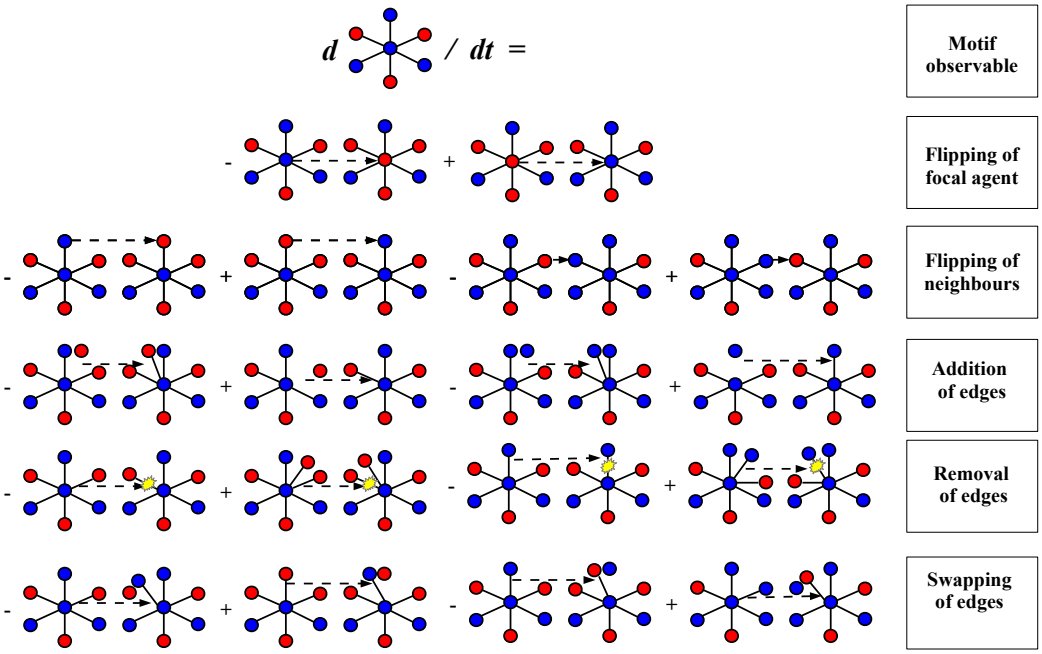

Figure 3.27: The dynamics of a star motif $A_{m,n}$ are illustrated by a series of flipping and swapping actions. The differential equation for $A_{m,n}$ involves the ones with the configurations of $B_{m,n}$, $A_{m\pm1,n}$, $A_{m,n\pm1}$ and $A_{m\pm1,n\pm1}$.

As illustrated in Figure 3.27, we obtain the master equation for $A_{m,n}$ to describe the adaptive dynamics. Similarly, we can also write the master equations for $B_{m,n}$. Let's suppose the maximal degree of a voter is $k_{\max}$, and the size of AME system is $2k_{\max}^2$, which is much bigger than the size of ODEs based on PA or IA.

$$\begin{aligned}
\tfrac{\mathrm{d}}{\mathrm{d}t}[A_{m,n}] \;=\;& -\lambda_{A_{m,n}}^{A\to B}[A_{m,n}] + \lambda_{A_{m,n}}^{B\to A}[B_{m,n}] \\
& - \textstyle\sum_{u\in NB(A_{m,n})\wedge s_u=A} \lambda_u^{A\to B}[A_{m,n}] + \sum_{u\in NB(A_{m,n})\wedge s_u=A} \lambda_u^{A\to B}[A_{m+1,n-1}] \\
& - \textstyle\sum_{u\in NB(A_{m,n})\wedge s_u=B} \lambda_u^{B\to A}[A_{m,n}] + \sum_{u\in NB(A_{m,n})\wedge s_u=B} \lambda_u^{B\to A}[A_{m-1,n+1}] \\
& - \mu_{A_{m,n}}^{-A}[A_{m,n}] - \mu_{A_{m,n}}^{-B}[A_{m,n}] + \mu_{A_{m+1,n}}^{-A}[A_{m+1,n}] + \mu_{A_{m,n+1}}^{-B}[A_{m,n+1}] \\
& - \mu_{A_{m,n}}^{+A}[A_{m,n}] - \mu_{A_{m,n}}^{+B}[A_{m,n}] + \mu_{A_{m-1,n}}^{+A}[A_{m-1,n}] + \mu_{A_{m,n-1}}^{+B}[A_{m,n-1}] \\
& - \mu_{A_{m,n}}^{-A+B}[A_{m,n}] - \mu_{A_{m,n}}^{+A-B}[A_{m,n}] + \mu_{A_{m-1,n+1}}^{+A-B}[A_{m-1,n+1}] + \mu_{A_{m+1,n-1}}^{-A+B}[A_{m+1,n-1}]
\end{aligned} \tag{3.31}$$

where $\lambda_{A_{m,n}}^{A\to B}$ indicates the rate for the transition $A_{m,n}\to B_{m,n}$; $\lambda_u^{A\to B}$ indicates the rate that a neighbouring agent $u\in NB(A_{m,n})\wedge s_u=A$ changes its state from A to B; $\mu_{A_{m,n}}^{-A}$ indicates the rate to remove a neighbour holding A from $A_{m,n}$; $\mu_{A_{m,n}}^{+A}$ indicates the rate to add a new neighbour holding A to $A_{m,n}$; and $\mu_{A_{m,n}}^{-A+B}$ indicates the rate for $A_{m,n}$ to disconnect a neighbour holding A but connect to a new one holding B.

Here, we should notice that the neighbourhood configurations of the neighbours are not mentioned. In Ref. (Durrett et al., 2012), for a star motif $A_{m,n}$, it is supposed that all the neighbours holding A are indifferent with a configuration $A_{1+[AAA]/[AA],[AAB]/[AA]}$; and all the neighbours holding B have a configuration $B_{1+[ABA]/[AB],[ABB]/[AB]}$. As for the star motif $B_{m,n}$, we can draw similar approximations. Figure 3.28 provides the corresponding neighbourhood configurations for the stars and their neighbours.

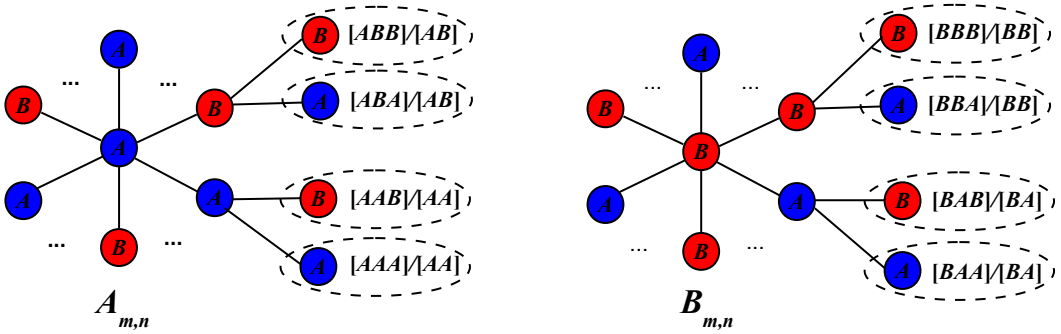

Figure 3.28: The approximate neighbourhood configurations of star motifs $A_{m,n}$ and $B_{m,n}$ in AME.

As for the number of various nodes, pairs and triplets, all of them can be approximated through those star motifs, for example the number of active triplets ABA can be calculated as $[ABA] = \sum_{m,n} m(m-1)[B_{m,n}]$.

3.6.2.2 Double Stars Approximation

Based on the previous AME, we intend to approximate the neighbourhood configurations more precisely. We can group two stars connected by an edge ij with isomorphic neighbourhood pairs in $\langle NB(i), NB(j)\rangle$, in this way a motif of "double stars" is obtained. Only finitely many of these monomials are not zero, so the above sum is finite. In double stars approximation (DSA), the doublet defined as $A_{m,n}B_{p,q}$ means the motif of two connected stars, where one star $A_{m,n}$ has m neighbours holding A and n neighbours holding B, the other star $B_{p,q}$ has p neighbours holding A and q neighbours holding B (Figure 3.29).

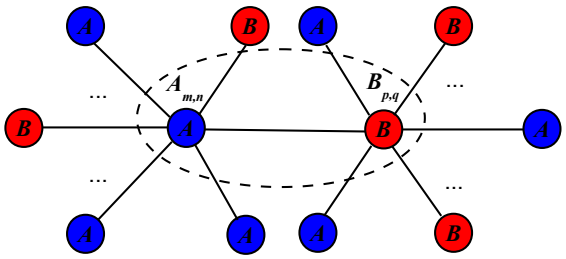

Figure 3.29: Double stars $A_{m,n}B_{p,q}$.

When we adapt DSA into the voter models, the rates for state evolution between neighbours (e.g. $AB \to AA$) can be calculated through the double stars observables. In detail, the following master equation can be obtained to capture the dynamics of $A_{m,n}$:

$$\begin{aligned}
\tfrac{\mathrm{d}}{\mathrm{d}t}[A_{m,n}] \;=\; & -\lambda^{A\to B}_{A_{m,n}}[A_{m,n}] + \lambda^{B\to A}_{B_{m,n}}[B_{m,n}] \\
& - \textstyle\sum_{p,q} \lambda^{B\to A}_{B_{p,q}}[A_{m,n}B_{p,q}] + \sum_{p,q} \lambda^{B\to A}_{B_{p,q}}[A_{m-1,n+1}B_{p,q}] \\
& - \textstyle\sum_{p,q} \lambda^{A\to B}_{A_{p,q}}[A_{m,n}A_{p,q}] + \sum_{p,q} \lambda^{A\to B}_{Ap,q}[A_{m+1,n-1}A_{p,q}] \\
& - \mu^{-A}_{A_{m,n}}[A_{m,n}] - \mu^{-B}_{A_{m,n}}[A_{m,n}] + \mu^{-A}_{A_{m+1,n}}[A_{m+1,n}] + \mu^{-B}_{A_{m,n+1}}[A_{m,n+1}] \\
& - \mu^{+A}_{A_{m,n}}[A_{m,n}] - \mu^{+B}_{A_{m,n}}[A_{m,n}] + \mu^{+A}_{A_{m-1,n}}[A_{m-1,n}] + \mu^{+B}_{A_{m,n-1}}[A_{m,n-1}] \\
& - \mu^{-A+B}_{A_{m,n}}[A_{m,n}] - \mu^{+A-B}_{A_{m,n}}[A_{m,n}] + \mu^{+A-B}_{A_{m-1,n+1}}[A_{m-1,n+1}] + \mu^{-A+B}_{A_{m+1,n-1}}[A_{m+1,n-1}]
\end{aligned} \tag{3.32}$$

where $\lambda^{A\to B}_{A_{m,n}}$ indicates the rate for the flipping $A_{m,n} \to B_{m,n}$; $\lambda^{B\to A}_{B_{p,q}}$ indicates the rate for the transition $B_{p,q} \to A_{p,q}$; $\mu^{-A}_{A_{m,n}}$ indicates the rate to remove a neighbour holding

A from $A_{m,n}$; $\mu^{+A}_{A_{m,n}}$ indicates the rate to add a new neighbour holding A to $A_{m,n}$; and $\mu^{-A+B}_{A_{m,n}}$ indicates the rate for $A_{m,n}$ to disconnect a neighbour holding A but connect to a new one holding B.

Notably, DSA captures the neighbourhood configurations by extending the observable from single star to double stars, which can obtain a more precise flipping rate for adjacent agents. In order to make the set of equations closed, we have following approximations (Figure 3.29) to decompose those double stars into stars. So the size of ODEs based on DSA is same as that based on AME.

$$\begin{aligned}
[A_{m,n}B_{p,q}] &\simeq [A_{m,n}] \times n \times \frac{p\times[B_{p,q}]}{\sum_{p,q} p\times[B_{p,q}]} = \frac{[A_{m,n}]\times n\times p\times[B_{p,q}]}{[AB]} \\
[A_{m,n}A_{p,q}] &\simeq [A_{m,n}] \times m \times \frac{p\times[A_{p,q}]}{\sum_{p,q} p\times[A_{p,q}]} = \frac{[A_{m,n}]\times m\times p\times[A_{p,q}]}{[AA]}
\end{aligned} \tag{3.33}$$

where $[AB] = \sum_{m,n}\sum_{p,q}[A_{m,n}B_{p,q}]$ and $[AA] = \sum_{m,n}\sum_{p,q}[A_{m,n}A_{p,q}]$.

3.6.2.3 Examples

(1) **Linear rate**

Let's first look back to the original adaptive voter model in Ref. (Durrett et al., 2012), where the flipping rate of an agent is linearly proportional to the number of neighbours holding a different state.

In AME, the rate to flip the state of a focal agent is calculated as: $\lambda^{A\to B}_{A_{m,n}} = n$ and $\lambda^{B\to A}_{B_{m,n}} = m$. While for the flipping of the neighbours of the focal agent, it is approximated through an **aggregate then compute** (ATC) method, which means that it will first estimate the "mean" neighbourhood configuration by aggregating all possible cases and then compute the rate based on that "mean" configuration.

For example, for a focal agent $A_{m,n}$, a neighbour u holding a state of A can be approximated as $A_{1+[AAA]/[AA],[AAB]/[AA]}$, who has a flipping rate $\lambda^{A\to B}_{u} = [AAB]/[AA]$. Considering that $A_{m,n}$ has m this kind of neighbours, and the sum of them means the rate of flipping from a neighbouring A to a neighbouring B:

$$\sum_{u\in NB(A_{m,n})\wedge s_u=A} \lambda^{A\to B}_{u}[A_{m,n}] = [A_{m,n}] \times m \times [AAB]/[AA] \tag{3.34}$$

Finally, we can write approximate master equations (AME) for the adaptive voter

model under rewire-to-random as:

$$\begin{aligned}\frac{\mathrm{d}}{\mathrm{d}t}[A_{m,n}] &= -(1-\alpha)n[A_{m,n}] + (1-\alpha)m[B_{m,n}] \\ &\quad -(1-\alpha)([AAB]/[AA])m[A_{m,n}] + (1-\alpha)([AAB]/[AA])(m+1)[A_{m+1,n-1}] \\ &\quad -(1-\alpha)([ABA]/[AB]+1)nA_{m,n} + (1-\alpha)([ABA]/[AB]+1)(n+1)[A_{m-1,n+1}] \\ &\quad +\alpha(-2+[B]/N)n[A_{m,n}] + \alpha([A]/N)(n+1)[A_{m-1,n+1}] + \alpha(n+1)[A_{m,n+1}] \\ &\quad +\alpha[AB](-2[A_{m,n}] + [A_{m,n-1}] + [A_{m-1,n}])/N\end{aligned} \tag{3.35}$$

When it comes to DSA in adaptive voter models, the flipping rate for the focal agent is same as AME, namely $\lambda_{A_{m,n}}^{A\to B} = n$ and $\lambda_{B_{m,n}}^{B\to A} = m$. However, the flipping of the neighbours of the focal agent is approximated through a **compute then aggregate** (CTA) method, which means that it will first compute the flipping rate for a certain doublet configuration and then obtain a "mean" rate by aggregating all possible configurations of doublets.

For example, $\lambda_{A_{p,q}}^{A\to B} = q$ is the flipping rate from a doublet $A_{m,n}A_{p,q}$ to $A_{m,n}B_{p,q}$. Aggregating the possible configurations of doublets connecting $A_{m,n}$, we can have:

$$\begin{aligned}\textstyle\sum_{p,q}\lambda_{A_{p,q}}^{A\to B}[A_{m,n}A_{p,q}] &\simeq \textstyle\sum_{p,q} q \times \frac{[A_{m,n}]\times m\times p\times[A_{p,q}]}{[AA]} \\ &= \frac{[A_{m,n}]\times m}{[AA]} \times \textstyle\sum_{p,q} q\times p\times[A_{p,q}] \\ &= \frac{[A_{m,n}]\times m}{[AA]} \times [AAB] \\ &= [A_{m,n}]\times m\times[AAB]/[AA]\end{aligned} \tag{3.36}$$

As we can see, in the case of linear imitation, the flipping rate based on AME (Eq. 3.34) is same as that based on DSA (Eq. 3.36). In this way, we can also write the master equations using DSA as:

$$\begin{aligned}\frac{\mathrm{d}}{\mathrm{d}t}[A_{m,n}] &= -(1-\alpha)n[A_{m,n}] + (1-\alpha)m[B_{m,n}] \\ &\quad -(1-\alpha)\textstyle\sum_{p,q}[A_{m,n}B_{p,q}]\times p + (1-\alpha)\sum_{p,q}[A_{m-1,n+1}B_{p,q}]\times p \\ &\quad -(1-\alpha)\textstyle\sum_{p,q}[A_{m,n}A_{p,q}]\times q + (1-\alpha)\sum_{p,q}[A_{m+1,n-1}A_{p,q}]\times q \\ &\quad +\alpha(-2+[B]/N)n[A_{m,n}] + \alpha([A]/N)(n+1)[A_{m-1,n+1}] + \alpha(n+1)[A_{m,n+1}] \\ &\quad +\alpha[AB](-2[A_{m,n}] + [A_{m,n-1}] + [A_{m-1,n}])/N\end{aligned} \tag{3.37}$$

Figure 3.30 illustrates the results obtained through numerical simulations and analytical approximations. Interestingly, the master equations based on AME and DSA present same results in this case of linear imitation, whose accuracy is much higher than approximations based on PA and IA introduced before (see Figure 3.23).

(2) **Non-linear rate**

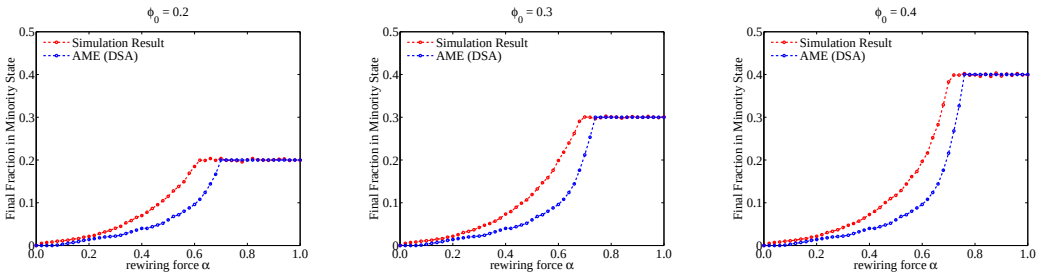

Figure 3.30: The final fraction of the minority under the strategy of rewire-to-random for varying rewiring force αs, and the initial fraction is $\phi_0 = 0.2, 0.3$ and 0.4 respectively. The numerical simulation, AME and DSA approximations are run in a random network with $N = 1000$, $E = 2000$ and $\langle k \rangle = 4$.

Now, let's consider a more complicated case where the flipping rate for state evolution is non-linear as we discussed in the weighted voter model. In this situation, the weight of a node is dependent on its state as well as the neighbourhood configuration.

In the case of AME, the state imitation is based on the **aggregate then compute** (ATC) method, namely we need to estimate the "mean" neighbourhood configuration first, and then compute the flipping rate. For an agent $A_{m,n}$, whose weight is computed as $\pi_{A_{m,n}} = R \times m + S \times n$. The number of neighbours holding B is n, each of which can be approximated as $B_{[ABA]/[AB]+1,[ABB]/[AB]}$, indicating that the "mean" B in the neighbourhood of $A_{m,n}$ has $[ABA]/[AB]+1$ neighbours of A and $[ABB]/[AB]$ neighbours of B. Therefore, the weight of this kind of "mean" neighbouring B is approximated as:

$$\begin{aligned}
\pi_{\bar{B}} &= T \times ([ABA]/[AB]+1) + P \times [ABB]/[AB] \\
&\simeq \sum_{p,q} T \times \frac{p \times [B_{p,q}] \times p}{[AB]} + P \times \frac{p \times [B_{p,q}] \times q}{[AB]} \\
&\simeq \sum_{p,q} \frac{p \times [B_{p,q}]}{[AB]} \times \pi_{B_{p,q}}
\end{aligned}$$

In this way, the flipping rate of the focal agent from $A_{m,n}$ to $B_{m,n}$ is approximated as:

$$\begin{aligned}
\lambda_{A_{m,n}}^{A \to B} &= [A_{m,n}] \times n \times \frac{1}{1+e^{-\beta(\pi_{\bar{B}} - \pi_{A_{m,n}})}} \\
&= [A_{m,n}] \times n \times \frac{1}{1+e^{-\beta(\sum_{p,q} \frac{p \times [B_{p,q}]}{[AB]} \times \pi_{B_{p,q}} - \pi_{A_{m,n}})}}
\end{aligned} \tag{3.38}$$

When it comes to DSA, the imitation rate is computed based on the **compute then aggregate** (CTA) method, where we need to compute the rate separately for each doublet, and then aggregate all those cases. Given a doublet $A_{m,n}B_{p,q}$, the flipping rate

from $A_{m,n}B_{p,q}$ to $B_{m,n}B_{p,q}$ is computed as:

$$p(A_{m,n}B_{p,q} \to B_{m,n}B_{p,q}) = [A_{m,n}B_{p,q}] \times \frac{1}{1+e^{-\beta(\pi_{B_{p,q}}-\pi_{A_{m,n}})}}$$

Aggregating all the cases of $B_{p,q}$ in $A_{m,n}B_{p,q}$, we can have the flipping rate for the focal agent from $A_{m,n}$ to $B_{m,n}$ as:

$$\begin{aligned} \lambda_{A_{m,n}}^{A\to B} &= \sum_{p,q}[A_{m,n}B_{p,q}] \times \frac{1}{1+e^{-\beta(\pi_{B_{p,q}}-\pi_{A_{m,n}})}} \\ &\simeq [A_{m,n}] \times n \times \sum_{p,q} \frac{p\times[B_{p,q}]}{[AB]} \times \frac{1}{1+e^{-\beta(\pi_{B_{p,q}}-\pi_{A_{m,n}})}} \end{aligned} \tag{3.39}$$

As we can see, in the case of non-linear imitation, the flipping rate shown in Eq. 3.38 based on AME is different from that Eq. 3.39 based on DSA. In general, let's define $f(x)$ as the flipping rate computed by:

$$f(x) = 1/(1+e^{-\beta(x-c)}) \tag{3.40}$$

In this case, the flipping rate based on AME is proportional to $f(\mathbb{E}[x])$, while the flipping rate based on DSA is proportional to $\mathbb{E}[f(x)]$.

Taking the weighted voter model as an example, we implement the above two approximation methods (AME and DSA) to characterize the adaptive dynamics. First, we take a set of weight parameters $T > R > P > S$ to build a prisoner's dilemma (PD) interaction payoff matrix. Figure 3.31 presents the performance of the analytical approximations based on AME and DSA relative to the numerical simulations.

When we change the weight parameters to a coordination game with $R \simeq P > S \simeq T$, we come to another example of weighted voter model. Figure 3.32 presents the performance of the two analytical approximations relative to the numerical simulations.

As we can see, AME and DSA have same approximation results in the case of linear imitation, but DSA performs a little bit better than AME in the case of non-linear imitation. Notably, the approximation performance obtained from AME and DSA (see Figure 3.31 and 3.32) is much better than that obtained from PA and IA (see Figure 3.24 and 3.25). Of course, the computation cost of ODEs based on AME and DSA is quite higher than that using PA and IA.

3.7 Summary

This chapter has explored the dynamics of adaptive voter models on the basis of pairwise imitation and link rewiring, where a transition from network consensus to fragmentation is obtained as the rewiring force gets stronger. As the connecting nodes are

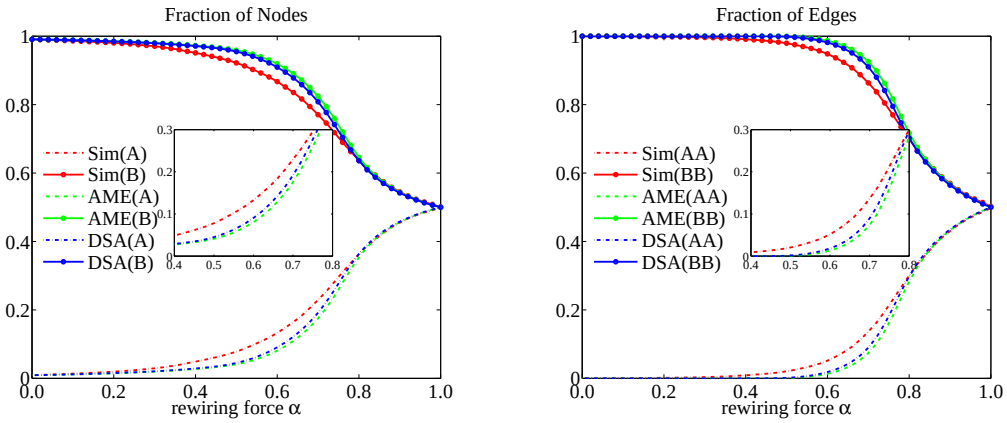

Figure 3.31: The final fraction of different types of nodes and edges under different rewiring force αs in the weighted voter model. With an initial fraction $\phi_0 = 0.5$, the numerical simulation, AME and DSA approximations are run in a random network with $N = 1000$, $E = 2000$ and $\langle k \rangle = 4$, and the selection strength is $\beta = 0.1$. The weight parameters are $R = 1.0$, $S = -1.0$, $T = 2.0$ and $P = 0.0$.

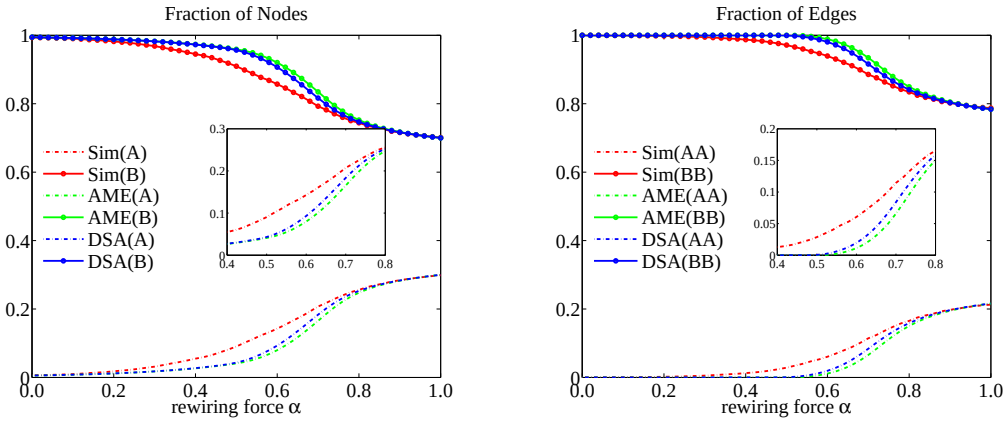

Figure 3.32: The final fraction of different types of nodes and edges under different rewiring force αs in the weighted voter model. With an initial fraction $\phi_0 = 0.3$, the numerical simulation, AME and DSA approximations are run in a random network with $N = 1000$, $E = 2000$ and $\langle k \rangle = 4$, and the selection strength is $\beta = 0.1$. The weight parameters are $R = 1.0$, $S = 0.0$, $T = 0.0$ and $P = 1.0$.

equally persuasive under direct competition, the average fraction of a certain type of nodes remains same as the initial fraction. First, we investigate a feasible rewiring strategy based on rewire-to-foaf numerically and analytically, where an early fragmentation can be observed. When a neutral state based on approximate majority is introduced, the system will converge to the consensus easily, and the initial minority loses

the chance to win. Besides the unbiased state imitation, we also enable the agents to hold weights which are dependent on their neighbourhood configurations, so that the evolution of state is biased by the weights in a form of Fermi distribution. In this weighted voter model, the network is more likely to reach consensus, where a small fraction of "powerful" voters are going to take over the whole population.

Some accurate and tractable approximation techniques are developed to estimate the evolution of the average basic observables. With same computation cost, the ODEs based on interface approximation (IA) performs much better than that based on pair approximation (PA). In addition, double stars approximation (DSA) has higher performance than approximate master equation (AME) in some special cases, where the rate for state evolution is non-linear.

Notably, information diffusion or opinion spreading in real world (Leskovec et al., 2008) is far more complicated than the situations discussed in this chapter, and some data mining methods are indispensable in revealing the dynamics of large-scale networks like Facebook or Twitter. It will be a promising direction to study adaptive networks by using the real data, and a large number of researches (Gomez Rodriguez et al., 2010; Cheng et al., 2014) have been launched to do that.

Chapter 4

Detecting the Loss of Cooperation in Evolving Communities

As we all know, the success and sustainability of structured biological, social, economic and ecological communities are often determined by the presence of evolutionary conflicts between cooperative individuals (cooperators) and defective individuals (cheaters). Cooperators are those paying cost for the success of population, but cheaters avoid the cost of contributing to the community. This chapter mainly investigates the rise and down of cooperation in an evolutionary population proposed by Ref. (Cavaliere et al., 2012), where state evolution and structure adaptation are implemented according to the principles of natural selection.

Starting from a cooperative population, an invading cheater may spread in the population occasionally leading to the collapse of cooperation. Such a collapse usually unfolds rapidly and unexpectedly bearing the traits of a critical transition (Scheffer et al., 2009). Although several factors can facilitate the spread of cheaters, it is an open question whether one can detect the rising risk of invasions by cheaters and loss of cooperation in an evolving community. Here, we combine evolutionary games with adaptive networks to study the abrupt loss of cooperation from the perspective of critical transitions. We follow the dynamics of the community upon the appearance of a single cheater and estimate the risk of invasion, leading to the collapse of cooperation. We associate this risk with a number of indicators based on network structure and population composition. Interestingly, some specific patterns in the indicators can signal the increasing risk of cooperation collapse, which highlights that it is possible to detect the community fragility even in such a complex adaptive system.

4.1 Introduction

The sustainability of many biological, social, economic, and ecological communities is determined by the interplays between individual actions and collective dynamics (Levin, 1999). The successful performance of a community is often based on the cooperative attitude of individuals that pay a personal cost to distribute general benefits (Nowak, 2006b). Nonetheless, although cooperation favours in general the success of a community, it can also facilitate the appearance of cheaters who take advantage of cooperators and spread in the community, and may even cause its collapse (Levin, 1999).

The failure of cooperation in the presence of cheaters has been observed in many systems at different scales (Rainey and Rainey, 2003; Popat et al., 2012; Travisano and Velicer, 2004; Haldane et al., 2009). In all these systems, a long-standing question has been to understand the mechanisms that allow cooperators to resist the reproductive advantage of selfish cheating individuals (Nowak, 2006b). Among the many theoretical and experimental studies on the maintenance of cooperation (Nowak, 2006b; Ohtsuki et al., 2006), scenarios where strategies co-evolve with population structure (Perc and Szolnoki, 2010) are of particular interest as they show how structural properties in the population can affect the evolution of cooperation (Perc and Szolnoki, 2010; Wardil and Hauert, 2014; Rand et al., 2011; Sanchez and Gore, 2013). For instance, it has been shown that not only the number of cheaters in the community is important, but also how and to whom they are connected (Cavaliere et al., 2012). The interplays between the population evolution and structure adaptation endogenously determine either the formation or the sudden collapse of cooperative communities (Levin, 1999). Despite our relatively good understanding of the conditions that promote the failure of cooperation in a community, in most scenarios, it is still difficult to predict whether the appearance of a cheater will actually lead to its spreading and to the eventual loss of cooperation (Ostrom, 2009; Bowles and Gintis, 2011). Thus, it is crucial to develop some indicators for detecting the risks of the collapse of cooperation in an evolving community.

Critical transitions (Scheffer et al., 2009) illustrate the abrupt shift triggered by gradually changing conditions. Recent work has suggested that the proximity to unexpected transitions can be announced by generic indicators based on the dynamical properties of the system. These indicators are generic in the sense that they do not depend on the particular system in question. On the contrary, they are solely deter-

mined by the mathematical phenomenon of critical slowing down (CSD) that occurs prior to the bifurcation point (Strogatz, 2014; Wissel, 1984). A bifurcation point represents a threshold where a qualitative change in the equilibrium of a system takes place: the iconic case is the shift between two alternative equilibria at a crossing of a fold bifurcation driven by gradual changes in external conditions. Close to the fold bifurcation, CSD means that the system takes longer to recover back to equilibrium after a disturbance (Scheffer et al., 2009; Van Nes and Scheffer, 2007). Direct consequence of a slow responsive system is that its dynamics become more variable (Carpenter and Brock, 2006) and more autocorrelated (Held and Kleinen, 2004) close to the transition. In other words, rising variance and autocorrelation can be used as generic indicators for the approaching critical transition (Scheffer et al., 2009; Dakos et al., 2012).

Here, for the first time to our knowledge, we combine evolutionary game theory with adaptive networks to detect the collapse of cooperation in an evolving community. To do this, we adopt a previously investigated model (Cavaliere et al., 2012) that displays recurrent cooperation collapses as a consequence of invasions by cheaters. The dynamical nature of the population is driven by the appearance and disappearance of cheaters and cooperators in dynamical networks, resulting from **state inheritance** (newcomers imitate the strategies of the parents) and **network reorganisation** (newcomers reconstruct the neighbourhood). The two features lead to recurrent collapses and recoveries of cooperation that are associated with dramatic changes in network topology. Interestingly, the chances that a newcomer imitates the social network of the selected role-model are controlled by some embedding parameters, that ultimately control the success of cooperation (Cavaliere et al., 2012). The embedding parameters reflect the increasing ability of newcomers to connect to a higher number of individuals already present in the network. Increasing such ability can generate higher prosperity in a network of cooperators, as it allows more interactions to take place, but it also facilitates the success of cheaters as they can profit from more cooperators.

In this chapter, we will highlight that the embedding parameters directly affect the resilience of cooperative networks by controlling the chances that a single cheater can invade a network full of cooperators. In particular, we modulate the resilience of a community by changing the embedding parameters, where the loss of cooperation resembles a critical transition. To detect the increasing fragility of cooperation, we propose a series of structural and non-structural indicators in the following. The results show that these indicators can be used as early-warning signals, but their detecting performance depends on the mechanism of evolution, the nature of each indicator and

the level of selection. Our contribution is two-fold. First, it demonstrates how the loss of cooperation in evolving communities bears the features of a critical transition. Second, it offers a set of indicators for detecting the approaching transitions.

4.2 Evolutionary Population Model

Adapting game theory into evolutionary population, we reach the field of evolutionary game theory (EGT) as shown in Figure 4.1. In general, the states of individuals co-evolve with the structure of network, driven by natural selection.

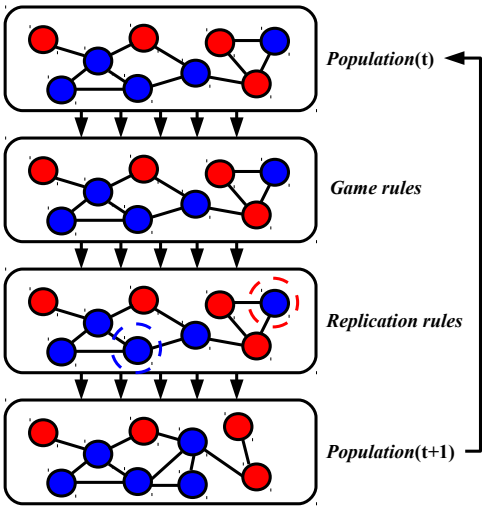

Figure 4.1: The generalised framework for the dynamics of evolutionary population. The game rules determine the payoffs of the individuals, based on which some nodes are allowed to reproduce and some are removed. Meanwhile, the structure of network is adjusted along with the appearance and disappearance of the players.

A rich landscape in Ref. (Cavaliere et al., 2012) has been illustrated to show the competing players in a structured community, and we will focus on the co-evolution of population and network based on that model. In detail, we will consider a network with a fixed number of nodes but with a non-fixed number of links: to whom and to how many neighbours an agent is connected varies during the evolution of the system.

Each agent in the network adopts one of the two strategies of the Prisoner's Dilemma (PD). A cooperator (C) pays a cost c to provide a benefit b to each of its neighbours, where $b > c > 0$; however, the cheaters (or defectors, D) pay no cost and distribute no benefit. Specifically, if a cooperator has m cooperative neighbours and n cheating

neighbours, its payoff is $m(b-c)-nc$. However, a cheater in the same neighbourhood has payoff mb. The payoff matrix can be represented by:

$$\Pi = \begin{matrix} \\ C \\ D \end{matrix} \begin{matrix} \begin{matrix} C & D \end{matrix} \\ \begin{pmatrix} R & S \\ T & P \end{pmatrix} \end{matrix} = \begin{matrix} \\ C \\ D \end{matrix} \begin{matrix} \begin{matrix} C & D \end{matrix} \\ \begin{pmatrix} b-c & -c \\ b & 0 \end{pmatrix} \end{matrix} \tag{4.1}$$

Evolutionary dynamics for a system can be defined by a discrete sequence of update steps as shown in Figure 4.2.

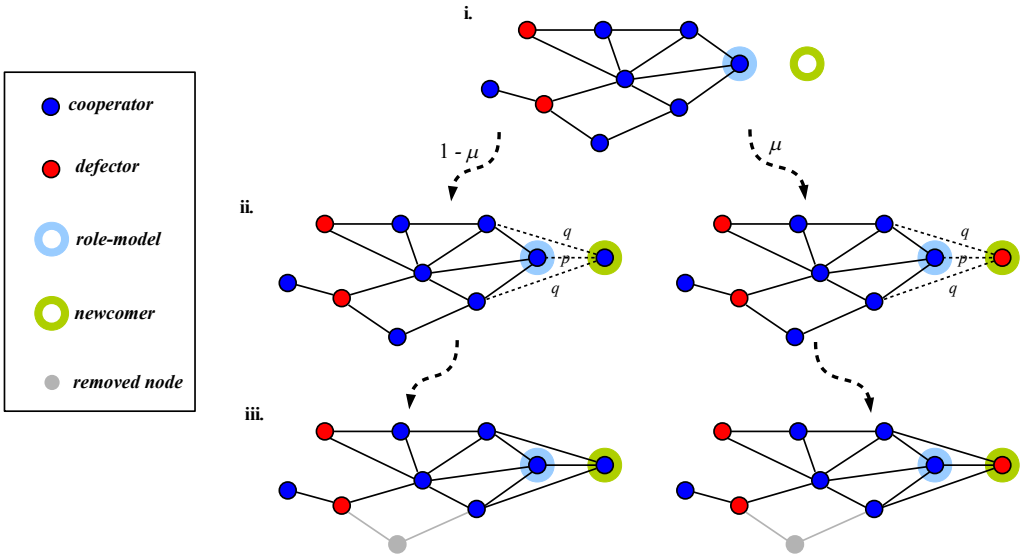

Figure 4.2: Evolutionary dynamics in a structured population. Each update step of the network follows these actions: (i) A role-model is selected to reproduce proportional to its effective payoff. (ii) The newcomer connects to the role-model with probability p (dashed line), connects to each of its neighbours with probability q (dotted lines) and emulates its strategy with probability $1-\mu$. p and q are called embedding parameters. (iii) A randomly selected node and all its connections are removed from the network.

At each update step, a node i is selected as a role-model to reproduce with probability proportional to its effective payoff, namely the fitness f_i:

$$f_i = (1+\delta)^{\pi_i} \tag{4.2}$$

where $\delta \geq 0$ specifies the **strength of selection** and π_i is the sum of payoffs through pairwise interactions to each neighbour. For $\delta = 0$ the selection probability is the same for all nodes, while increasing δ makes it more likely that a node with a higher payoff

is selected to reproduce. In addition, a randomly chosen existing node is removed from the population, so that the number of nodes is constant.

We assume that the newcomer adopts the strategy of the chosen role-model with probability $1-\mu$, otherwise adopts the alternative strategy with probability μ, where $1 \gg \mu \geq 0$ is a very tiny real number indicating the **mutation rate**. In the process of network reorganisation, the newcomer connects to the role-model with probability p as well as to each of the role-model's neighbours with probability q. The parameters p and q are called **embedding parameters**, as they explicitly determine the ability of the newcomer to copy the role-model's social network (Cavaliere et al., 2012).

4.2.1 Evolution Without Games

When $\delta = 0$, we have $f_i = 1$ for any individual in the network, where the evolution is independent of the game parameters and graph structure. In this special case, we can have the transitions from a state $([C]_t, [D]_t)$ to:

- $([C]_t + 1, [D]_t - 1)$ with probability $p^+ = \frac{[C]_t}{N}(1-\mu)\frac{[D]_t}{N} + \frac{[D]_t}{N}\mu\frac{[D]_t}{N}$;
- $([C]_t - 1, [D]_t + 1)$ with probability $p^- = \frac{[C]_t}{N}\mu\frac{[C]_t}{N} + \frac{[D]_t}{N}(1-\mu)\frac{[C]_t}{N}$;
- $([C]_t, [D]_t)$ with probability $1 - p^+ - p^-$.

Now, let's derive the ordinary differential equation (ODE) for the average number of cooperators $[C]$, which can be written as:

$$\begin{aligned} \frac{\mathrm{d}}{\mathrm{d}t}[C]_t &= \frac{[C]_t}{N}(1-\mu)\frac{[D]_t}{N} + \frac{[D]_t}{N}\mu\frac{[D]_t}{N} \\ &\quad - \frac{[C]_t}{N}\mu\frac{[C]_t}{N} - \frac{[D]_t}{N}(1-\mu)\frac{[C]_t}{N} \\ &= \mu\frac{[D]_t^2 - [C]_t^2}{N^2} = \mu\frac{N^2 - 2N[C]_t}{N^2} \end{aligned} \tag{4.3}$$

It is easy to see that the average number of cooperators and detectors will be $\mathbb{E}([C]) = \mathbb{E}([D]) = N/2$ at stationary state. Specifically, the analytical solution for the evolution of $[C]$ in a large-scale population can be obtained as:

$$[C]_t = Ae^{-2\mu t/N} + N/2 \tag{4.4}$$

where A is given by the formula $A = [C]_0 - N/2$. If we start from a network with all cooperators $[C]_0 = N$, then $A = N/2$; otherwise if we start from a network with all

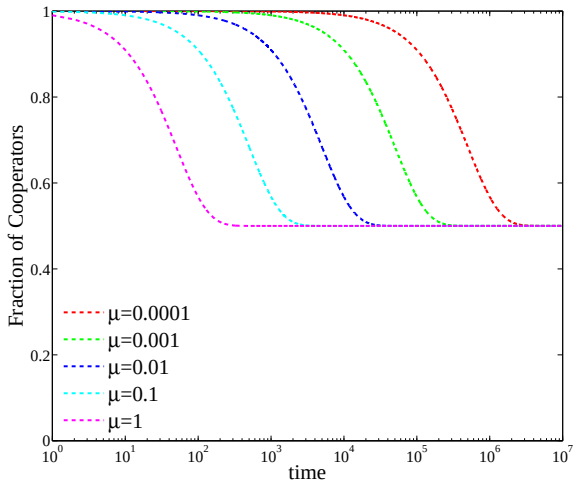

Figure 4.3: The evolution of analytical solutions for the average fraction of cooperators at $\delta = 0$. Various mutation rate μs are illustrated, where a smaller μ gives rise to slower convergence.

cheaters $[C]_0 = 0$, then $A = -N/2$. As we can see in Figure 4.3, the convergence rate decays with the decrease of μ exponentially.

Even though the average fraction of cooperators eventually will converge to 0.5, the system still can keep a good stability at $[C]_t \to N$ when the mutation rate is quite small. Interestingly, the system alternates between $[C] = 0$ and $[C] = N$ at a smaller μ, which leads to a phenomenon of bi-stability. But when the mutation rate is bigger, the system keeps stable around $[C] = N/2$ illustrating a situation of uni-stability (Figure 4.4).

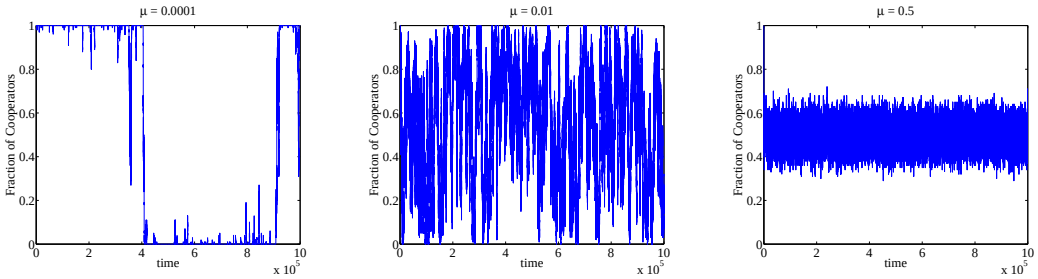

Figure 4.4: Numerical simulation for the fraction of cooperators at $\delta = 0$ and $N = 100$ under different mutation rates: $\mu = 0.0001$ (left), $\mu = 0.01$ (middle) and $\mu = 0.5$ (right).

With the increase of mutation rate μ, the distributions for the fraction of cooperators are illustrated in Figure 4.5, where a shift from bi-stability to uni-stability is obtained.

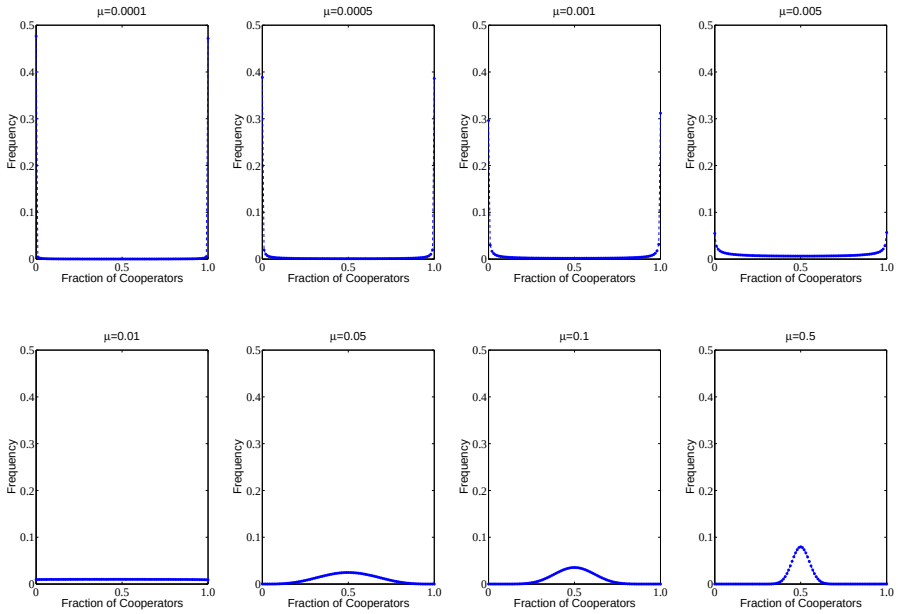

Figure 4.5: The distributions for the fraction of cooperators under varying μs at $\delta = 0$. For each μ, the evolution process lasts for $t_{\max} = 10^8$ steps. Each simulation starts from a population of $N = 100$ cooperators.

When the mutation rate μ is increasing, the distribution for the fraction of cooperators transforms from a bimodal one to a unimodal one. At a bigger μ, the newcomer would like to adopt the state different from that of the role-model, and the system converges to the uni-stability case around half cooperators and half cheaters.

4.2.2 Long-term Evolution

Now, let's introduce the PD game into the evolutionary population with $b/c = 3$ and the selection strength is $\delta = 0.01$. Considering the fact that the mutation rate is usually a very small number, we set $\mu = 0.0001$. The dynamics of evolutionary population is illustrated like Figure 4.6 with a given $p = 0.6$, where three embedding parameters $q = 0.8$, $q = 0.9$ and $q = 0.95$ are presented respectively.

Interestingly, we can observe recurrent collapses and recoveries of cooperation, a network full of cooperators appears highly connected while a network full of cheaters appears mostly fragmented when the embedding parameter q is not large enough. As for the reason, the cooperative newcomers provide positive feedbacks to the role-models, and the payoffs of the cooperators will increase. However, the invading cheater

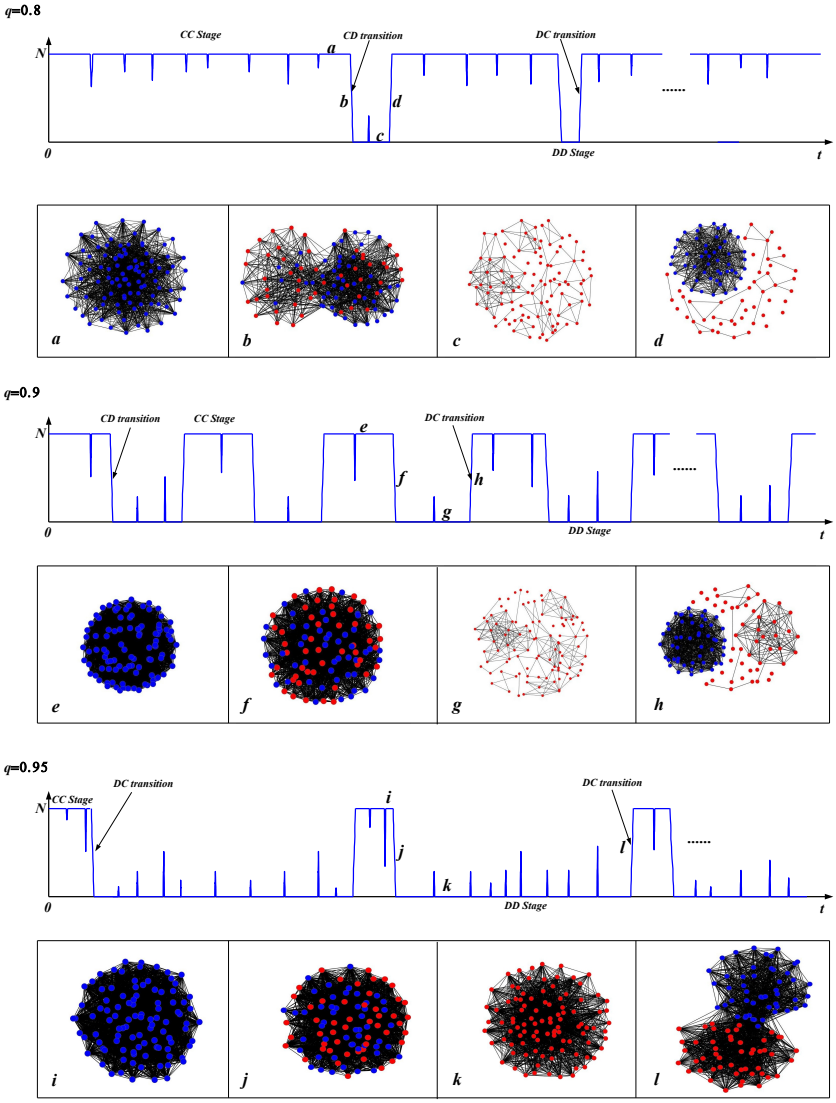

Figure 4.6: Long-term evolution with endogenous mutation at $\mu = 0.0001$ and selection $\delta = 0.01$. A schematic illustration shows the evolution of dynamical networks at different embedding parameters $q = 0.8$, $q = 0.9$ and $q = 0.95$. We consider a network with $N = 100$ individuals, interacting in the PD game with $b/c = 3$. Specifically, we can identify four typical stages: CC (a, e and i), CD(b, f and j), DD (c, g and k) and DC (d, h and l). A mutant appears with a strategy different from the rest of the population, followed by a recovery to its initial state or a full invasion. For instance in the upper row, starting from a community of only cooperators in a, the cheaters invade until an entire collapse (from b to c), and the system ultimately returns to its original state in d. Notably, the number of transitions from the state of only Cs to the state of only Ds follows a non-monotonous curve: first increases and then decreases as q gets bigger.

will diminish the payoffs of the neighbours, which acts as negative feedbacks for the reproduction (see Ref. (Cavaliere et al., 2012) for more details), as a result the network becomes less connected.

Here, it should be noted that the embedding parameters p and q determine the reconstruction of network structure, which will influence population compositions in turn. In Figure 4.6, we can find that the invasion by cheaters is easier with the increase of q, but cooperation recovery gets harder and harder. In the following part, a variety of collective dynamics will be presented by varying the embedding parameters.

4.2.3 The Collapse of Cooperation

The embedding parameters influence the network structure locally, which in turn affects some global properties, such as the average fraction of cooperators, network connectivity and the number of transitions (Figure 4.7). In particular, the embedding parameter q used to connect the neighbours of the role-model is quite crucial for the dynamics of population, where a great loss of cooperation is obtained when q is reaching a big value. Let t_0 and $t_{\max}$ be the starting and ending time of the long-term evolution, and then some measurements for the evolutionary system are provided.

- the average number of cooperators in the long-term evolution is computed by:

$$[C] = \frac{\sum_{t=t_0}^{t_{\max}} [C]_t}{t_{\max} - t_0} \tag{4.5}$$

  where $[C]_t$ is the number of cooperators in the network at step t.

- the connectivity of network can be computed by:

$$\langle k \rangle = \frac{\sum_{t=t_0}^{t_{\max}} \langle k \rangle_t}{t_{\max} - t_0} \tag{4.6}$$

  where $\langle k \rangle_t$ is the network average degree at step t.

- the number of transitions indicates the total number of transitions from all-cooperators case ($[C] = N$) to all-cheaters case ($[C] = 0$) or from all-cheaters case to all-cooperators case. Here the frequency of transitions shows the stability of the system.

As we can see in Figure 4.7, a single parameter q can lead to a complex dynamics for the structure and population. With the increase of q, the long-term network connectivity increases up to a peak, where the fraction of cooperators is close to 1. At a

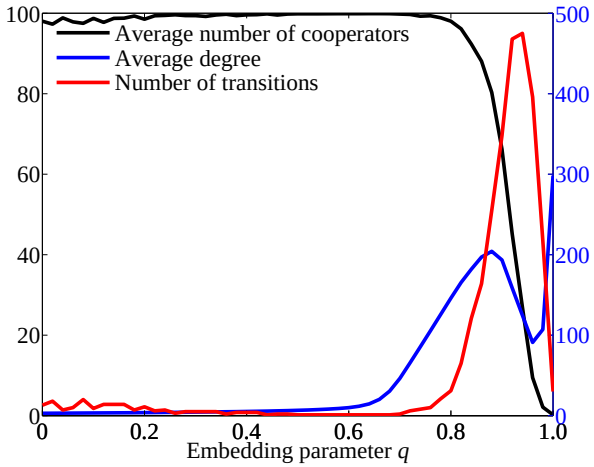

Figure 4.7: The long-term cooperation and network structure for varying embedding parameter qs. With a given $p = 0.6$, we start from a random network with $N = 100$ players to capture the dynamical properties. The benefit to cost ratio is $b/c = 3$, the selection strength is $\delta = 0.01$ and the mutation rate is $\mu = 0.0001$. At each q, we consider a simulation of 10^8 steps to obtain the illustrated properties.

relatively bigger q, the network is highly connected and the cheating newcomer would exploit the cooperators heavily, which leads to an invasion by cheaters and then a rapid decline of network connectivity. At the same time, the transitions between cooperation regime and defection regime are frequent. When q is close to 1, even the defectors can form highly-connected components, leading to the failure of cooperation recovery. In this way, the number of transitions decreases to a low value again. As shown in Figure 4.7, a stable cooperation is obtained at smaller qs, at the price of low connectivity. The network connectivity is non-monotonous with the increase of q, and the decline of connectivity from $q = 0.85$ to $q = 0.9$ is caused by the fragmented clusters of cheaters. The fraction of cooperators alone is not enough to capture the coupled dynamics, which also covers the interplay between connectivity and stability.

Another factor should be considered is the selection strength δ, which controls the fitness of a player as $f_i = (1+\delta)^{\pi_i}$. Figure 4.8 illustrates the average fraction of cooperators under different selection strengths.

When the selection is weak, the average fraction of cooperators is non-monotonous: it increases at smaller qs and reaches the maximal at intermediate levels of q, followed by a collapse as q gets larger. This non-monotonicity is caused by the relatively even distribution of fitness in a sparse network when q is sufficiently low, where the chance that a mutant cheater invades a community of cooperators is same as that a mutant

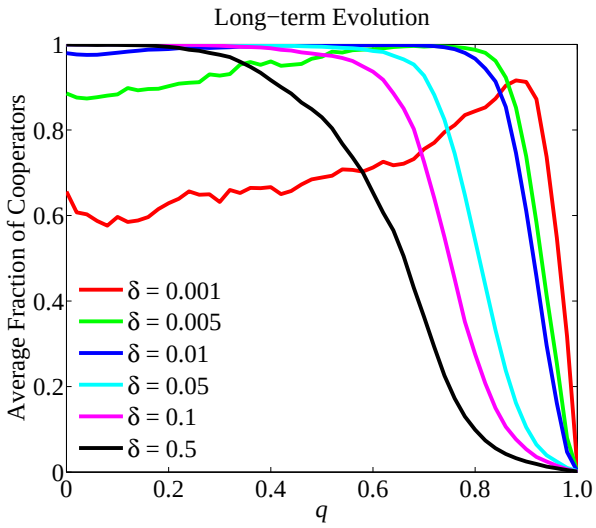

Figure 4.8: The average fraction of cooperators in the long-term evolution. The benefit to cost ratio is $b/c = 3$ and the mutation rate is $\mu = 0.0001$. With a given embedding parameter $p = 0.6$ and varying $q \in [0, 1]$, the evolution starts from a random network with $N = 100$ players. At each q, we consider a simulation of 10^8 steps to obtain the average fraction of cooperators. When the selection strength is changing from weak to strong, the loss of cooperators is increasingly deteriorated. A non-monotonous trend is obtained when the selection strength is weak.

cooperator invades a community of cheaters. When q is increasing but not that large, the network is a little more connected, and the cooperation level is increased due to the fragmented structure caused by imitating the invading cheaters. Under this circumstance, the component of cooperators will get more and more connected, which contributes to relatively higher fitness through mutual benefit and then better persistence of cooperation. However, when q goes on increasing, the invading cheaters will be highly connected and the cooperators are intensively exploited, which leads to the collapse of cooperation. In a highly connected group of cheaters, a restoring cooperator can't get rid of the lower fitness, and the recovery of cooperation is doomed to fail.

When the selection is strong, the average fraction of cooperators changes in a monotonous way with the increase of q. Even at a smaller q, the big value of δ brings high fitness to the invading cheaters in the beginning, followed by the fragmented networks. In this way, some cooperators may be maintained, which are separated from the cheaters. And then those cooperators will get clustered to promote the cooperation. The collapse of cooperation is triggered when the embedding parameter q increases to a large value, where the invading cheaters exploit heavily due to the higher connec-

tivity and stronger selection. As a result, the growth of cheaters is enhanced and the population turns into the regime of defection.

As we can see, even some simple parameters can give rise to a rich landscape for the evolutionary population. Here, we are very interested in the collapse of cooperation as the embedding parameter q increases, which is quite crucial in many real-world applications.

4.3 The Loss of Cooperation in Perturbation Experiments

At a critical transition, a system is radically changing from one equilibrium to an alternative contrasting one at the crossing of a threshold in external conditions (Scheffer et al., 2001, 2009). In the vicinity of such a critical transition, the probability that a small disturbance induces a shift from one equilibrium to another increases, in other words the resilience of the system becomes low (Holling, 1973). As we are concerned, many realistic situations bear the traits of a critical transition.

4.3.1 Perturbation Experiments

In an evolving community, the regime of cooperation may collapse depending on the way a cheater invades the population. When cooperators and cheaters spontaneously appear due to endogenous mutations, such loss of cooperation has been shown to be a transient behaviour that can occur rapidly, and the collapse is usually followed by the restoration. As it is difficult to analytically track the behaviour of such kind of evolving networks and establish the existence of a critical transition in long-term evolution, we follow an alternative numerical approach. Here, we will study the progressive loss of the resilience of cooperation by performing a series of perturbation experiments at the equilibrium of a dominant strategy.

A **perturbation** consists of the introduction of a mutant in a network where all agents are holding the opposite strategy. We initially evaluate the resilience of cooperation under that disturbance, and the mutation rate then is set to $\mu = 0$, which means that the population composition is only dependent on the fitness-based selection. More specifically, the network is updated for a large number of steps to remove transients and to establish a stable network topology. We then perturb the network by introducing a mutant newcomer (for instance, a cheater comes into a network of only cooperators) and the system is updated until one of the two outcomes is reached: either a **recovery**,

the mutant fails to invade and the system returns to the original state, or a **transition**, the mutant invades successfully and the original state collapses. In the case of collapse, we say the perturbation is successful. Starting from a cooperative community invaded by cheaters, we illustrate the two outcomes in Figure 4.9.

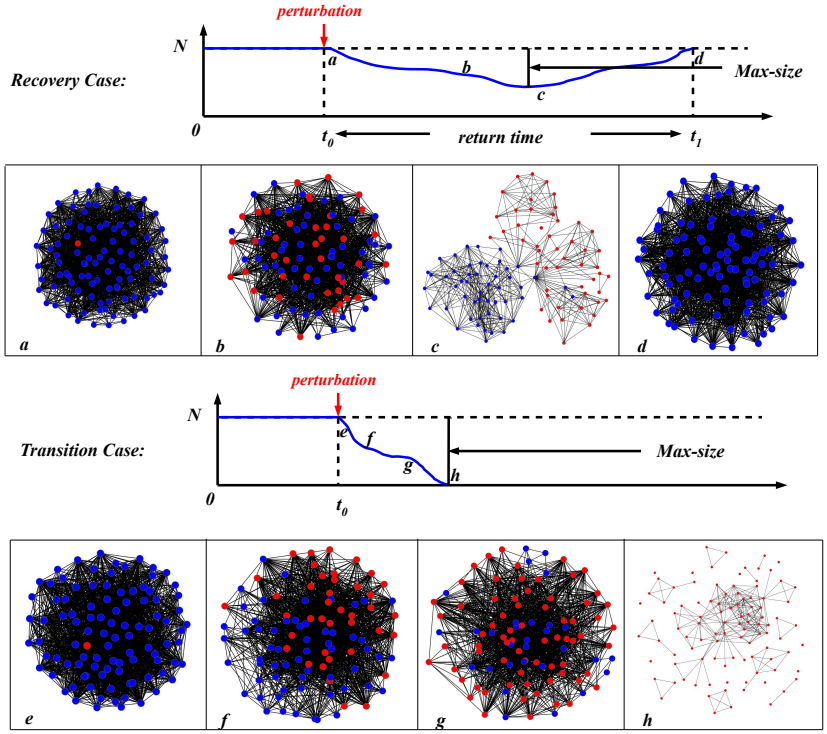

Figure 4.9: Perturbations lead to the recoveries and transitions. Recovery and collapse of cooperation following the addition of a single mutant in a network with agents of the opposite strategy. We show the two possible outcomes from a perturbation obtained by adding a cheater in a network of only cooperators. The first row shows the typical case of an unsuccessful perturbation where cooperators resist while the bottom row shows the typical case of a successful perturbation where cheaters invade gradually, and in both cases $p = 0.6$, $q = 0.8$ and $\delta = 0.01$.

4.3.2 Persistence and Restoration of Cooperation

In the following, we will evaluate the fraction of perturbations that are successful for increasing embedding parameter q at different selection strengths. This fraction of transitions represents the probability that a mutant will overturn the original regime (i.e. the probability for the mutants to dominate). For a given p, q and δ, the fraction

of transitions can be computed as:

$$\phi = \frac{\#\ transitions}{\#\ perturbations} \tag{4.7}$$

where we define $\phi(C \to D)$ as the fraction of transitions by adding a cheater in a network of only cooperators, and similarly $\phi(D \to C)$ means the fraction of transitions by adding a cooperator in a network of only cheaters.

Starting from a community full of cooperators, we evaluate the **persistence of cooperation** as the ratio between the number of unsuccessful perturbations by cheaters and the total number of perturbations. This ratio indicates the probability that a system recovers from a cheater's perturbation to the regime of cooperation ($[C] = N$), which can be computed as $1 - \phi(C \to D)$.

On the other hand, the **restoration of cooperation** in a community full of cheaters can be measured by the ratio between the number of successful perturbations by cooperators and the total number of perturbations. This ratio indicates the probability that a system returns from the regime of defection ($[D] = N$) to the regime of cooperation ($[C] = N$), which can be computed as $\phi(D \to C)$.

From the perspective of cooperation, we find that the probability that a single cheater can invade and destroy the cooperation rapidly once the embedding parameter q crosses a threshold (Figure 4.10(A)). The exact value of the threshold depends on the selection strength δ. After this threshold, even a slight disturbance will lead to a successful invasion by cheaters, which implies the extinction of cooperators. This pattern of cooperation collapse resembles a critical transition as the external condition changes gradually .

For a single perturbation, there must exist a maximal number of mutants during the process of evolution. In detail, the max-size of mutants in a perturbation starting from t_0 to t_{end} can be calculated as:

$$max\text{-}size = \max\{[M]_t \mid t_0 \leq t \leq t_{end}\} \tag{4.8}$$

where $[M]_t$ is the number of mutants at step t. In the case of a perturbation to a network of cooperators, the mutants are cheaters, and $[M]_t = [D]_t$. When a perturbation leads to a transition, the max-size is N.

For a given embedding parameter $p = 0.6$ and the selection strength is $\delta = 0.01$, we have the distributions for the max-size of cheaters at some embedding parameters from $q = 0.75$ to $q = 1.0$ (Figure 4.11). With the increase of q, the max-size distributions shift from right-skewed to left-skewed, which indicates the deterioration of the resilience of cooperation.

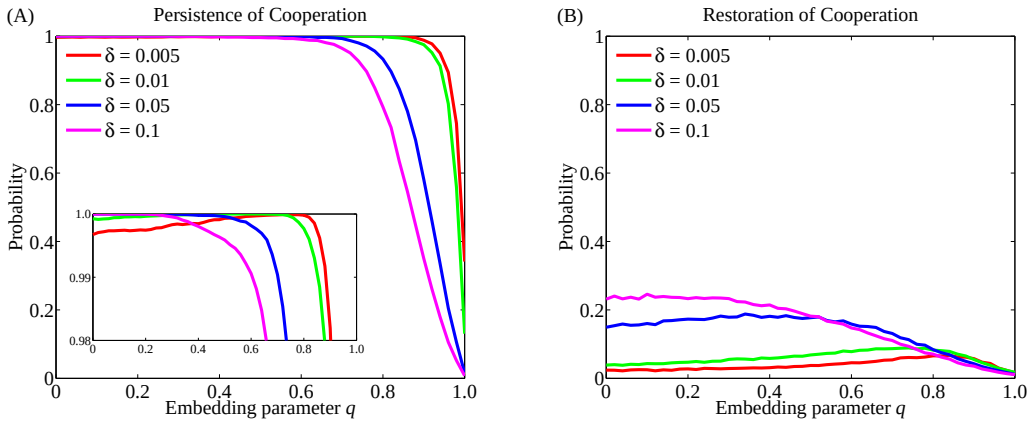

Figure 4.10: Persistence and restoration of cooperation. (A) The persistence of cooperation is present as a function of the embedding parameter q for various selection strength δs. Note the non-monotonicity of the curves: for low selection the persistence of cooperation reaches a maximum before collapsing (the non-monotonicity is visible more clearly in the inset panel that zooms in the relevant part). In the case of strong selection, however, the persistence of cooperation is decreasing monotonically. (B) The restoration of cooperation is present as a function of the embedding parameter q for various selection strength δs, which is computed as the fraction of successful perturbations. For a given δ and q, we consider 20000 perturbations, each of which is carried out by updating a network for a long time until the addition of a mutant at t_0 in a network of (A) only cooperators or (B) only cheaters. All results are shown under the embedding parameter $p = 0.6$ and another parameter $q \in [0, 1]$.

Furthermore, we also reverse the conditions and study the probability of restoring cooperation in a network of only cheaters. In Figure 4.10(B), the probability that a single cooperator restores a network of cheaters successfully increases when decreasing the embedding parameter q, but it never reaches a large value. This means that once cooperation is lost it is difficult to be recovered: on the route to restoration there is no critical transition. We find no hysteresis in this case, indicating that the dominance of cheaters is much more resilient than the dominance of cooperators. Restoring cooperation would only be possible by a strong perturbation, in fact a successful recovery from the community of cheaters will be possible only when the cooperators have reached a certain mass.

This asymmetry in the resilience of cooperators and cheaters is caused by the characteristics of the dynamical network structure, the way newcomers are embedded in the community and the payoff setups of the game. When q is sufficiently low, the

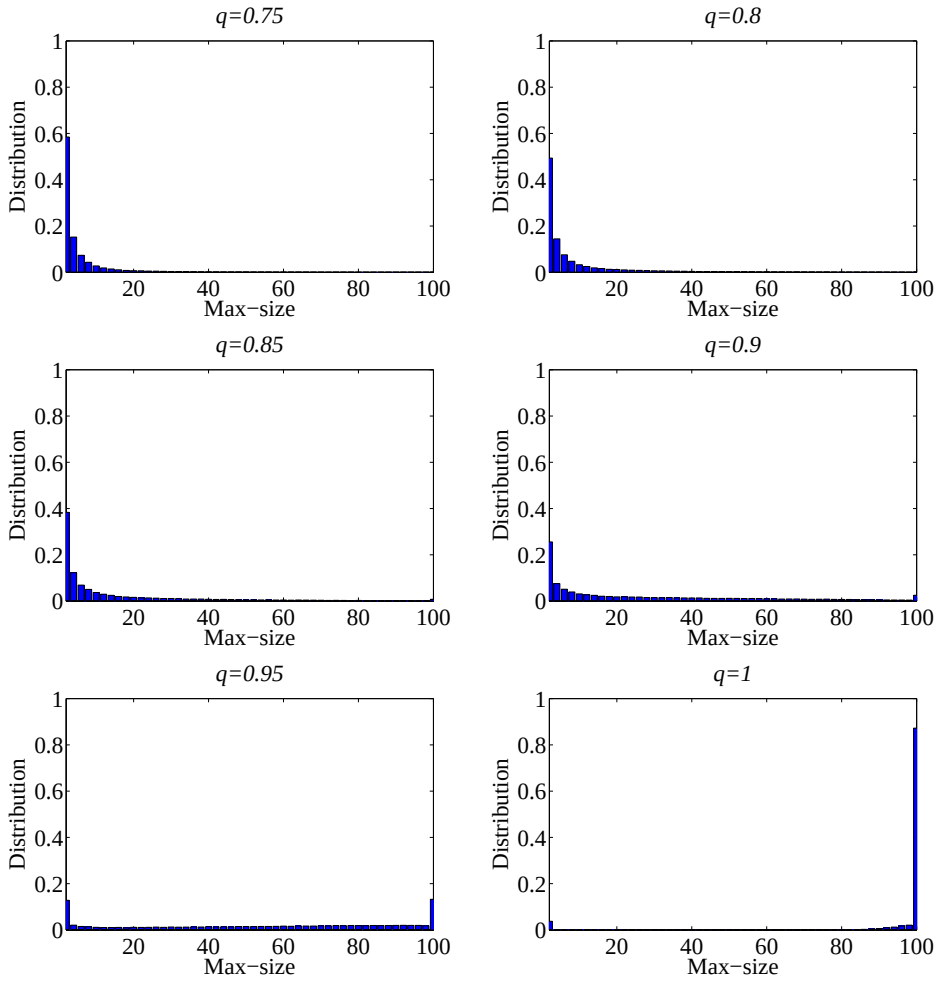

Figure 4.11: The distributions for the max-size of cheaters at different qs. At each q, we consider 20000 cheater's perturbations in a network of only cooperators with a size $N = 100$, and each perturbation is updated for a long time until the addition of a cheater at t_0.

network of cooperators is sparsely connected. Only a few connections are present and all nodes get similar payoffs (especially when δ is small enough, namely weak selection), therefore the chance that a single cheater invades is exclusive to neutral drift. As q increases the network becomes a little bit connected and the invading cheater will acquire some links to the cooperators, but those cheaters will become fragmented gradually due to the deterioration of fitness caused by *DD* links. However, the cooperators far away from the cheaters may be favoured by getting together, which results in a higher chance for the cooperator to be selected as a role-model. This gives rise

to a decrease in the chances of invasions by cheaters, consequently the intermediate increase in cooperation persistence (highlighted in the inset panel red curve in Figure 4.10(A)). Only as q increases to a large value, the invading cheaters become highly connected in the network and a large number of links to cooperators provide a tremendous advantage to them, even under weak selection. After this point, the spreading of cheaters is highly enhanced, which increases the risk of cooperation collapse.

On the contrary, the networks of only cheaters at higher qs are well connected (Figure 4.9). A single cooperator gets embedded in a mass of cheaters, obtaining very poor fitness. This isolation makes it quite hard for the newcomers to adopt the strategy of cooperation. Even if the embedding parameter q decreases, the chance of imitating cooperators does not increase substantially. The restoration of cooperation seeded by a single cooperative mutant is then doomed to fail.

4.3.3 More Cooperators Promote the Restoration of Cooperation

After adding a single mutant at t_0 in the perturbation experiment, the number of mutants will increase. When the mutants reach a certain density ρ in the population, we can measure the fraction of successful perturbations conditional on ρ as:

$$\phi_\rho = \frac{\#\ transitions}{\#\ perturbations\ reaching\ \rho} \tag{4.9}$$

Here, we intend to explore how many mutants are required to bring about a transition from the original regime to the opposite one. As described in the section above, we know that most cooperator's perturbations in a network of only cheaters are unsuccessful. It is very difficult to restore the cooperation once the cheaters have fully invaded the community, unless the population of cooperators is able to reach a certain size (Figure 4.12).

As shown in Figure 4.12, the density of mutants reaches ρ and the fraction of successful perturbations corresponds to ϕ_ρ. Interestingly, with the increase of the density of cheaters, the persistence of cooperation doesn't drop sharply under both weak and strong selections (left column in Figure 4.12). The max-size of cheaters in the process of perturbation may reach a big value due to the high fitness in the beginning (Figure 4.11). However, when we start from a community of only cheaters, the restoration of cooperation is quite different when the density of cooperators is increasing. In the right column of Figure 4.12, when the density of cooperators increases from $\rho = 0$ to $\rho = 0.5$, it is generally easier for the cooperators to restore from the defective community. Especially under strong selection, the cooperation can be restored completely

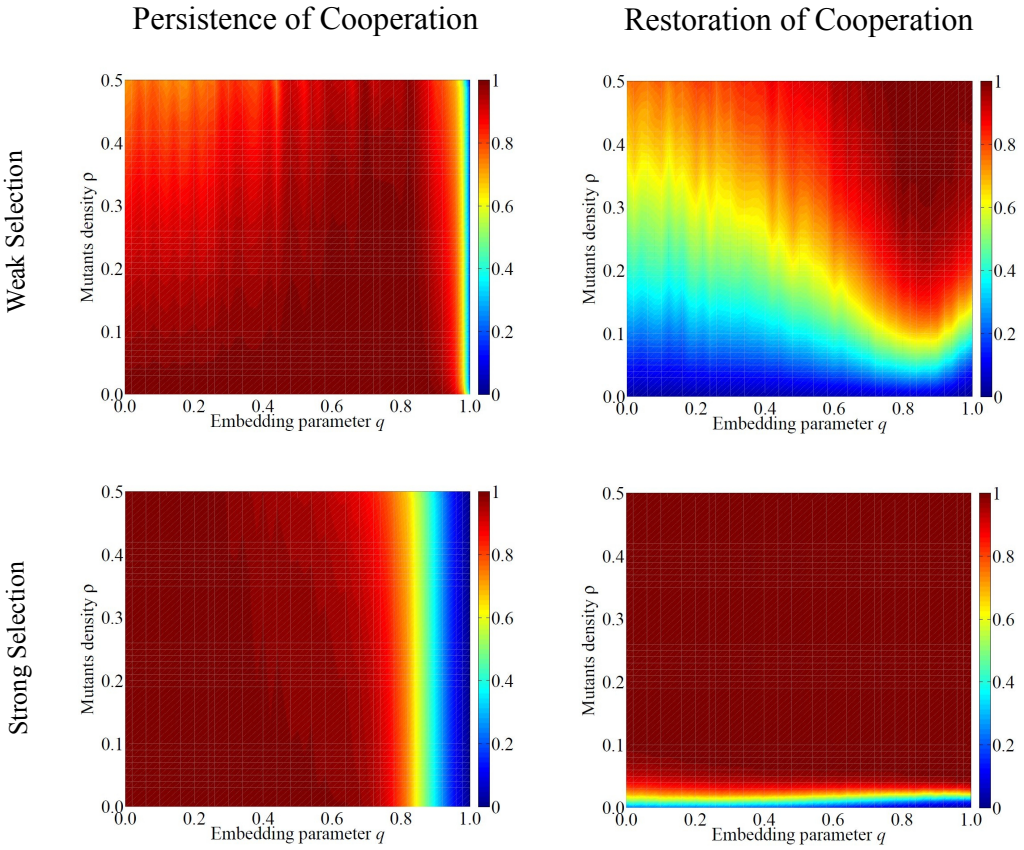

Figure 4.12: Cooperation persistence (left column) and restoration (right column) as a function of the embedding parameter q and mutant density ρ. We measure ϕ_ρ conditional on the density of mutants ρ under weak selection $\delta = 0.005$ and strong selection $\delta = 0.1$, where the persistence of cooperation is computed by $1 - \phi_\rho(C \to D)$ and the restoration of cooperation is computed by $\phi_\rho(D \to C)$. The results are obtained from 20000 perturbations at each q and each perturbation is implemented by updating a network with $N = 100$ players for a long time until the addition of a mutant agent at t_0.

when cooperators have reached a certain mass. However, despite it is very likely for the cooperators to restore a network full of cheaters (when the density of cooperators has already reached a certain value), there is still no critical transition that can be observed with the increase of q.

4.3.4 The Effects of the Embedding Parameter p

To reveal the effects of another embedding parameter p, which is the probability for the new-born to connect the role-model (i.e. parent) itself, we plot the persistence of cooperation as a function of the embedding parameter q in Figure 4.13. Three differ-

ent parameters are explored at: (a) $p = 0.2$, (b) $p = 0.6$ and (c) $p = 1.0$. Starting from a network full of cooperators, we have the persistence of cooperation under various selections, where the dynamics of the system is hardly influenced by the embedding parameter p. It is the embedding parameter q, the probability to connect each neighbour of the role-model, that affects the resilience of the population.

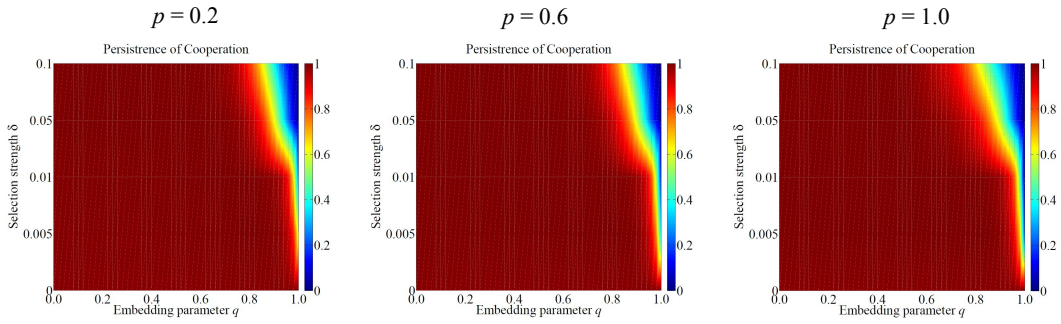

Figure 4.13: At different ps, we have the persistence of cooperation as a function of the embedding parameter q and selection strength δ. The results are obtained by considering 20000 perturbations for a given q and δ, and each perturbation is carried out by updating a network of only cooperators for t_0 steps followed by the addition of a cheater.

In the following, we will fix one embedding parameter $p = 0.6$ but vary another embedding parameter q from 0 to 1 to detect the loss of cooperation, where a perturbation of cheaters is introduced in a network of only cooperators at t_0.

4.4 Detecting the Loss of Cooperation

The rapidly increasing chance of invasions by cheaters (especially when the embedding parameter q crosses a threshold) indicates that the changes in the persistence of cooperation are far from linear. With enough detailed knowledge on the embedding parameter q and selection strength δ, one could estimate the probability that the invading cheaters dominate the community full of cooperators. However, in most cases, one cannot assume such detailed knowledge and therefore should consider the possibility of alternative ways that could indirectly signal the rising risk for the collapse of cooperation.

4.4.1 The Evaluation of the Indicators

Motivated by the generic indicators for critical transitions (Scheffer et al., 2009), we evaluate two broad classes of indicators: those based on the dynamics of the population composition (as known as *non-structural* indicators) and those based on the network structure (as known as *structural* indicators). The difference between the two classes is that non-structural indicators reflect the changes in the numbers of cheaters and cooperators, whereas structural indicators reflect the changes in the interactions between the players.

We compute the structural and non-structural indicators for each perturbation experiment, where a single invading cheater is introduced into a network of only cooperators. To remove the transients, the initial network with N players is updated for t_0 steps. After that, the community co-evolves until one of the two outcomes is reached: either recovery, the cheater fails to invade; or transition, the cheater invades successfully and the cooperation collapses. For each perturbation, we identify by t_0 the beginning of the perturbation and with t_{end} the end of the perturbation.

4.4.1.1 Non-structural Indicators

In particular, we estimate two non-structural indicators, which are (1) return rate: the inverse of the time it takes for the system to recover back to its original state of all cooperators after the addition of a single cheater; and (2) maximum size: the maximal amount of cheaters reached after a perturbation.

- Return rate is defined as:

$$return\ rate = \frac{1}{return\ time} \tag{4.10}$$

  where *return time* is the number of update steps the system takes to go back to its original state following a perturbation (Scheffer et al., 2009).

  Hence, if the perturbation is unsuccessful, then the return time is calculated as $t_{end} - t_0$. Otherwise if the perturbation is successful, then the return rate is defined to be 0.

- Max-size (of cheaters) is the maximal number of cheaters recorded during a perturbation to a network of cooperators.

$$max\text{-}size = \max\{[D]_t \mid t_0 \leq t \leq t_{end}\} \tag{4.11}$$

where $[D]_t$ is the number of cheaters at step t. It is the size of the population *max-size* $= N$ if the perturbation of cheaters is successful.

4.4.1.2 Structural Indiators

In terms of structural indicators, we estimate (1) average connectivity of the network, and (2) structural coefficient σ^*, which is the fraction of beneficial interactions between cooperators over the exploitative interactions between cooperators and cheaters.

- Average connectivity is the average number of links per node recorded during a perturbation to a network of cooperators. We can compute it in a dynamical network as:

$$\langle k \rangle = \frac{\sum_{t=t_0}^{t_{end}} \langle k \rangle_t}{t_{end} - t_0} \tag{4.12}$$

  where $\langle k \rangle_t$ is the average degree of the network at step t.

- Structural coefficients σ^*, which is computed by

$$\sigma^* = \frac{\sum_{t=t_0}^{t_{end}} [CC]_t}{\sum_{t=t_0}^{t_{end}} [CD]_t} \tag{4.13}$$

  where $[CC]_t$ is the total number of CC links (doesn't discount as the symmetry), $[CD]_t$ is the total number of CD links in the network at step t.

  Intuitively, σ^* evaluates the ratio between the beneficial payoff (generated by purely cooperative interactions) and the detrimental payoff (generated by cheaters connected to cooperators). This coefficient is inspired by the structural parameter introduced in Refs. (Tarnita et al., 2009; Nowak et al., 2010).

4.4.2 The Pattern of the Indicators

We estimate the above four indicators in the perturbation experiments under different selections and varying embedding parameters (q from 0 to 1). In Figure 4.14, we plot the median values of those indicators from 20000 perturbations performed at each q.

We find that both non-structural and structural indicators change in perceivable ways before the persistence of cooperation falls below 0.5, which is defined as a threshold for the collapse of cooperation. The corresponding embedding parameter is denoted as $q(0.5)$, as known as the **tipping point** in critical transitions. Strikingly, the return rate decreases in a manner that resembles the critical slowing down (CSD) prior to the tipping point (Figure 4.14 (A) and (C)) supporting the idea that the loss

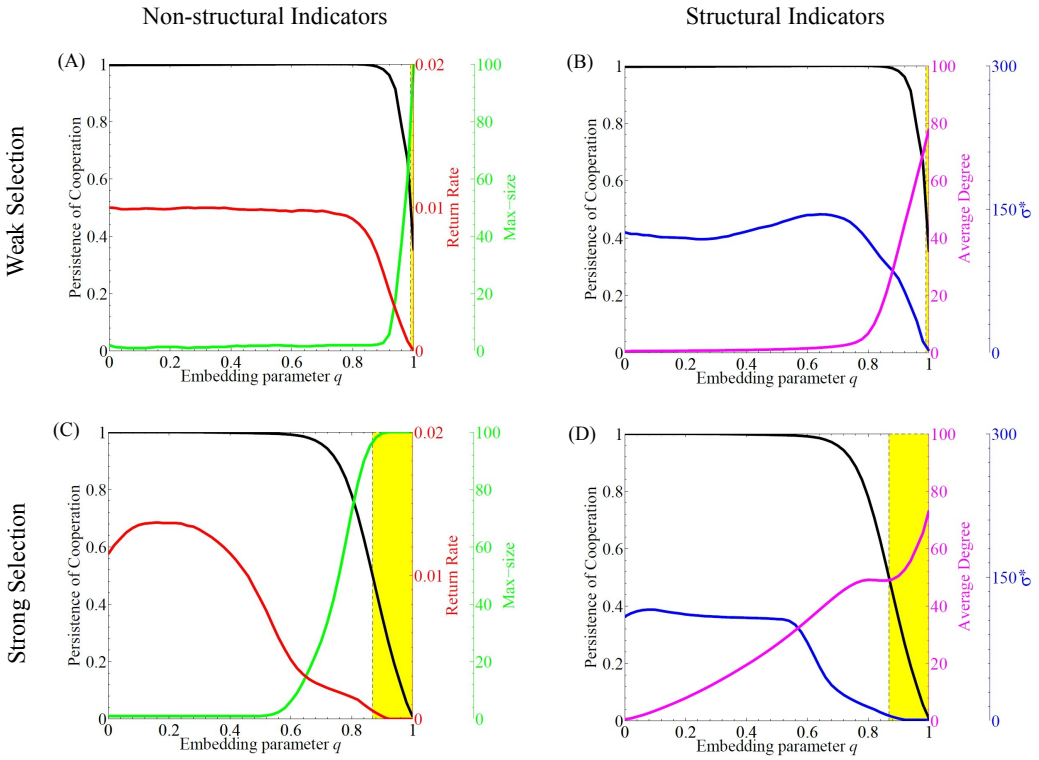

Figure 4.14: The pattern of indicators adopted to detect the loss of cooperation. Non-structural (left column) and structural (right column) indicators are measured in our perturbation experiments. We plot the trends of indicators in the case of weak selection $\delta = 0.005$ (upper row), and strong selection $\delta = 0.1$ (lower row). The black curve denotes the persistence of cooperation. The yellow shaded area identifies the values of q where the persistence of cooperation is below 0.5. The x-axis represents the embedding parameter q, and the other embedding parameter p is fixed to 0.6. Each point in the indicators is the median estimated out of the considering 20000 perturbations, and each perturbation is starting from the addition of a cheater in a network of only cooperators with $N = 100$.

of cooperation in dynamical networks might be perceived as a critical transition. In addition, the changes in the indicators are dependent on the selection strength δ, where strong selection leads to more pronounced and earlier changes in the indicators when compared to weak selection. In order to capture the distribution of the indicators at each q, we present the median of the indicators as well as the range between 25% percentile and 75% percentile in Figure 4.15.

Although the pattern of the a random sequence from $q = 0$ to $q(0.5)$ maybe misleading, where the value of a certain indicator at each q is randomly picked from all 20000 perturbations, the overall distributions of these indicators shown in Figure 4.15

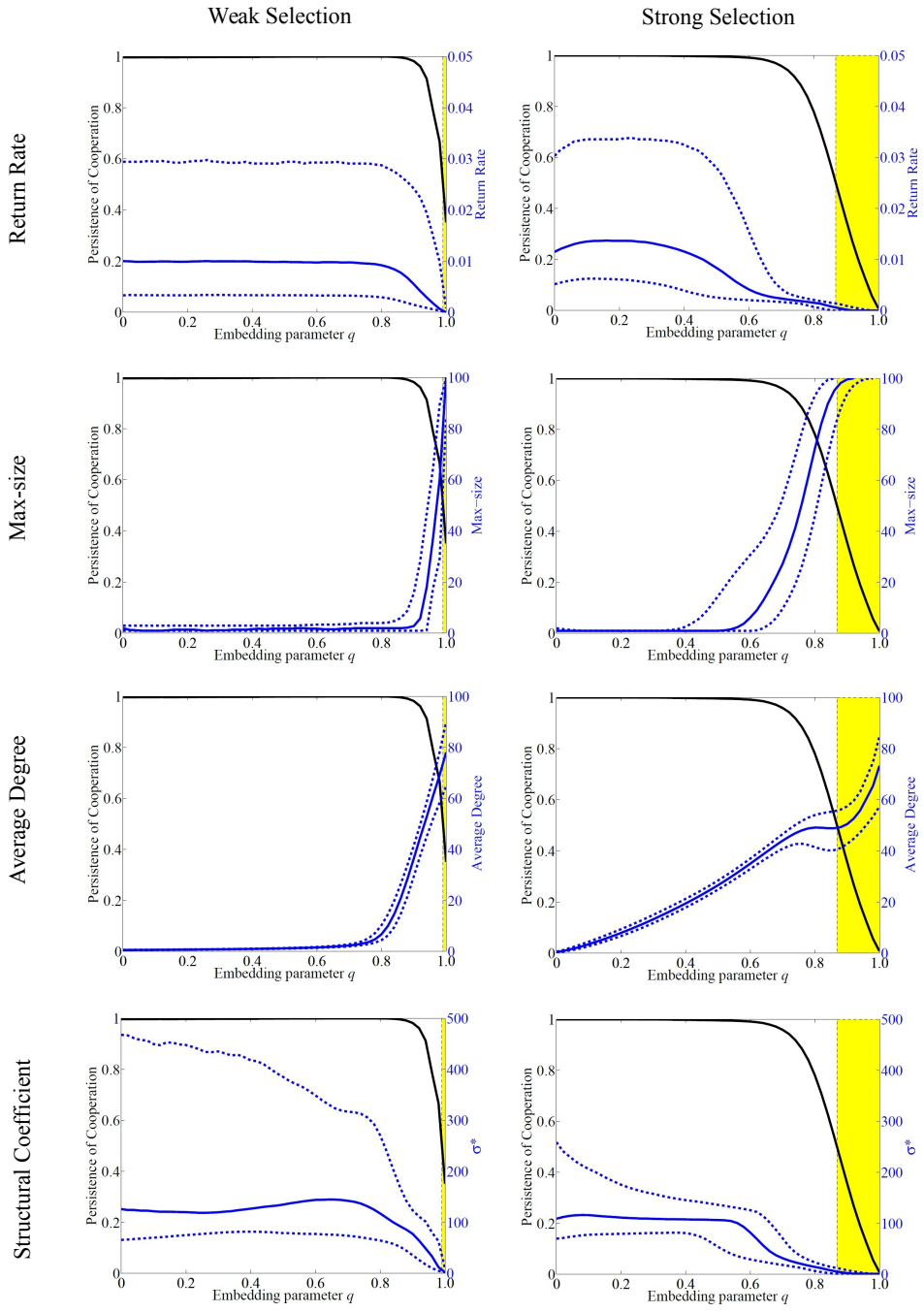

Figure 4.15: The distributions of various indicators with percentiles. The blue solid curves are the median values obtained by considering 20000 perturbation experiments. The blue dashed curves denote the 25% and 75% percentiles for the distribution of the indicators. Yellow area starts from the tipping point where the persistence of cooperation (black curve) falls below 0.5. The rest numerical simulation parameters are same as before (Figure 4.14).

still confer a promising pattern. In particular, the return rate and structural coefficient σ^* present a wide distribution at smaller qs but converge around their median values before the collapse of the cooperation. On the contrary, the max-size and average degree diverge before the collapse of the cooperation. These two opposite phenomena illustrate some early warnings for the loss of cooperation.

To measure the performance of the indicators in detecting the loss of cooperation, some qualitative and quantitative measurements are required. In the following, we will analyse the consistency and accuracy of the indicators compared to the persistence of cooperation.

4.4.3 Consistency of the Indicators through Kendall Correlations

Although we observe conceivable changes in the indicators, these changes are not always monotonic to the changes in the embedding parameter q. Instead, an indicator is informative, and thus useful, only if it is changing in a correlated way to the persistence of cooperation independently of the selection strength.

In this section, we intend to test such informative consistency by computing the Kendall τ rank correlation coefficient (Abdi, 2007) between the sequence of indicators and the persistence of cooperation.

4.4.3.1 Kendall τ Rank Correlation

Kendall τ rank coefficient is used to measure the association between two measured quantities. For any pair of data (x_i, y_i) and (x_j, y_j), we can measure them as:

- concordant pair

  if $x_i > x_j \wedge y_i > y_j$ or $x_i < x_j \wedge y_i < y_j$;

- discordant pair

  if $x_i > x_j \wedge y_i < y_j$ or $x_i < x_j \wedge y_i > y_j$.

Suppose we have n observations $(x_1, y_1), (x_2, y_2), \cdots (x_n, y_n)$ in a 2-dimensional data space, and then we can compute the number of concordant pairs defined as cp and that of discordant pairs defined as dp by comparing any pair of them. The Kendall τ coefficient is computed as:

$$\tau = \frac{cp - dp}{n(n-1)/2} \tag{4.14}$$

where n is the size of data space. As we can see, the Kendall τ rank correlation coefficient follows that $-1 \leq \tau \leq 1$. When $\tau > 0$, it indicates that the two sets of data are positively correlated; otherwise when $\tau < 0$, it indicates that the two sets of data are negatively correlated. In particular, the correlation is strong when $|\tau| \to 1$.

4.4.3.2 The Distribution of Kendall τ Coefficients

In the perturbation experiments, we also have two sets of data for a certain indicator: one is the sequence of indicators (see Figure 4.15) and the other is the persistence of cooperation (see Figure 4.10(A)). As shown in Figure 4.16, we illustrate a schematic diagram to show the computation of Kendall τ coefficient between them, where the range of qs is from $q = 0$ to $q(0.5)$ (which indicates the tipping point at which the persistence of cooperation falls below 0.5).

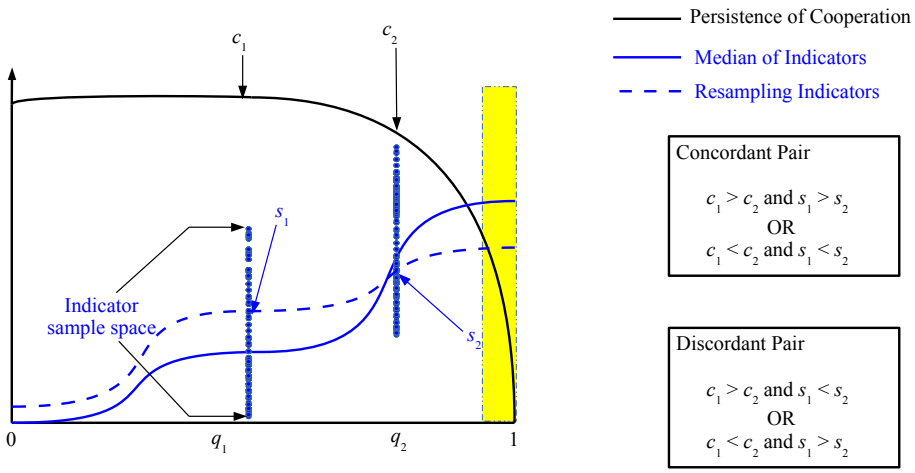

Figure 4.16: Detecting the consistency between the persistence of cooperation and the indicators. A schematic diagram is presented to show how to compute the Kendall τ coefficient. For any given indicator, we intend to test the data before the collapse of cooperation, namely $q(0.5)$. We have a sample space at each q, which contains all indicator values corresponding to 20000 perturbations. Randomly pick an indicator value at each q, and then we can have a sequence of resampling indicators from $q = 0$ to $q(0.5)$. In this way, we are able to compute the Kendall τ coefficient by comparing the persistence of cooperation with that sequence of resampling indicators.

For a given indicator, we compute the Kendall τ rank correlation coefficient by constructing a sequence of resampling indicator values from $q = 0$ to $q(0.5)$, and at each q the indicator value is taken randomly out of the sample space obtained from

the perturbations. Repeating the above process, a large number of sequences will be constructed following a bootstrap approach without replacement, so will be as many as Kendall τ coefficients. In detail, the Kendall τ distribution (Figure 4.17) can be obtained as follows to depict the consistency of that indicator:

- Construct a sequence of indicator values after randomly picking one from all the perturbations at each q;
- Compute the Kendall τ coefficient between such a constructed sequence and the persistence of cooperation up to the decided tipping point $q(0.5)$.
- Repeat the above process to a large number of iterations, and we obtain lots of Kendall τ values.
- Fit those Kendall τ coefficients as a Gaussian distribution.

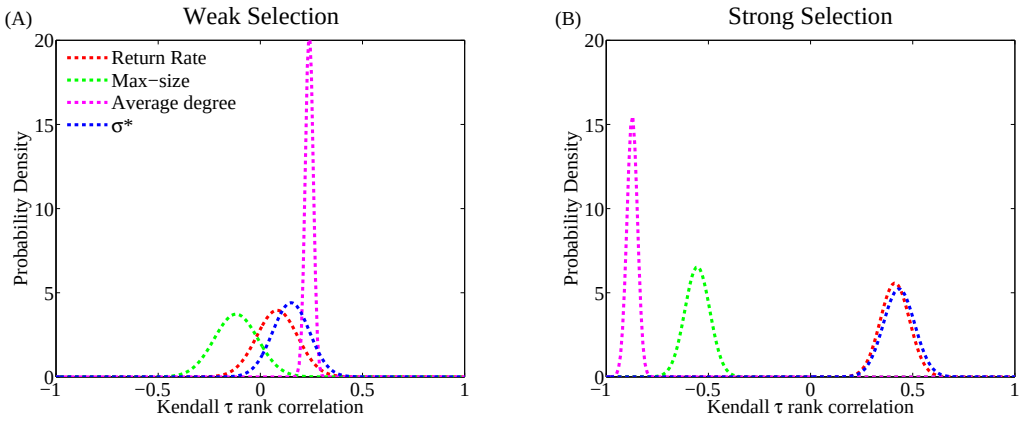

Figure 4.17: Kendall τ distributions of the indicators under weak $\delta = 0.005$ and strong selection $\delta = 0.1$. As we can see, most of the indicators are consistent with the increase of selection strength except the average degree, which changes the sign from positive to negative. As before, we conduct 20000 perturbations at each q, and for each perturbation a random network with $N = 100$ cooperators is updated until the addition of an invading cheater at t_0. The perturbation stops when either transition or recovery is obtained.

Intuitively, one indicator is more consistent than another if the range of the obtained Kendall distribution tends to fall on the same side (either positive or negative) of the x-axis, independent of the considered selection strength.

Furthermore, the consistency of indicators with varying selections is illustrated in Figure 4.18. By comparing the mean values and standard deviations of the Kendall τ

distributions, we can find that the consistency is dependent on the selection strength. In particular, the max-size and structural coefficient σ^* perform consistently with the persistence of cooperation. On the other hand, the average degree is the most inconsistent indicator as the selection increases. Under weak selection, the trends of average degree are positively correlated with the persistence of cooperation, while when selection is strong the trends become negatively correlated. This inconsistency presented in some indicators actually highlights that the reliable interpretation of the trends requires the knowledge of underlying evolutionary process.

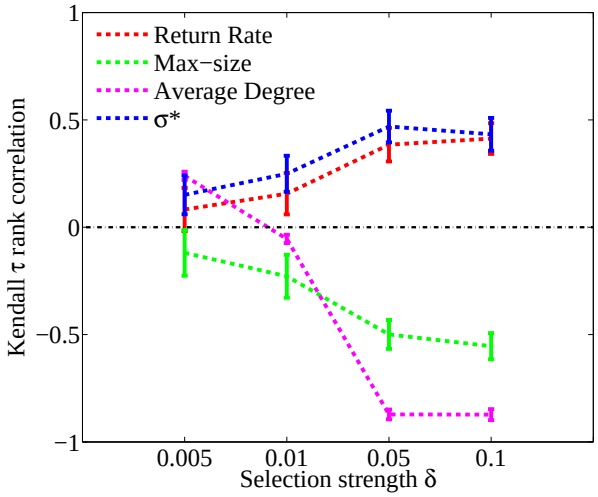

Figure 4.18: Consistency of the indicators at different selection strengths. Mean values and standard deviations of the distributions for Kendall τ coefficients are illustrated as the selection strength δ increases. Non-structural indicators are (1) return rate and (2) max-size; and the structural indicators are (1) structural coefficient σ^* and (2) average degree. It is clearly that the average degree is inconsistent as the mean value of its Kendall distribution changes sign when the selection strength is increasing, even though it shows a quite high correlation under some selections. In addition, the correlations of other indicators generally get stronger with the increase of selection strength. The parameters used for numerical simulations are same as before (Figure 4.14).

4.4.3.3 The Influences of Tipping Point

The data space used to compute the consistency is ranging from $q = 0$ to the tipping point, at which a critical transition from the regime of cooperation to that of defection is defined. In general, we have the tipping point in the loss of cooperation defined as $q(0.5)$, namely the point at which the persistence of cooperation falls below 0.5.

When the defined tipping point is changed to some earlier ones, for example $q(0.75)$ and $q(0.95)$, the data space is smaller and we have Figure 4.19 to illustrate the respective Kendall τ distributions under weak ($\delta = 0.005$) and strong selection ($\delta = 0.1$). Interestingly, an increasing tipping point generally leads to an increase in the correlation between the indicators and cooperation persistence.

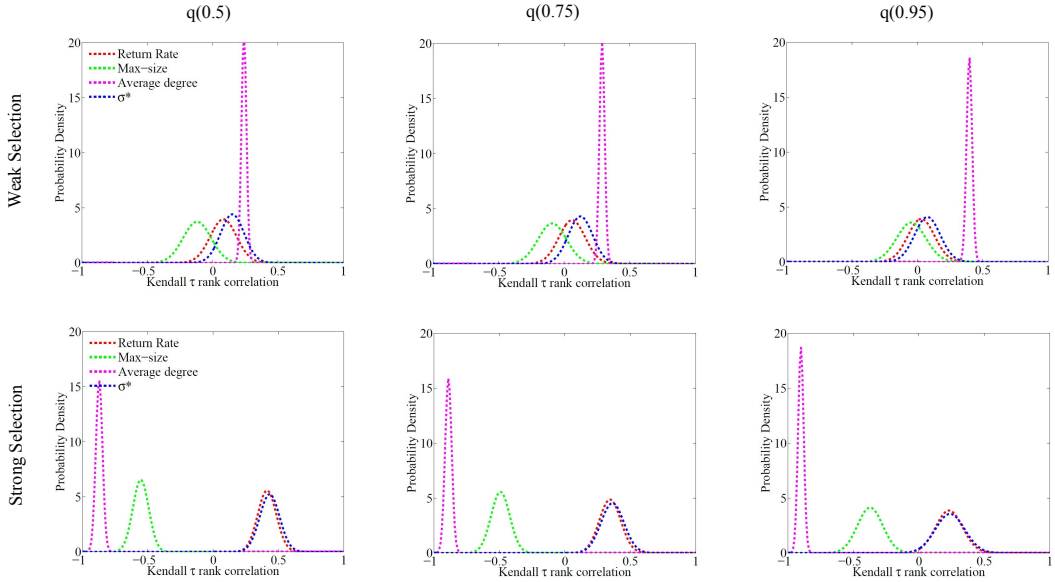

Figure 4.19: The distributions of Kendall τ coefficients at different tipping points. We consider the tipping point as the value of q, which corresponds to the persistence of cooperation is 0.5 (left column), 0.75 (middle column) and 0.95 (right column) respectively. The parameters used for numerical simulations are same as before (Figure 4.14).

The inconsistency of some indicators for identifying the increasing risks of cooperation loss actually highlights the complexity of interpreting such trends in coupled dynamics of finite population. When the selection strength is small, the population suffers the risk of invasions by cheaters only when the embedding parameter q becomes sufficiently large. As discussed earlier, under weak selection, the persistence of cooperation follows a non-monotonous curve. Only when the selection is strong, the risk increases monotonously and the trends in the indicators become consistent. Nonetheless, these features highlight the following two aspects. First, the search for consistent indicators at any level of selection may be non-trivial: only indicators that display a correlated non-monotonous trend can consistently detect the risk of invasions by cheaters. Secondly, the trends can be more informative of the underlying mechanistic process rather than signalling the risk: they can help to deduce the degree of selection and to identify an underlying evolutionary mechanism.

4.4.4 Accuracy of the Indicators through ROC

Next to the consistency, we also need to analyse the accuracy of the indicators in detecting the loss of cooperation. Here, we analyse the accuracy by defining the cases of false positives (false alarms) and false negatives (no alarms) prior to the collapse of cooperation at the tipping point. We conduct the detection accuracy by using the receiver operating characteristic (ROC) curves (Boettiger and Hastings, 2012) in this study. In general, ROC curves are obtained by plotting the true positive rates (TPR) versus the false positive rates (FPR) for the indicators at various discrimination levels. Larger area under the ROC curve (AUC), more accurately an indicator identifies the rising risk of invasions by cheaters. However, if the area is smaller than 0.5, then it means that the indicator trend carries no accurate information about the risk of invasions.

4.4.4.1 Receiver Operating Characteristic (ROC)

Receiver operating characteristic (ROC) curve, is usually used to describe a binary classifier system with the change of its discrimination threshold. In a ROC curve, the true positive rate and false positive rate are presented at various thresholds. Similar to the diagnostic decision making, we use ROC to detect whether an indicator behaves correctly corresponding to the persistence of cooperation.

There are two prediction outcomes and two actual results as well: *positive* and *negative*, and then four possible combinations are presented:

- True Positive (TP): if the prediction result is positive and the actual result is positive as well.
- False Positive (FP): if the prediction result is positive but the actual result is negative.
- True Negative (TN): if both the prediction result and actual result are negative.
- False Negative (FN): if the prediction result is negative while the actual result is positive.

Each point in the ROC space is defined by the true positive rate (TPR) and false positive rate (FPR) under a certain threshold. The TPR shows the fraction of correct positive predictions in the whole positive samples, namely

$$\mathrm{TPR} = \frac{\#TP}{\#TP + \#FN} \tag{4.15}$$

Similarly, the FPR indicates the fraction of incorrect positive predictions in the whole negative samples, namely

$$\text{FPR} = \frac{\#FP}{\#FP + \#TN} \tag{4.16}$$

For a given threshold θ, we have a pair of TPR and FPR. When we change the threshold from very small to very big, we obtain a curve of ROC constituted by those TPR and FPR pairs (see Figure 4.20). The diagonal in the ROC space from $(0,0)$ to $(1,1)$, known as random guess line, divides the ROC space into two parts: points above the random guess line represent good classification results (better than random); on the contrary, points below the line indicate poor prediction results (worse than random).

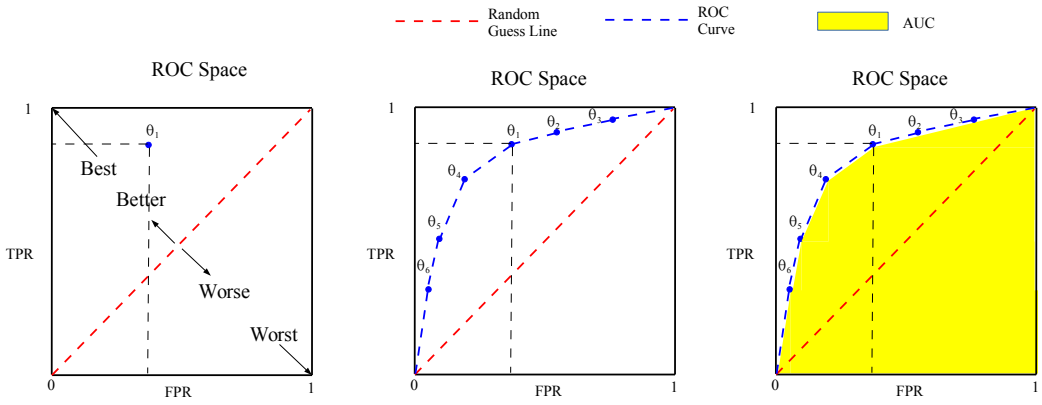

Figure 4.20: A schematic diagram illustrates the mechanism of ROC curve. For a given threshold θ, one can obtain a pair of TPR and FPR by considering the numbers of TP, FP, TN, and FN. When more thresholds are taken into account, a curve is formed in the ROC space. The area under the ROC curve indicates the probability that "positive" ranks higher than "negative".

Now, let's consider the accuracy of an indicator in detecting the loss of cooperation within a given **observational window** starting from $q = 0$ to q', where $q' \leq q(0.5)$. Given two arbitrary points q_1, q_2 between $q = 0$ and q', with $q_1 < q_2$, we randomly pick two values from the indicator sample space at q_1 and at q_2 and denote them by s_1 and s_2 respectively. Similarly, we denote by c_1 and c_2 the values of cooperation persistence at q_1 and q_2 respectively. In this case, the values of s_1 and s_2 tuned by θ will provide the prediction outcomes, while c_1 and c_2 will provide the actual results.

For a given observational window, we use a **discrimination threshold** θ to define the cases of true/false positive/negative. The parameter θ indicates a criterion value to discriminate the prediction outcomes. Specifically, for each indicator we need to

constitute two distinct ROC curves, which correspond to two possible discrimination conditions in judging whether the prediction of that indicator is positive or negative.

Condition (I):

- If $(1+\theta)s_1 < s_2$ and $c_1 \geq c_2$, then it is a true positive (TP).
- If $(1+\theta)s_1 < s_2$ and $c_1 < c_2$, then it is a false positive (FP).
- If $(1+\theta)s_1 \geq s_2$ and $c_1 < c_2$, then it is a true negative (TN).
- If $(1+\theta)s_1 \geq s_2$ and $c_1 \geq c_2$, then it is a false negative (FN).

Condition (II):

- If $(1+\theta)s_1 \geq s_2$ and $c_1 \geq c_2$, then it is a true positive (TP).
- If $(1+\theta)s_1 \geq s_2$ and $c_1 < c_2$, then it is a false positive (FP).
- If $(1+\theta)s_1 < s_2$ and $c_1 < c_2$, then it is a true negative (TN).
- If $(1+\theta)s_1 < s_2$ and $c_1 \geq c_2$, then it is a false negative (FN).

As the sample space at each q is large enough, we can produce a large number of indicator pairs (s_1, s_2) and cooperation pairs (c_1, c_2) between $q = 0$ and q', which are used to evaluate, for each indicator, the total number of TP, FP, TN and FN based on either condition (I) or condition (II). Once these numbers are obtained, we can compute the sensitivity and specificity for each indicator under that threshold θ:

$$\text{Sensitivity} = \text{true positive rate (TPR)}$$

$$\text{Specificity} = \text{1-false positive rate (FPR)}$$

The calculated pair (TPR, FPR) constitutes a single point in the ROC curve. Repeating the above described process for as many as possible thresholds θs (from very small to very large), we can obtain a set of (TPR, FPR) pairs, which constitute a full ROC curve.

Notably, each indicator has two possible symmetric ROC curves - depending on whether the condition used to determine FP, FN, TP and TN is either (I), or (II). For convention, we choose the condition that gives the larger area under the curve (AUC) within the largest observational window (namely $q' = q(0.5)$) as the **effective discrimination condition**. In this study, the indicators of max-size and average degree would adopt the condition (I), while the indicators of return rate and structural coefficient σ^*

would adopt the condition (II) to detect the loss of cooperation. For completeness, we present the ROC curves in Figure 4.21, whose observational window is largest, namely from $q = 0$ to $q(0.5)$.

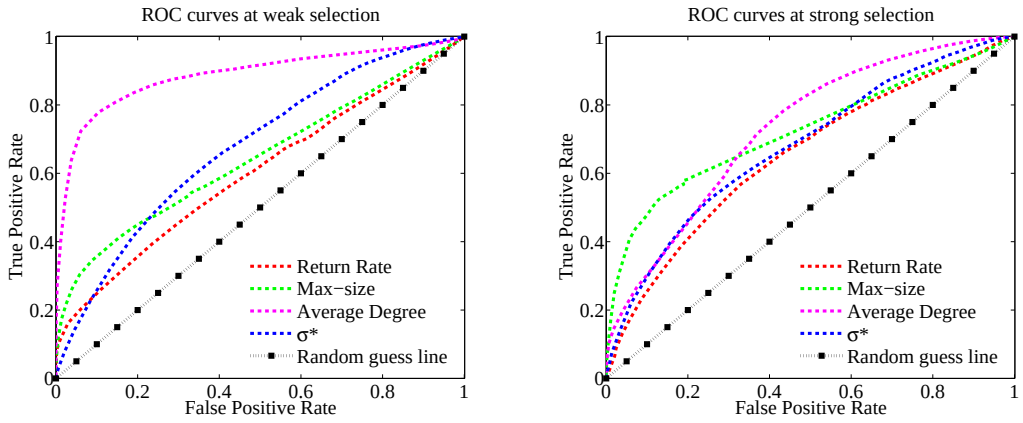

(a) Weak Selection (b) Strong Selection

Figure 4.21: ROC curves of the indicators within the largest observational window are obtained by using all data from $q = 0$ to $q(0.5)$. Based on the condition that gives the larger AUC, we plot the ROC curves for the indicators under weak ($\delta = 0.005$) and strong selection ($\delta = 0.1$). The parameters used for numerical simulations are same as before (Figure 4.14).

4.4.4.2 Varying Observational Windows

The discussions above shed light upon the accuracy of indicators within a certain observational window, namely the data is picked from the space ranging from $q = 0$ to $q(0.5)$. In this section, let's investigate the influence of data space on the ROC curves, where we will vary the size of the observational window.

We estimate the area under the ROC curves (AUC) for each indicator through a range of observational window sizes in Figure 4.22. Intuitively, an observational window characterizes the distance from the collapse of cooperation: increasing the size of the window means to estimate the accuracy closer to the transition. Specifically, with the increase of selection strength and observational window size, most of the indicators work very well in detecting the loss of cooperation. Under weak selection, return rate, max size and σ^* are almost inaccurate for small observational windows, where the AUC is close to 0.5 (Figure 4.22 (A)). However, the indicator of average degree has a high false positive rate when the observational window is small but outperforms the rest indicators when the observational window is large, which provides misleading in-

formation in the detection of collapse. On the other hand, when the selection is strong, most of the indicators become accurate following the same pattern with the increase of observational window (Figure 4.22 (B)), where their accuracy is already evident far from the collapse of cooperation at the tipping point.

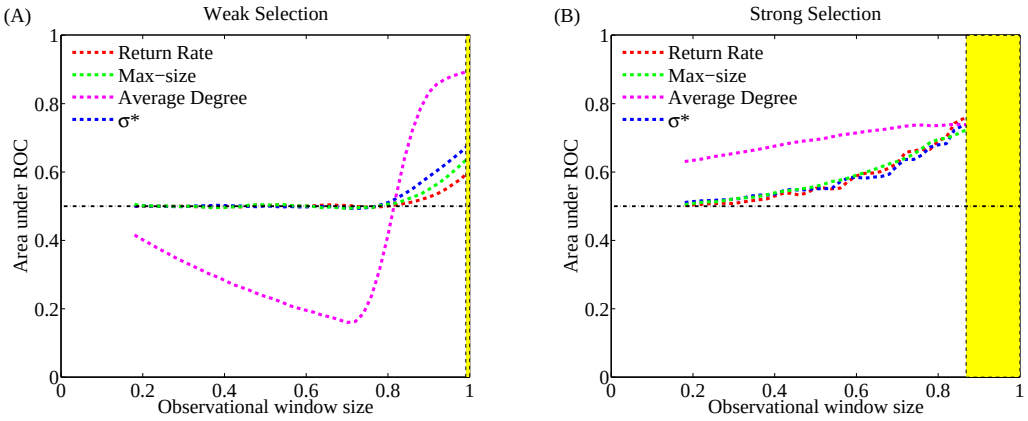

Figure 4.22: Accuracy of the indicators for varying observational window sizes. We plot the area under the curve (AUC) for structural and non-structural indicators under weak ($\delta = 0.005$) and strong selection ($\delta = 0.1$), where each point indicates an observational window from $q = 0$ to the corresponding q. An observational window defines the distance from the transition: a large window corresponds to comparing changes in the indicators for values close to the collapse of cooperation. An AUC of 1 represents a perfect test; an area of 0.5 represents a random test. Under weak selection, the average degree is inconsistent for varying observational windows, and the indicators are more accurate under strong selection. The parameters used for numerical simulations are same as before (Figure 4.14).

4.5 Summary

Combining evolutionary mechanism with game theory, the evolution of cooperation in dynamical networks presents many fascinating properties. How to recognize the conditions that favour the spreading of cheating behaviour and then the collapse of cooperation in a community has been a major objective in the study of evolutionary population (Levin, 1999, 2010; Bowles and Gintis, 2011). Here we approach this issue from a different perspective and look at the dynamics of cheaters, cooperators, and their interactions to infer the risk of cooperation collapse. Specifically, we argue that the collapse of cooperation can be approximated to a critical transition: an abrupt

change in equilibrium dynamics at the crossing of a bifurcation point. Although, it is difficult to make analytically a clear link of the dynamics in our model to such a bifurcation point, we find that return rate (i.e. inverse of the time necessary for a cheater to get expelled from the community) gradually decreases prior to the collapse in our numerical experiments (Figure 4.14). Such a slowing down resembles the critical slowing down effect prior to the bifurcations point (Scheffer et al., 2009; Wissel, 1984) and appears clearly in our complex adaptive system, even if the transition we study may not belong to the same dynamical family.

We actually demonstrate that the abrupt loss of cooperation can be detected in advance by a handful of structural as well as non-structural indicators that are associated to the critical slowing down. In particular, the few studies on critical transitions on networks assume fixed topologies and use non-structural indicators to detect dynamical instabilities (Dakos et al., 2015; Suweis and D'Odorico, 2014), and the structural indicators have not yet been developed for detecting the instabilities in evolutionary communities. In the considered population, the structure is not static but co-evolving with the spreading of strategies, which allows us to monitor its dynamics using a suite of complex network metrics. Among the structural indicators we tested (including varying links, connectivity, structural coefficients, etc.), we showed that the decreasing ratio of beneficial interactions (between cooperators) to detrimental ones (between cheaters and cooperators) could detect the increasing risk of invasions by cheaters effectively.

In addition, our results also show that the success of early warnings in the evolutionary population is crucially linked to the selection strength, where some indicators may be effective for a larger range of selection strengths, but some are effective for a smaller range. In this adaptive situation, the level of selection defines the effective payoff returned to an agent. Stronger selection increases the chance that a cheating invader connects to better-off individuals and can benefit more. Not surprisingly, this difference makes the risk of collapse to increase earlier and more abruptly when the selection is strong (Figure 4.10), driving similar patterns in the indicators. In general, the reliable detection of the collapse of cooperation in dynamical networks is affected by the level of selection and the size of observational window, where most of the indicators become more accurate and consistent under stronger selection and bigger window.

Despite our work is based on a specific adaptive network model, where the dynamics of state and structure are triggered by the birth-death mechanism, our approach and indicators can be extended to other models of evolutionary population (Lieberman

et al., 2005; Tarnita et al., 2009). For example, some structural indicators like connectance, clustering, assortativity, etc. may be useful in other models of structured populations. The presented results suggest that it is possible to evaluate the resilience of cooperation by monitoring the interactions and following the behaviour of individuals in a community, in practice such information might be difficult to obtain. Identifying cheaters from cooperators, or even following their interactions in time seems a daunting task. Still, the difficulty for evaluating the proposed signals may depend on the specific application, the type, and the scale of the community in question. Perhaps the most novel conclusion of this work is that we can identify the progressive loss of cooperation persistence by combining non-structural and structural indicators. Although the patterns we reported have high standard errors due to the stochastic component in our model, they still confer a promising pattern. As such our study paves the way for testing and developing similar indicators in a variety of evolutionary subjects, ranging from biological systems to ecological communities and even socio-economic networks.

Chapter 5

Distributed Learning in Adaptive Agents Coordination

The main purpose of this chapter is to illustrate how a generalised work-learn-adapt (WLA) framework can lead to high organisation performance in cooperative adaptive networks. We ground this WLA framework into the paradigm of adaptive agents coordination, where a number of cooperative agents need to complete some complicated tasks in a distributed manner. In this situation, the organisation performance is highly dependent on the functional agents and their interacting relationships. Under the framework of WLA, all agents work according to their corresponding functionality without a central control, meanwhile they are able to learn and recognize the environment by aggregating local and historical information. At a slower rate, the agents will implement state evolution and structure adaptation rationally based on the knowledge obtained from distributed learning, such that a favourable organisation configuration can arise. Notably, the dynamics of state and structure are driven by real-time agent learning, which contributes to the division of labour. This WLA framework is implemented by agents in a local, distributed and quantitative manner, and can be widely used in many real-world applications.

5.1 Introduction

Our previous chapters have studied voter models and evolutionary population in adaptive networks to reason about the highly connected world. As mentioned before, the dynamics in adaptive voter model is driven by pairwise imitation (Chapter 3), while the dynamics in evolutionary population is characterized by natural selection (Chapter 4).

In this chapter, we intend to incorporate distributed learning into adaptive networks, where each agent has a local view on its neighbourhood and is able to acquire and aggregate local information to guide state evolution and structure adaptation. In this way, these individuals can work rationally to achieve desired improvement without external or central control entities.

How to improve the organisation performance through adaptive dynamics has been studied for a long time. Considering the cost for communication and synchronization, it is very difficult to manage a networked system under a centralised mechanism, especially when the size of the system is quite large. With the increasing technological complexity in real world, more and more distributed systems are developed to improve the organisation performance with lower cost.

Effective structures fostered by local interactions are usually characterized by self-organisation (Kohonen, 1988), which has been widely observed in biology, chemistry, economy and even sociology (Prehofer and Bettstetter, 2005). In nature, for example, the flocking behaviour of fish, birds, ants, etc. can self-organise themselves in a local manner to form a robust structure, which enables them to survive and live in a severe environment. The term of self-organisation occurs in many different subjects, and with different definitions, but some of the common principles are: locality, functionality, emergence, adaptability, robustness and scalability (Prehofer and Bettstetter, 2005). In addition, modern intelligent systems are required to self-adapt their structures and states in real time with the changes of external environments, so that there is no overall collapse under a random disturbance or attack. Many agile organisations have arisen by means of self-adaptation, which has been widely used to design and manage complex multi-agent systems.

It is known that local behaviours can facilitate the emergence of global coordination, but many details still remain for further exploration. In particular, a main challenge lies in how to give rise to effective individual behaviours.

5.1.1 WLA Framework

Recently, some generic frameworks for adaptive agent organisation have been developed to tackle the dynamism and complexity in MAS discipline, where the adaptive pattern follows the procedure of acting, collecting, decision-making and reconfiguring (Argente et al., 2013; Brun et al., 2009). In this chapter, we consider a simple framework of work-learn-adapt (WLA) in adaptive networks, where distributed learning is

integrated into the evolution of state and the adaptation of structure. As a result, a network with advantageous topology can be built, which leverages individual behaviours to achieve global coordination.

From a more generalised perspective, the agents embedded in a structured community are required to implement tasks according to their corresponding functionality. Meanwhile, they are able to acquire and aggregate external environment information in real time, and revise prior knowledge as environment changes. After that, the agents will adapt their structures and states quantitatively relative to the prior knowledge of what is a good network. Figure 5.1 illustrates a schematic procedure for the WLA framework in an organisation of agents.

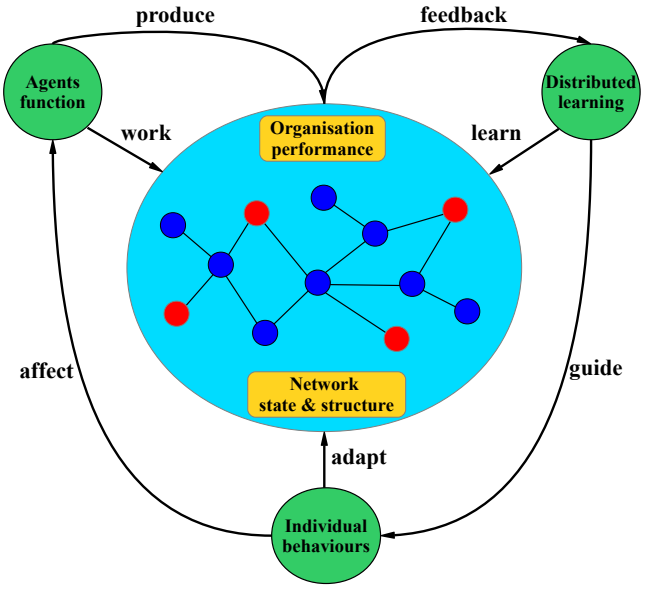

Figure 5.1: A schematic diagram is presented to show the WLA framework. In structured multi-agent systems, agents' functionality together with network structure will determine the organisation performance, which in turn provides some feedbacks used in the process of learning. Based on the information aggregated from learning, the individuals are able to adapt their states and structures in a rational way.

In the following, we will study a model of agents team formation (section 5.2 to 5.5) to elaborate the framework of work-learn-adapt (WLA). In this model, the agents need to form teams in a decentralized manner to complete some complicated tasks, which require a variety of skill suppliers. The change of agent's role is characterized by state evolution, and the adjustment of interactions corresponds to structure adaptation. In particular, a universal leader-follower mechanism is adopted to promote the division of labour. Distributed learning is incorporated into this framework to guide

the coupled dynamics quantitatively and rationally. Analytical and numerical investigations are conducted to show that the learning rates together with task size and skill set would have a big influence on both team wastefulness and task completion. Finally, an example of distributed task allocation (section 5.6) is explored to verify the effectiveness of this WLA framework.

5.2 Agents Team Formation

As mentioned above, it is the effective strategies for state evolution and structure adaptation that bring about agents organisations with favourable structures. In real world, we have already witnessed a large number of successful applications driven by adaptive dynamics. Here, we will study agents team formation on top of adaptive networks to demonstrate how this framework of work-learn-adapt (WLA) can operate as a whole for the coordination of agents.

5.2.1 Motivation

Agent-organised networks (AONs) (Gaston and desJardins, 2005) are organisations resulting from interdependent and interacting agents, where team formation is one of the most essential topics for the coordination of agents. Here, a team consists of a number of cooperative agents which are inter-connected, equipped with some kinds of skills and have agreed to work together toward a common complex task that none of the team members can complete independently. The applications of AON in real world include business alliances (de Weerdt et al., 2012), dynamic supply chains (Thadakamaila et al., 2004), robotic team (Vig and Adams, 2007), sensor networks (Glinton et al., 2008a), etc. AON studies have established that not only does organisational structure have a direct impact on performance, but also that simple strategies to adjust the structure dynamically can lead to remarkable improvements in team quality, task completion, and consequently global performance.

The research on agents team formation mainly focuses on the coordination among cooperative agents, whose behaviours usually determine the performance of task completion. Many operational research methods (Shehory and Kraus, 1998; Bulka et al., 2007; Adams et al., 2011; Dos Santos and Bazzan, 2012; de Weerdt et al., 2012) have been applied to the optimization of task allocation in a network. However, the blocking problem caused by insufficient or unreachable skills (especially in a network with an

unfavourable structure) still is a bottleneck for high-performance team formation. Let's see the following examples: task T_1 and T_2 need to be completed by two teams (red and blue) with the required skills to do so. Figure 5.2(a) shows the blocking caused by insufficient skills, where both teams try to compete for a skill 'S_2', but neither can successfully grab it. Figure 5.2(b) shows a form of 'spatial' blocking caused by unreachable skills, where the required skills are separated from one team by the growth of the other one. Therefore, a universal concept of *division of labour* is necessary to avoid the contention for resources.

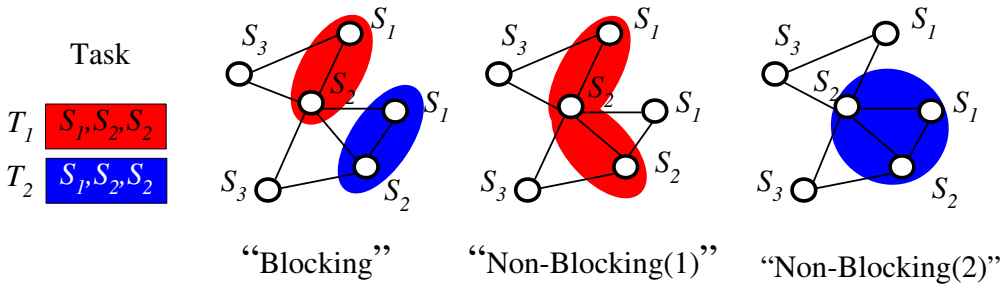

(a) Example 1: Blocking by insufficient skills. If both of the two incomplete teams: red team and blue team, are initiated to implement their tasks, neither of them will succeed because of the insufficient skills. However, if one of them gives up, then the other team will implement its task successfully.

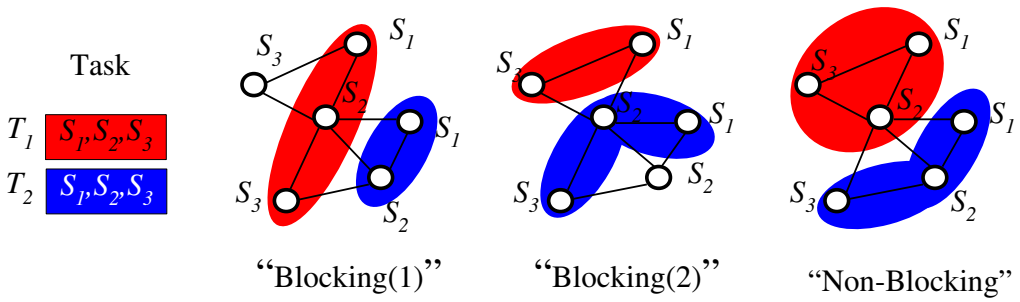

(b) Example 2: Blocking by unreachable skills. When the required skills are enough to form two complete teams, it is possible that some skills required by the blue (or red) team are blocked by the red (or blue) team, and then become unreachable because of the unfavourable structure. If the teams are formed by agents with reasonable structures, then the blocking by unreachable skills will be resolved.

Figure 5.2: Blockings and non-blockings in networked agents team formation.

As the task flow usually follows some distributions in open environments, which may change over time, a static network is manifestly disadvantageous to effective team formation. Recently, some people have proposed various adaptation strategies to re-

shape the network structures (Gaston and desJardins, 2005; Abdallah and Lesser, 2007; Kota et al., 2012; Ye et al., 2012) so as to achieve better organisation performance. The effects of network structure on team formation have been investigated by Gaston *et al.* (Gaston and desJardins, 2005; Gaston, 2005), and many extensions (Glinton et al., 2008b,a; Barton and Allan, 2007a,b, 2008) are provided to handle the issues regarding the organisation performance and network adaptation. However, the question of how individual behaviours can promote collective benefit still remains for further exploration.

5.2.2 Agent-organised Networks

Based on the work of Gaston (Gaston and desJardins, 2005; Gaston, 2005), we proceed to a formal description of agents team formation as what follows, where tasks need to be completed by agents in teams.

Agent-organised networks (AONs) are presented in terms of labelled undirected graphs, where the nodes correspond to the agents and the labels encode the respective skill of each agent. The set of networks of a given size correspond to the state space on which adaptive algorithms are to be defined.

- $N = \{a_1, a_2, a_3, ..., a_N\}$ is a finite set of agents.
- $E = (e_{ij})_{N\times N}$ is a $0-1$ symmetric adjacency matrix s.t. $e_{ij} = 1$ iff there is an edge between agents a_i and a_j.
- $NB(a_i) = \{a_j \mid e_{ij} = 1\}$ is the set of neighbours of a_i, and its neighbours' neighbours are in a set $NB^2(a_i) = \{a_k \mid e_{ij}e_{jk} > 0 \wedge e_{ik} = 0\}$.
- $S = \{S_1, S_2, ...S_\xi\}$ is a finite set of skills with a size of ξ.
- $s : N \to S$ maps agent a_i to the respective skill $s(a_i)$, also noted s_i for short. In general, the skills are uniformly distributed among the agents.

At each step, γ tasks are generated, and each task is a multiset of skills with a fixed size $|T|$. The contents in the task are drawn from S uniformly at random. To avoid overload, the requirement of tasks should be smaller than the supply of network, i.e. $\gamma|T| < N$. Each task is associated with a unique team, which is a set of agents supposed to provide the required skills. A valid team is defined as *a set of agents which induces a connected subgraph and whose skill multiset fulfils the skill requirements for the*

given task (Gaston, 2005). The process of agents team formation in a network can be described as Figure 5.3.

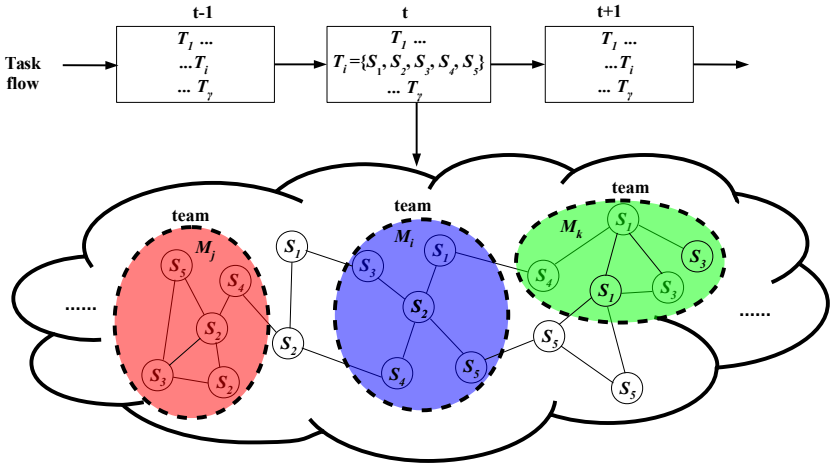

Figure 5.3: Agents team formation in a network. At each step, γ tasks are imported to the network and globally advertised to the agents. If a team M_i can provide all the skills required by the task T_i, then that task will be completed. Here, we use different colours to represent different teams.

There are two main performance measurements in agents team formation, which are solely for the purpose of evaluating the system from outside.

- **Task success rate** (TSR) is defined by the ratio between the number of completed tasks (CT) and that of imported tasks (IT) averaged over a long time.

$$TSR = \lim_{t \to +\infty} \frac{1}{t} \sum_{u<t} CT(u)/IT(u) \tag{5.1}$$

- **Team waste rate** (TWR) means the average ratio between surplus team size and actual task size. This measure captures the idea that the skill supply in a team should not be too large on average.

$$TWR = \lim_{t \to +\infty} \frac{1}{t} \sum_{u<t} \left(\frac{\sum_i m_i(u)}{\sum_i |T_i|(u)} - 1 \right) \tag{5.2}$$

  where $m_i(u)$ is the size of a team M_i at the time of u, and the corresponding task is T_i.

5.2.3 Division of Labour

The division of labour in adaptive networks (Gross and Blasius, 2008) means to differentiate agents according to their functionality. In the most decentralised case, any agent

can bid for the task, which may lead to the blockings easily. In order to have access to unreachable skills meanwhile avoid disordered allocation, a universal leader-follower approach is applied in our study to manage the teams. Reconfiguring the network into some hub-and-spoke clusters can help to reduce the collisions for resources and then avoid blockings caused by unreachable skills (Gaston, 2005), thus we ground our particular AON model on a multi-star structure. The concept of leaders and followers are explained in what follows.

Concretely, the agent-organised model presented before is extended by a mapping r to show the roles of the agents in taking the tasks:

- $r : N \to \{leader, follower\}$ maps the agents to their roles, and $r(a_i)$ or r_i for short means the functional role played by a_i.

The set of leaders is defined by L, whose size shows how many teams (or hubs) are in the network. Given a leader agent $a_i \in L$, the corresponding followers are a group of neighbours playing the role of *follower*.

$$F(a_i) = \{a_j \mid a_j \in NB(a_i) \wedge r_i = leader \wedge r_j = follower\}$$

A leader and its followers form a team to implement the tasks by providing the equipped skills. For example, a team led by agent a_i is a group of agents in $M_i = \{a_i\} \cup F(a_i)$. Note that some followers may be attached to more than one leader, from which they randomly pick a team to join (one can imagine they work part-time). The effective size of a team M_i led by a_i is defined as:

$$m_i = 1 + \sum_{a_j \in F(a_i)} 1/d(a_j) \tag{5.3}$$

where d_j is the number of leaders connecting a_j. The reason we add 1 is because the leader a_i itself provides a skill.

In order to reduce the chances of disordered team formation, it is assumed that only the leaders are allowed to take tasks and recruit teams. That is to say, at each step, the tasks are evenly uniformly taken by the leaders, and then implemented by the corresponding teams. This configuration can stabilize the relationships between cooperative agents, which conforms to the patterns of modern intelligent systems.

Under the framework of work-learn-adapt (WLA), the above described leader-follower mechanism is in the module of *working*, which contains team recruitment and task implementation. To form an organisation of agents with dynamically changing topology, we need to provide an intelligent approach (namely *learning*) to guide the behaviours of evolution and adaptation (namely *adapting*).

5.3 Adaptive Dynamics Based on Distributed Learning

To design an efficient adaptive strategy, we need first to specify what we want. Indeed, two problems should be addressed further: (1) how many leaders (or teams) are required for the completion of tasks; (2) how do the leaders adjust their teams to match the requirements of tasks.

5.3.1 Leader-Follower Flipping

As we can see, the number of leaders should be neither too small nor too large, where too few leaders may bring about big-size teams and then fragile network, while too many leaders may lead to numerous small-size teams with insufficient skills and then unsuccessful teams. There are two extreme solutions for task allocation: one is maximally decentralised case, where the number of leaders is equal to the number of tasks, namely one task per team; the other is the most centralised case where only one leader with a quite large team is in the network to do all tasks.

In practice, the cost (of communication, cognition, management, etc.) used for a leader to manage a big-size team will be very high. In addition, the network will become fragile if the leader agent is under attack. Considering the cost as well as network resilience, it is necessary to set a limitation on the size of a team (namely $m \ll N$), meanwhile we need to make sure that the team can provide enough skills for the completion of a task (namely $m > |T|$). Therefore, the most decentralised leader-follower approach is adopted in our study, where the number of teams is equal to the number of tasks, namely $|L| = \gamma$. In this way, we have enough capable teams to complete the tasks.

For a leader agent $a_i \in L$, an evolving parameter $\lambda : L \to \mathbb{R}$ is defined to characterize the expected number of tasks taken by itself, indicating the load to the corresponding team. In this model, we adopt a simple weighted moving average method to update the value of λ recursively:

$$\lambda_i \leftarrow \alpha\lambda_i + (1-\alpha)x_t \tag{5.4}$$

where x_t is the number of tasks taken by a_i at time t. This method can smooth out the accidental fluctuations meanwhile highlight the inevitable trends. A smaller α discounts the older observations faster, and a bigger one discounts them slowly. The λ_i obtained through this simple update strategy can be used to show whether the leader is overloaded ($\lambda_i > 1$, more than one task per team) or underloaded ($\lambda_i < 1$,less than one task per team).

The evolution of state means the change of an agent's role from follower to leader or the other way around, which will be implemented based on the evolving parameter λ. In detail, the state flipping (*leader* $\leftrightarrows$ *follower*) occurs with a small probability p_e (a quite small value) at each step. If the agent a_i is a follower, then nothing happens. Otherwise, if the agent a_i is a leader, then we need to either promote a random follower or demote the leader herself/himself based on the corresponding λ_i (shown in Figure 5.4).

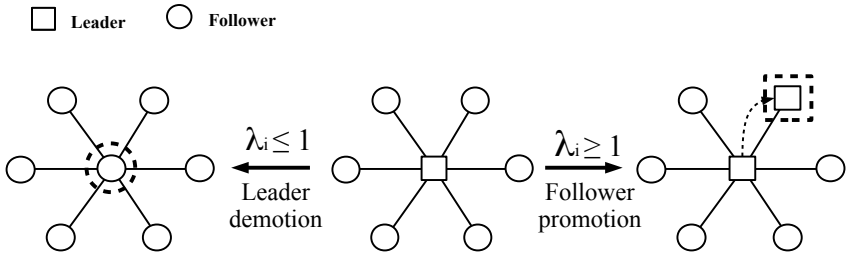

Figure 5.4: The evolution of state is quantified by the weighted moving average value λ, which characterizes the average number of tasks taken by the leader. If $\lambda_i \geq 1$, it means too many tasks are allocated to a team, then more leaders are required; otherwise if $\lambda_i \leq 1$, it means the teams are underloaded, then fewer leaders are required.

- if $\lambda_i \geq 1$, then the leader promotes a random follower to a leader with probability $\min(\lambda_i - 1, 1)$.
- if $\lambda_i \leq 1$, then the leader demotes herself/himself to a follower with probability $1 - \lambda_i$.

The flipping of role is led by agents in a distributed manner, which can react promptly to the change of the number of tasks γ. At stationary state, we have $\lambda_i = 1$ for any leader $a_i \in L$, so that the number of teams is consistent with the number of tasks. In this way, task allocation is carried out in the maximally decentralised way.

5.3.2 Risk-averse Learning

Generally speaking, the real division of labour cares not only the number of teams in the network but also the composition of skills in teams. In other words, the skills provided by a team should be consistent with the requirements of the imported tasks. Considering the dynamics of tasks, the leaders need to update some internal targets

continuously to track the requirements of tasks, and then establish effective teams based on those internal targets.

In order to characterize the composition of a desired team, for each leader agent, we define a ξ-vector θ as the **leader internal target** for various types of skills. Specifically, if a_i is a leader, then θ_i is defined in the following way to represent the desired team:

$$\theta_i = [\theta_i(S_1), \theta_i(S_2), ...\theta_i(S_\xi)]$$

where $\theta_i(S_j)$ means the desired number of team members holding skill S_j, and ξ is the size of skill set.

At each step, the tasks taken by a leader a_i can be defined in the form of **task skill requirement**, namely:

$$\psi_i = [\psi_i(S_1), \psi_i(S_2), ...\psi_i(S_\xi)]$$

where $\psi_i(S_i)$ is the number of skill S_i required to be completed. At stationary state, we have one task for each team and the sum for all skills is equal to the size of a task, namely $\sum_{S_i \in S} \psi_i(S_i) = |T|$.

When taking a task, the leader agent will update and adjust its internal target θ to track the requirements of task. Here, we will adopt a heuristic of "Win or Learn Fast" (WoLF) (Bowling and Veloso, 2002) to learn θ. In detail, we want to track the task using θ with different sensitivities depending on whether the actual task demand is below the internal target or above. The learning of θ gives rise to an appropriate predictor for task size and skill composition, which will be used to guide the formation of effective teams.

In general, the leaders are usually more sensitive to the case of underestimation $\theta_i(S_j) < \psi_i(S_j)$ than the overestimation $\theta_i(S_j) \geq \psi_i(S_j)$. Therefore, at each step, a leader agent a_i will compare current internal target θ_i with actual task requirement ψ_i, and then update θ_i as follows:

- if $\theta_i(S_j) \geq \psi_i(S_j)$

$$\theta_i(S_j) \leftarrow \theta_i(S_j) + \eta_-[\psi_i(S_j) - \theta_i(S_j)]$$

- if $\theta_i(S_j) < \psi_i(S_j)$

$$\theta_i(S_j) \leftarrow \theta_i(S_j) + \eta_+[\psi_i(S_j) - \theta_i(S_j)]$$

where $j \in \{1, 2, 3, ...\xi\}$ is the index of skills, and the learning rates are small real numbers satisfying that $0 < \eta_- \leq \eta_+$. The idea of $\eta_- \leq \eta_+$ is from the risk-averse

strategy (Holt and Laury, 2002; Gaston, 2005), indicating that if you don't have enough skills to meet the requirements, then you will lose everything. The bigger ratio of η_-/η_+ will bring a relatively bigger team size and then higher success rate, but the waste of skills will be higher at the same time.

This learning is distributed and conducted by agents continuously, which can lead to a rational estimation for the task-flow. Based on the internal target θ, the network will be adapted to meet the requirements quantitatively.

5.3.3 Energy-based Network Adaptation

Let ϕ_i be a ξ-vector to show the **team skill supply** in a team led by a leader a_i, reflecting how many skills of different types are available in current team:

$$\phi_i = [\phi_i(S_1), \phi_i(S_2), ...\phi_i(S_\xi)]$$

where $\phi_i(S_j)$ means the number of agents holding skill S_j in the team. The difference between the leader internal target θ and the team skill supply ϕ tells the agents how to adapt their structures.

In other words, we need to drive any given network structure to a favourable one fulfilling the requirements. Specifically, we will modify network structure based on a thermodynamics approach (Danos et al., 2013), where the *energy* is defined in a non-linear form (exponential, quadratic, etc.) to demonstrate how good a network is. With the change of network structures, the corresponding energy is going to change as well: the lower energy, the better structure.

In detail, the energy of a team is used to show the extent whether current team supply (ϕ) can match the internal target (θ), where a higher energy means the team needs more skills. In our study, the energy of a team led by a_i is defined to be an exponential form as:

$$e_i = \sum_{j=1}^{\xi} \exp^{\theta_i(S_j)-\phi_i(S_j)} \tag{5.5}$$

As for the network energy $\mathcal{E}$, we compute it through the sum of all teams:

$$\mathcal{E} = \sum_{a_i \in L} e_i = \sum_{a_i \in L} \sum_{j=1}^{\xi} \exp^{\theta_i(S_j)-\phi_i(S_j)} \tag{5.6}$$

Using the form of non-linear energy, we can balance the distribution of skills within the network. The network energy will decrease more when the required skills are

attached to the more "needy" agents. Without loss of generality, we suppose that $0 < x_1 \leq x_2$, for any given small change $\delta \leq (x_2 - x_1)$, we can have the following inequality:

$$\exp^{x_2} - \exp^{x_2-\delta} \geq \exp^{x_1} - \exp^{x_1-\delta}$$

In addition, this kind of energy also makes it possible that the skills from "rich" agents can be attached to the "needy" ones as:

$$\exp^{x_1} + \exp^{x_2} \geq \exp^{x_1+\delta} + \exp^{x_2-\delta}$$

Figure 5.5 illustrates an example that the non-linear energy instead of a linear one can distribute the skills evenly among different teams.

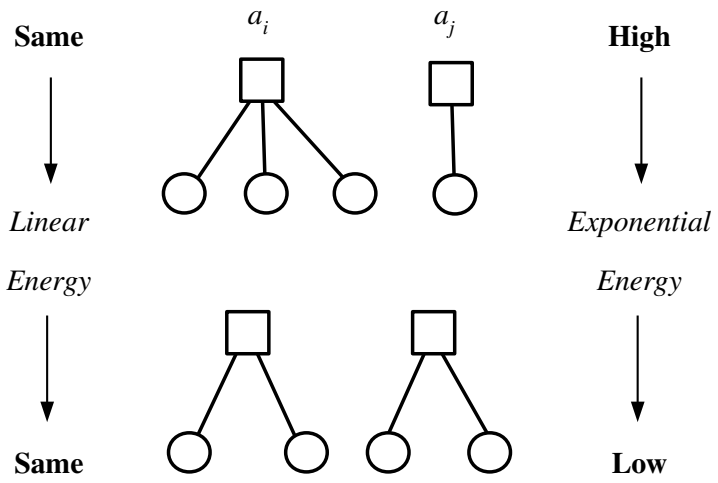

Figure 5.5: A simple example is presented to show the difference between non-linear energy and linear one. For the linear energy, suppose the initial energy of a_i is $\theta_i - \phi_i = \theta_i - 3$, and the initial energy of a_j is $\theta_j - 1$, so the total energy is $\theta_j + \theta_j - 4$. After rewiring, the total energy keeps same, still $\theta_j + \theta_j - 4$. For the exponential energy, however, the initial energy of a_i is $e^{\theta_i - 3}$, and that of a_j is $e^{\theta_j - 1}$, and the total energy is $e^{\theta_i - 3} + e^{\theta_j - 1}$. After rewiring, the total energy becomes $e^{\theta_i - 2} + e^{\theta_j - 2}$, which is smaller than before.

In the following, let's consider how to integrate network energy into the adaptation of network. As we all know, Metropolis et al. (Metropolis et al., 1953) introduced the successive state transitions using Markov chains, and the detailed balance equation can be obtained as:

$$p(G)W(G \to G') = p(G')W(G' \to G) \tag{5.7}$$

where G and G' are two states in the space of network structures, and $p(G)$ is the probability at state G, and $W(G \to G')$ indicates the transition rate from state G to G'.

Applying the Boltzmann's prescription to describe the distribution of networks, we have

$$p(G) = \frac{\exp^{-\beta\mathcal{E}(G)}}{Z} \tag{5.8}$$

where $Z = \sum_G \exp^{-\beta\mathcal{E}(G)}$ and β is a parameter seen as the inverse of a temperature.

Therefore, the ratio of transition rate between the move $G \to G'$ and its inverse move $G' \to G$ is:

$$\frac{W(G \to G')}{W(G' \to G)} = \frac{p(G')}{p(G)} = \exp^{-\beta(\mathcal{E}(G')-\mathcal{E}(G))} \tag{5.9}$$

In this model, we set the transition probability from state G to G' as follows:

$$W(G \to G') = \min(1, \exp^{-\beta\Delta\mathcal{E}}) \tag{5.10}$$

where $\Delta\mathcal{E} = \mathcal{E}(G') - \mathcal{E}(G)$. As shown in Figure 5.6, the adaptation of network is driven by the change of energy, which can be calculated locally.

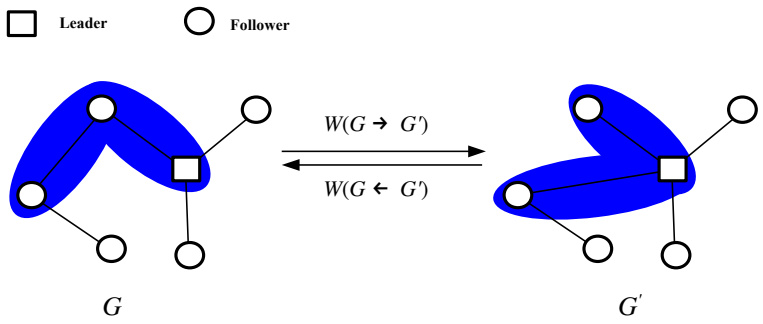

Figure 5.6: Graph transformation based on energy. Here, the structure of network are the states in Markov chains. The transition from state G to state G' is driven by the change of network energy, where a decrease of network energy would foster a better structure and consequently higher organisation performance.

As for the adaptation strategy, we adopt a **triangle rewiring** (Gaston, 2005) to guarantee the connectedness in graph transformation, where an agent disconnects one neighbour and connects to that neighbour's neighbour. It is possible to transfer any connected network G to another connected network G' based on this triangle rewiring strategy. The only difference between the two networks is that there exists an edge $a_i a_j$ in G but not in G', and there is anther edge $a_k a_l$ in G' but not in G.

To conclude, the energy-based network adaptation procedure will run with a small probability p_a at each step: an edge $a_i a_j$ and a random neighbour's neighbour a_k are

selected, and then a_i rewires from a_j to a_k with probability $\min(1, \exp^{-\beta\Delta\mathcal{E}})$. The energy difference before and after rewiring is calculated as:

$$\Delta\mathcal{E} = \mathcal{E}(a_i a_k a_j) - \mathcal{E}(a_i a_j a_k) \tag{5.11}$$

5.3.4 Connectedness in Graph Transformation

Now, let's consider the above mentioned triangle rewiring in an undirected graph, where a node disconnects one neighbour and connects to that neighbour's neighbour. We can write the rule of triangle rewiring as: if $e_{uv} = e_{uw} = 1$ and $e_{vw} = 0$ in graph G, then $e_{uw} = e_{vw} = 1$ and $e_{uv} = 0$ in the transformed graph G'. This class of transformations has three interesting properties: (I) it preserves the number of edges; (II) it preserves connectedness, and (III) it is ergodic in the sense that any two connected graphs on the same set of vertices can be related by a series of such rewirings.

Lemma 5.3.1. *Let G be a connected graph, v and w are connected by a path π, and all the nodes on the path excluding w are connected with u. The original G can be transformed to G' by the rule of triangle rewiring, where $e_{uv} = 0$, $e_{uw} = 1$ and any other pair is unchanged.*

Proof. We need to show we can swap the edge uv with uw, leaving everything else unchanged. The transformations can be shown as Figure 5.7, and the path from v to w is:

$$\pi : v \to k_1 \to k_2 \to \cdots \to k_m \to w$$

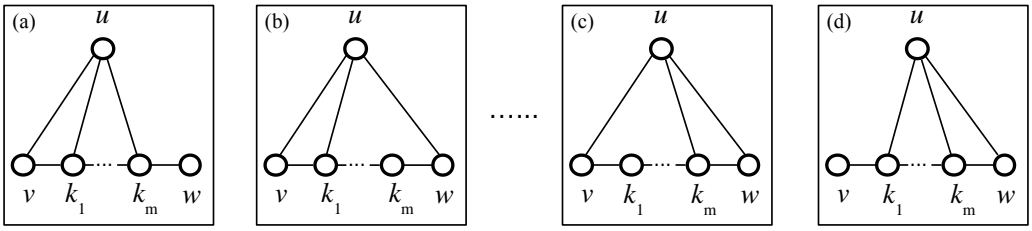

Figure 5.7: Edge swapping by triangle rewiring. The edge uv can be replaced by the uw along a series of triangle rewiring along the path from v to w.

To do that, we first forward the edge uk_m to uw, and then forward the edges of $uk_{m-1}, \cdots uk_1, uk_v$ one by one along the path until the edge uv is forwarded to uk_1.

□ □

The above lemma tells us that the source edge (i.e. uv) can "jump" over existing edges along a path to an unoccupied target (i.e. uw).

Let $\mathcal{G}_E^N$ be the set of connected graphs with N nodes and E edges. We can use the following theorem to show that any two graphs in $\mathcal{G}_E^N$ can be transformed through a series of triangle rewirings.

First, we consider a situation to transfer an edge from uv to uw.

Theorem 5.3.2. *Let G be a connected graph in $\mathcal{G}_E^N$, and u, v, w are some nodes in G, where $e_{uv} = 1$, $e_{uw} = 0$. If G' is a connected graph with $e_{uv} = 0$, $e_{uw} = 1$ and everything else is same as G, then G' can be transformed from G under triangle rewiring.*

Proof. By the fact that both G and G' are connected, there must exist a path from v to w excluding edge uv:

$$\pi : v \to k_1 \to k_2 \to \cdots \to k_m \to w$$

For any k_i $(1 \leq i \leq m)$ on the path, if $e_{uk_i} = 0$, we forward the source edge uv edge directly; otherwise if $e_{uk_i} = 1$, we use Lemma 5.3.1 to "jump" over those existing edges. Finally, we can have the edge uv replaced by uw. The transformations can be shown as Figure 5.8.

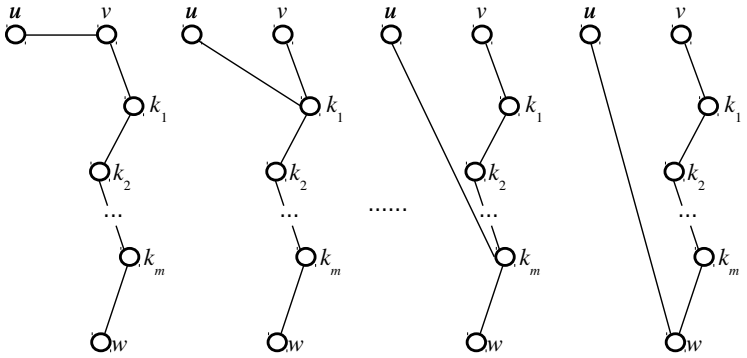

Figure 5.8: Edge permutation from uv to uw along a path from v to w.

□ □

After that, we need to consider the permutation between any two pairs of nodes in a graph, let's say they are uv and wx.

Theorem 5.3.3. *Let G be a connected graph in $\mathcal{G}_E^N$, and we have $e_{uv} = 1$ and $e_{wx} = 0$ in G. Let G' be a connected graph as well, we have $e_{uv} = 0$ and $e_{wx} = 1$ in G', and everything else is same as G. There exist a sequence of transformations from G to G' under triangle rewiring.*

Proof. Both G and G' are connected graphs, and we need to consider the following two cases in graph transformation:

- Case 1: there exist two paths in G: π_1 is starting from u to w, and π_2 is starting from v to x. Neither path includes the edge uv.

$$\pi_1 : u \to l_1 \to l_2 \to \cdots \to l_n \to w$$
$$\pi_2 : v \to k_1 \to k_2 \to \cdots \to k_m \to x$$

In this case, we say we have two "parallel" paths: π_1 and π_2. And then we can do the transformations in two steps: the first step is to connect u and x with an edge following the edges transformations on π_2; and the second step is to transform xu to xw along the path π_1. The transformations can be shown as Figure 5.9.

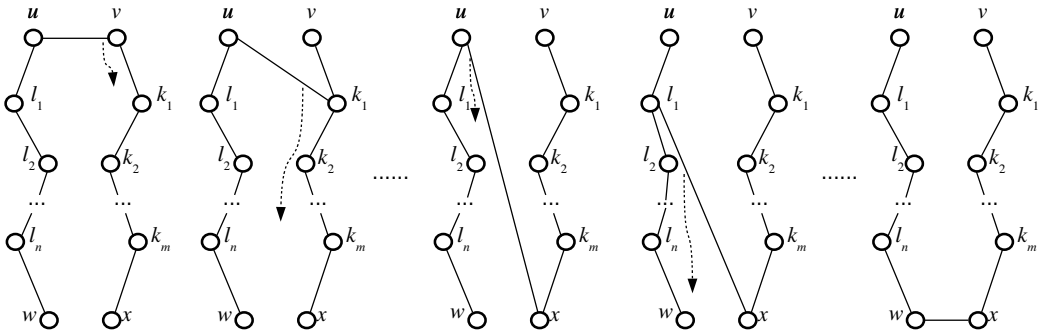

Figure 5.9: Case 1: Edge permutation along two " parallel" paths π_1 and π_2.

- Case 2: there are two paths in G: π_1 is starting from u to w, and π_2 is starting v and x. Both of the two paths include the edge uv.

$$\pi_1 : u \to v \to l_1 \to l_2 \to \cdots \to l_n \to w$$
$$\pi_2 : v \to u \to k_1 \to k_2 \to \cdots \to k_m \to x$$

In this case, we say we have two "cross" paths: π_1 and π_2. And then we can do the transformations in two steps as follows. First, we transfer the edge uv along the path π_1 to connect u and w. The second step is to transfer the edge wu along the path π_2 to connect w and x. In this way, the edge uv is replaced by wx. The transformations can be shown as Figure 5.10.

Notably, if we find a case where the path π_1 starting from u to w includes the edge uv but the path π_2 starting from v to x excludes uv, then we must can find another path

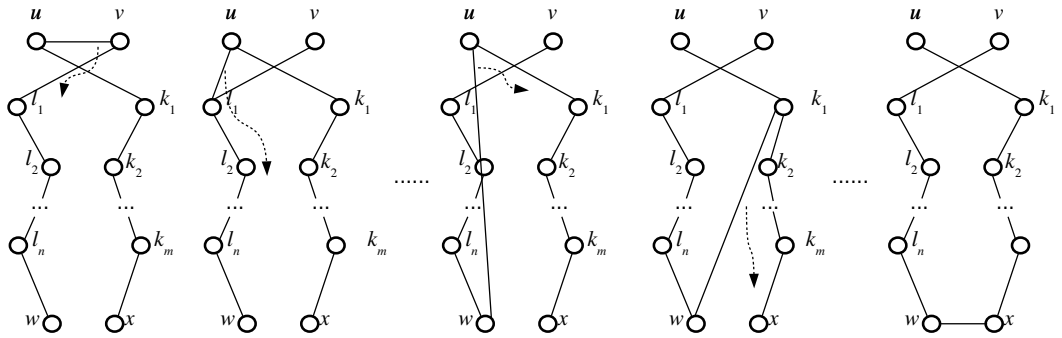

Figure 5.10: Case 2: Edge permutation along two "cross" paths π_1 and π_2.

π_1' (dashed curves) which connects u and w (or x) excluding the edge uv, otherwise G' won't be connected (see Figure 5.11). In this way, the above case belongs to either case 1 or case 2, and we can transfer the edge from uv to wx under triangle rewiring.

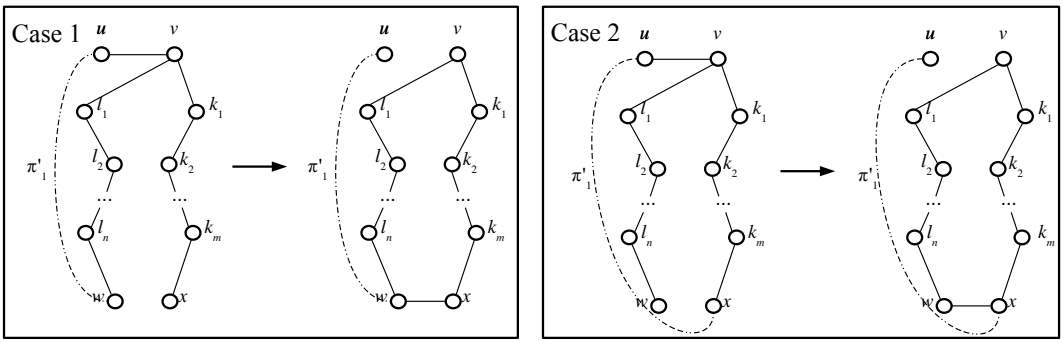

Figure 5.11: For the case where path π_1 connecting u and w includes the edge uv but the path π_2 connecting v and x excludes uv, there must be another path π_1' (dashed curves) connecting u and w which is equivalent to case 1, or connecting u and x which is equivalent to case 2. Otherwise, the transformed network will not be connected.

□ □

As we can see, for any two connected graphs G and G' with an edge permutation, we can transfer from one to the other based on the rule of triangle rewiring. Therefore, the connectedness in graph transformation is preserved.

5.3.5 Algorithm

We can now summarise our full distributed algorithm. We start from a connected random network with one arbitrary leader agent, and iterate *ad libitum* the following

round. The 'role change' and 'edge rotation' probabilities are defined above and depend respectively on learned parameters λ and θ.

Algorithm 1 Agents team formation in adaptive networks

Require: initial state N, E, S, γ, r, λ, and θ

$t \leftarrow 0$
while $t < t_{\max}$ **do**
  $t \leftarrow t+1$
  tasks are distributed to the leaders evenly uniformly
  for $a_i \in N$ **do**
    implement the tasks by providing skills
    if $r(a_i) =$*leader* **then**
      Update λ and θ
      with probability p_e try role change
    end if
  end for
  for $a_i \in N$ **do**
    pick uniformly a redex (if any) to try edge rotation with probability p_a
  end for
end while

As explained before, γ tasks are allocated to the leaders uniformly at each time step, and then the teams will implement the received tasks by providing the required skills. At the same time, the leaders will update their evolution parameter λ used for role flipping and the adaptation parameter θ used for triangle rewiring. After that, the event of state evolution will occur with probability p_e, where the leader will promote a follower or demote herself/himself according to the value of λ. And the event of structure adaptation will occur with probability p_a, where the triangle rewiring is made based on the energy computed through θ. In particular, both p_e and p_a are very small real numbers, indicating the relatively slow module of *adapting* relative to the modules of *working* and *learning*.

5.4 Analytical Investigations

In this section, we are going to analyse the effects of this work-learn-adapt (WLA) framework on network structure and organisation performance by some mathemati-

cal calculations. As described in the agent-organised model, the generation of tasks follows a multinomial distribution:

$$T \sim f(\psi(S_1), \psi(S_2), ...\psi(S_\xi), |T|, p_1, p_2, ...p_\xi) \tag{5.12}$$

where $\sum_{i=1}^{\xi} \psi(S_i) = |T|$ and $\sum_{i=1}^{\xi} p_i = 1$.

All the skills are uniformly selected for each task slot, and each skill is selected with probability $p_i = 1/\xi$. When the size of a task $|T|$ is large enough, according to the central limit theorem (CLT), the number of skill S_i in the task follows a distribution as:

$$\psi(S_i) \sim |T| p_i + \sqrt{|T|}\mathcal{N}(0, \sigma_i^2) \tag{5.13}$$

where $\sigma_i^2 = p_i(1-p_i)$ means the variance of skill number in the task and $\mathcal{N}$ indicates the normal distribution.

We update the leader internal target $\theta(S_i)$ for skill S_i as follows based on the risk-averse learning:

$$\Delta\theta(S_i) \leftarrow \begin{cases} \eta_-[\psi(S_i) - \theta(S_i)] & \text{if } \theta(S_i) \geq \psi(S_i) \\ \eta_+[\psi(S_i) - \theta(S_i)] & \text{if } \theta(S_i) < \psi(S_i) \end{cases} \tag{5.14}$$

For a certain skill S_i, we define a variable ε_i as the difference between the actual task skill requirement $\psi(S_i)$ and the leader internal target $\theta(S_i)$, namely $\varepsilon_i = \psi(S_i) - \theta(S_i)$, and then we can have ε_i at stationary state:

$$\varepsilon_i \sim \sqrt{|T|}\mathcal{N}(0, \sigma_i^2) + |T| p_i - \theta^\star(S_i)$$

where $\theta^\star(S_i)$ is the stationary leader internal target for skill S_i.

Rewriting the above equation, we have:

$$\varepsilon_i \sim \mathcal{N}(|T| p_i - \theta^\star(S_i), |T|\sigma_i^2) \tag{5.15}$$

where the probability density function (pdf) can be computed as:

$$p_{\varepsilon_i} = \frac{1}{\sigma_i\sqrt{2\pi|T|}} \exp^{-\frac{(\varepsilon_i - |T| p_i + \theta^\star(S_i))^2}{2|T|\sigma_i^2}} \tag{5.16}$$

Following the "kick-up" adjustment of $\theta(S_i)$ with η_+ and "kick-down" adjustment with η_-, the stationary state can be obtained when:

$$\eta_+ \int_0^{+\infty} \varepsilon_i p_{\varepsilon_i} \, d\varepsilon_i = \eta_- \int_{-\infty}^{0} -\varepsilon_i p_{\varepsilon_i} \, d\varepsilon_i \tag{5.17}$$

where $\eta_- \leq \eta_+$ and both of them are quite small compared to $\psi(S_i) - \theta(S_i)$.

Using integration by parts, we can obtain the stationary condition for $\theta^\star(S_i)$ under a certain pair of η_- and η_+.

$$\frac{|T|p_i-\theta^\star(S_i)}{-\sigma_i\sqrt{|T|}}\big[\eta_+-(\eta_+-\eta_-)\Phi(\frac{|T|p_i-\theta^\star(S_i)}{-\sigma_i\sqrt{|T|}})\big] = (\eta_+-\eta_-)\frac{1}{\sqrt{2\pi}}e^{-\frac{(|T|p_i-\theta^\star(S_i))^2}{2|T|\sigma_i^2}} \tag{5.18}$$

where $\Phi(x)$ is the cumulative distribution function (CDF) of the normal distribution.

Let's define an **intermediate variable** a as:

$$a=\frac{|T|p_i-\theta^\star(S_i)}{-\sigma_i\sqrt{|T|}} \tag{5.19}$$

Replacing $\frac{|T|p_i-\theta^\star(S_i)}{-\sigma_i\sqrt{|T|}}$ by a, we can rewrite the stationary condition Eq. 5.18 as:

$$a\big[\eta_+-(\eta_+-\eta_-)\Phi(a)\big]=(\eta_+-\eta_-)\frac{1}{\sqrt{2\pi}}e^{-a^2/2} \tag{5.20}$$

where it is clear that the intermediate variable a is only dependent on the learning rates η_+ and η_-. We say $a^\star$ is the solution of Eq. 5.20 for a given pair of η_+ and η_-.

5.4.1 The Effects of Learning Rates

If the two learning rates are equal, namely $\eta_+=\eta_-$, then we can obtain $a^\star=0$ by solving Eq. 5.20. When we come to Eq. 5.19 using $a^\star=0$, it is clear that:

$$a^\star=\frac{|T|p_i-\theta^\star(S_i)}{-\sigma_i\sqrt{|T|}}=0$$

In this case, the stationary leader internal target is equal to the average number of skill S_i in a task.

$$\theta^\star(S_i)=|T|p_i \tag{5.21}$$

If $\eta_+>\eta_->0$, then $a^\star>0$, and Eq. 5.20 can be rewritten as:

$$a\big[\frac{\eta_+}{\eta_+-\eta_-}-\Phi(a)\big]=a\big[\frac{1}{1-\eta_-/\eta_+}-\Phi(a)\big]=\frac{1}{\sqrt{2\pi}}e^{-\frac{a^2}{2}} \tag{5.22}$$

where we can see that the solution $a^\star$ for that equation only depends on $\eta_+/(\eta_+-\eta_-)$, essentially η_-/η_+. By solving Eq. 5.22, Figure 5.12 presents the solution of $a^\star$ as a decreasing function of η_-/η_+, which ranges from 0 to 1.

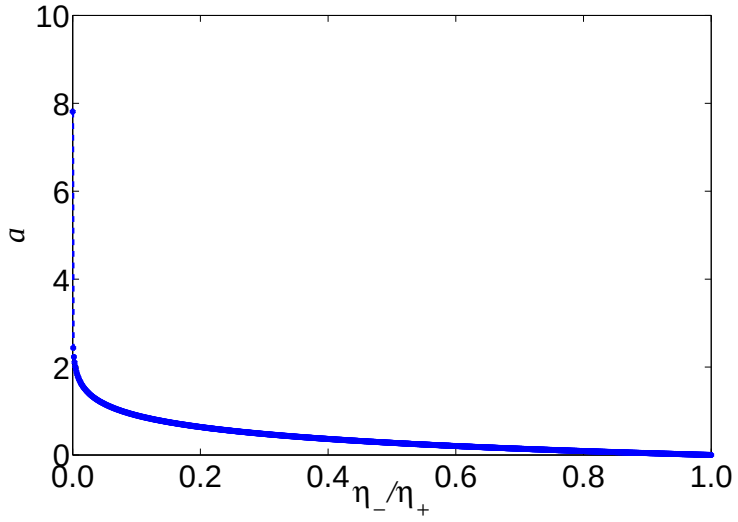

Figure 5.12: The solution $a^\star$ changes as η_-/η_+ goes from 0 to 1, where it is clear that with the increase of η_-/η_+, the solution of $a^\star$ decreases monotonously.

5.4.2 Bigger-size Tasks Bring Smaller Team Waste

For a given skill S_i, we have the solution $a^\star = \frac{|T|p_i - \theta^\star(S_i)}{-\sigma_i\sqrt{|T|}}$, which can be rewritten as:

$$\theta^\star(S_i) - |T|p_i = a^\star \times \sigma_i\sqrt{|T|} \tag{5.23}$$

From the above equation, the difference between the stationary leader internal target $\theta^\star(S_i)$ and the average skill number $|T|p_i$ can be decomposed into three contributors: $a^\star$ (which is only dependent on the ratio of learning rates η_-/η_+ as shown in Figure 5.12), σ_i (standard deviation for the number of skill S_i) and $|T|$ (task size). And then we can obtain following equation to show the ratio $\theta^\star(S_i)/|T|$:

$$\frac{\theta^\star(S_i)}{|T|} \simeq p_i + a^\star \times \frac{\sigma_i}{\sqrt{|T|}} \tag{5.24}$$

where we can see that with the decrease of $a^\star$, or the increase of task size, or the decrease of skill variance, the ratio between the stationary internal target $\theta^\star(S_i)$ and task size $|T|$ will decrease and converge to p_i.

When we consider all the skills in S, we have $\theta^\star = \sum_{i=1}^{i=\xi}\theta^\star(S_i)$, and Eq. 5.24 can be extended by the following equation:

$$\begin{aligned} \frac{\theta^\star}{|T|} &\simeq 1 + a^\star \times \frac{\sum_i \sigma_i}{\sqrt{|T|}} \\ &= 1 + a^\star \times \frac{\sum_i \sqrt{p_i(1-p_i)}}{\sqrt{|T|}} \end{aligned} \tag{5.25}$$

In particular, when all the skills are uniformly selected to constitute the task, namely $p_i = 1/\xi$, the standard deviation for the number of a certain skill S_i is $\sigma_i = \sqrt{\frac{1}{\xi}(1-\frac{1}{\xi})}$, and the sum will be $\sum_i \sigma_i = \sqrt{\xi - 1}$. Thus we can rewrite Eq. 5.25 as:

$$\frac{\theta^\star}{|T|} \simeq 1 + a^\star \times \frac{\sqrt{\xi - 1}}{\sqrt{|T|}} \tag{5.26}$$

where a smaller skill set will lead to a smaller difference between the leader internal target $\theta^\star$ and actual task size $|T|$. It is clear that $\theta^\star \simeq |T|$ when $\xi = 1$, namely there is only one single skill in the network.

Suppose the team skill supply ϕ can match the leader internal target θ through network adaptation at stationary state, namely $\phi^\star \simeq \theta^\star$, where $\phi^\star = \sum_i \phi(S_i)^\star$ is the sum of all skills provided by the team. In this situation, team waste rate (TWR) can be approximated as:

$$\begin{aligned} TWR &= \frac{\phi^\star}{|T|} - 1 \simeq \frac{\theta^\star}{|T|} - 1 \\ &\simeq a^\star \times \frac{\sqrt{\xi - 1}}{\sqrt{|T|}} \end{aligned} \tag{5.27}$$

5.4.3 A Larger Skill Set Decreases the Task Completion

For a certain skill S_i, the number of agents holding S_i in a team at stationary state can be approximated by the corresponding leader internal target, namely:

$$\phi(S_i)^\star \simeq \theta^\star(S_i) \simeq |T| p_i + a^\star \sigma_i \sqrt{|T|}$$

Meanwhile, the actual number of skill S_i in a task follows the distribution:

$$\psi(S_i) \sim |T| p_i + \sqrt{|T|}\mathcal{N}(0, \sigma_i^2)$$

Given a task T, if its skill S_i is fulfilled by a team, then the team should provide enough number of skill S_i such that $\phi^\star(S_i) \geq \psi(S_i)$, namely

$$|T| p_i + a^\star \sigma_i \sqrt{|T|} \geq |T| p_i + \sqrt{|T|}\mathcal{N}(0, \sigma_i^2) \tag{5.28}$$

and the probability satisfies the above inequality is:

$$p(\phi^\star(S_i) \geq \psi(S_i)) = \Phi_{0,\sigma_i^2}(a^\star \sigma_i) \tag{5.29}$$

where Φ indicates the cumulative distribution function (CDF).

Similarly, the task will be completed if all ξ skills are fulfilled, and the probability for task completion can be approximated by:

$$\prod_{i=1}^{\xi} p(\phi^{\star}(S_i) \geq \psi(S_i)) = \prod_{i=1}^{\xi} \Phi_{0,\sigma_i^2}(a^{\star}\sigma_i) \tag{5.30}$$

As all the skills are uniformly picked to constitute a task, task success rate (TSR) can be computed roughly as:

$$\begin{aligned} TSR &\simeq \prod_{i=1}^{\xi} \Phi_{0,\sigma_i^2}(a^{\star}\sigma_i) \\ &\simeq \Phi_{0,\sigma_i^2}(a^{\star}\sigma_i)^{\xi} \\ &\simeq \left(\frac{1}{2}\left[1+\mathrm{erf}(\frac{a^{\star}}{\sqrt{2}})\right]\right)^{\xi} \end{aligned} \tag{5.31}$$

where $\mathrm{erf}(x)$ is the error function.

As we can see, for a given $a^{\star}$, the probability for task completion decreases exponentially with the increase of the size of skill set, namely ξ, but is independent of the size of a task.

5.5 Numerical Simulations

This section will present a series of numerical simulations to verify the above analytical calculations. Under the framework of work-learn-adapt (WLA), we solve agents team formation by considering the differentiation between leaders and followers. Several important observables are captured during the process of network evolution and adaptation, such as the leader internal target θ, the team skill supply ϕ and the organisation performance (including TSR and TWR).

The simulations are undertaken on the synthetic data within a random connected network with a size $N = 500$ and average degree $\langle k \rangle = 4$. At each step, γ tasks are introduced into the network. Role and edge changes both use the same probability $p_e = p_a = 0.002$, which reflects the fact that the adaptation module should have a slow time scale relative to the learning one. The "kick-up" learning rate is $\eta_+ = 0.01$ and the "kick-down" learning rate η_- is varying from 0 to η_+, so it is clear $\eta_-/\eta_+ \in [0,1]$. The whole simulation lasts 10^5 steps according to the procedures presented in our Algorithm 1.

5.5.1 Baseline

In this part, we have the size of a task $|T| = 100$ and the number of tasks introduced at each step is $\gamma = 4$, so that $\gamma|T| < N$ is satisfied. The size of skill set is $\xi = 2$ and each skill is selected with same probability $p_i = 0.5$. As the generation of tasks follows a multinomial distribution, the standard deviation for the number of a single skill is computed by: $\sigma_i = \sqrt{p_i(1-p_i)} = 0.5$.

Run the WLA framework described above and the ratio of learning rates is $\eta_-/\eta_+ = 0.1$. At stationary state, we have the snapshot of network in Figure 5.13 (left panel), where 4 evident hubs are obtained (namely the leaders). The red and blue nodes indicate the two different skills, which are uniformly assigned to the agents at random.

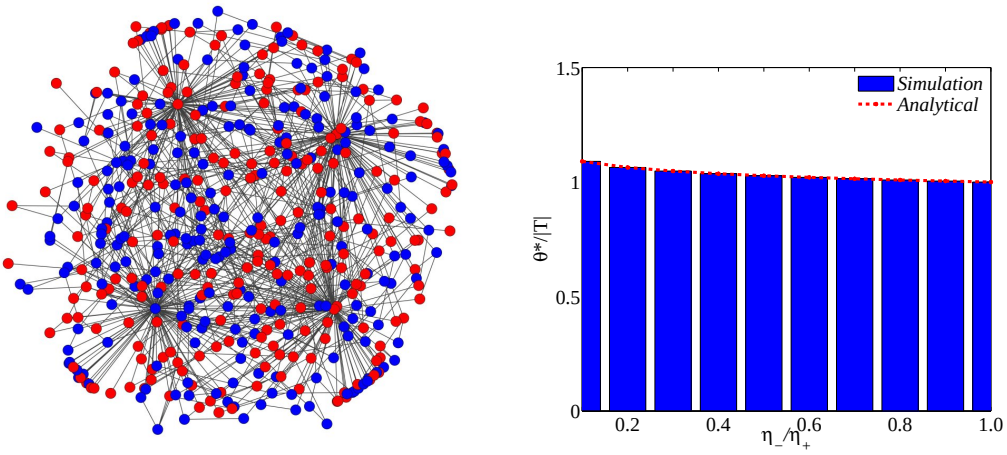

Figure 5.13: Given a certain ratio $\eta_-/\eta_+ = 0.1$, the network structure with $N = 500$ nodes and average degree $\langle k \rangle = 4$ is illustrated in the left panel. When η_-/η_+ increases, the numerical and analytical values for $\theta^\star/|T|$ at stationary state are presented in the right panel. In the simulations, $\gamma = 4$ tasks are introduced into the network at each step, each of which has a size of $|T| = 100$, and the size of skill set is $\xi = 2$.

As discussed in Section 5.4, the ratio between the leader internal target $\theta^\star$ and the size of a task $|T|$ at stationary state follows that:

$$\frac{\theta^\star}{|T|} \simeq 1 + a^\star \sqrt{(\xi - 1)/|T|}$$

where the numerical solution of $a^\star$ can be obtained in Figure 5.12 as a function of η_-/η_+.

Using the same parameters introduced above, the numerical and analytical values for $\theta^\star/|T|$ under varying η_-/η_+ are presented in Figure 5.13 (right panel). As we can

see, the simulation results match the analytical solutions very well, which verifies the effectiveness of our analytical investigations in Section 5.4.

When the ratio of learning rates varies (namely η_-/η_+ changes from 0.1 to 0.9), we have Figure 5.14 to show the evolution of task size $|T|$ and the leader internal target θ. As we can see, the value of θ is a little bit bigger than actual task size $|T|$, especially when the ratio η_-/η_+ is small, where the leaders are very sensitive to the loss case of $\theta < \psi$, where the leader internal target θ is below the actual task requirement ψ.

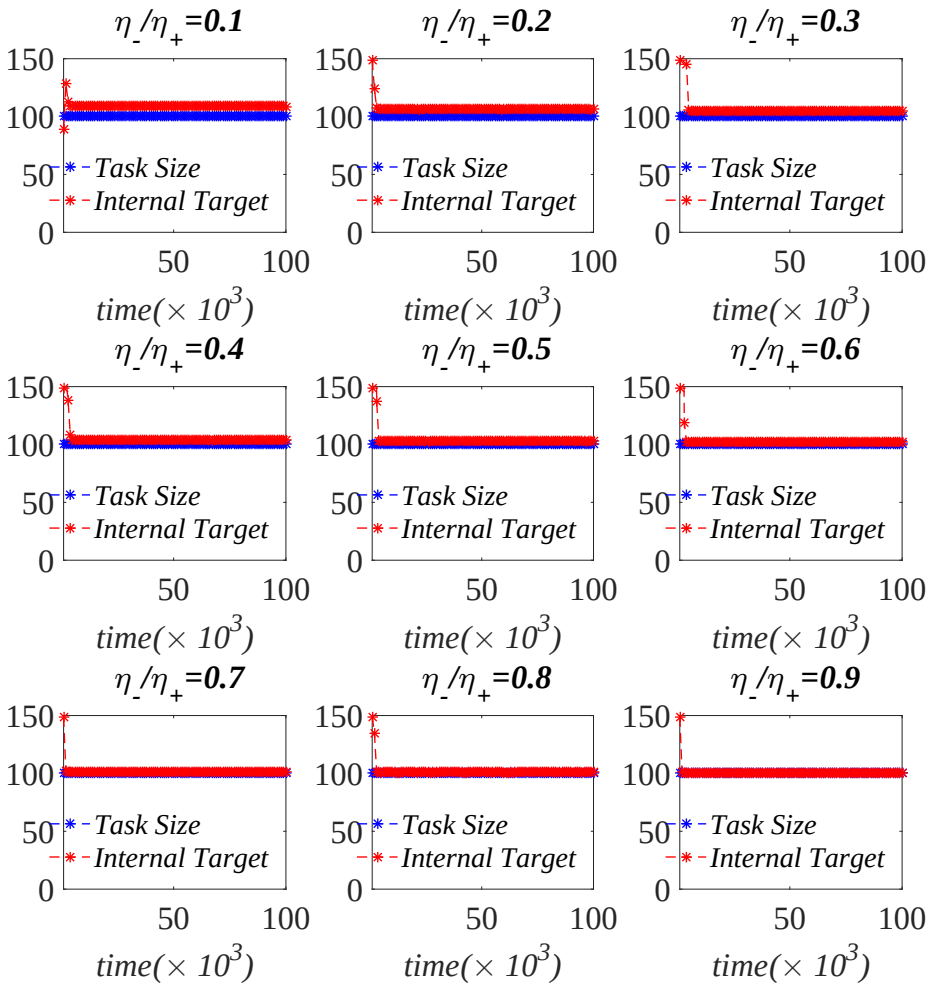

Figure 5.14: The leader internal target θ and the size of a task $|T|$ change with the evolution of network at different values of η_-/η_+. When the ratio η_-/η_+ is small e.g. $\eta_-/\eta_+ = 0.1$, the leader internal target is bigger than the actual task size. With the increase of η_-/η_+, the difference between the two curves is smaller and smaller. Finally, the two curves overlap in the end when η_- is close to η_+.

Furthermore, Figure 5.15 presents the evolution of team skill supply ϕ when the ratio η_-/η_+ varies. Here, the size of a team reflects the degree of resource wastefulness in agents team formation. Ideally, the size of a team ϕ should be equal to the size of a task $|T|$ at stationary state. Considering the uncertainty in task requirements, some surplus skill suppliers in the team are necessary in case of skill shortage. In particular, we can find an evident gap between team supply and task demand at a smaller η_-/η_+.

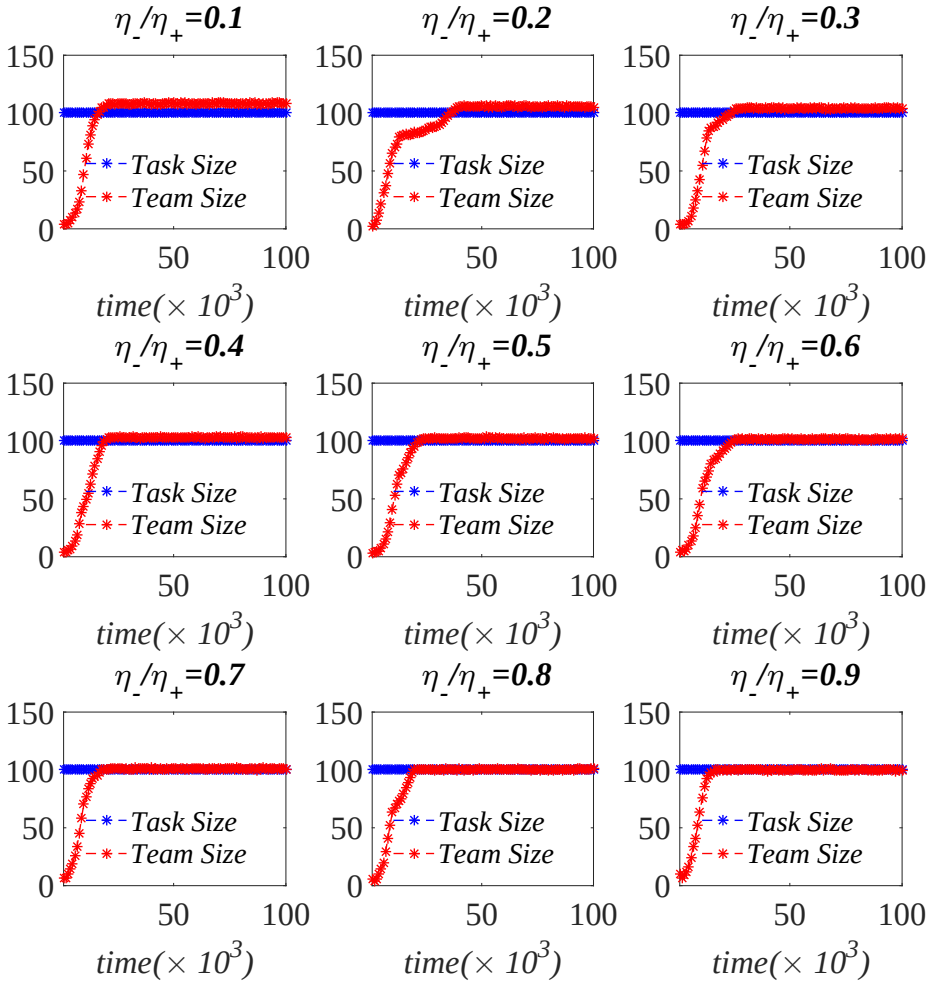

Figure 5.15: The size of a team ϕ and the size of a task $|T|$ change with the evolution of network at different values of η_-/η_+. Here, the size of a team can be interpreted as the skill supply for team formation and bigger team size means higher resource wastefulness. Similarly, with the increase of η_-/η_+, the size of a team is smaller due to the decrease of the leader internal target θ. And the difference between the two curves of $|T|$ and ϕ is smaller and smaller when η_-/η_+ is close to 1.

In Figure 5.16, we present the dynamics of task success rate (TSR) at different η_-/η_+. It is clear that, when the ratio η_-/η_+ is smaller, team size is bigger than task size so that task success rate is higher; on the contrary, when the ratio η_-/η_+ is bigger, team size is close to task size gradually and task success rate drops to a quite low level. It is a trade-off between team wastefulness (i.e. TWR) and task completion (i.e. TSR), where higher completion performance usually comes along with bigger resource wastefulness, which indicates "*there's no such thing as a free lunch*".

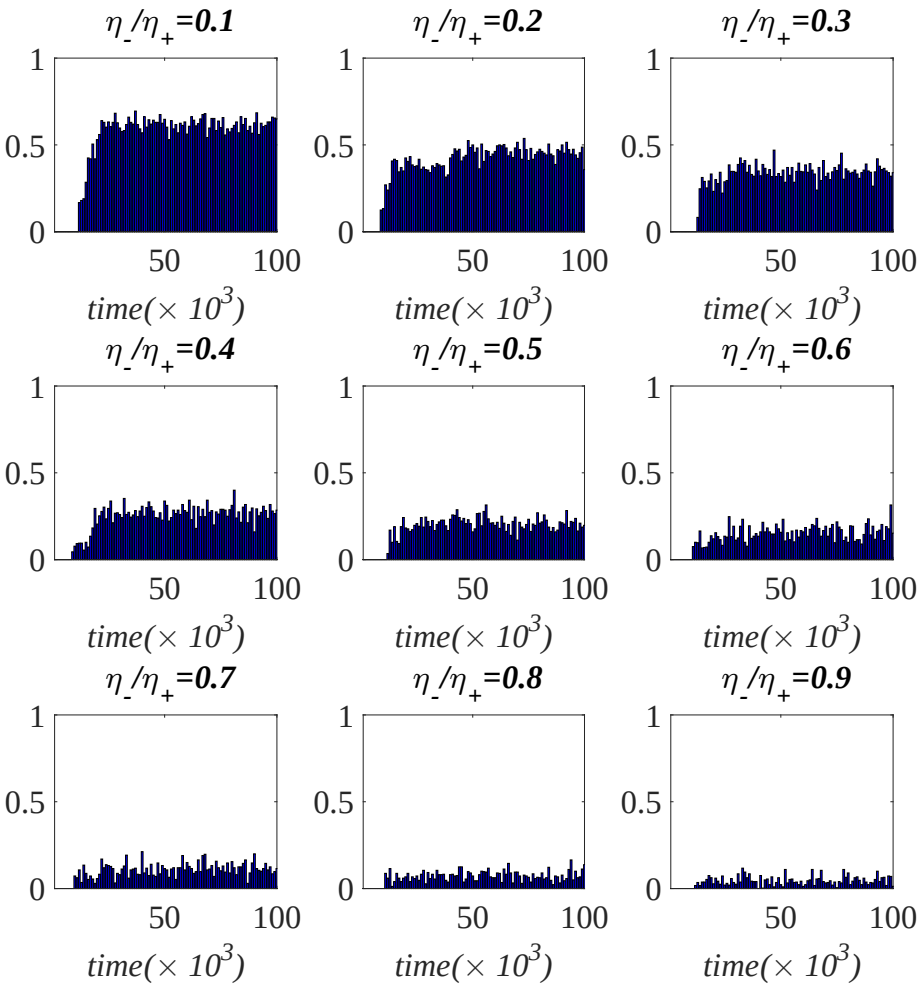

Figure 5.16: Task success rate (TSR) changes with the evolution of network at different values of η_-/η_+. A higher task completion is obtained when η_-/η_+ is smaller (e.g. $\eta_-/\eta_+ = 0.1$), where team size is bigger than task size. With the increase of η_-/η_+, TSR drops to a small value, where team size is close to task size.

In the following, we will take the above case as a baseline and change some pa-

rameters (the size of skill set ξ and the size of a task $|T|$) to observe their influences on team wastefulness and task completion.

5.5.2 Increasing the Size of Skill Set

In this part, we intend to check the influence of the size of skill set ξ on network structure and organisation performance. Keeping task size $|T| = 100$ and the number of tasks $\gamma = 4$, we increase the size of skill set from $\xi = 2$ to $\xi = 4$. As before, the skills are selected uniformly with probability $p_i = 1/\xi$. The standard deviation for the number of a single skill now increases to $\sigma_i = \sqrt{p_i(1-p_i)} = \sqrt{3}/4$, which is higher than the previous baseline value where $\sigma_i = 1/2$. Figure 5.17 presents the comparisons between the case of baseline (left column) and the case of bigger skill set (right column).

As we can see, there are 4 hubs (corresponding to the team leaders) in both snapshots, but the composition of team is diverse in the right column, where different colours indicate different skills.

At stationary state, the resource wastefulness (i.e. TWR) is bigger when the skill set is increased to double size, especially when η_-/η_+ is smaller. This phenomenon can be explained by Eq. 5.27, where team waste rate is associated with both task size (inversely proportional to $\sqrt{|T|}$) and skill set size (proportional to $\sqrt{\xi - 1}$). Therefore, when the size of skill set increases from $\xi = 2$ to $\xi = 4$, the size of a team at stationary state becomes bigger.

In addition, the probability for task completion (i.e. TSR) is sharply reduced as the size of skill set increases, which has been explained in Section 5.4 Eq. 5.31. In this case, task success rate (TSR) decrease exponentially with the increase of ξ.

5.5.3 Increasing the Size of a Task

In this part, we will check the influence of task size on network structures and organisation performance. In detail, we increase the size of a task from $|T| = 100$ to $|T| = 400$ and the number of tasks introduced at each step is decreased to $\gamma = 1$, so that the system is not overloaded ($\gamma|T| < N$). Meanwhile, we keep the size of skill set as $\xi = 2$, and each skill will be selected with same probability $p_i = 0.5$. In this way, the standard deviation for the number of a single skill will not be affected by increasing task size.

Figure 5.18 illustrates the case of baseline ($|T| = 100$) in the left column and the

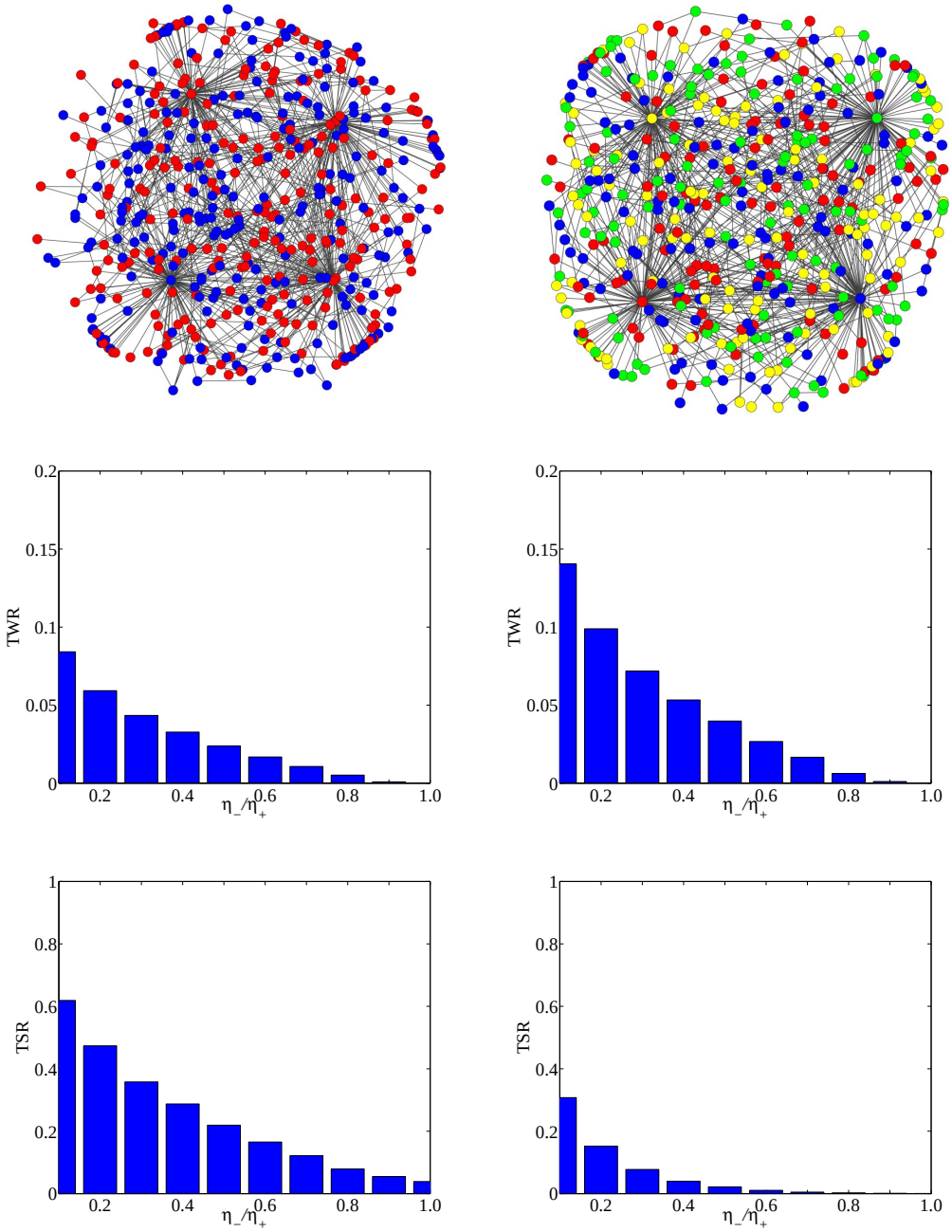

Figure 5.17: Network structures and organisation performance change as the size of skill set increases, where the left column illustrates the case of baseline and the right column presents the case of increasing skill set. Two snapshots for network structures are presented at $\eta_-/\eta_+ = 0.1$ (upper row). For a given η_-/η_+, team waste rate (TWR) is much higher in the case of increasing skill set (middle row). Task success rate (TSR) is dramatically decreased when the skill set is increased to double size (lower row). Parameters settings: task size $|T| = 100$, task number $\gamma = 4$, skill set size $\xi = 2$ (left column: baseline), and $\xi = 4$ (right column: increasing ξ).

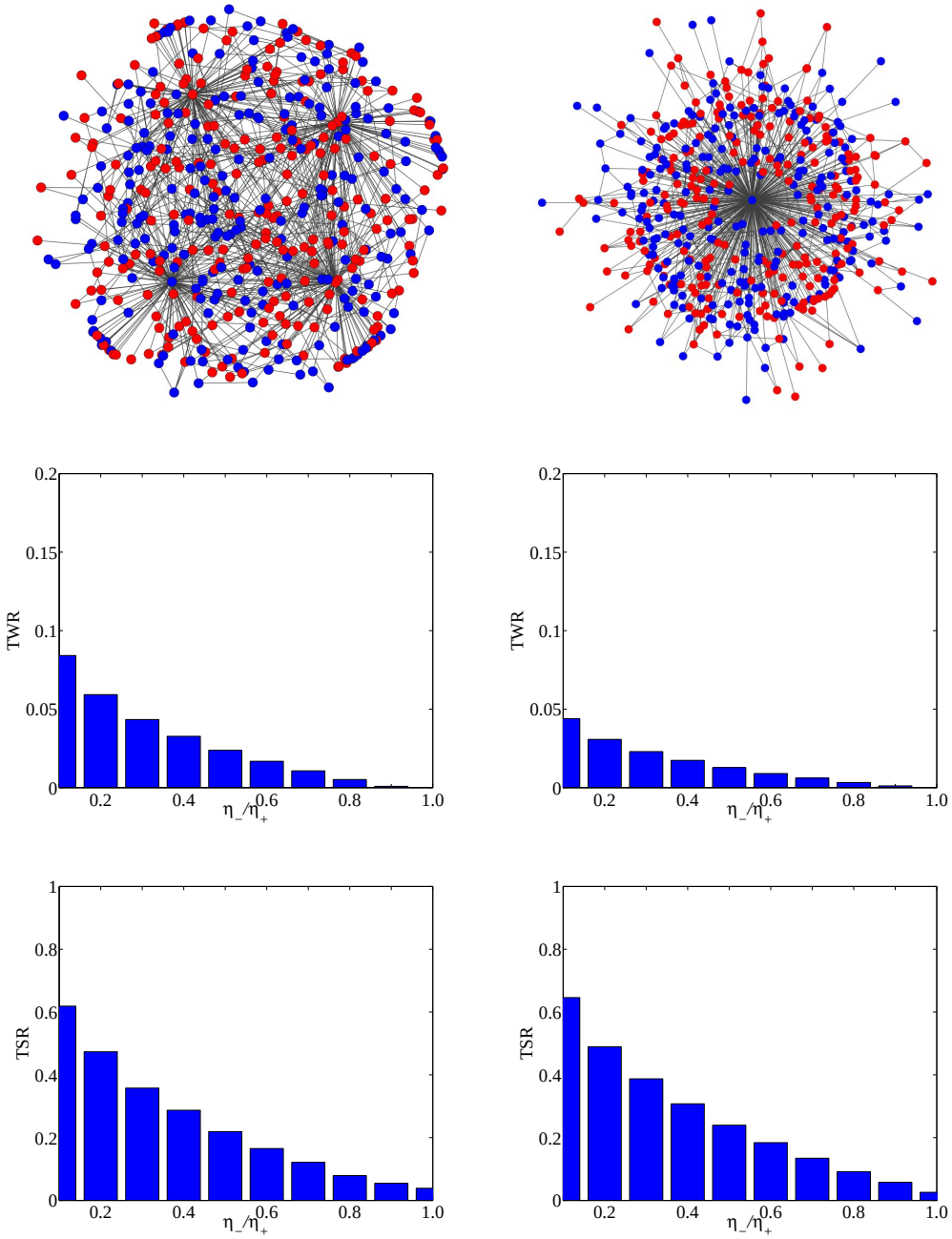

Figure 5.18: Network structures and organisation performance change as task size increases, where the left column illustrates the case of baseline and the right column shows the case of increasing task size. Two network snapshots are presented at $\eta_-/\eta_+ = 0.1$ (upper row). For a given η_-/η_+, team waste rate (TWR) becomes smaller in the case of increasing task size (middle row). Task success rate (TSR) in the case of increasing task size is similar to the baseline (lower row). Parameters settings: skill set size $\xi = 2$, task number $\gamma = 4$, task size $|T| = 100$ (left column: baseline), and task number $\gamma = 1$, task size $|T| = 400$ (right column: increasing $|T|$).

case of bigger task size ($|T| = 400$) in the right column. As we can see, the number of teams (or hubs) in the network decreases from 4 to 1, but the size of team is expanding to a large one. Specifically, team waste rate (TWR) at stationary state is inversely proportional to $\sqrt{|T|}$ (see Eq. 5.27), which means that TWR will decrease when task size is bigger. When it comes to task success rate (TSR), we can find that the organisation performance is well maintained in both cases, where task completion is independent of task size as presented in Eq. 5.31.

5.5.4 The Evolution of Teams with Dynamical Tasks

Considering the dynamics of task requirements in real world, an intelligent and robust distributed algorithm is able to detect those changes and react to them quickly. The adaptive network mechanism explored in this chapter enables the leader agents to aggregate historical information and adjust the internal targets continuously to keep up with the task requirements. In this way, we can implement state evolution and structure adaptation quantitatively when the task requirements are changing. Starting form the baseline settings with $\xi = 2$, $|T| = 100$ and $\gamma = 4$, we change the task requirements during the evolution by varying task size $|T|$ to observe its influence on the size of a team.

With $\gamma|T| < N$, we vary the size of a task in the simulation, and then the number of tasks generated per round is changed as well. Specifically, the size of a task is increased from $|T| = 100$ to $|T| = 200$ after a certain step, when the teams are adjusted to attract more followers so as to match those bigger-size tasks. On the other hand, the size of a team becomes smaller when the size of a task is decreased from $|T| = 200$ to $|T| = 100$. Figure 5.19 illustrates the dynamical process for the evolution of teams as task size increases or decreases during the simulation.

5.6 Distributed Task Allocation

As mentioned above, how to allocate tasks to the right agents is an important topic in multi-agent systems, and a large number of researches (Shehory and Kraus, 1998; de Weerdt et al., 2012; Abdallah and Lesser, 2007; Ye et al., 2012) have been launched to address this problem based on intelligent allocation algorithms and dynamically changing structures. In this section, we generalise the leader-follower mechanism introduced before by considering that all agents in the organisation are able to learn

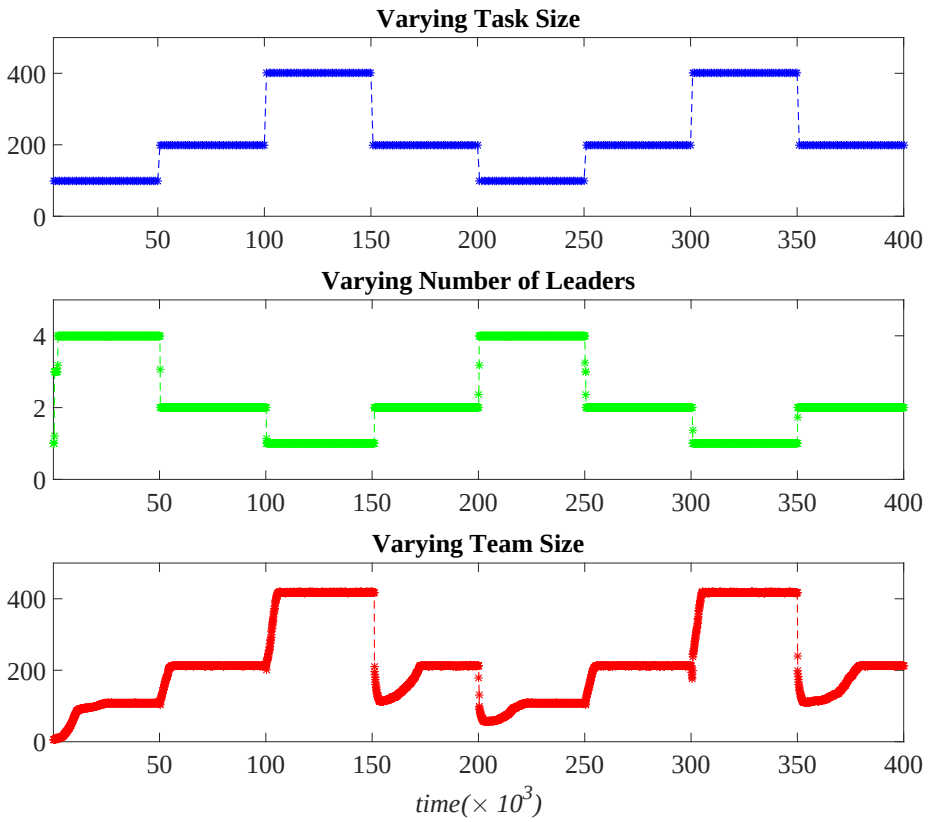

Figure 5.19: The evolution of team size goes with the changes of task requirements. The upper row shows the changes of task size, followed by the number of leaders in the middle row and the lower row is the corresponding changes of team size. The simulation parameters are: the ratio of learning rates $\eta_-/\eta_+ = 0.1$ and the size of skill set $\xi = 2$.

and adapt. A simple case study of distributed task allocation is present to illustrate the framework of work-learn-adapt (WLA). Our model is adapted from the self-organisation for load balance (Abdallah and Lesser, 2007) and task solving (Kota et al., 2009), where the agents are able to learn from environment (task flow, neighbourhood configuration, interactive information, etc.) and then adjust the network. Notably, the nodes in our model are heterogeneous with different abilities, and the edges are heterogeneous as well indicating various affinities between the connecting nodes. We are interested in how an agent reorganises its neighbourhood in a distributed way in order to accomplish the task effectively, when only local information is available.

5.6.1 Model Description

We ground the model of distributed task allocation on a weighted directed network.

Agents are in a set $N = \{a_1, a_2, \cdots, a_N\}$. In our model, each agent can solve the task with a certain service rate $\mu : N \to \mathbb{R}$. A real number $q : N \to \mathbb{R}$ indicates the size of tasks in an agent's queue, which need to be solved by the agent.

The agents are interacting in a weighted directed network denoted by W, where W_{ij} indicates the link strength from a_i to a_j. In this model, we define $0 \leq W_{ij} \leq 1$, and a bigger weight means closer relationship. If $W_{ij} = 0$, then a_i has no access to a_j.

In detail, we divide the agents in the neighbourhood into n layers (Figure 5.20), so that the weights are discrete. For an agent a_i, we set the weight of an edge connecting to a neighbour a_j on the k-th layer ($1 \leq k \leq n-1$) as:

$$W_{ij} = 1/k \tag{5.32}$$

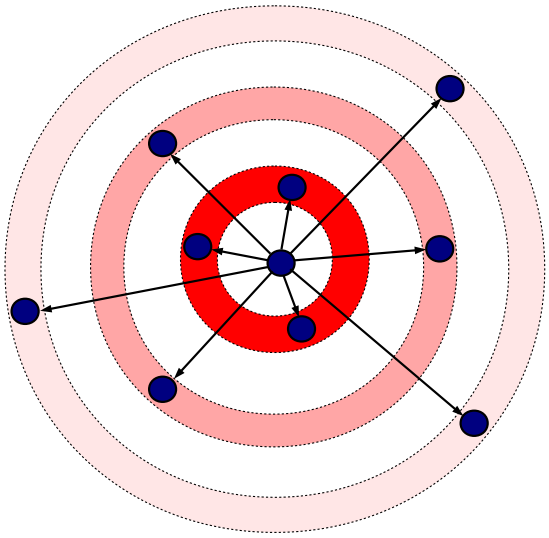

Figure 5.20: Neighbourhood diversity with tiered structure.

Those agents on the n-th layer are disconnected from a_i, and the corresponding weight is set to be 0. The tiered structures have been found in many realistic networks Kota et al. (2009); Saramäki et al. (2014); Dunbar (2016), indicating the heterogeneity in interactions, namely how easy an agent has access to its neighbours.

Tasks arrive at the agents locally with a certain arrival rate $\lambda : N \to \mathbb{R}$. In general, it is supposed that the task can be decomposable continuously, and it is completed by different agents in the neighbourhood.

- Allocation

At step t, a task with a size of λ_i (i.e. arrival rate) arrives at agent a_i, and then that agent will allocate the task to its neighbours according to the affinity (Figure 5.21). We define f_{ij}^t as the task flow from a_i to a_j at that step, and it is proportional to W_{ij}, which indicates that a closer neighbour helps to do more work.

$$f_{ij}^t = \lambda_i \frac{W_{ij}}{\sum_k W_{ik}} \tag{5.33}$$

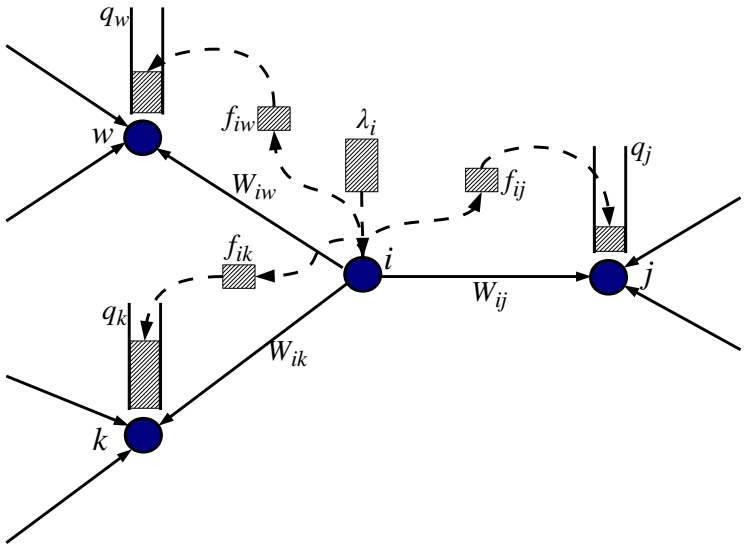

Figure 5.21: Task allocation in weighted networks.

Notably, agents will not re-distribute the tasks received from their neighbours. In the case of $\sum_i \lambda_i = \sum_i \mu_i$, the optimal allocation strategy should be $\sum_i f_{ij}^t = \mu_j$ for any agent a_j.

We measure the organisation performance using the utilization rate (UR), which is defined as the ratio between the total size of served tasks and the system service ability. At a given step t, we can calculate UR through:

$$UR^t = \sum_i s_i^t / \sum_i \mu_i \tag{5.34}$$

where s_i^t is the size of served tasks by a_i and μ_i is the corresponding service ability. If there are some underloaded agents, then there must be some overloaded agents, and the utilization rate is less than 1.

5.6.2 Work, Learn and Adapt

Given the distributed task allocation model described above, we adopt the work-learn-adapt framework to solve the tasks in adaptive networks. In this model, we incorporate state evolution and structure adaptation into the changes of W, where the state of an agent a_i can be represented by the weight vector $[W_{1i}, W_{2i}, \cdots, W_{Ni}]$.

- Work

At the beginning of a certain step t, agent a_i pushes all the received tasks from neighbours into its queue and the size of agent's queue will be updated as:

$$q_i \leftarrow q_i + \sum_j f_{ji}^t \tag{5.35}$$

Afterwards, the tasks in the queue will be implemented with a rate μ_i. At the end of that step, the size of queue changes to $q_i \leftarrow q_i - s_i^t$, where s_i^t indicates the size of served tasks during t.

$$s_i^t = \begin{cases} \mu_i, & \text{if } q_i \geq \mu_i \\ q_i, & \text{if } q_i < \mu_i \end{cases} \tag{5.36}$$

The above process can be shown as Figure 5.22.

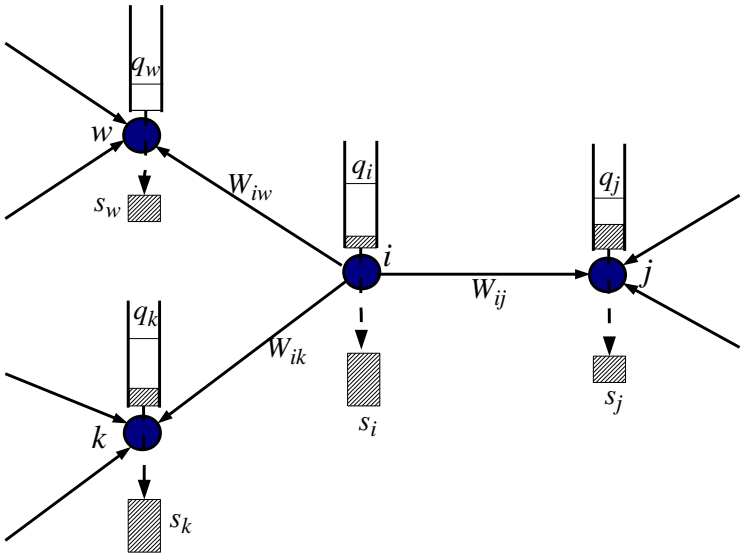

Figure 5.22: Task solving in weighted networks.

- Learn

At each step, the agent will track the size of received tasks, based on which to figure out whether current neighbourhood configuration can balance the load-input and load-output. Under this learning method that is implemented by agents locally, we don't need to consider too large state space. We define $l : N \to \mathbb{R}$ as the average size of received tasks per step, which is updated in real time to characterize the information of agent's load influenced by neighbourhood configuration:

$$l_i \leftarrow \alpha l_i + (1-\alpha)\sum_j f_{ji}^t \tag{5.37}$$

where α is the learning rate, and a smaller value discounts the older observations faster.

- Adapt

The adapting actions are implemented at a slower rate compared to the working and learning processes. At each step, each agent a_i will adapt the link to a random neighbour (or potential neighbour) a_j with probability

- p_a, if $W_{ij} > 0$;
- $p_a\beta$, if $W_{ij} = 0$.

We have the **adaptation rate** $p_a \ll 1$ and β ($0 \leq \beta \leq 1$) is defined as an **exploration rate**. In this way, some unreachable agents ($W_{ij} = 0$) can be upgraded and inserted into the neighbourhood.

We change the weight of an edge based on the estimated task input l and actual service ability μ. For a given directed edge $i \to j$, the weight W_{ij} will more likely to be increased when $l_j < \mu_j$, namely the agent a_j is underloaded. On the contrary, W_{ij} will more likely to be decreased when $l_j > \mu_j$, namely the agent a_j is overloaded.

In general, if an agent a_j is on the k-th layer, then the link weight is $W_{ij} = 1/k$. When the adaptation occurs, we will update the weight of an edge through three types of actions: *upgrading* ($W_{ij} \leftarrow 1/(k-1)$), *unchanging* ($W_{ij} \leftarrow 1/k$)), and *downgrading* ($W_{ij} \leftarrow 1/(k+1)$). The corresponding willingness (p_{ij}^+,$p_{ij}^=$ and p_{ij}^-) to implement those actions can be calculated by:

- if $l_j \geq \mu_j$

$$\begin{aligned} p_{ij}^+ &= 0 \\ p_{ij}^= &= \exp^{(\mu_j - l_j)} \\ p_{ij}^- &= 1 - \exp^{(\mu_j - l_j)} \end{aligned}$$

- if $l_j < \mu_j$

$$\begin{aligned} p_{ij}^+ &= 1 - \exp^{(l_j - \mu_j)} \\ p_{ij}^= &= \exp^{(l_j - \mu_j)} \\ p_{ij}^- &= 0 \end{aligned}$$

5.6.3 Numerical Simulations

Starting from an ER random network with $N = 100$ and average out-degree $\langle k_{out} \rangle = 4$, we have agents uniformly distrusted with different service rates, where half of them are *fast* in a set F with $\mu_F = 4$ and half of them are *slow* in a set S with $\mu_S = 2$. Tasks arrive at a certain agent a_i with an arrival rate λ_i. When $\sum_i \lambda_i = \sum_i \mu_i$, the utilization rate is $UR = 1$ under the centralised allocation, where $\sum_i f_{ij} = \mu_j$. The agents are differentiated into n layers, and the weight of agent on the layer of k ($1 \leq k \leq n-1$) is $W_{ij} = 1/k$. For neighbours of $W_{ij} > 0$, they are assigned to different layers uniformly at random in the beginning. The adaptation rate is $p_\alpha = 0.01$.

5.6.3.1 Static Networks

When $\lambda_i = \lambda$ for any agent, we have a uniform task input distribution. If $p_\alpha = 0$, then the network is static. In an ER random network, the fast agent $a_i \in F$ receives same amount of tasks as the slow one $a_j \in S$ on average, namely $\langle \sum_k f_{ki} \rangle = \langle \sum_k f_{kj} \rangle = \lambda$. As $\langle \sum_k f_{ki} \rangle < \mu_F$ while $\langle \sum_k f_{kj} \rangle > \mu_S$, the fast ones are always underloaded but the slow ones are always overloaded. Therefore, the utilization rate can be calculated approximately by:

$$UR \approx \frac{\mu_S N/2 + \lambda N/2}{\mu_S N/2 + \mu_F N/2} = \frac{\mu_S + \lambda}{\mu_S + \mu_F} \tag{5.38}$$

5.6.3.2 Neighbourhood Configurations

In the neighbourhood of a_i, we have the inputting load to fast agents proportional to $\sum_{a_j \in F} W_{ij}$, similarly the inputting load to slow agents is proportional to $\sum_{a_j \in S} W_{ij}$. The optimal structure should satisfy that:

$$\frac{\langle \sum_{a_j \in F} W_{ij} \rangle}{\langle \sum_{a_j \in S} W_{ij} \rangle} = \frac{W(F)}{W(S)} = \frac{\mu_F}{\mu_S} \tag{5.39}$$

where we define $W(F) = \langle \sum_{a_j \in F} W_{ij} \rangle$ as the average weighted number of fast neighbours, and $W(S) = \langle \sum_{a_j \in S} W_{ij} \rangle$ means the average weighted number of slow neighbours.

In the following, we take a specific case $n = 3$ and $\lambda = 3$ as an example to implement the framework of work-learn-adapt. When the exploration rate is $\beta = 0$, the access to the disconnected agents with $W_{ij} = 0$ is impossible while some overloaded agents may be "pushed" out from the neighbourhood, so the network gets sparse gradually as shown in Figure 5.23. When the exploration rate gets bigger, it is possible to

"pull" some disconnected agents into the neighbourhood. As a result, the favourable configuration with $W(F)/W(S) \simeq \mu_F/\mu_S$ can be achieved and the utilization rate is close to 1.

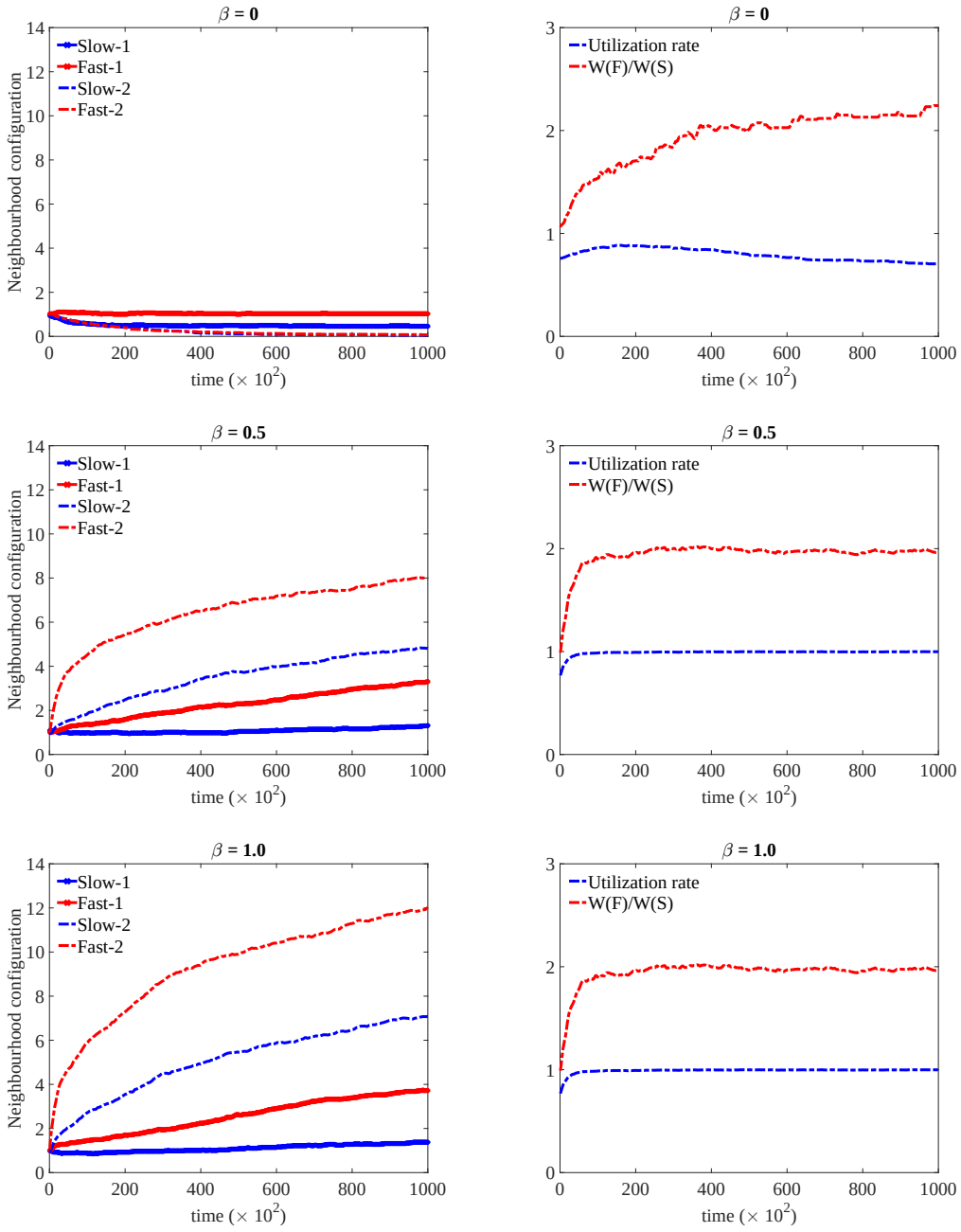

Figure 5.23: Neighbourhood configurations and utilization rate are illustrated when the exploration rate is $\beta = 0, 0.5$ and 1 respectively, where "Fast-1" means the fast agents on the first layer. The simulation runs up to $t_{\max} = 10^5$.

At the end of simulation, we obtain the stationary neighbourhood configurations by varying exploration rate β in Figure 5.24. With the increase of β, the density of

neighbours on the second layer is increasing, but slow neighbours are still around the agent to balance the system load.

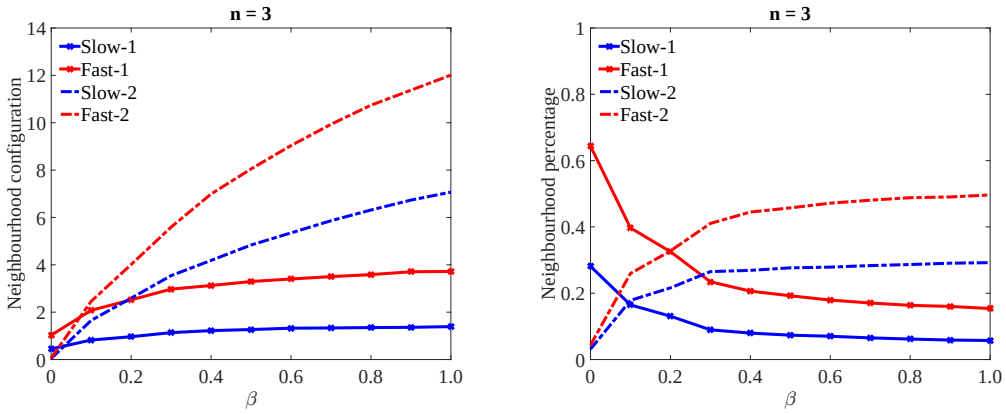

Figure 5.24: Neighbourhood configurations and percentages at stationary state are shown by varying exploration rate β from 0 to 1. The left panel illustrates how many fast and slow neighbours are on the first and second layers, and the right panel presents the percentages of various types of neighbours.

5.6.3.3 The Activities of Agents

We also explore the activities of agents in the adaptation of neighbourhood in the case of $n = 3$ and $\lambda = 3$. Let's define $In(F)$ as the average number of *coming-in* fast neighbours and $Out(F)$ as the average number of *going-out* fast neighbours. Similarly, we have $In(S)$ and $Out(S)$ for the activities of slow neighbours. Figure 5.25 illustrates the dynamical processes resulting from individual upgrading/downgrading. With the increase of the exploration rate β, more and more agents come into the neighbourhood, but the number of *going-out* neighbours changes rarely. Interestingly, the fast agents are more likely to be inserted into the neighbourhood than the slow ones.

5.6.3.4 The Effects of the Number of Layers

When the number of layers is bigger, the neighbourhood is more diverse. Figure 5.26 displays the average number of slow/fast neighbours, as well as the average weighted number of slow/fast neighbours under different tiered networks. As we can see, the weighted number of neighbours gets smaller when the number of layers (namely n) is bigger, but the average number of neighbours is invariant.

In real world, more cost usually comes along with the closer neighbours as we need to maintain them at the expense of time, energy and even money. Through this tiered

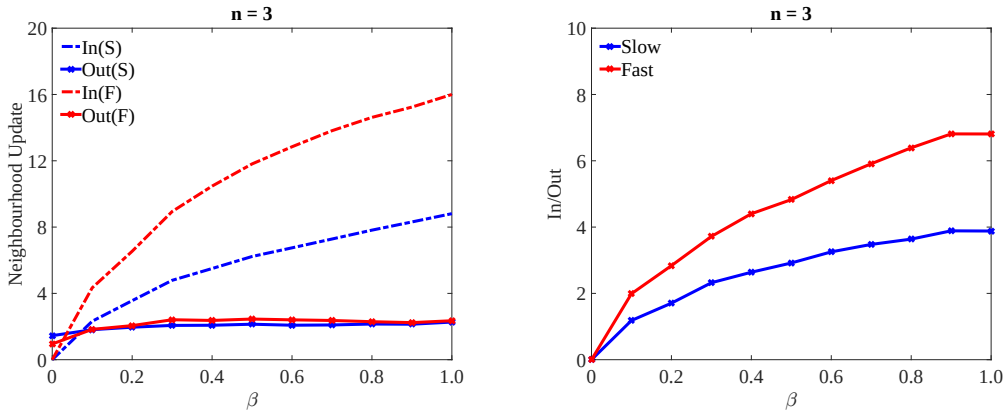

Figure 5.25: Neighbourhood is updated by varying exploration rate β from 0 to 1. Here, we use $In(S)$ to show the average number of slow agents coming in the neighbourhood, while $Out(S)$ is the average number of slow agents going out from the neighbourhood. The right panel illustrates the ratio between the number of *coming-in* neighbours and that of *going-out* neighbours (namely $In(S)/Out(S)$ and $In(F)/Out(F)$), where we can find that the fast agents are more likely to be inserted into the neighbourhood.

structure, tasks can be accomplished with less cost (namely, smaller weighted number of neighbours).

5.7 Summary

This chapter incorporates state evolution, structure adaptation and distributed learning into adaptive networks, for high-performance and resilient agent coordination. Through continuous learning, a series of local adjustments reshape the roles of agents and their connectivity.

Key to the overall performance, is a dynamic division of labour between leaders and followers. This local form of order avoid locks caused by insufficient or unreachable resources. To reach an efficient configuration, a risk-averse learning mechanism is strapped on the leaders so that they continuously refresh the picture of the local structure they are targetting, and seek to attain by rewiring their neighbourhoods. For radical changes in patterns of demand, leaders also track their loads and are able to demote themselves or promote neighbours as the case may appear. The ratio of target learning rates η_-/η_+, the probabilities of adaptation, together with the task size, and the number of different skill types, have an influence on both team wastefulness (over-accumulation of followers) and task completion rates.

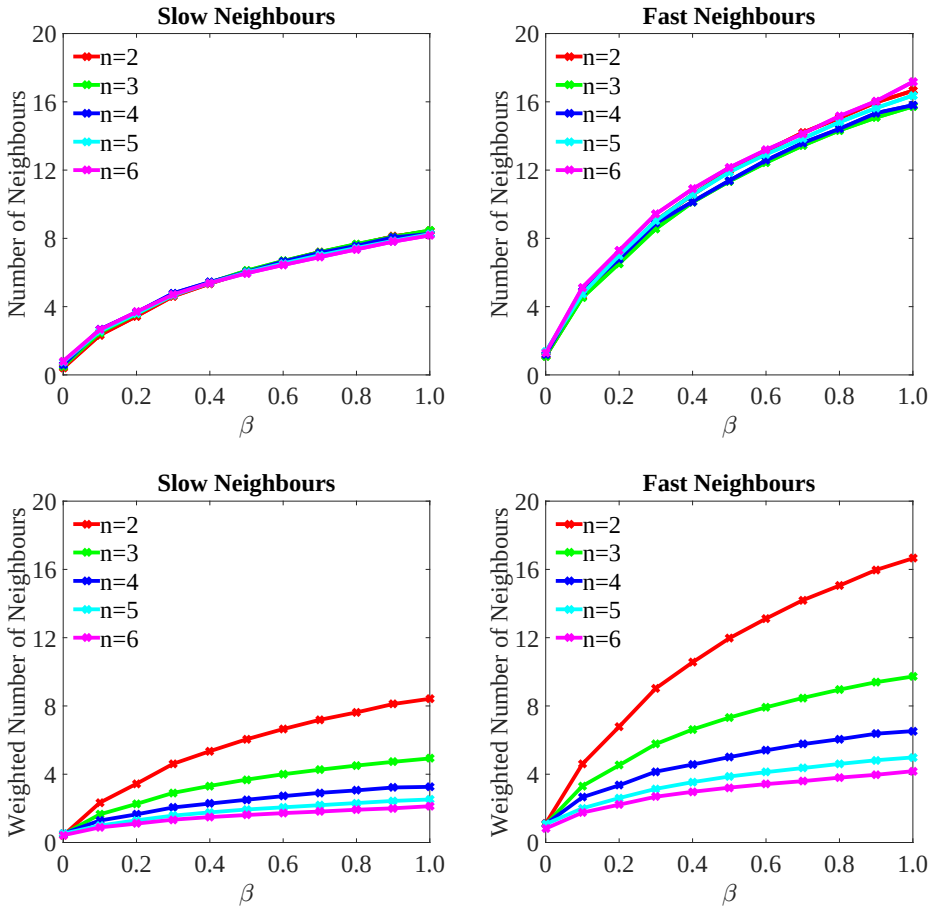

Figure 5.26: Neighbourhood configuration in weighted networks. Five different networks (whose number of layers is $n = 2,3,4,5,6$ respectively) are used to implement the framework of work-learn-adapt. Note that the number of neighbours (slow or fast) is independent on the number of layers, while the weighted number of neighbours ($W(S)$ or $W(F)$) gets smaller when the neighbourhood diversity is strong (namely bigger number of layers n).

Increasing the number of skill types decreases the organisation performance. A diverse demand in skills seem to require larger assemblies to be dealt with well. A situation familiar to people living in small groups. In contrast, increasing the typical size of a task will lead to more efficient teams with smaller resource waste rate. Our self-organizing decentralised method, where no one exerts global control, does not know a priori about the type of skill demand it is going to face. As result, it works well in a dynamical environment while incurring a relatively low loss of performance compared to a centralised solution.

In the real world, more and more systems are open to new incoming agents and built by largely interdependent components, who are supposed to manage and adapt

their relationships with others intelligently based on local and historical information. Elaborations of our simple distributed work-learn-adapt model might be useful in these more complicated settings. One limitation, is that our agents are cooperative (especially in the example of distributed task allocation, where some overloaded agents get upgraded to take more tasks). There are many situations in organisations where this is not the case. A line of research we feel would be worth pursuing, would be to take self-interested agents (Miyashita et al., 2015) into consideration, and integrate to the design of the learn-and-adapt model elements of game theory and incentives to handle these more realistic situations.

Chapter 6

Conclusions

In the dynamical world, many complex adaptive systems consist of a large number agents interacting with each other, where macroscopic phenomena emerge out of microscopic interactions. In the fields of sociology, biology and economics, a variety of investigations (Gross and Blasius, 2008; Blasius and Gross, 2009; Sayama et al., 2013) have been conducted to shed light upon the interplay between global properties and local behaviours, that we are just in the beginning to understand. As the dynamics of complex systems lies in both temporal and spatial aspects, it is a quite promising direction to study the coupled dynamics between states and structures, and then reveal the emergent order from chaos. Two core questions are: (1) where do the dynamics of state and structure originate; (2) how do the collective patterns emerge out of individual behaviours.

6.1 Thesis Summary

In this thesis, we have studied the collective dynamics on top of complex adaptive networks, which are entangled by state evolution and structure adaptation. Three adaptive network models based on various levels of learning are discussed in our work, namely adaptive voter model, evolutionary population model and adaptive agents coordination. All these models are characterized by the interplay between the dynamics *of* networks and the dynamics *on* networks, but the origins of their respective dynamics are different.

Firstly, we focus on an adaptive voter model, whose dynamics originates from a form of social learning by a series of pairwise imitation and link rewiring. When the rewiring force gets stronger, the adaptive system transforms from consensus to frag-

mentation. In Chapter 3, we have explored some interesting directions to study the influences of various evolution and adaptation strategies on the collective patterns. Specifically, a strategy of rewire-to-foaf can lead to an early fragmentation by forming numerous smaller monochrome communities. When a neutral state is introduced, network consensus is enhanced based on the method of approximate majority. Considering the heterogeneity of the nodes, a weighted voter model is proposed to illustrate the influences of biased imitation on collective dynamics. In addition, the adaptive dynamics can be derived by approximate differential equations, which may be inaccurate due to the emergent correlations. To address this difficulty, we have explored interface approximation (IA) and double stars approximation (DSA) to truncate bigger moments using smaller ones. A series of numerical simulations have shown that the accuracy is highly improved through these approximation methods.

Secondly, we study the evolution of cooperation in a group of structured population in Chapter 4, where the dynamics originates from natural selection. Based on the framework of evolutionary game theory, the players are provided with the strategy of either cooperation or defection, where cooperators are those paying cost for the success of population, but defectors (or cheaters) avoid the cost of contributing to the community. The state and structure co-evolve under natural selection and social inheritance. A critical phase transition from the regime of cooperation to that of defection is obtained with the change of a certain structure adaptation parameter (i.e. the embedding parameter q). To detect the loss of cooperation, some indicators are proposed as early-warning signals for the critical slowing down. Furthermore, Kendall τ correlation and ROC curves are adopted to measure the consistency and accuracy of the indicators in detecting the collapse of cooperation. Our results highlight that it is possible to detect the community fragility even in such a complex adaptive system. This work is quite promising nowadays in the fields of financial market, economics and ecology, where the risk of collapse is a fatal problem like Achilles' heel.

Finally, the adaptive dynamics is incorporated by state evolution, structure adaptation and distributed learning in Chapter 5. We have explored the adaptive agents coordination under the framework of work-learn-adapt (WLA), where the interacting agents need to complete the coming tasks cooperatively. Considering the uncertainty of tasks, the agents are able to adapt their states and structure in real time. In the case of agents team formation, the division of labour is achieved by the differentiation between leaders and followers. Importantly, the agents implement state evolution and structure adaptation based on quantitative information obtained from learning. This mechanism

extends the state-structure dynamics by allowing distributed learning, which can give rise to better organisation performance in a more natural and rational way. This WLA framework is decentralised, robust and sustainable in many real-world applications.

The above models are embedded into complex adaptive networks coupled by dynamical states and structures, but the endogenous dynamics are driven by different levels of learning. In the adaptive voter model, the dynamics originates from pairwise imitation. When it comes to the evolutionary population, natural selection is the main power for the evolution of cooperation. As for the dynamics in adaptive agents coordination, distributed learning guides the co-evolution of state and structure rationally. Through these models, we have gained much deeper insights into the adaptive dynamics from different perspectives.

6.2 Future Work

Even though many amazing fruits have been obtained at present in modelling and analysing complex adaptive systems, there are still many obstacles on the way ahead. In the following, we will point out some future challenges in this field.

- **Extracting rules form data**

The models adopted to study the adaptive dynamics are mostly conceptual, and how to combine theoretical work with real-world applications is always an important subject. As we all know, the models usually trade realism for generality. When we come to some realistic applications, the rules are almost unknown and we need to uncover the hidden information from real data. Therefore, the mechanisms for adaptive networks should be extracted from large-scale temporal and structured data.

Let's first suppose the state of a node is one-dimensional (namely a scalar), which means $s_i \in S_1$. At a certain step t, the whole network data defined by G_t will be the states of all nodes N and the topology information $N \times N$. The situation will be more complicated if some nodes (edges) are created or removed. When the time is advancing, we can have access to all network information G_t at each step. After that, the problem will be how to extract the dynamical mechanisms from the big data. Some machine learning methods (neural networks, deep learning, linear regression, etc.) will be helpful in dealing with this kind of regression problems.

Furthermore, when the state of a node is multi-dimensional (namely a vector), for example $s_i \in S_1 \times S_2 \times \cdots \times S_m$, the problem becomes more complicated, where we

need to consider the interdependence among the attributes as well as the interactions among the nodes.

- **Strategic learning**

When we are modelling adaptive agents coordination, all the agents are cooperative and make contributions to collective benefit. It will be a quite interesting problem to incorporate the self-interested agents into adaptive networks, where the learning will be strategic. This family of models should consider the trade-off between individual interest and global benefit, just like the Prisoner's Dilemma (PD) discussed in Chapter 4. Therefore, the model combining strategic agents with distributed learning will be a promising direction in the future.

- **Inference and decision-making**

Adaptive dynamics based on learning provides us a robust technology to build systems. In reality, the dynamics is far from linear one, and may follow some distributions. How to do the inference and make decisions under stochastic dynamics is another key problem for future research.

Bibliography

Abdallah, S. and Lesser, V. (2006). Learning the task allocation game. In *Proceedings of the fifth international joint conference on Autonomous agents and multiagent systems*, pages 850–857. ACM.

Abdallah, S. and Lesser, V. (2007). Multiagent reinforcement learning and self-organization in a network of agents. In *Proceedings of the 6th international joint conference on Autonomous agents and multiagent systems*, pages 172–179. ACM.

Abdi, H. (2007). The kendall rank correlation coefficient. *Encyclopedia of Measurement and Statistics. Sage, Thousand Oaks, CA*, pages 508–510.

Adams, J. A. et al. (2011). Coalition formation for task allocation: theory and algorithms. *Autonomous Agents and Multi-Agent Systems*, 22(2):225–248.

Albert, R. and Barabási, A.-L. (2002). Statistical mechanics of complex networks. *Reviews of modern physics*, 74(1):47.

Albert, R., Jeong, H., and Barabási, A.-L. (1999). Internet: Diameter of the world-wide web. *Nature*, 401(6749):130–131.

Allen, B., Nowak, M. A., and Dieckmann, U. (2013). Adaptive dynamics with interaction structure. *The American Naturalist*, 181(6):E139–E163.

Angluin, D., Aspnes, J., and Eisenstat, D. (2008). A simple population protocol for fast robust approximate majority. *Distributed Computing*, 21(2):87–102.

Argente, E., Billhardt, H., Cuesta, C. E., Esparcia, S., Görmer, J., Hermoso, R., Kirikal, K., Lujak, M., Pérez-Sotelo, J.-S., and Taveter, K. (2013). Adaptive agent organisations. In *Agreement Technologies*, pages 321–353. Springer.

Aspnes, J. and Ruppert, E. (2009). An introduction to population protocols. In *Middleware for Network Eccentric and Mobile Applications*, pages 97–120. Springer.

Axelrod, R. (1997). The dissemination of culture: a model with local convergence and global polarization. *Journal of conflict resolution*, 41(2):203–226.

Barabási, A.-L. and Albert, R. (1999). Emergence of scaling in random networks. *science*, 286(5439):509–512.

Barrat, A., Barthelemy, M., and Vespignani, A. (2008). *Dynamical processes on complex networks*. Cambridge University Press.

Barrat, A. and Weigt, M. (2000). On the properties of small-world network models. *The European Physical Journal B-Condensed Matter and Complex Systems*, 13(3):547–560.

Barthélémy, M. and Amaral, L. A. N. (1999). Small-world networks: Evidence for a crossover picture. *Physical Review Letters*, 82(15):3180.

Barto, A. G. (1998). *Reinforcement learning: An introduction*. MIT press.

Barton, L. and Allan, V. (2007a). Information sharing in an agent organized network. In *Proceedings of the 2008 IEEE/WIC/ACM International Conference on Web Intelligence and Intelligent Agent Technology*, pages 89–92. IEEE Computer Society.

Barton, L. and Allan, V. (2007b). Methods for coalition formation in adaptation-based social networks. *Cooperative Information Agents XI*, pages 285–297.

Barton, L. and Allan, V. (2008). Adapting to changing resource requirements for coalition formation in self-organized social networks. In *Proceedings of the 2007 IEEE/WIC/ACM International Conference on Web Intelligence and Intelligent Agent Technology*, volume 2, pages 282–285. IEEE.

Benczik, I., Benczik, S., Schmittmann, B., and Zia, R. (2008). Lack of consensus in social systems. *EPL (Europhysics Letters)*, 82(4):48006.

Benczik, I., Benczik, S., Schmittmann, B., and Zia, R. (2009). Opinion dynamics on an adaptive random network. *Physical Review E*, 79(4):046104.

Bender, E. A. and Canfield, E. R. (1978). The asymptotic number of labeled graphs with given degree sequences. *Journal of Combinatorial Theory, Series A*, 24(3):296–307.

Blasius, B. and Gross, T. (2009). Dynamic and topological interplay in adaptive networks. *Reviews of Nonlinear Dynamics and complexity, Wiley-VCH, Weinheim*.

Boccaletti, S., Latora, V., Moreno, Y., Chavez, M., and Hwang, D.-U. (2006). Complex networks: Structure and dynamics. *Physics reports*, 424(4):175–308.

Boettiger, C. and Hastings, A. (2012). Quantifying limits to detection of early warning for critical transitions. *Journal of The Royal Society Interface*, 9(75):2527–2539.

Bollobás, B. (1981). The diameter of random graphs. *Transactions of the American Mathematical Society*, 267(1):41–52.

Bollobás, B. (2001). Random graphs, volume 73 of cambridge studies in advanced mathematics.

Bollobás, B., Kozma, R., and Miklos, D. (2010). *Handbook of large-scale random networks*, volume 18. Springer Science & Business Media.

Bollobás, B. and Riordan, O. M. (2003). Mathematical results on scale-free random graphs. *Handbook of graphs and networks: from the genome to the internet*, pages 1–34.

Bork, P., Jensen, L. J., von Mering, C., Ramani, A. K., Lee, I., and Marcotte, E. M. (2004). Protein interaction networks from yeast to human. *Current opinion in structural biology*, 14(3):292–299.

Bornholdt, S. and Rohlf, T. (2000). Topological evolution of dynamical networks: Global criticality from local dynamics. *Physical Review Letters*, 84(26):6114.

Bornholdt, S. and Schuster, H. G. (2006). *Handbook of graphs and networks: from the genome to the internet*. John Wiley & Sons.

Bowles, S. and Gintis, H. (2011). *A cooperative species: Human reciprocity and its evolution*. Princeton University Press.

Bowling, M. and Veloso, M. (2002). Multiagent learning using a variable learning rate. *Artificial Intelligence*, 136(2):215–250.

Brun, Y., Serugendo, G. D. M., Gacek, C., Giese, H., Kienle, H., Litoiu, M., Müller, H., Pezzè, M., and Shaw, M. (2009). Engineering self-adaptive systems through feedback loops. In *Software engineering for self-adaptive systems*, pages 48–70. Springer.

Bulka, B., Gaston, M., and Desjardins, M. (2007). Local strategy learning in networked multi-agent team formation. *Autonomous Agents and Multi-Agent Systems*, 15(1):29–45.

Cardelli, L. and Csikász-Nagy, A. (2012). The cell cycle switch computes approximate majority. *Scientific reports*, 2.

Carpenter, S. and Brock, W. (2006). Rising variance: a leading indicator of ecological transition. *Ecology letters*, 9(3):311–318.

Castellano, C., Fortunato, S., and Loreto, V. (2009). Statistical physics of social dynamics. *Reviews of modern physics*, 81(2):591.

Castellano, C., Marsili, M., and Vespignani, A. (2000). Nonequilibrium phase transition in a model for social influence. *Physical Review Letters*, 85(16):3536.

Castellano, C., Vilone, D., and Vespignani, A. (2003). Incomplete ordering of the voter model on small-world networks. *EPL (Europhysics Letters)*, 63(1):153.

Castelló, X., Eguíluz, V. M., and San Miguel, M. (2006). Ordering dynamics with two non-excluding options: bilingualism in language competition. *New Journal of Physics*, 8(12):308.

Cavaliere, M., Sedwards, S., Tarnita, C. E., Nowak, M. A., and Csikász-Nagy, A. (2012). Prosperity is associated with instability in dynamical networks. *Journal of theoretical biology*, 299:126–138.

Charlesworth, B. (2009). Effective population size and patterns of molecular evolution and variation. *Nature Reviews Genetics*, 10(3):195–205.

Chen, P. and Redner, S. (2005). Majority rule dynamics in finite dimensions. *Physical review E*, 71(3):036101.

Cheng, J., Adamic, L., Dow, P. A., Kleinberg, J. M., and Leskovec, J. (2014). Can cascades be predicted? In *Proceedings of the 23rd international conference on World wide web*, pages 925–936. ACM.

Clifford, P. and Sudbury, A. (1973). A model for spatial conflict. *Biometrika*, 60(3):581–588.

Colaiori, F. and Castellano, C. (2015). Interplay between media and social influence in the collective behavior of opinion dynamics. *Physical Review E*, 92(4):042815.

Colaiori, F., Castellano, C., Cuskley, C. F., Loreto, V., Pugliese, M., and Tria, F. (2015). General three-state model with biased population replacement: Analytical solution and application to language dynamics. *Physical Review E*, 91(1):012808.

Collet, P., Martínez, S., and San Martín, J. (2012). *Quasi-stationary distributions: Markov chains, diffusions and dynamical systems*. Springer Science & Business Media.

Conte, R. and Paolucci, M. (2001). Intelligent social learning. *Journal of Artificial Societies and Social Simulation*, 4(1):U61–U82.

Dakos, V., Carpenter, S. R., Brock, W. A., Ellison, A. M., Guttal, V., Ives, A. R., Kefi, S., Livina, V., Seekell, D. A., van Nes, E. H., et al. (2012). Methods for detecting early warnings of critical transitions in time series illustrated using simulated ecological data. *PloS one*, 7(7):e41010.

Dakos, V., Carpenter, S. R., van Nes, E. H., and Scheffer, M. (2015). Resilience indicators: prospects and limitations for early warnings of regime shifts. *Philosophical Transactions of the Royal Society B: Biological Sciences*, 370(1659):20130263.

Danos, V., Harmer, R., and Honorato-Zimmer, R. (2013). Thermodynamic graph-rewriting. *Lecture Notes in Computer Science*, 11(2):380–394.

Danos, V., Heindel, T., Honorato-Zimmer, R., and Stucki, S. (2014). Approximations for stochastic graph rewriting. In *Formal Methods and Software Engineering*, pages 1–10. Springer.

Danos, V., Heindel, T., Honorato-Zimmer, R., and Stucki, S. (2015a). Computing approximations for graph transformation systems. *MeMo 2015*, page 33.

Danos, V., Heindel, T., Honorato-Zimmer, R., and Stucki, S. (2015b). Moment semantics for reversible rule-based systems. In *Reversible Computation*, pages 3–26. Springer.

Darwin, C. and Bynum, W. F. (2009). *The origin of species by means of natural selection: or, the preservation of favored races in the struggle for life*. AL Burt.

de Weerdt, M. M., Zhang, Y., and Klos, T. (2012). Multiagent task allocation in social networks. *Autonomous Agents and Multi-Agent Systems*, 25(1):46–86.

Deffuant, G., Neau, D., Amblard, F., and Weisbuch, G. (2000). Mixing beliefs among interacting agents. *Advances in Complex Systems*, 3(01n04):87–98.

Demirel, G., Vazquez, F., Böhme, G., and Gross, T. (2014). Moment-closure approximations for discrete adaptive networks. *Physica D: Nonlinear Phenomena*, 267:68–80.

Dornic, I., Chaté, H., Chave, J., and Hinrichsen, H. (2001). Critical coarsening without surface tension: The universality class of the voter model. *Physical Review Letters*, 87(4):045701.

Dorogovtsev, S. N. and Mendes, J. F. (2002). Evolution of networks. *Advances in physics*, 51(4):1079–1187.

Dorogovtsev, S. N., Mendes, J. F. F., and Samukhin, A. N. (2000). Structure of growing networks with preferential linking. *Physical review letters*, 85(21):4633.

Dos Santos, D. S. and Bazzan, A. L. (2012). Distributed clustering for group formation and task allocation in multiagent systems: a swarm intelligence approach. *Applied Soft Computing*.

Dunbar, R. I. (2016). Do online social media cut through the constraints that limit the size of offline social networks? *Royal Society Open Science*, 3(1).

Dunne, J. A., Williams, R. J., and Martinez, N. D. (2002). Food-web structure and network theory: the role of connectance and size. *Proceedings of the National Academy of Sciences*, 99(20):12917–12922.

Durrett, R., Gleeson, J. P., Lloyd, A. L., Mucha, P. J., Shi, F., Sivakoff, D., Socolar, J. E., and Varghese, C. (2012). Graph fission in an evolving voter model. *Proceedings of the National Academy of Sciences*, 109(10):3682–3687.

Durrett, R., Steif, J. E., et al. (1993). Fixation results for threshold voter systems. *The Annals of Probability*, 21(1):232–247.

Easley, D. and Kleinberg, J. (2010). *Networks, crowds, and markets: Reasoning about a highly connected world*. Cambridge University Press.

Ellner, S. P. (2001). Pair approximation for lattice models with multiple interaction scales. *Journal of theoretical biology*, 210(4):435–447.

Erdős, P. and Rényi, A. (1959). On random graphs. *Publicationes Mathematicae Debrecen*, 6:290–297.

Erdős, P. and Rényi, A. (1960). On the evolution of random graphs. *Publ. Math. Inst. Hungar. Acad. Sci*, 5:17–61.

Erdős, P. and Rényi, A. (1961). On the strength of connectedness of a random graph. *Acta Mathematica Hungarica*, 12(1):261–267.

Ferber, J. (1999). *Multi-agent systems: an introduction to distributed artificial intelligence*, volume 1. Addison-Wesley Reading.

Fisher, R. A. (1930). *The genetical theory of natural selection: a complete variorum edition*. Oxford University Press.

Fu, F., Hauert, C., Nowak, M. A., and Wang, L. (2008). Reputation-based partner choice promotes cooperation in social networks. *Physical Review E*, 78(2):026117.

Fu, F. and Wang, L. (2008). Coevolutionary dynamics of opinions and networks: From diversity to uniformity. *Physical Review E*, 78(1):016104.

Galam, S. (2002). Minority opinion spreading in random geometry. *The European Physical Journal B-Condensed Matter and Complex Systems*, 25(4):403–406.

Gaston, M. E. (2005). *Organizational learning and network adaptation in multi-agent systems*. University of Maryland at Baltimore County.

Gaston, M. E. and desJardins, M. (2005). Agent-organized networks for dynamic team formation. In *Proceedings of the fourth international joint conference on Autonomous agents and multiagent systems*, pages 230–237. ACM.

Gilks, W. R. (2005). *Markov chain monte carlo*. Wiley Online Library.

Gleeson, J. P. (2011). High-accuracy approximation of binary-state dynamics on networks. *Physical Review Letters*, 107(6):068701.

Gleeson, J. P. (2013). Binary-state dynamics on complex networks: pair approximation and beyond. *Physical Review X*, 3(2):021004.

Gleeson, J. P., Melnik, S., Ward, J. A., Porter, M. A., and Mucha, P. J. (2012). Accuracy of mean-field theory for dynamics on real-world networks. *Physical Review E*, 85(2):026106.

Glinton, R., Scerri, P., and Sycara, K. (2008a). Agent-based sensor coalition formation. In *Information Fusion, 2008 11th International Conference on*, pages 1–7. IEEE.

Glinton, R., Sycara, K., and Scerri, P. (2008b). Agent organized networks redux. *Proceedings of the Twenty-Second AAAI Conference on Artificial Intelligence*, pages 83–88.

Gomez Rodriguez, M., Leskovec, J., and Krause, A. (2010). Inferring networks of diffusion and influence. In *Proceedings of the 16th ACM SIGKDD international conference on Knowledge discovery and data mining*, pages 1019–1028. ACM.

Gross, T. and Blasius, B. (2008). Adaptive coevolutionary networks: a review. *Journal of The Royal Society Interface*, 5(20):259–271.

Gross, T., DLima, C. J. D., and Blasius, B. (2006). Epidemic dynamics on an adaptive network. *Physical review letters*, 96(20):208701.

Gross, T. and Sayama, H. (2009). *Adaptive networks*. Springer.

Guerra, B. and Gómez-Gardeñes, J. (2010). Annealed and mean-field formulations of disease dynamics on static and adaptive networks. *Physical Review E*, 82(3):035101.

Guimerà, R., Diaz-Guilera, A., Vega-Redondo, F., Cabrales, A., and Arenas, A. (2002). Optimal network topologies for local search with congestion. *Physical review letters*, 89(24):248701.

Guimera, R., Mossa, S., Turtschi, A., and Amaral, L. N. (2005). The worldwide air transportation network: Anomalous centrality, community structure, and cities' global roles. *Proceedings of the National Academy of Sciences*, 102(22):7794–7799.

Haldane, A. G. et al. (2009). Rethinking the financial network. *Speech delivered at the Financial Student Association, Amsterdam, April*, pages 1–26.

Heindel, T. (2010). *A category theoretical approach to the concurrent semantics of rewriting: adhesive categories and related concepts*. PhD thesis, Universität Duisburg-Essen, Fakultät für Ingenieurwissenschaften Informatik und Angewandte Kognitionswissenschaft.

Held, H. and Kleinen, T. (2004). Detection of climate system bifurcations by degenerate fingerprinting. *Geophysical Research Letters*, 31(23).

Hinton, G. E. and Nowlan, S. J. (1987). How learning can guide evolution. *Complex systems*, 1(3):495–502.

Hofbauer, J. and Sigmund, K. (1998). *Evolutionary games and population dynamics*. Cambridge University Press.

Hofmann, L.-M., Chakraborty, N., and Sycara, K. (2011). The evolution of cooperation in self-interested agent societies: a critical study. In *The 10th International Conference on Autonomous Agents and Multiagent Systems-Volume 2*, pages 685–692.

Holland, J. H. (1992). Complex adaptive systems. *Daedalus*, pages 17–30.

Holland, J. H. (2006). Studying complex adaptive systems. *Journal of Systems Science and Complexity*, 19(1):1–8.

Holley, R. A. and Liggett, T. M. (1975). Ergodic theorems for weakly interacting infinite systems and the voter model. *The annals of probability*, pages 643–663.

Holling, C. S. (1973). Resilience and stability of ecological systems. *Annual review of ecology and systematics*, pages 1–23.

Holme, P. and Newman, M. E. (2006). Nonequilibrium phase transition in the coevolution of networks and opinions. *Physical Review E*, 74(5):056108.

Holt, C. A. and Laury, S. K. (2002). Risk aversion and incentive effects. *American economic review*, 92(5):1644–1655.

Hudson, R. R. (2002). Generating samples under a wright–fisher neutral model of genetic variation. *Bioinformatics*, 18(2):337–338.

Jackson, M. O. et al. (2008). *Social and economic networks*, volume 3. Princeton University Press Princeton.

Jeong, H., Tombor, B., Albert, R., Oltvai, Z. N., and Barabási, A.-L. (2000). The large-scale organization of metabolic networks. *Nature*, 407(6804):651–654.

Jiang, C., Chen, Y., and Liu, K. R. (2013). Distributed adaptive networks: A graphical evolutionary game-theoretic view. *Signal Processing, IEEE Transactions on*, 61(22):5675–5688.

Jin, Q., Wang, Z., and Wang, Y.-L. (2012). Strategy changing penalty promotes cooperation in spatial prisoners dilemma game. *Chaos, Solitons & Fractals*, 45(4):395–401.

Karinthy, F. (1929). Chain-links. *Everything is the Other Way*.

Kimura, D. and Hayakawa, Y. (2008). Coevolutionary networks with homophily and heterophily. *Physical Review E*, 78(1):016103.

Kleinberg, J. M. (2000). Navigation in a small world. *Nature*, 406(6798):845–845.

Klemm, K. and Eguiluz, V. M. (2002a). Growing scale-free networks with small-world behavior. *Physical Review E*, 65(5):057102.

Klemm, K. and Eguiluz, V. M. (2002b). Highly clustered scale-free networks. *Physical Review E*, 65(3):036123.

Kohonen, T. (1988). Self-organization and associative memory. *Self-Organization and Associative Memory, 100 figs. XV, 312 pages.. Springer-Verlag Berlin Heidelberg New York. Also Springer Series in Information Sciences, volume 8*, 1.

Kota, R., Gibbins, N., and Jennings, N. (2009). Self-organising agent organisations. In *Proceedings of the 8th International Conference on Autonomous Agents and Multiagent Systems-Volume 2*, pages 797–804. International Foundation for Autonomous Agents and Multiagent Systems.

Kota, R., Gibbins, N., and Jennings, N. (2012). Decentralized approaches for self-adaptation in agent organizations. *ACM Transactions on Autonomous and Adaptive Systems (TAAS)*, 7(1):1–36.

Kozma, B. and Barrat, A. (2008). Consensus formation on adaptive networks. *Physical Review E*, 77(1):016102.

Krapivsky, P. and Redner, S. (2003). Dynamics of majority rule in two-state interacting spin systems. *Physical Review Letters*, 90(23):238701.

Krapivsky, P. L., Redner, S., and Leyvraz, F. (2000). Connectivity of growing random networks. *Physical review letters*, 85(21):4629.

Leskovec, J., Backstrom, L., Kumar, R., and Tomkins, A. (2008). Microscopic evolution of social networks. In *Proceedings of the 14th ACM SIGKDD international conference on Knowledge discovery and data mining*, pages 462–470. ACM.

Levin, S. (1999). Fragile dominion: Complexity and the commons (perseus, reading, ma).

Levin, S. (2003). Complex adaptive systems: exploring the known, the unknown and the unknowable. *Bulletin of the American Mathematical Society*, 40(1):3–19.

Levin, S. (2010). Crossing scales, crossing disciplines: collective motion and collective action in the global commons. *Philosophical Transactions of the Royal Society B: Biological Sciences*, 365(1537):13–18.

Lieberman, E., Hauert, C., and Nowak, M. A. (2005). Evolutionary dynamics on graphs. *Nature*, 433(7023):312–316.

Liggett, T. M. (2013). *Stochastic interacting systems: contact, voter and exclusion processes*, volume 324. Springer Science & Business Media.

Macy, M. W. and Flache, A. (2002). Learning dynamics in social dilemmas. *Proceedings of the National Academy of Sciences*, 99(suppl 3):7229–7236.

Masel, J. (2011). Genetic drift. *Current Biology*, 21(20):R837–R838.

Mellor, A., Mobilia, M., Redner, S., Rucklidge, A. M., and Ward, J. A. (2015). Role of luddism on innovation diffusion. *arXiv preprint arXiv:1505.02020*.

Merton, R. K. (1968). The matthew effect in science. *Science*, 159(3810):56–63.

Metropolis, N., Rosenbluth, A. W., Rosenbluth, M. N., Teller, A. H., and Teller, E. (1953). Equation of state calculations by fast computing machines. *The journal of chemical physics*, 21(6):1087–1092.

Miller, J. H. and Page, S. E. (2009). *Complex adaptive systems: an introduction to computational models of social life: an introduction to computational models of social life*. Princeton university press.

Miller, N. E. and Dollard, J. (1941). Social learning and imitation.

Miyashita, Y., Hayano, M., and Sugawara, T. (2015). Self-organizational reciprocal agents for conflict avoidance in allocation problems. In *Self-Adaptive and Self-Organizing Systems (SASO), 2015 IEEE 9th International Conference on*, pages 150–155. IEEE.

Molloy, M. and Reed, B. (1995). A critical point for random graphs with a given degree sequence. *Random structures & algorithms*, 6(2-3):161–180.

Moran, P. A. P. (1958). Random processes in genetics. In *Mathematical Proceedings of the Cambridge Philosophical Society*, volume 54, pages 60–71. Cambridge Univ Press.

Moran, P. A. P. et al. (1962). The statistical processes of evolutionary theory. *The statistical processes of evolutionary theory.*

Myers, S. A. and Leskovec, J. (2014). The bursty dynamics of the twitter information network. In *Proceedings of the 23rd international conference on World wide web*, pages 913–924. ACM.

Newman, M. E. (2001). The structure of scientific collaboration networks. *Proceedings of the National Academy of Sciences*, 98(2):404–409.

Newman, M. E. (2003). The structure and function of complex networks. *SIAM review*, 45(2):167–256.

Newman, M. E., Strogatz, S. H., and Watts, D. J. (2001). Random graphs with arbitrary degree distributions and their applications. *Physical review E*, 64(2):026118.

Norris, J. R. (1998). *Markov chains*. Cambridge university press.

Nowak, M. A. (2006a). *Evolutionary dynamics*. Harvard University Press.

Nowak, M. A. (2006b). Five rules for the evolution of cooperation. *science*, 314(5805):1560–1563.

Nowak, M. A. (2012). Evolving cooperation. *Journal of theoretical biology*, 299:1–8.

Nowak, M. A. and May, R. M. (1992). Evolutionary games and spatial chaos. *Nature*, 359(6398):826–829.

Nowak, M. A., Tarnita, C. E., and Antal, T. (2010). Evolutionary dynamics in structured populations. *Philosophical Transactions of the Royal Society B: Biological Sciences*, 365(1537):19–30.

Ohtsuki, H., Hauert, C., Lieberman, E., and Nowak, M. A. (2006). A simple rule for the evolution of cooperation on graphs and social networks. *Nature*, 441(7092):502–505.

Olfati-Saber, R., Fax, A., and Murray, R. M. (2007). Consensus and cooperation in networked multi-agent systems. *Proceedings of the IEEE*, 95(1):215–233.

Ostrom, E. (2009). *Understanding institutional diversity*. Princeton university press.

Pacheco, J. M., Lenaerts, T., and Santos, F. C. (2007). Evolution of cooperation in a population of selfish adaptive agents. In *Advances in Artificial Life*, pages 535–544. Springer.

Pacheco, J. M., Traulsen, A., and Nowak, M. A. (2006a). Active linking in evolutionary games. *Journal of theoretical biology*, 243(3):437–443.

Pacheco, J. M., Traulsen, A., and Nowak, M. A. (2006b). Coevolution of strategy and structure in complex networks with dynamical linking. *Physical Review Letters*, 97(25):258103.

Pastor-Satorras, R. and Vespignani, A. (2001). Epidemic dynamics and endemic states in complex networks. *Physical Review E*, 63(6):066117.

Perc, M. (2014). The matthew effect in empirical data. *Journal of The Royal Society Interface*, 11(98):20140378.

Perc, M. and Szolnoki, A. (2010). Coevolutionary gamesa mini review. *BioSystems*, 99(2):109–125.

Poncela, J., Gómez-Gardeñes, J., Traulsen, A., and Moreno, Y. (2009). Evolutionary game dynamics in a growing structured population. *New Journal of Physics*, 11(8):083031.

Popat, R., Crusz, S. A., Messina, M., Williams, P., West, S. A., and Diggle, S. P. (2012). Quorum-sensing and cheating in bacterial biofilms. *Proceedings of the Royal Society B: Biological Sciences*, page rspb20121976.

Porter, M. A. and Gleeson, J. P. (2014). Dynamical systems on networks: a tutorial. *arXiv preprint arXiv:1403.7663*.

Prehofer, C. and Bettstetter, C. (2005). Self-organization in communication networks: principles and design paradigms. *IEEE Communications Magazine*, 43(7):78–85.

Rainey, P. B. and Rainey, K. (2003). Evolution of cooperation and conflict in experimental bacterial populations. *Nature*, 425(6953):72–74.

Rand, D. G., Arbesman, S., and Christakis, N. A. (2011). Dynamic social networks promote cooperation in experiments with humans. *Proceedings of the National Academy of Sciences*, 108(48):19193–19198.

Ranjbar-Sahraei, B., Bou Ammar, H., Bloembergen, D., Tuyls, K., and Weiss, G. (2014). Evolution of cooperation in arbitrary complex networks. In *Proceedings of the 2014 international conference on Autonomous agents and multi-agent systems*, pages 677–684.

Redner, S. (1998). How popular is your paper? an empirical study of the citation distribution. *The European Physical Journal B-Condensed Matter and Complex Systems*, 4(2):131–134.

Rogers, T. and Gross, T. (2013). Consensus time and conformity in the adaptive voter model. *Physical Review E*, 88(3):030102.

San Miguel, M., Eguiluz, V. M., Toral, R., Klemm, K., et al. (2005). Binary and multivariate stochastic models of consensus formation. *Computing in Science and Engineering*, 7(6):67–73.

Sanchez, A. and Gore, J. (2013). Feedback between population and evolutionary dynamics determines the fate of social microbial populations. *PLoS biology*, 11(4):e1001547.

Sánchez, J. R. (2004). A modified one-dimensional sznajd model. *arXiv preprint cond-mat/0408518*.

Santos, F. C., Pacheco, J. M., and Lenaerts, T. (2006). Cooperation prevails when individuals adjust their social ties. *PLoS Computational Biology*, 2(10):e140.

Santos, F. C., Pacheco, J. M., and Skyrms, B. (2011). Co-evolution of pre-play signaling and cooperation. *Journal of Theoretical Biology*, 274(1):30–35.

Santos, F. C., Pinheiro, F. L., Lenaerts, T., and Pacheco, J. M. (2012). The role of diversity in the evolution of cooperation. *Journal of theoretical biology*, 299:88–96.

Saramäki, J., Leicht, E. A., López, E., Roberts, S. G., Reed-Tsochas, F., and Dunbar, R. I. (2014). Persistence of social signatures in human communication. *Proceedings of the National Academy of Sciences*, 111(3):942–947.

Sayama, H., Pestov, I., Schmidt, J., Bush, B. J., Wong, C., Yamanoi, J., and Gross, T. (2013). Modeling complex systems with adaptive networks. *Computers & Mathematics with Applications*, 65(10):1645–1664.

Sayed, A. H. (2014). Adaptive networks. *Proceedings of the IEEE*, 102(4):460–497.

Scheffer, M., Bascompte, J., Brock, W. A., Brovkin, V., Carpenter, S. R., Dakos, V., Held, H., Van Nes, E. H., Rietkerk, M., and Sugihara, G. (2009). Early-warning signals for critical transitions. *Nature*, 461(7260):53–59.

Scheffer, M., Carpenter, S., Foley, J. A., Folke, C., and Walker, B. (2001). Catastrophic shifts in ecosystems. *Nature*, 413(6856):591–596.

Scheucher, M. and Spohn, H. (1988). A soluble kinetic model for spinodal decomposition. *Journal of statistical physics*, 53(1-2):279–294.

Schuster, P. and Sigmund, K. (1983). Replicator dynamics. *Journal of theoretical biology*, 100(3):533–538.

Sen, S. and Weiss, G. (1999). Learning in multiagent systems. *Multiagent systems: A modern approach to distributed artificial intelligence*, page 259.

Shakarian, P., Roos, P., and Johnson, A. (2012). A review of evolutionary graph theory with applications to game theory. *Biosystems*, 107(2):66–80.

Sharp, H. (1968). Cardinality of finite topologies. *Journal of Combinatorial Theory*, 5(1):82–86.

Shehory, O. and Kraus, S. (1998). Methods for task allocation via agent coalition formation. *Artificial Intelligence*, 101(1):165–200.

Smith, J. M. and Price, G. (1973). The logic of animal conflict. *Nature*, 246:15.

Sood, V., Antal, T., and Redner, S. (2008). Voter models on heterogeneous networks. *Physical Review E*, 77(4):041121.

Sood, V. and Redner, S. (2005). Voter model on heterogeneous graphs. *Physical review letters*, 94(17):178701.

Strogatz, S. H. (2001). Exploring complex networks. *Nature*, 410(6825):268–276.

Strogatz, S. H. (2014). *Nonlinear dynamics and chaos: with applications to physics, biology, chemistry, and engineering*. Westview press.

Suchecki, K., Eguiluz, V. M., and San Miguel, M. (2005). Conservation laws for the voter model in complex networks. *EPL (Europhysics Letters)*, 69(2):228.

Suweis, S. and D'Odorico, P. (2014). Early warning signs in social-ecological networks. *PloS one*, 9(7):e101851.

Szabó, G., Alava, M., and Kertész, J. (2003). Structural transitions in scale-free networks. *Physical Review E*, 67(5):056102.

Sznajd-Weron, K. (2005). Sznajd model and its applications. *arXiv preprint physics/0503239*.

Sznajd-Weron, K. and Sznajd, J. (2000). Opinion evolution in closed community. *International Journal of Modern Physics C*, 11(06):1157–1165.

Szolnoki, A. and Perc, M. (2008). Coevolution of teaching activity promotes cooperation. *New Journal of Physics*, 10(4):043036.

Szolnoki, A., Perc, M., and Danku, Z. (2008). Making new connections towards cooperation in the prisoner's dilemma game. *EPL (Europhysics Letters)*, 84(5):50007.

Szolnoki, A., Perc, M., and Mobilia, M. (2014). Facilitators on networks reveal optimal interplay between information exchange and reciprocity. *Physical Review E*, 89(4):042802.

Tarnita, C. E., Ohtsuki, H., Antal, T., Fu, F., and Nowak, M. A. (2009). Strategy selection in structured populations. *Journal of theoretical biology*, 259(3):570–581.

Thadakamaila, H., Raghavan, U. N., Kumara, S., and Albert, R. (2004). Survivability of multiagent-based supply networks: a topological perspect. *Intelligent Systems, IEEE*, 19(5):24–31.

Traulsen, A. and Nowak, M. A. (2006). Evolution of cooperation by multilevel selection. *Proceedings of the National Academy of Sciences*, 103(29):10952–10955.

Traulsen, A., Nowak, M. A., and Pacheco, J. M. (2006). Stochastic dynamics of invasion and fixation. *Physical Review E*, 74(1):011909.

Traulsen, A., Shoresh, N., and Nowak, M. A. (2008). Analytical results for individual and group selection of any intensity. *Bulletin of mathematical biology*, 70(5):1410–1424.

Travisano, M. and Velicer, G. J. (2004). Strategies of microbial cheater control. *Trends in microbiology*, 12(2):72–78.

Van Der Hofstad, R. (2009). Random graphs and complex networks. *Available on http://www. win. tue. nl/rhofstad/NotesRGCN. pdf*.

Van Nes, E. H. and Scheffer, M. (2007). Slow recovery from perturbations as a generic indicator of a nearby catastrophic shift. *The American Naturalist*, 169(6):738–747.

Van Noort, V., Snel, B., and Huynen, M. A. (2004). The yeast coexpression network has a small-world, scale-free architecture and can be explained by a simple model. *EMBO reports*, 5(3):280–284.

Van Segbroeck, S., Santos, F. C., Lenaerts, T., and Pacheco, J. M. (2009). Reacting differently to adverse ties promotes cooperation in social networks. *Physical review letters*, 102(5):058105.

Van Segbroeck, S., Santos, F. C., Lenaerts, T., and Pacheco, J. M. (2011). Selection pressure transforms the nature of social dilemmas in adaptive networks. *New Journal of Physics*, 13(1):013007.

Van Segbroeck, S., Santos, F. C., Nowé, A., Pacheco, J. M., and Lenaerts, T. (2008). The evolution of prompt reaction to adverse ties. *BMC evolutionary biology*, 8(1):287.

Varghese, C. and Durrett, R. (2013). Phase transitions in the quadratic contact process on complex networks. *Physical Review E*, 87(6):062819.

Vazquez, F. (2013). Opinion dynamics on coevolving networks. In *Dynamics On and Of Complex Networks, Volume 2*, pages 89–107. Springer.

Vazquez, F., Eguíluz, V. M., and San Miguel, M. (2008). Generic absorbing transition in coevolution dynamics. *Physical review letters*, 100(10):108702.

Vazquez, F., Krapivsky, P. L., and Redner, S. (2003). Constrained opinion dynamics: Freezing and slow evolution. *Journal of Physics A: Mathematical and General*, 36(3):L61.

Vig, L. and Adams, J. A. (2007). Coalition formation: From software agents to robots. *Journal of Intelligent and Robotic Systems*, 50(1):85–118.

Vincent, T. L. and Brown, J. S. (2005). *Evolutionary game theory, natural selection, and Darwinian dynamics*. Cambridge University Press.

Vural, D. C., Isakov, A., and Mahadevan, L. (2015). The organization and control of an evolving interdependent population. *Journal of the Royal Society Interface*, 12(108):2021–2025.

Wardil, L. and Hauert, C. (2014). Origin and structure of dynamic cooperative networks. *Scientific reports*, 4.

Wasserman, S. (1994). *Social network analysis: Methods and applications*, volume 8. Cambridge university press.

Watts, D. J. and Strogatz, S. H. (1998). Collective dynamics of small-world networks. *nature*, 393(6684):440–442.

Weibull, J. W. (1997). *Evolutionary game theory*. MIT press.

Weng, L., Ratkiewicz, J., Perra, N., Gonçalves, B., Castillo, C., Bonchi, F., Schifanella, R., Menczer, F., and Flammini, A. (2013). The role of information diffusion in the evolution of social networks. In *Proceedings of the 19th ACM SIGKDD international conference on Knowledge discovery and data mining*, pages 356–364. ACM.

West, D. B. et al. (2001). *Introduction to graph theory*, volume 2. Prentice hall Upper Saddle River.

Wissel, C. (1984). A universal law of the characteristic return time near thresholds. *Oecologia*, 65(1):101–107.

Wright, S. (1931). Evolution in mendelian populations. *Genetics*, 16(2):97.

Wu, B., Zhou, D., Fu, F., Luo, Q., Wang, L., and Traulsen, A. (2010). Evolution of cooperation on stochastic dynamical networks. *PLoS One*, 5(6):e11187.

Xie, J., Sreenivasan, S., Korniss, G., Zhang, W., Lim, C., and Szymanski, B. K. (2011). Social consensus through the influence of committed minorities. *Physical Review E*, 84(1):011130.

Yang, G., Huang, J., and Zhang, W. (2014). Older partner selection promotes the prevalence of cooperation in evolutionary games. *Journal of theoretical biology*, 359:171–183.

Yang, G., Zhang, W., and Xiu, B. (2015). Neighbourhood reaction in the evolution of cooperation. *Journal of theoretical biology*, 372:118–127.

Ye, D., Zhang, M., and Sutanto, D. (2012). Self-organization in an agent network: A mechanism and a potential application. *Decision Support Systems*, 53:406–417.

Zanette, D. H. and Gil, S. (2006). Opinion spreading and agent segregation on evolving networks. *Physica D: Nonlinear Phenomena*, 224(1):156–165.

Zimmermann, M. G. and Eguíluz, V. M. (2005). Cooperation, social networks, and the emergence of leadership in a prisoner's dilemma with adaptive local interactions. *Physical Review E*, 72(5):056118.

Zimmermann, M. G., Eguíluz, V. M., and San Miguel, M. (2004). Coevolution of dynamical states and interactions in dynamic networks. *Physical Review E*, 69(6):065102.

Zschaler, G. (2012). Adaptive-network models of collective dynamics. *The European Physical Journal Special Topics*, 211(1):1–101.

Zschaler, G., Böhme, G. A., Seißinger, M., Huepe, C., and Gross, T. (2012). Early fragmentation in the adaptive voter model on directed networks. *Physical Review E*, 85(4):046107.